Tip-Clearance Effects in Axial Compressors

Anna Mollie Young
Jesus College

A dissertation submitted for the degree of
Doctor of Philosophy

Whittle Laboratory
Department of Engineering
University of Cambridge
April 2012

Tip-Clearance Effects in Axial Compressors

Anna Mollie Young

Summary

The flow in the tip-clearance gap of a compressor has a profound effect on its performance, but understanding of the actual flow phenomena involved is limited. The current work aims to improve the situation through a comprehensive set of tests on a compressor with different clearance sizes and levels of eccentricity.

The size of the tip-clearance gap is shown to affect both the flow coefficient at which the compressor stalls and the mechanism by which stall inception occurs (spikes or modes). Furthermore, the industry 'rule of thumb' that the stalling flow coefficient of an eccentric compressor is determined by the maximum tip-clearance is shown to be overly cautious. In this thesis it is shown that the more stable, small tip-clearance part of the annulus has a stabilising influence on the large clearance sector.

The second part of the thesis focuses on pre-stall disturbances in the rotor tip region and their link to stall inception. Past work has found that the signature generated by passing rotor blades becomes more irregular as the compressor approaches stall. Various attempts have been made to develop stall warning systems based on this irregularity, but without understanding its underlying cause.

It has been revealed that the increase in irregularity depends on both the tip-clearance size and the eccentricity level in the compressor. When the clearance is small and uniform, reducing the flow rate leads to a modest increase in irregularity. If the tip-clearance is large, there will be a sharp rise in irregularity all around the annulus as the compressor moves towards stall. In a compressor with eccentric tip-clearance, the irregularity will only increase in the large tip-clearance sector. This presents a major obstacle to reliable stall warning as tip-clearance size and eccentricity change during each flight and over the life of an engine.

Having examined the conditions under which pre-stall irregularity is most pronounced, the cause of the irregularity itself is investigated. The tip region is shown to be occupied by discrete disturbances that have been named 'blue holes'. The techniques developed as part of the work described in this thesis enable these disturbances to be investigated in detail. The experimental data gives strong evidence that the blue holes are caused by radial vortices, and this is confirmed by computational results.

The connection between blue holes and stall inception is also investigated. In a compressor with small tip-clearance, the formation of blue holes is found to lead directly to spike formation. A compressor with larger tip-clearance supports blue hole activity while continuing to operate stably. These blue holes are initially within the blade passage and do not appear to cause stall until they reach the rotor leading edge plane.

Declaration

The research presented in this dissertation was conducted at the Whittle Laboratory in the Cambridge University Engineering Department between October 2008 and March 2012.

This dissertation is the work of the author alone, and includes nothing which is the outcome of work done in collaboration, except where specifically indicated to the contrary. The computational results in Chapters 7 and 8 are from a collaborative project with Dr Graham Pullan. None of the work presented in this dissertation has been submitted to any other University or Institution for any other qualification.

This dissertation contains approximately 53,000 words and 95 figures.

Anna Mollie Young
April 2012

Publications

Young, A M, Day, I J and Pullan, G, 2011. 'Stall Warning by Blade Pressure Signature Analysis'. Paper presented at ASME Turbo Expo, Vancouver, Canada. Accepted for Publication in the *ASME Journal of Turbomachinery*.

Pullan, G, Young, A M, Day, I J, Greitzer, E M and Spakovszky, Z, 2012. 'Origins and Structure of Spike-Type Rotating Stall'. Paper to be presented at ASME Turbo Expo, Copenhagen, Denmark. Accepted for Publication in the *ASME Journal of Turbomachinery*.

Acknowledgements

I would not have been able to complete this thesis without the help of several people along the way. First of all, I would like to thank my supervisor, Dr Ivor Day. I am lucky to have been able to benefit from his vast knowledge of turbomachinery and experimental methods. Over the past three and a half years, Ivor has been a continuous source of advice, help and chocolate biscuits, and his patience in helping me to turn various draft documents from 'Double Dutch' into refined prose has been remarkable.

I am also indebted to my advisor, Dr John Longley, in particular for his help with the analytical modelling. I am thankful to Dr Graham Pullan for sharing his computational work with me and allowing me to use some of his data.

I would also like to thank Mr Chris Freeman for the time he has spent talking through various results with me and telling me about how things work in the real world. I am also grateful to Dr John Adamczyk and Dr Nick Cumpsty for many useful conversations.

No experimentalist would survive long without a technician, and I am particularly grateful to Mr David Barlow for his assistance, and for his patience in helping me dismantle and rebuild the compressor - often several times a day - and for always being prepared to drill 'another couple of holes' in the casing.

Other students at the Whittle Laboratory have also provided vital help to me during this project. In particular, I am indebted to Dr Tim Houghton for giving me his MATLAB and LabVIEW codes and to Dr Stephanie Weichert for her advice on experimental technique.

Finally, I am grateful to the EPSRC and Rolls-Royce Plc. for sponsoring me for the past three and a half years, and to Simon Gallimore and Nick Baker for taking an interest in my work.

Contents

Nomenclature

Roman Letters

$B = 1 - \frac{\text{Effective Flow Area}}{\text{Geometric Annulus Area}}$	Blockage (Effective flow area - accounting for endwall boundary layer displacement thickness)
b	Blade Chord
Δh	Enthalpy Rise over Stage
$g_{\text{t}} = \frac{\text{Pitch}}{\cos\gamma}$	Staggered spacing
I	Turbulence Intensity
j	Measurement number (in time)
$\dot{m}$	Mass Flow Rate
n	Revolution number
p	Pressure
$Re = \frac{\rho W b}{\mu}$	Reynolds' Number (Based on Chord)
r	Radius
s	Blade Span
S_{u}	Spanwise Non-Uniformity
U	Blade Speed
V	Absolute Velocity
W	Relative Velocity

Greek Letters

α	Flow Angle (absolute)
β	Flow Angle (relative)
γ	Blade stagger angle
δ	Difference between ensemble-average and instantaneous pressure
$\delta^* \approx Bs$	Displacement thickness
ϵ	Tip-clearance
θ	Tangential direction
$\lambda = \frac{b_{\mathrm{X}}}{\frac{1}{2} r \cos^2 \gamma}$	Inertia parameter
λ_2	Vortex Criterion
μ	Dynamic Viscosity
ρ	Density
τ	Angle between tip-leakage vortex and tangential
$\phi = \frac{V_{\mathrm{X}}}{U_{\mathrm{mid}}}$	Flow Coefficient
$\psi_{\mathrm{T\text{-}S}} = \frac{p_2 - p_{01}}{\frac{1}{2}\rho U_{\mathrm{mid}}^2}$	Total-to-static Pressure Rise Coefficient
ω	Rotational Speed

Superscripts/Subscripts

$[\bar{\ }]$	Mean
$[\ ]'$	Fluctuation
$[\ ]_0$	Stagnation Quantity
$[\ ]_{\mathrm{max}}$	Maximum
$[\ ]_{\mathrm{mid}}$	Mid-span value
$[\ ]_{\mathrm{min}}$	Minimum
$[\ ]_{\mathrm{RMS}}$	Root Mean Square Value
$[\ ]_{\mathrm{T\text{-}S}}$	Total-to-static
$[\ ]_{\mathrm{T\text{-}T}}$	Total-to-total
$[\ ]_{\mathrm{X}}$	Axial Component
$[\ ]_\theta$	Tangential Component

Chapter 1

Introduction

Axial compressors are widely used in aero-engines, where size and weight are important, so designers are always striving to improve performance. This means the largest possible pressure rise must be produced from the smallest possible work input, in the smallest possible space.

This sought-after performance is known to be adversely affected by the flow in the tip-clearance gap between the rotating compressor blades and the engine casing (necessary to prevent rubbing). The size of the tip-clearance gap affects the efficiency and pressure rise of the compressor and also has an impact on its stability when operating at off-design conditions.

It is therefore not surprising that a lot of work has previously been done on the tip-clearance gap and the associated tip-leakage flows. However, many questions remain unanswered. This thesis aims to study the effects of tip-clearance size and distribution on compressor performance and stability, and to improve understanding of the flowfield in the tip-clearance region.

The overall performance of a compressor is reflected in its performance map, which is a plot of pressure rise against mass flow rate at various operating speeds. A sketch of a typical performance map is shown in Diagram 1.1. At a given speed, the compressor will operate on one of the characteristic lines - the one highlighted in yellow, for example. The design point (green circle) is the normal operating point of the compressor at that speed. If the flow rate through the compressor is reduced, the pressure rise will increase, i.e. the operating point moves up and to the left.

The flow rate through the compressor cannot, of course, be reduced indefinitely, so at some point the low-flow stability limit of the compressor will be reached. This is the stall point, and is denoted by the red circle in Diagram 1.1. At this point, there is a sudden breakdown of the orderly flow in the compressor, leading to a loss of pressure rise. At higher rotational speeds, stall can lead to surge, which can potentially lead to engine damage.

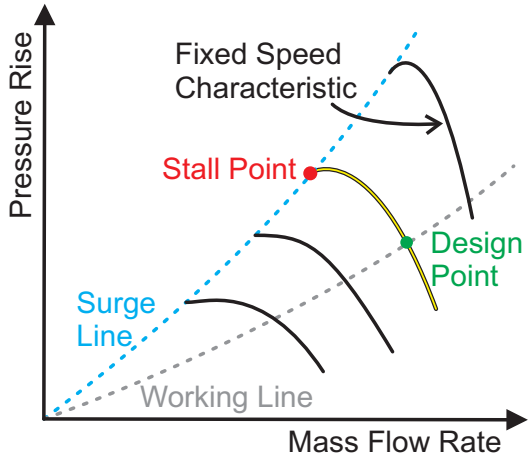

Diagram 1.1: *Sketch of a Typical Compressor Performance Map.*

Because of the potentially disastrous effects of stall, it must be avoided at all costs. This necessitates a large margin between the stall point and the design point of the compressor - i.e. the design point is purposely kept well to the right of the stall point on the characteristic. At its design point, the compressor therefore produces a pressure rise that is lower than the maximum possible.

If the compressor could operate closer to its stall point without compromising safety, it would produce a larger pressure rise (and, in most cases, operate with higher efficiency). This would mean it would be possible to have a smaller, lighter compressor, which would clearly be advantageous. In order to achieve this, either a more accurate understanding of how and when the compressor will stall is required, or a system needs to be developed which can, in real time, calculate the proximity of the current operating point to the stall point. This thesis contains contributions to both subjects.

The first part of this thesis contains what is believed to be the most comprehensive set of tests on the effects of tip-clearance size and eccentricity. This subject is not only of academic interest, as the tip-clearance is known to change during flight in a

real engine.

For the first time, the size of the tip-clearance gap has been found to affect the stall inception mechanism of the compressor (spike or modal). This work has also shown that, beyond a certain gap size, further increases in clearance cease to be detrimental in terms of the stalling flow coefficient of the machine.

It is generally accepted in industry that the stalling flow coefficient of an eccentric compressor can be determined using Freeman's rule of thumb [2]. This rule states that the stalling flow coefficient of a machine with tip-clearance asymmetry will be the same as that of a compressor with concentric clearance equal to the maximum gap. Tests on the compressor in both concentric and eccentric configurations with different levels of average clearance, have shown this rule of thumb to be somewhat pessimistic, as the more stable, smaller tip-clearance part of the annulus has a stabilising influence on the large clearance sector.

In the second part of the thesis, attention is turned to pre-stall disturbances in the rotor tip region and their link to the stall inception process. In recent times, several researchers have concentrated on measuring the pressure fluctuation caused by each blade as it passes over the casing, referred to here as the 'blade passing signature'. These researchers have generally found that the level of irregularity in the blade passing signal increases as the flow rate through the compressor is reduced. Attempts have been made to develop stall warning systems based on the level of blade passing irregularity, and General Electric have patented this idea [3]. Little effort has been made, however, to characterise the irregularity itself, or to understand its underlying causes.

Through a careful experimental program, the current work has revealed for the first time that the increase in irregularity in the blade passing signature is highly dependent on both the tip-clearance size and eccentricity. In a compressor with small, uniform, tip-clearance, the increase in irregularity which accompanies a reduction in flow rate will be modest. If the tip-clearance is enlarged, however, there will be a bigger rise in irregularity all around the annulus. In a compressor with eccentric tip-clearance, the irregularity will only increase in the large tip-clearance sector.

This finding is then used to argue that the level of irregularity in the blade passing signature cannot be used on its own to provide reliable stall warning in a real engine.

At least one other parameter would have to be measured, and so the system patented by General Electric will not work reliably in its current form.

Once the conditions under which once can expect to see a pre-stall ramp-up in irregularity have been defined, the actual cause of the irregularity will be investigated. The results of a detailed study of the unsteady pressure field on the rotor casing will be used to show that the increased irregularity is caused by discrete disturbances that have now been named 'blue holes'.

It is thought that this is the first time that these blue holes have been clearly shown to exist. Previous researchers have suggested such disturbances, but their work has mainly been based on frequency analysis of data from one spatial location and they have not obtained measurements of the flow in the tip region of the compressor. It is particularly notable that the blue holes in this work have been seen in a compressor that is operating stably and is not in a partially-stalled state. Furthermore, this work unifies the previously separate subjects of stall warning using irregularity measurements and the presence of blue holes in the flowfield at near-stall conditions.

The link between blue hole activity and stall inception will also be considered. This work is part of a collaborative project with Dr Pullan, whose computational work is used to see further details of the structure of the blue holes. In particular, new insight is gained into the spike-stall inception process.

Chapter 2

Literature Review

Compressor performance and tip-clearance flows have been the subject of numerous research projects over the past fifty years. Despite this, understanding of the precise effects that tip-clearance size and eccentricity have on compressor performance remains limited. Furthermore, agreement has not been reached on the existence or otherwise of pre-stall disturbances and there is no clear consensus as to the precise role of the tip-leakage flow in stall inception.

This chapter presents a review of the key literature on stall inception, starting with a description of the Emmons model for stall, and the two accepted stall inception mechanisms, modes and spikes. The current understanding of the role played by the tip clearance flow in determining compressor performance and stall inception is considered then, and previous work on the effect of blockage is also discussed.

Existing work on detecting and avoiding stall is then reviewed, and work on the legitimacy of low-speed testing (as carried out in this project) is then presented. Finally, conclusions are drawn and the basis for the current work is established.

2.1 The Emmons Model for Rotating Stall

Early work by Emmons et al. [4] separated the low-flow instabilities of compressors into two separate phenomena - stall, which is a rotating disturbance in the blade rows, and surge, which is a 1-D instability of the entire compressor. They proposed

a basic model for the propagation mechanism of a rotating stall cell in an axial compressor. This is illustrated in Diagram 2.1. Their idea was that, in a compressor operating near stall, a transient disturbance in one passage would cause flow separation on one blade, marked 'B' in Diagram 2.1, leading to significant blockage in that passage and thus diverting the approaching flow into adjacent passages. This in turn causes higher incidence on the next blade (blade 'A'), making it more likely to stall, and lower incidence on the previous blade (blade 'C'), making it more stable. It is evident that the process will repeat itself, with blades stalling, and unstalling in turn, such that the stall cell propagates relative to the blades in the direction opposite to rotor rotation.

Using a similar model and small perturbation analysis, Stenning [5] proposed that stall will occur at the peak of the total-to-static pressure rise characteristic, though it has been proven that this theoretical limit is not always adhered to in real compressors, which can stall before, at, or even after the peak of the characteristic (see, for example, the experimental work of Camp and Day [6]).

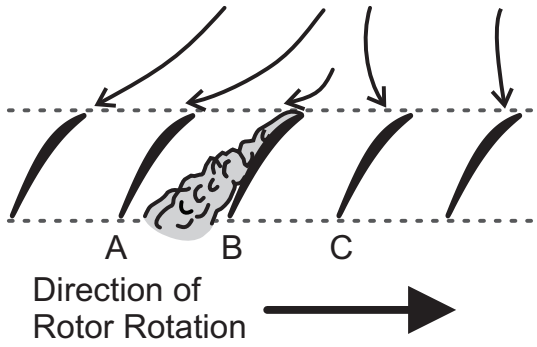

Diagram 2.1: *Stall Inception Model Proposed by Emmons/Stenning [4], [5].*

In addition to the general distinction between stall and surge, stall can be further divided into full-span and part-span stall. In full-span stall, the whole blade span is stalled, whereas only a portion of the span is involved in part-span stall and the rest of the span continues to operate normally. It is generally found that several small stall cells will be visible in a compressor operating in part-span stall, whereas in full-span stall one large cell will be observed.

Part-span stall often occurs in low hub-to-tip ratio blades (aero-engine fans, for example) at low-speed [7]. In his review paper on stall, however, Greitzer [8] points out that it is not only low hub-to-tip ratio compressors which exhibit part-span stall. Further discussion on this subject is given by Day et al. [9], where full- and part-span

stall are shown to occur in a high hub-to-tip ratio compressor. In the same work, Day et al. showed that stage loading and the proportion of the annulus blocked by the stall cell(s) are key factors in determining whether or not part-span stall will be observed.

2.2 Stall Inception Mechanisms

One of the early analytical models of stall inception was developed by Moore and Greitzer [10] [11], who used linearised stability theory to propose that stall inception would be preceded by modal waves. These modal waves are perturbations in the velocity distribution around the entire circumference of the compressor, which grow and eventually cause the breakdown of the flow and the onset of rotating stall, as shown in Diagram 2.2 (a). Modal waves were first observed in a compressor by McDougall [12], using measurements from hotwire probes located on the rotor blade surface and in the flowfield upstream and downstream of the blade rows. It is well-documented that modes can exist for many revolutions before stall.

It was, however, later observed by Day [13] that modal waves were not a necessary precursor for stall, and that there was at least one other mechanism of stall inception in a compressor, in which a stall cell developed independently of any modal perturbations. This work was followed up by Camp and Day [6], who showed how a short lengthscale disturbance, known as a spike, could lead to stall. This mechanism is illustrated in Diagram 2.2 (b) (note the similarity of this inception mechanism to that proposed by Emmons et al. [4]). In the early stages of development, spikes are three-dimensional disturbances that propagate around the annulus of the compressor. Spikes are initially only two or three blade pitches in circumferential extent, and are confined to the blade tip region. The spikes rapidly grow in magnitude as they rotate and develop into rotating stall within a few revolutions.

Camp and Day concluded that there are two routes to rotating stall, spike and modal, and that spikes would be most likely to occur if the compressor stalled on the negatively sloped part of the total-to-static characteristic, while modal stall would occur if the gradient of the characteristic was zero at stall. They also proposed that spike stall would always occur when the rotor blades reached a 'critical incidence', but further work by Young [14] has found this to be too simplistic.

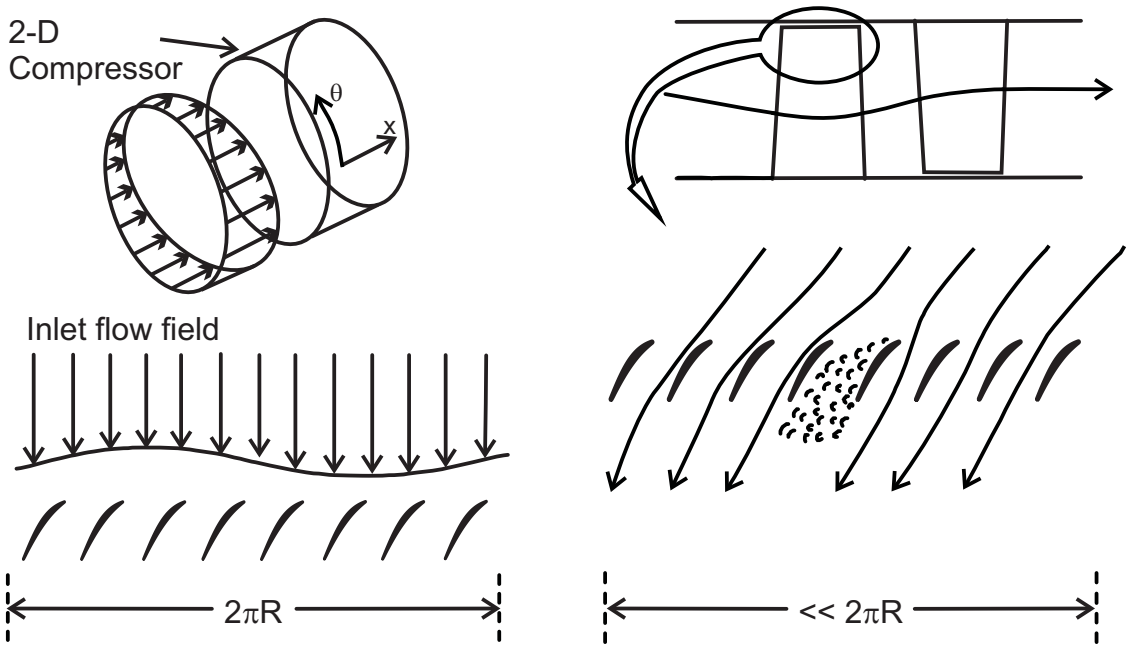

(a) Modal stall inception.

(b) Spike stall inception.

Diagram 2.2: *Sketches of Stall Inception Mechanisms (Courtesy of J.P. Longley/I. J. Day).*

The reason why a compressor should exhibit one type of stall inception rather than the other remains unclear. In his PhD work, Dickens tested four different blade designs [15], two of which tended to stall via modes while the other two stalled via spikes. He suggested that the spanwise location of blockage might be related to this (see Section 2.4).

It has also been shown by Simpson and Longley [16] that the stall inception mechanism can be changed from spike to modal by re-staggering the stator blades or changing the inlet flow profile. This is because these changes alter the spanwise loading distribution on the rotor blades, so that the location of flow breakdown changes from the hub to the tip for a change from modes to spikes (or from tip to hub for a change from spikes to modes). Despite this work, it is not currently possible for a designer to predict which mechanism a compressor will favour.

2.3 Tip-Clearance Flow

The flow in the clearance gap between the rotor blade tips and the casing is known to have a profound effect on the performance of a compressor and is thought to play

an important role in stall inception. This link has been pursued most keenly in the case of spike-type stall inception, which starts with a disturbance forming near the rotor blade tips.

Much previous work has focused on tip-clearance flows, which can be divided into five parts. First, the structure of the tip-clearance flow will be described. Next, the effect of the size of the tip-clearance gap on compressor stall margin and pressure rise is discussed, and tip-clearance flow models will be presented. Then the evidence for the involvement of the tip-clearance flow in stall inception will be reviewed, and finally tip-clearance asymmetry will be discussed in terms of its effect on stall inception.

2.3.1 Structure of the Tip-Clearance Flow

The flow through the clearance gap is shown schematically in Diagram 2.3. The flow between the blade tip and the casing is driven by the pressure difference between the pressure side and the suction side of the blade. This is shown in Diagram 2.3 (a).

The high-momentum tip-leakage flow collides with the main incoming flow along the interface (or lift-off) line as shown in Diagram 2.3 (b). At the interface between the two flows, a tip-leakage vortex forms slightly inboard of the blade tips. The angle of the interface line (marked τ in Diagram 2.3 (b)) will depend on the momentum balance between the two flows. As the compressor is throttled, the axial momentum of the main flow will decrease because of the reduction in flow coefficient. At the same time, the higher loading on the blades at this reduced flow coefficient leads to a bigger pressure difference across the blade tip, and so the leakage flow becomes stronger. This means that the tip-leakage vortex swings round towards the rotor leading edge plane as the compressor is throttled towards stall, i.e. there is a reduction in τ.

2.3.2 Effect of Tip-Clearance Gap Size on Compressor Performance

As early as 1949, the reduction in efficiency and work output caused by operating with a large tip-clearance was documented by Bowden and Jefferson [17]. Since then,

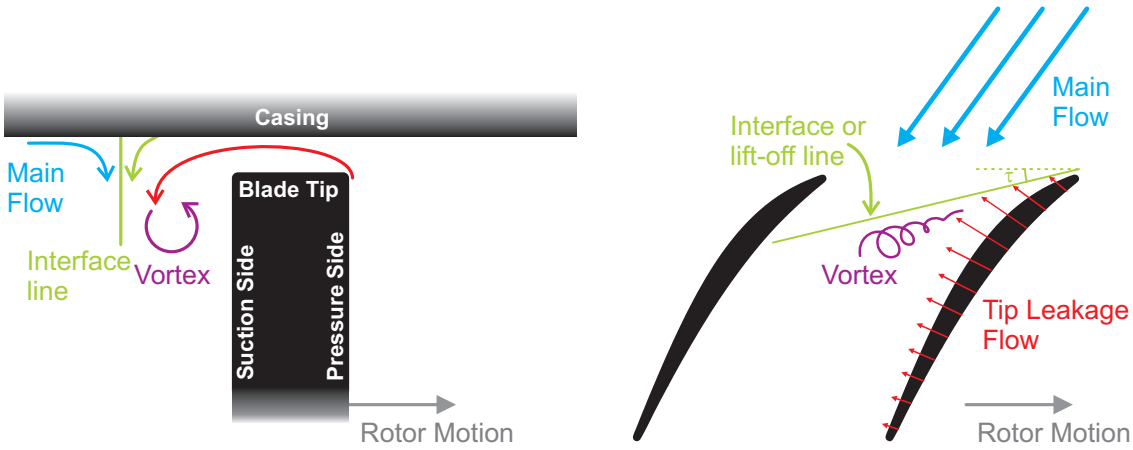

(a) Axial view.

(b) Radially Inwards.

Diagram 2.3: *Sketch of tip-clearance flow (in the rotor relative frame).*

numerous researchers have confirmed these findings and shown that an increase in tip-clearance can also cause a loss of stall margin.

A review paper by Peacock [18] brought together much of the early research on tip-clearance and showed a general consensus towards a linear relationship between tip-clearance size and compressor efficiency. Peacock also pointed out that some researchers had suggested that a small tip-clearance might be beneficial to compressor performance, as it could suppress corner separations and secondary flows. This would mean that there was an optimum tip-clearance, below which efficiency would drop, though this optimum clearance might well be lower than the minimum practical clearance imposed by mechanical constraints.

Experiments by Wennerstrom [19] in a transonic machine showed this to be the case. He found that there was an optimum clearance at which the secondary flows were just counteracted by tip-leakage flows, leading to a minimum loss. Wisler et al [20] also investigated the effects of tip-clearance size in a four-stage low-speed machine. They tested two blade designs, and found that one showed an optimum clearance greater than the minimum possible clearance, while the other design showed all increases in clearance to be detrimental. This shows that the optimum clearance is very much dependent on blade and compressor design.

Koch undertook an extensive study into the maximum pressure rise of compressors [21]. In this work he showed the relationship between tip-clearance and pressure rise to be approximately linear at moderate to large clearances. With smaller

gap sizes, his results show pressure rise increasing more rapidly with decreasing tip-clearance, i.e. a slightly non-linear relationship.

At the other end of the tip-clearance range, i.e. where the clearance is very large, there have been some suggestions that beyond a certain point, the stalling flow coefficient is constant regardless of the tip-clearance size. This can be seen in the results of Smith and Cumpsty [22], where the stalling flow coefficient increased when the clearance was opened from 1% to 3.5% chord, but there was no further increase in the test with 6% clearance.

2.3.3 Modelling the Tip-Clearance Flow and Associated Losses

Because of the profound effect of the tip-clearance flow on compressor performance, many attempts have been made to model this flow and the associated losses. These models were of particular importance in the time before large-scale CFD studies could be carried out. These models remain useful for understanding the fundamental physics of the flow.

Storer and Cumpsty [23] studied the tip-leakage flow in a cascade with cantilevered blades and found that the vortex became stronger and bigger as the tip-clearance gap was made larger. They also found that the transverse leakage flow separates and does not reattach as it passes over the blade tip. This is in contrast to the clearance flow in a turbine, where the flow reattaches because the ratio of blade thickness to gap size is much larger. They then developed a simple model for the tip-clearance flow based on the work of Rains [24], which assumes negligible mixing in the tip gap. Later work by the same authors [25] found that the loss due to the tip-clearance flow is proportional to the tip-clearance gap size.

The work of Lakshminarayana was instrumental in developing early models for the tip-clearance flow and associated losses [26], [27]. He showed that tip-clearance loss arises from lost circulation from the blades, and so the loss is dependent on the proportion of lift maintained at the tip.

Having developed an expression for this retained lift, Lakshminarayana argued that the stagnation pressure loss due to tip-leakage flow consists of two parts: one part due to the shed vorticity, and another part due to the kinetic energy of the tip-

clearance flow. He then developed expressions for the induced drag due to the shed vorticity and for the loss due to the kinetic energy of the leakage flow. The drag due to shed vorticity is a function of the lift coefficient and tip-clearance size only, while the loss due to kinetic energy comes from considering the pressure difference across the blade. Lakshminarayana used data from a compressor cascade with a double-sized tip-clearance gap in the centre of the span to test his model.

Horlock and Denton [28] produced a modern appraisal of Lakshminarayana's ideas and undertook some computational work which was in agreement with his results. They also emphasise the importance of the proportion of lift retained at the blade tip in determining the magnitude of the tip-clearance loss. The issue of how much lift is maintained at the blade tip was also tackled by Horlock in his review paper on blockage [29], where he suggests a relationship between tip-clearance size and shed lift.

Recently, an extensive experimental and computational project has been undertaken by Williams and others at Durham University to investigate tip-leakage flows in a compressor cascade [30], [31]. Of particular interest here are their calculations of blade loading with different tip-clearance sizes.

The measurements are discussed in detail by Walker et al. [32], where it is shown that the tip-leakage flow has an influence on the loading up to approximately 3 gap-heights inboard of the blade tips. With small clearances (3% span and under), the loading drops towards the blade tip as expected. However, in their calculations with larger clearances (6% span and higher), they observed an increase in loading near tip.

Walker et al. were unable to provide a complete explanation for this effect, though they postulated that it is due to the stagnation of the tip-leakage jet on the blade pressure surface and high velocities induced by the jet on the suction side of the blade, leading to a bigger pressure difference and thus higher loading.

In an aero-engine compressor, the tip-clearance will vary with operating conditions due to the changing load on the blades and thermal growth. This means that the clearance may be relatively large at some engine operating points and small at others, as explained by Freeman in his VKI lecture series [2]. In the same lecture, Freeman gave various 'rules of thumb' for the effect of tip-clearance on compressor

efficiency, stall margin and work output. He also argued that simple correlations are not always reliable, motivating more work on the fundamental flow physics driving these correlations.

The recent NASA N+3 project asked six teams comprised of universities and airframe and engine manufacturers to design concept aircraft which could enter service in 2030-35 [33]. These concept aircraft tended to make use of engines with compact cores (open rotor designs, for example). This work suggests that core sizes are likely to get smaller, and so tip-clearance sizes will get proportionally bigger due to mechanical constraints. It is thus becoming more important to understand the effect of changing the tip-clearance gap on compressor performance and stability. Some work towards this is presented in Chapter 4.

2.3.4 The Role of Tip-Clearance Flow in Stall Inception

It seems likely that the tip leakage flow plays a part in stall inception, particularly spike-type stall, as this originates in the tip region of the compressor. However, the exact way in which the tip leakage flow contributes to stall is unclear.

Vo, in his PhD work [34] and subsequent paper [35], undertook unsteady CFD calculations to try to understand the conditions under which spike stall occurs. He found the stability limit of the compressor using a single-passage calculation and then examined the transients that developed once the flow became unstable.

In Vo's work, the interface between the main incoming flow and the tip-clearance flow (see Diagram 2.3 (b)) is denoted by a region of high entropy gradient, which marks the most axially-forward extent of the tip-leakage vortex. From his single-passage studies, Vo found that this interface lined up with the rotor leading-edge plane at the stability limit (i.e. $\alpha = 0$ at stall).

Using the single-passage calculations, Vo concluded that there are two necessary criteria for spike stall inception. These are shown schematically in Diagram 2.4 and are:

1. Backflow, which occurs when the tip-clearance flow from one passage flows around the trailing edge of one blade and back into the next passage along.

This is seen as negative mass flow inboard of the blade tip at the trailing edge (shown in red).

2. Forward spillage of the tip-clearance flow into the adjacent passage upstream of the rotor leading edge and just inboard from the blade tip (shown in blue). This is a logical consequence of the interface between the main flow and the tip-clearance flow reaching the rotor leading edge plane.

According to Vo, these two flow features are both necessary criteria for spike stall. The spillage of tip-clearance flow into the next blade passage at the leading edge of the blade allows the backflow from the trailing edge to move upstream and create increased blockage. If there is no spillage, the backflow must convect downstream, or pass through the next tip-clearance gap.

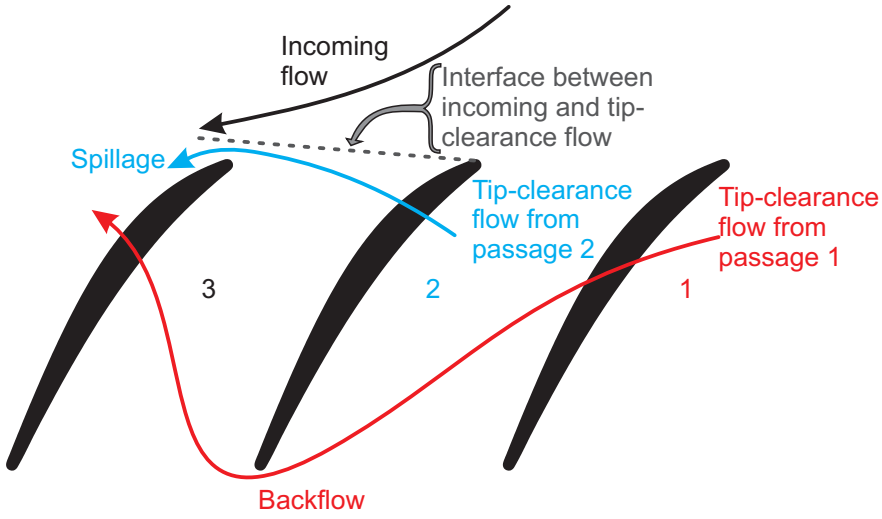

Diagram 2.4: *Schematic Diagram of Spillage and Backflow as Defined by Vo [34].*

In order to clarify the link between these two criteria and spike stall inception, Vo also performed some calculations in a 6-rotor passage segment. Again, he observed stall inception at the same point as the onset of spillage and backflow. There is limited experimental evidence in the literature to back up Vo's work, and that which exists is often contradictory. Some of the ideas presented in the literature are discussed below.

The centre of the tip-clearance vortex can be seen in experimental data as a trough in static pressure on the rotor casing. This was shown by Inoue and Kuromaru [36], who measured the static pressure on the compressor casing over the rotor blade

tips. They then compared the static pressure field with radial velocity measurements from the tip-clearance gap near the casing. They found a trough in the pressure field which coincided with a change in direction of the radial velocity, indicating that the flow was moving towards the casing on one side of the minimum pressure line and away from it on the other, suggesting the presence of a tangential vortex. This showed that the centre of the tip-clearance vortex could be located using the casing static pressure field.

The upstream limit of the tip-clearance vortex is, however, more difficult to locate from experimental data. Entropy cannot be measured directly, so the high entropy gradient found by Vo cannot be directly checked. Cameron et al. [37] have attempted to solve this problem by using CFD to calculate the axial shear stress on the casing of a compressor, and say that this matches up with the high entropy gradient seen in their CFD calculations. However, axial shear stress is also difficult to measure in a compressor, and Cameron et al. rely on flow visualisation.

In the absence of a quantitative measure of the upstream extent of the tip-clearance vortex, the main experimental validation of Vo's work is from flow visualisation, where oil or paint is applied to a surface in the experimental rig and the operating point is kept fixed while the paint dries. This gives a time-averaged picture of the flow. Saathoff and Stark [38] undertook oil flow visualisation and measured the casing static pressure in a compressor and a cascade rig. The compressor they tested stalled at the peak of its total-to-static characteristic, suggesting that it showed modal stall inception.

They observed a 'black line' in the casing flow visualisation pictures from the compressor. This black line was caused by the flow visualisation oil being scoured off the compressor casing, leaving the casing exposed (which was painted black). Saathoff and Stark interpreted this line as the point at which the flow on the casing separated and became axially reversed. This separation line was seen to move forwards as the compressor was throttled, and was actually upstream of the rotor leading edge plane at stall. Saathoff and Stark also observed spillage of the tip-clearance flow in the cascade rig, but not in the compressor. These observations were made from casing static pressure measurements.

Deppe et al. [39], then repeated Saathoff and Stark's work in 3 different compressors, all of which showed spike-type stall inception. They managed to delay stall onset

by using air injection to keep the tip-leakage vortex downstream of the rotor leading edge plane. This may suggest a link between the movement of the vortex and stall inception or it may be coincidental and the air injection may have served some other purpose, such as suppressing the growth of spikes in the tip region.

A major problem with flow visualisation techniques is that they give a time-averaged picture of what is a highly unsteady and extremely complicated flowfield. This means that any conclusions drawn from them must be treated with caution. Houghton and Day's recent work [40] shed more light on the cause of the 'black line' by using CFD in conjunction with flow visualisation. Houghton discussed this in more detail in his thesis [41], where he showed that that the 'black line' is due to a 3-D separation point on the interface line between the incoming and tip-leakage flows. At this point, the flow is simultaneously pushed inwards from all sides, and so it moves inboard of the casing. This 3-D separation point is not stationary, but moves along the casing with the rotors. The black line is, therefore, the time-averaged representation of an unsteady phenomenon.

Suder and Celestina [42] saw spillage at the onset of spike stall in a transonic compressor. They state that there is a strong link between spillage and spike stall inception, but that it is unclear whether the spillage actually causes spike stall, or is the spike stall itself. Cumpsty [43] also observed spillage at stall in a compressor fitted with part-circumference casing treatment, but did not suggest a causal link between spillage and spike stall inception.

Work by Brouckaert et al. [44] has shown that modal stall is not affected or caused by the behaviour of the tip-clearance flow. This is to be expected because modal stall is a whole-annulus phenomenon, whereas spike stall is caused by a disturbance formed in the tip region, so there is no reason why the tip-clearance flow should influence modal stall.

Work by Weichert and Day [45] using detailed unsteady pressure and velocity measurements in the tip-clearance and on the rotor casing has shown that the spike stall cell grows from a small disturbance within the blade passage, and that these early signs of a disturbance *precede* any detection of spillage. They also state that the process of spike formation may indeed vary from one compressor to the next.

The latest work by Pullan et al. [1], has highlighted the fact that spike-type stall

has been observed experimentally in compressors with zero tip-clearance (i.e. with shrouded rotor blades). Pullan et al. also show computational results for spike stall inception in a compressor with zero clearance. These results cast doubt on the idea that the tip-clearance flow itself is the cause of spike stall, as assumed in much of the work above.

In conclusion, no firm link has been established between the tip-clearance flow and spike-type stall inception. There is also limited evidence for the theory that backflow of the leakage flow at the trailing edge in combination with spillage of the tip-leakage vortex at the leading edge of the rotor are the cause of spike stall (as proposed by Vo [35]). More work is required to understand how the different elements of the flow interact to cause stall.

2.3.5 Lessons from Casing Treatment Studies

Applying casing treatment to a compressor involves altering the rotor casing, usually using circumferential grooves or axial slots, as a means of extending its stable operating range. For a full overview of previous studies, which are not of direct relevance here, see Houghton's thesis [41]. As casing treatment alters the behaviour of the flow in the rotor tip region, studies into its effectiveness often involve detailed measurement of the tip-clearance flow and its connection to stall inception. It is these measurements which are of interest here.

In his PhD work, Seitz [46] undertook detailed measurements in a low-speed compressor, which he backed up with computational work. In the tests without casing treatment, he observed a small low-pressure disturbance in the passage immediately before the formation of a spike stall cell. Seitz stated that this low pressure spot caused a blockage in the rotor tip region, which in turn led to forward spillage and stall inception. Whether or not his experimental data shows forward spillage before stall is a subject of debate.

This is similar to that reported by Weichert and Day [45] and Pullan et al. [1], which is discussed in detail in Chapter 8. In the current work, the low-pressure spot is shown to be caused by shed vorticity from the leading-edge of the rotor tip.

It is interesting to note that Seitz insisted that the low-pressure spot was initially

rotor-locked, whereas the more recent studies ([45], [1]) have shown a disturbance which propagates as soon as it forms.

From studying the rotor exit flowfield, Seitz suggested that casing treatment provided stall margin improvement by re-energising the tip-clearance flow and reducing the rotor exit tip blockage. More recent work on the same compressor by Houghton [41], however, has shown near-identical levels of blockage in the compressor with and without circumferential groove casing treatment, suggesting that suppressing blockage is not the reason why casing treatments create a stall margin improvement.

In the same project, Houghton and Day [40] showed that a stall margin improvement can be created by interfering with the development of the tip-clearance vortex, but that a groove placed downstream of the vortex can also give the same stability improvement while having no apparent effect on the vortex. As discussed in the previous section, this suggests that the relationship between the tip-clearance flow and the stall point is not straightforward.

2.3.6 Effect of Tip-Clearance Asymmetry

A real aero-engine will not have a perfectly round casing at all times, and the engine shaft will not always be mounted concentrically. This means that the tip-clearance gap will always have some degree of asymmetry, i.e. the gap will be larger in some sections of the annulus than others. As explained above, the size of the tip-clearance gap has a major effect on the strength of the tip-leakage vortex, on efficiency, and on the stall margin of the compressor. This means that it is important to understand the effect of having a larger gap on one side of the compressor than the other.

Graf et al. [47] measured the stall margin of a compressor with an off-centre casing, such that the asymmetry was stationary in the absolute frame. Their results showed that an asymmetric tip-clearance gives a much smaller stall margin than a constant tip-clearance with the same average value. They also found that the stall margin of an eccentric compressor is almost as poor as if the compressor had a uniform tip-clearance equal to the maximum value in the eccentric case. This finding is in line with Freeman's [2] rule of thumb that the stall margin of a compressor is determined by the worst clearance sector.

In their paper, Graf et al. [47] also developed a model for the flow in a compressor with asymmetric tip-clearance. This was based on the model for flow redistribution in a compressor operating with inlet distortion that had previously been developed by Hynes and Greitzer [48]. This model uses the parallel compressor argument: The compressor is constrained to provide the same exit static pressure at all circumferential locations, so the total-to-static pressure rise must be constant around the annulus of the eccentric compressor. However, a compressor with a smaller tip-clearance will provide a higher pressure rise at a given flow coefficient than one with a larger tip-clearance. This means that the compressor will have a higher flow coefficient in the small tip-clearance region and a lower flow coefficient in the large tip-clearance region. This is shown schematically in Diagram 2.5.

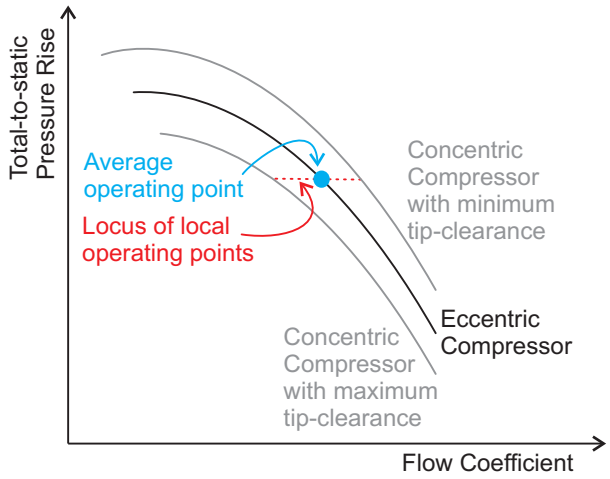

Diagram 2.5: *Parallel compressor argument for an eccentric machine [47].*

As discussed in Section 2.3.2, the stalling flow coefficient varies with tip-clearance, so the 'natural' stalling point (i.e. the point at which an axisymmetric compressor with the local tip-clearance) of the compressor will vary around the annulus. This means that some parts of the annulus will be more stable than others at a given flow coefficient. This circumferential variation in stability, along with the flow redistribution, is thought to be the cause of the loss of stall margin due to eccentricity and will be discussed in Chapter 5.

Tip-clearance asymmetry and the associated flow redistribution also changes the stall inception behaviour of a compressor. Researchers at Notre Dame University (Cameron et al. [49] and Bennington et al. [50]) studied the development of spike-type disturbances in a compressor with non-axisymmetric tip-clearance. They showed that, very close to the stall point, spike-like disturbances appear in the region with

the largest tip-clearance, and then decay in the part of the annulus where the tip-clearance is smaller.

Eventually, one of these disturbances completes an entire revolution of the annulus without fully decaying and then grows rapidly into a stall cell. They postulated that this phenomenon is due to the stronger tip-leakage vortex in the large tip-clearance causing forward spillage to occur first at this location.

The same authors also developed a simple model which uses a momentum balance to try to predict the operating point at which spillage will occur [50]. This model assumes that the location of the vortex is analogous to the separation point in a flow with a wall-bounded jet meeting an incoming uniform flow. Their experimental results agreed well with the model outputs, however the model is of dubious utility because the origin of the tip-leakage jet must be known (this is effectively a constant that can be adjusted to fit experimental data). Also, the analysis in the model is two-dimensional and steady, while the actual flowfield is highly three-dimensional and unsteady (a comparison of unsteady CFD and flow visualisation experiments is reported in Houghton's PhD thesis [41]).

It is clear that tip-clearance asymmetry is of interest both in academia, where it may be useful in understanding the fundamentals of stall inception, and in industry, where it presents an exacting design challenge. The lack of work in this area means the effect of both tip-clearance size and asymmetry on compressor stability remains poorly understood, with design calculations being based on rules of thumb. This is surprising given the devastating effect an enlarged tip-clearance can have on the performance of a compressor.

New work which may enable design rules to be improved is presented in Chapters 4 and 5, where the effects of a wide range of tip-clearance sizes and eccentricity levels will be discussed. The analytical model proposed by Graf et al. [47] for flow redistribution due to eccentricity will also be compared with experimental data.

2.4 Blockage

Blockage is a term used to define the loss of flow area in a compressor bladerow caused by wakes and boundary layers. It is commonly defined as:

$$B = 1 - \frac{\text{Effective Area}}{\text{Geometric Area}}$$

Different researchers have used different methods of calculating blockage depending on the data available to them.

Blockage tends to increase as the compressor moves from its design point to higher loading, as boundary layers and wakes grow and losses increase. This has led to attempts to find a blockage level at which stall will occur.

The effect of tip-clearance size on blockage was investigated by Smith [51], who conducted traverses in the rear two stages of a four-stage low-speed compressor. Smith's definition of blockage was based on measurements of displacement thickness of the endwall boundary layers at the hub and tip. This method requires the ideal velocity profile (with no blockage) to be defined. Smith showed that the blockage rises rapidly as the compressor operating point is moved towards stall.

Smith repeated his tests with different tip-clearance levels, and his data led him to suggest that the near-stall blockage level in the tip region rises linearly with increased clearance. As Smith says in the paper, this relationship is based more on engineering judgment than on an understanding of the flow phenomena involved.

Suder [52] used a two-dimensional analysis to determine blockage (as opposed to Smith's 1-D analysis). His experiments were undertaken in a transonic compressor and show that the end-wall blockage is two to three times larger than the blockage from wakes in the core flow. This end-wall blockage is mainly due to the tip-clearance flow and the shock-boundary layer interaction. He also showed that the blockage rises as the compressor operating point is moved towards stall, and that this increase is mainly in the hub and tip regions.

Khalid et al. [53] also measured blockage using a 2-D definition. As with Smith's data, Khalid et al.'s results showed blockage to be proportional to tip-clearance size for clearances greater than 1%.

Using a non-dimensional loading parameter, Khalid et al. were able to show that the blockage level reaches an asymptote as the compressor reaches its stall point. They also showed that the tip-clearance blockage is the limiting factor for stage pressure rise with larger clearances, whereas the pressure rise is constrained by the suction-surface boundary layer when the clearance is smaller.

One issue with the blockage measures described above is that they require assumptions to be made about the flow in the absence of blockage. In order to remove the need for these subjective judgments, Simpson and Longley [16] calculated spanwise non-uniformity (S_u) as a measure of blockage. They defined spanwise non-uniformity as:

$$S_u = \frac{\int_{hub}^{tip} V_x^2 dA}{\left(\int_{hub}^{tip} V_x dA\right)^2} x \int_{hub}^{tip} dA \tag{2.1}$$

where a spanwise non-uniformity of 1 would describe uniform flow. From a series of experiments in a single-stage compressor, Simpson and Longley concluded that the spanwise non-uniformity was lower in compressors which exhibited spike stall than in those which entered stall via modes. The reasons for this are unclear.

Dickens [15] also measured the flowfield downstream of the rotor bladerow in four different compressors. His results suggested that the blockage would be higher near the hub in compressors which showed spike stall, whereas machines which stalled via modes tended to show a large loss near the blade tips. Again, the reasons for this link are unclear.

Intuitively, it seems that blockage ought to be a useful measure of stall proximity, as high blockage means large losses, and so suggests that the flow is breaking down and the compressor is therefore close to instability. However, it seems that the blockage level alone is not a good predictor of when a compressor will stall. In their work on casing treatments, Smith and Cumpsty [22] suggested that the location of the

blockage is also important. Their experimental results showed that the compressor could operate stably with large blockage on the suction side of the passage, but the same blockage on the pressure surface would lead to stall. More work is required to understand whether or not blockage is a good measure of stall proximity and what, if anything, links the blockage distribution to the stall inception mechanism. This will be discussed in Chapter 4.

2.5 Detecting and Avoiding Stall

Because of the catastrophic effects of stall on engine performance, and the efficiency penalty associated with having a large stall margin, a vast amount of work has been undertaken on the subject of detecting and avoiding stall. This has included detecting precursors to stall inception, developing 'active control' systems to sense and suppress embryonic stall cells and using unsteady over-tip pressure measurements to estimate stall margin.

2.5.1 Pre-Stall Disturbances

There has been some debate as to the existence or otherwise of precursors to spike stall, i.e. rotating disturbances that can be detected before the formation of a spike, but which do not lead immediately to stall. Various pre-stall disturbances have been reported in the literature, but a clear picture has not really emerged.

Mailach et al. [54], [55] reported seeing 'rotating instabilities' in the third stage of a four-stage low-speed compressor when the tip-clearance was increased in the third stage. However, when very similar experiments were carried out by Wisler et al. [20] on an identical machine but with the tip-clearance enlarged on all four stages, the disturbances were not seen. From this result, Wisler et al. concluded that the disturbances seen by Mailach were due to the third stage being pushed beyond its stability limit and artificially supported by the other three, more stable, stages.

Inoue et al. [56], [57] observed short lengthscale disturbances that were like small stall cells but did not grow. These were dismissed by Cumpsty in his discussion of their paper as part-span stall cells [58] (part-span stall is when a stall cell does

not extend over the full span of the blades, so the compressor is able to continue operating almost at full capacity). The part-span assertion by Cumpsty is supported by the shape of the characteristic, which shows a sharp drop in pressure rise before the flow rate at which the disturbances were seen. Cumpsty also pointed out that the compressor appears to show modal stall, so these disturbances are not linked to spike stall.

In their second paper on the subject [57], Inoue et al. suggest a structure for the short lengthscale disturbances. Having observed low pressure patches on the rotor casing, they propose that these are caused by a vortex which is attached to the blade suction surface at one end and the casing at the other. It is not clear from the paper what evidence they have for this model, though a vortex is the most plausible explanation of the low pressure patches measured on the casing.

März et al also showed similar 'rotating instabilities' in a fan with low hub-tip ratio and operating at part speed. Again, Wisler et al. [20], discuss this result, and argue that the positive slope of the characteristic in the region where the disturbances are seen suggests that the fan is not operating stably. Work on a different fan by Kameier and Neise [59] showed disturbances in a similar frequency range. As fans are known to be prone to part-span stall, especially when operating at part speed, it is difficult to distinguish between the disturbances seen by März et al. and Kameier and Neise and part-span stall cells.

It is worth noting that März et al. [60], Mailach et al. [54], [55] and Kameier and Neise [59] all made use of frequency analysis to argue for the existence of the rotating instabilities. They did not attempt to make direct measurements of the disturbances themselves.

Fourier analysis of stall inception measurements by Day [13] showed that while disturbances are clearly visible well in advance of modal stall, there are no such wave-like precursors to warn of spike stall. It is therefore generally accepted that stall onset with this mechanism is a stochastic process that develops in just a few rotor revolutions.

It is clear that the existence of pre-stall disturbances is not universally accepted. In fact, the main protagonists in the rotating instabilities story seem to be clustered in one or two institutions. The results discussed in Chapters 6 and 7 help to explain

the reason for this controversy as they show the circumstances under which clear disturbances are observed while the compressor is still operating on the stable part of its characteristic. In other words, the existence of these rotating instabilities can now be confirmed and explained.

2.5.2 Active control

As engine designers have responded to demands for higher efficiency, there has been great interest in active control as a means of operating with reduced stall margin without compromising safety - an approach initially suggested by Epstein et al. [61]. Day [13] used discrete air injection to suppress both spikes and modes, and to prevent surge, leading to a 6% improvement in stall margin. Furthermore, a system devised by Paduano et al. [62] was shown to be effective in suppressing modal stall.

Later work, by Day et al. [63] states that a fully functional active control system is a long way from reality because no system yet exists that can detect stall onset in all situations. This issue is compounded in high-speed, multi-stage machines because the stage-matching affects the stall inception mechanism, with stall occurring in the front stages of the compressor at low speed, all stages simultaneously in the middle of the speed range, and in the rear stages at high speed [64].

There has recently been renewed interest in active control, but progress towards a reliable system has been slow, as the systems that have been developed have to be tailored to the behaviour of each individual engine. An example of this is the work of Bindl et al. [65].

If the goal of operating compressors with reduced stall margins is to be achieved, either understanding of the stall inception process will have to be dramatically improved, or a method other than active control must be developed. For example, better casing treatment is one area in which progress has recently been made [40].

2.5.3 Stall Warning

Related to active control is the concept of stall warning. The difference between the two is that, while active control seeks to detect embryonic stall cells and damp them

out, stall warning systems aim to detect a build-up in pre-stall activity and thus avoid stall by moving the compressor operating point to a higher flow rate. As has been discussed above, no precursors to spike stall have been found, so the formation of a stall cell cannot be anticipated. Some researchers have, however, found that the blade passing signature to be a possible source of stall warning.

The term 'blade passing signature' is used to describe the pressure fluctuation on the rotor casing which accompanies the passing of each blade. The signature of each blade resembles a sawtooth wave, due to the rise in pressure as the pressure side of the blade passes followed by a sudden drop as the suction side follows. One avenue of research has been to measure the changes in the blade passing signature from one revolution to the next as stall is approached to see if there is any early indication that the compressor is approaching its stall point.

Dhingra et al. [66] measured the repeatability of the blade passing signature using a correlation function. They found that this correlation function dropped as stall was approached. This trend was seen in both low- and high-speed compressors, suggesting some generality in the observed patterns. In a later paper, Liu et al. [67] defined this drop in repeatability of the blade passing signature as an 'event' and measured 'event rate' against stall margin. They found that the event rate ramped up rapidly as the flow rate through the compressor was reduced towards the stall point.

An example of this ramp-up in event rate is shown in Diagram 2.6, which is a plot of event rate against stall margin taken from Dhingra's PhD Thesis [68]. The different lines show results for different correlation measure thresholds (a higher threshold means an event is defined by a smaller drop in correlation measure). It can be seen that the event rate rises rapidly near stall, and that a higher threshold leads to a much sharper rise.

Using the correlation function technique, Christensen et al. [69] describe a system that warns of imminent stall in time for the engine operating point to be adjusted away from danger. This system was tested successfully in an engine, though the data shown in the paper suggest that the probes are in fact detecting embryonic stall cells and so this is more like an active control system (see previous section) than a stall warning system.

This relationship between event rate and stall margin was used to develop a control system that was tested on a theoretical model of an engine with degraded parts. The computations met with apparent success, as reported by Liu et al. [67]. As shown in Diagram 2.6, the rise in event rate with throttling is very gradual when the compressor is far from stall, so the accuracy with which the stall margin can be measured in these conditions is poor. This meant that the correlation measure method on its own was found to give false alarms; these were prevented by using empirically determined stall margin data in the control system.

The success of this system in laboratory tests and on theoretical models has led to considerable interest from parties in industry, and a patent for implementing such a system on a real engine has been granted to General Electric [3].

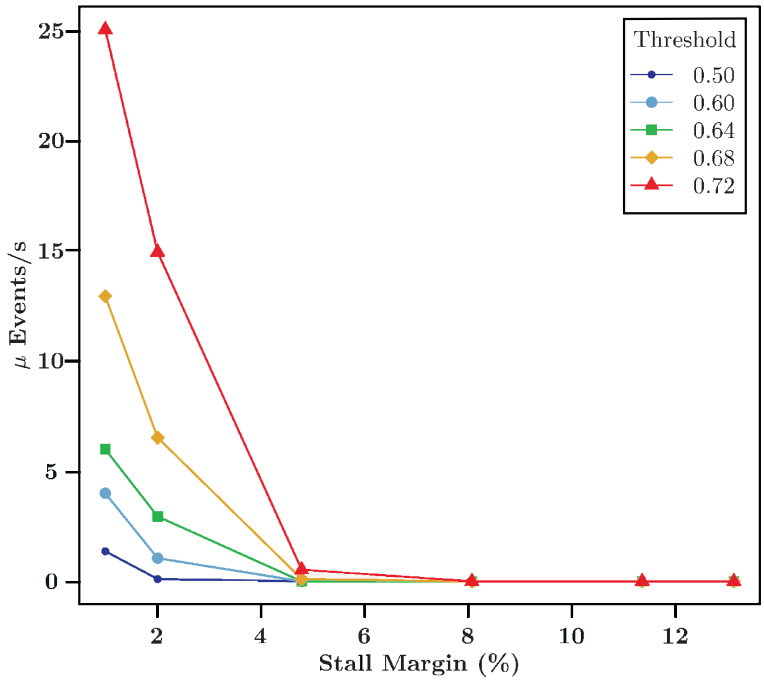

Diagram 2.6: *Graph of 'Event Rate' Against Stall Margin (taken from Dhingra [68]).*

The big issue with this field of study is that some researchers have reported seeing a ramp up in the irregularity of the blade passing signal as stall is approached, while many others have not. Doubt has been cast on the relationship between irregularity of the blade passing signature and stall proximity in recent work by Gannon et al. [70]. They measured the variation in blade passing signal in a transonic compressor at different speeds and did not find a consistent ramp-up in irregularity as stall was approached.

These conflicting results highlight the need to understand the basic physics behind the disturbances being measured. The rise in irregularity could be due to a structured disturbance in the tip-clearance region, or simply a general increase in turbulent behaviour prior to stall. If there is indeed a distinct structure to the disturbance, it could be related to the stall inception process or it could be an entirely independent flow feature. It is unlikely that a stall warning system can be based on a disturbance that is not directly related to the stall inception process. The basic cause of the irregularity in the blade passing signature will be examined in Chapter 7. Direct measurements of individual disturbances (as opposed to statistical event analysis) will be reported for the first time.

Graf et al. [47], in their work on asymmetric tip-clearance (see Section 2.3.6), found that the unsteady pressure signal upstream of the rotor at near stall conditions was most irregular in the region of large tip-clearance. In this thesis, detailed work using multiple probes spaced around the circumference of a compressor has been undertaken to clarify this issue and is also reported in Chapter 6.

An interesting question is whether the rise in blade passing signal irregularity will be seen if the compressor shows modal stall. As with active control systems, any stall warning mechanism must be capable of detecting all possible routes into instability or it will be unreliable. More details are reported in Chapter 6.

2.6 The Validity of Low-Speed Testing

Much of the testing done in laboratories is carried out on low-speed compressors, as opposed to high-speed engines. The reasons for this include cost and ease of instrumentation. High-speed tests are very expensive, and can be difficult to set up, so it is not possible to undertake extensive parametric studies, or measure the flowfield in great detail. In a low-speed machine, the sampling rates required to achieve reasonable resolution of flow features are much lower and generally the process of stripping and rebuilding the compressor will be far simpler and less time-consuming. It is, however, important to assess the validity of relying on low-speed testing, as some key flow features will be absent in a low-speed compressor.

As pointed out by Wisler [71], dynamical similarity is important for accurate testing.

This means that geometry, Reynolds' number and Mach number should be kept constant between the low speed tests and the engine they are meant to represent. The Mach number cannot be kept constant between the engine and the low-speed tests, but the Prandtl-Glauert equation can be used when designing the low-speed blading to correct for the reduction in speed. In particular, the blades in a low-speed research compressor will be thicker than those in a real engine. This changes the ratio of the tip thickness to the tip-clearance gap and may have implications for the behaviour of the tip leakage flow.

Most low-speed compressors, however, operate at much lower Reynolds' numbers than those found in an engine, so dynamical similarity is not achieved. Not all aspects of the flow will therefore be the same in a low-speed rig as in a real engine. The main work in support of low-speed testing for research into stall is that of Day and Freeman [7], in which stall inception data from stall and surge experiments in a low-speed research compressor were compared with those of a high-speed engine. They found that the key features of the stall inception process were the same in both cases, though some minor details of the flow differed. They thus concluded that low-speed testing is a valid and inexpensive way of understanding the stall inception process. The low-speed compressor used for their work had a Reynolds' number of $1.7x10^5$, so their conclusion is valid at least down to this Reynolds' number.

2.7 Conclusions and New Work

As shown above, much work has been done in the past to try to develop a model for stall inception and stall prediction, but there is still a lack of clear understanding. The precise effects of the tip-clearance gap dimensions on compressor behaviour also remain unknown.

What is known is that there are two mechanisms of stall inception; modal and spike. Modal stall can be modelled using linearised theory, but spike stall appears to be a stochastic process. Spike stall appears to be initiated in the tip region of the rotor blades, but a clear link to the tip-clearance flow has not been established.

In a rotor, the vortex which is formed by the interaction of the tip-leakage flow and the main flow through the passage changes in strength and direction as stall

is approached. There is controversy over the influence of the tip-leakage vortex on stall inception, especially over whether or not spillage of tip-leakage flow round the rotor leading edges, accompanied by flow reversal at the trailing edge of the blade, are actually the cause of spike stall. This issue is compounded by the difficulty of measuring the position of the tip-leakage vortex in an experiment and the fact that it is not yet possible to use CFD to predict the stall point of a compressor with confidence.

Enlarging the tip-clearance gap is known to be detrimental in terms of the pressure rise, stall margin and efficiency of a compressor, and several researchers have developed models for the losses associated with the tip-clearance flow. However, many questions remain unanswered, so new research on this topic will be shown in Chapter 4.

Tip-clearance eccentricity has also been a topic of study in the past, but so far nobody has been able to improve on Freeman's rule of thumb that stall margin is governed by the worst tip-clearance while efficiency is determined by the average clearance. Work to improve this rule of thumb and better understand the effect of tip-clearance asymmetry on the flowfield in the compressor will be shown in Chapter 5.

Active control systems aim to detect stall cells as soon as they develop and then damp them out. It is unlikely that these will ever be able to detect stall in all situations, so attention has turned to stall warning systems, which detect changes in the flowfield that suggest stall is imminent. The main area of interest is the blade passing signal, which appears to become more irregular as the compressor approaches the stability limit. There is a lack of understanding as to why some researchers see this irregularity and others do not, so a more detailed investigation of the blade passing signal has been undertaken. This is described in Chapter 6.

As well as a lack of understanding of the relationship between stall margin and blade passing irregularity, very little work has been done to identify the *cause* of this irregularity - whether it is a structured disturbance or simply a rise in turbulent fluctuations. Furthermore, nobody has established whether or not the cause of the irregularity is directly linked to the stall inception process.

The cause of the rise in irregularity will be explored in Chapter 7, and the link to stall inception will be discussed in Chapter 8. In these chapters, the latest computational

results, from calculations by Dr Graham Pullan, which show disturbances that match the experimental data, will be discussed. The simulation results are used to gain further insight into the structures in the flowfield that cause the disturbances. This work is part of a joint project and is published in Pullan et al. [1].

Chapter 3

Experimental Methods

This chapter explains the apparatus used in this project and the experiments which were undertaken. First, the test compressor is described, followed by details of the changes made to the tip-clearance size and eccentricity. Finally, both the steady and unsteady data acquisition methods are discussed. The measurements themselves are presented in Chapters 4 to 7, along with relevant information concerning data analysis.

3.1 Yellow Compressor

The experimental work for this project was carried out on a single-stage low-speed compressor (the Yellow Compressor) at the Whittle Laboratory. The compressor is fitted with controlled diffusion blades designed by Rolls-Royce (1998 design), and its key parameters are given in Table 3.1. The mid-span blade profiles for the rotor and stator are shown in Fig. 3.1.

When set up with the datum tip-clearance and stagger angles given, the compressor shows spike-type stall inception, and the stalling flow coefficient is 0.406 and the stage loading at stall is 0.67. The layout of the compressor and main instrumentation locations are shown in Diagram 3.1.

Rotor Reynolds' number (based on chord)	$1.7x10^5$
Hub Radius	184 mm
Hub-to-tip ratio	0.75
Rotational Speed	2985 rpm
Number of rotor blades	58
Number of stator blades	56
Design Flow Coefficient	0.5
Design Stage Loading	0.57
Design Reaction (%)	68
Rotor Stagger (hub, setting angle)	35°
Stator Stagger (setting angle)	22°
Mid-span solidity (rotor)	1.55
Rotor Chord	36 mm
Rotor Tip Clearance	0.6 mm (1.7% chord)

Table 3.1: *Key parameters of the Yellow Compressor.*

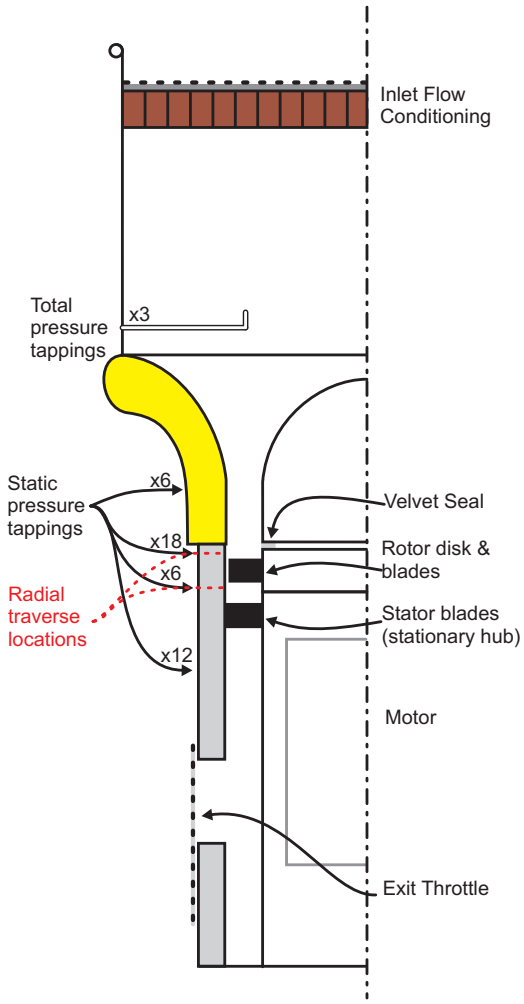

Diagram 3.1: *Schematic diagram of the Yellow Compressor.*

3.1.1 Flow Conditioning

Upstream of the blade row, there is a flow conditioning section which consists of a gauze, filter and honeycomb straightener, followed by a cylindrical plenum. The inlet section is designed to remove any large fluctuations from the incoming flow. The flow then passes through a strong contraction (5.4:1), before entering the parallel working section. The parallel section begins approximately 8 rotor mid-span axial chord lengths upstream of the rotor leading edge

The turbulence level of the incoming flow was calculated from a hotwire traverse upstream of the rotor blades. From the hotwire measurements, the turbulence intensity was found using the following equation:

$$I = \sqrt{\frac{v'}{V}}$$

Where v' is the size of the velocity fluctuations (as defined by the standard deviation of the set of velocity measurements) and V is the *local* mean velocity.

The incoming turbulence intensity was found to vary from approximately 1 to 2% in the free-stream, rising to 10% in the hub and casing boundary layer regions. The free-stream value is lower than that found by Camp and Shin [72] in an embedded stage, but almost up to the value of 2% suggested by Schlichting and Das [73] for flow behind the first rotor of a multistage machine. Schlichting and Das also showed that for a compressor operating at a Reynolds' number of 1.6×10^5 with turbulence intensities lower than 2.5%, transition took place via a laminar separation bubble, while at higher turbulence intensities, the flow was turbulent from the leading edge. With the original set of blades, it is thought that the flow was turbulent right from the leading edge due to blade surface roughness[1].

A brief study of the effect of fitting a turbulence grid upstream of the stage was carried out. The grid was the same as the one used by Simpson [74], which he measured to give a turbulence intensity of 4%. The grid restricted the flow range of the compressor at open throttle, but did not significantly alter the stall point of the machine, and the stall inception mechanism did not change. The use of a turbulence grid is not without problems, particularly with regard to measuring the total pressure downstream of the grid. Furthermore, the issue of the effect of inflow turbulence on compressor behaviour is far from clear (see [74] and [75]). It was therefore decided not to use a turbulence grid, as this would not improve the general consistency of the results.

The inlet flow profile obtained from a three-hole probe traverse 43% chord upstream of the rotor is shown in Fig. 3.2. The static pressure profile shows some variation across the span, which is thought to be due to streamline curvature. It can be seen from the total pressure plot that the endwall boundary layer extends to 6% span at the hub while the tip boundary layer is thicker, extending to 11% span in from

[1]Some of the final tests were carried out with a new set of blades, that appeared to behave slightly differently - laminar flow due to lower blade roughness is thought to be the reason for this.

the casing. The endwall boundary layers may be slightly thinner than in an embedded stage of the high-presure compressor in an aero-engine, though approximately representative of those found in an intermediate-pressure compressor. This is not expected to affect the results obtained in this thesis (for example, the rotor tips are well within the boundary layer, even with the maximum tip-clearance).

3.1.2 Working Section

The working section consists of the rotor and stator rows - there are no inlet guide vanes. Both sets of blades are cantilevered, and no sealant is used on either blade row, as the gap between blade and mounting surface (hub or casing) is very small. The rotor hub rotates from 49% axial chord (b_x) upstream of the rotor blades to 7% b_x downstream of the blades. The stator hub is stationary, allowing for a tight fit between the stator blades and the hub. This minimises leakage. The spacing between the rotor and stator rows is 45% axial chord (b_x) at the hub.

The blade stagger angle was set using specially manufactured setting tools. The tools were designed to sit on the rotor hub or stator casing as appropriate and the blade was lined up such that it just touched the tool at the leading and trailing edge. The setting tool was initially set using a protractor. This method means that while there could be an error of up to 0.25°in the absolute blade angle, the variation in blade stagger angle around the annulus would be significantly less than this.

The flow through the compressor is controlled by means of an exit throttle. This allows the flow coefficient to be varied precisely and held at any required operating point from full flow to stall.

As explained in Section 2.6, it is generally found that the stall inception process is very similar in low- and high-speed machines [7]. The fact that the compressor used here is of low-speed design is not thought to affect the general validity of the results, and should not diminish their applicability to real aero-engines.

3.2 Tip-Clearance and Rotor Eccentricity

During the course of the work described here, both tip-clearance size and eccentricity were changed, as shown schematically in Diagram 3.2. The tip-clearance size was adjusted by cutting back the rotor blade tips, to reduce the blade height. This cutting back process was done with the blades fitted to the rotor, so uniform blade height was maintained.

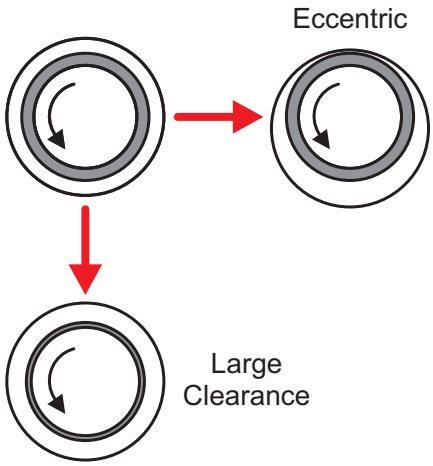

Diagram 3.2: *Schematic diagram of tip-clearance changes made in this project.*

There are two kinds of tip-clearance asymmetry which can occur in a compressor rotor; stationary, and rotating [47]. Stationary asymmetry is caused by casing ovality or by an off-centred rotor, while rotating asymmetry is due to rotor shaft bending, or irregular blade height. The Yellow Compressor was found to have negligible geometric asymmetry when stationary (tested by rotating the rotor while measuring the tip-clearance at a fixed point) and because the shaft over-hang is short, the rotating asymmetry at full speed is assumed to be negligible. For this project, a special rotor casing was manufactured to give minimal out-of-roundness. The combination of geometric asymmetry, rotor bending and casing out-of-roundness gave a total eccentricity of no more than 0.03 mm when the compressor was in the concentric configuration (5% of the datum tip-clearance).

In this project, stationary tip-clearance asymmetry due to an offset casing was studied. The asymmetry in the Yellow Compressor is achieved by altering the concentricity of the casing relative to the rotor, as shown schematically in Diagram 3.3.

The definition of eccentricity used in this work is as follows:

$$\text{Eccentricity (\%)} \quad = \quad \frac{\epsilon_{\max} - \epsilon_{\min}}{\bar{\epsilon}} \text{ x } 100 \tag{3.1}$$

where ϵ denotes tip-clearance. This is shown schematically in Diagram 3.3.

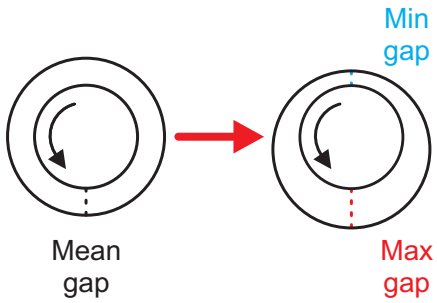

Diagram 3.3: *Schematic diagram of tip-clearance eccentricity.*

The physical technique for adjusting the casing is shown in Diagram 3.4. Before adjustment, the rotor is removed to allow access to the shaft. Once the bolts which hold the casing down have been slackened, the casing can be moved relative to the rotor shaft, and the eccentricity is measured using a dial gauge fitted to the centre of the shaft. In this way, the entire compressor casing, from inlet to exit, is moved, so there is no step in the casing in the working section.

During the adjustment process, the retaining bolts in the stator hub are also slackened, as shown in Diagram 3.4. This allows the stator blades and hub to move together as the casing is moved. This technique prevents the stator hub gap from becoming eccentric, which would change the behaviour of the hub corner separation on the stator suction surface.

In order to investigate the effect of both tip-clearance size and asymmetry on compressor performance, the compressor was altered systematically through a series of tip-clearances with different levels of eccentricity. The stall warning measurements were carried out on tip-clearances of 1.7 to 4.2% chord, with up to 75% eccentricity, while extra builds with tip-clearances of up to 10% chord were tested for the compressor stability study. A summary of all the configurations tested is shown in Table 3.2.

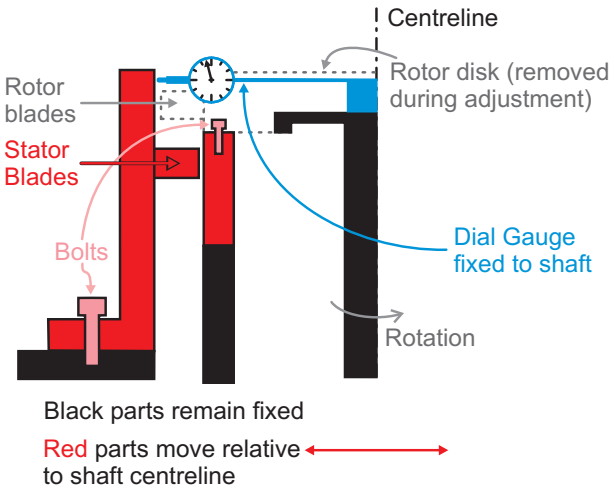

Diagram 3.4: *Schematic of eccentricity adjustment technique.*

3.3 Instrumentation

3.3.1 Computer Hardware and Software

All data was recorded using National Instruments data acquisition cards, controlled and monitored using LabVIEW. The cards have 16-bit resolution, meaning that quantisation uncertainty is small (0.15mV for a 10V range, or 15μV for a 1V range). Each data logging card is capable of logging at 1 million samples per second (i.e. 1 MHz on one channel, or 100 kHz on each of 10 channels).

In general, unsteady data was acquired at 100 kHz, to give approximately 34 points per rotor passing period. The comparatively high logging frequency used meant that, in cases where more than 10 channels were logged at once, two cards had to be used simultaneously so that up to 20 channels could be measured simultaneously. The data logging programs were altered to allow for synchronised logging from two cards, and the once-per-rev trigger signal was recorded on both cards so that the synchronisation could be checked. This meant that data from up to 18 probes could be recorded at once. Data processing was performed in MATLAB.

	Average Tip-Clearance(% chord)	Tip-Clearance Eccentricity (%)
Stall warning study	1.1	8
	1.7	5, 25, 50, 75
	2.4	4, 25, 50, 75
	3.3	3, 38, 75
	4.2	2, 30, 75
Extra tip-clearances for stability study	4.9	2, 26, 51, 75, 100
	5.8	2, 9, 21, 29, 43, 75
	6.7	2, 19, 75
	8.5	2
	10.0	2

Table 3.2: *Compressor tip-clearance and eccentricity levels.*

3.3.2 Steady Pressure Measurements

The pressure transducers used for logging steady pressures had a 1 psi range and were calibrated using a micromanometer. The same micromanometer was used throughout all the tests. The zero levels of the transducers were recorded at the start of each set of experiments and hourly during longer runs. This, along with choosing the pressure transducers with the greatest zero level stability for the most sensitive measurements, minimised the error due to drift in the transducers. Typical drift between zero-level measurements was found to be $\pm$0.2-2.5 mV. Combined with the errors due to quantisation (0.1 Pa) and calibration (0.2% of calibration gradient), the maximum error in steady pressure measurements was $\pm$4Pa, or 0.6% of inlet dynamic head (though for the lower-drift transducers, the error was less than $\pm$2Pa, or 0.3% of dynamic head).

Three-Hole Probe A three-hole cobra probe was used to obtain time-averaged pressures and thus deduce the average flow speed and direction. The probe is compact enough to pass through a 3 mm traverse hole. The probe head thickness is 0.8 mm.

The three-hole probe was calibrated in a steady-flow wind tunnel at angles from -

45°to +45°. The calibration was checked over a range of flow speeds, and was found to be independent of Reynolds' number at small to moderate angles (under 30°).

During the calibration process, the errors in the measured static and stagnation pressures were both found to be within 1% of dynamic head. The minimum rotational step size is 0.3°, so flow angles were accurate to $\pm 0.5°$.

3.3.3 Unsteady Pressure Measurements

Fast-response pressure transducers (Kulites) were used to measure the unsteady pressure on the rotor casing. These transducers can measure at up to 100 kHz, which is considerably above the highest frequencies observed in the flowfield. The data was usually low-pass filtered (electronically) at 50 kHz, to avoid aliasing[2].

The pressure transducers used have a 5 psi range, and were calibrated periodically using the same micromanometer mentioned above. The calibration gradient (Pa/V) was found to change very little and generally remained constant to within 2%. The zero levels, however, drifted rapidly such that the transducers could only be used to measure fluctuations in pressure, not absolute values. When absolute pressure measurements were required, the steady (time-averaged) pressure level was acquired at the same location (using the pressure transducers described in Section 3.3.2 above) and added to the unsteady measurements. The quantisation uncertainty for a 1 V peak-to-peak signal - the size of the blade passing signature - is 0.015%, which is small enough to be neglected.

3.3.4 Unsteady Velocity Measurements

Standard Hotwire Probe A single-filament hotwire was used to measure the turbulence intensity upstream of the rotor blades, and the unsteady flowfield at rotor exit. The hotwire was calibrated daily in the vast majority of cases, using a steady-flow wind tunnel over a range of velocities from 10 m/s to 45 m/s (this range covers most of the flow speeds present in the compressor). A fourth-order polynomial was

[2]Ideally, a lower frequency, say 40 kHz, would be used, as the filter is not an ideal filter and so has some roll-off, but 50 kHz is better than the available alternatives of 10 or 100 kHz.

fitted to the measurements to produce the calibration curve. During tests, the zero level of the hotwire was recorded hourly to minimise the error due to drift. The Bearman correction was used to correct the results obtained for changes in atmospheric temperature.

The main source of error in hotwire measurements is from drift in the zero-level of the signal. The absolute values of velocity obtained in repeated tests were found to vary by up to 6.1% from each other (or 2.3 m/s). However, when the results were divided by the passage average velocity, to give a normalised spanwise velocity distribution, the variation was only 1.8%. This means that the use of hotwire measurements to obtain absolute velocity values should be done with caution, but the spanwise axial velocity distributions obtained from hotwires are the correct shape.

To reduce the error due to drift, each traverse was repeated three times, and the average was taken - after any clear outliers had been rejected.

Tip-clearance Hotwires As well as standard hotwire probes, special short-stemmed probes were used to measure the flow in the tip-clearance gap and near the casing downstream of the rotor blades. The difference between the two types of probe is shown in Diagram 3.5. It can be seen that the standard probe (shown on the left-hand side in Diagram 3.5) tapers in steps towards the prongs. When measuring well away from the casing, this design minimises the interference of the probe with the flow, but leads to errors when measuring near the wall.

In the case of the special short-stemmed probe, shown on the right-hand side in Diagram 3.5, the prongs are attached directly to the probe stem, so the probe stem always fits flush with the casing wall. This means that there is no hole in the casing and thus any chance of flow recirculation in the probe hole is removed. The special hotwires were manufactured with various prong lengths from 0.8 mm to 6 mm.

The tip-clearance hotwires were calibrated in the same manner as the standard probes, but in a different wind tunnel so that they could be fitted flush with the wall during calibration. Due to the risk of damage from repeatedly fitting and dismounting the hotwires, and the desire to obtain a qualitative rather than a quantitative picture of the flow field, these probes were only calibrated once each, at the start of the experiments.

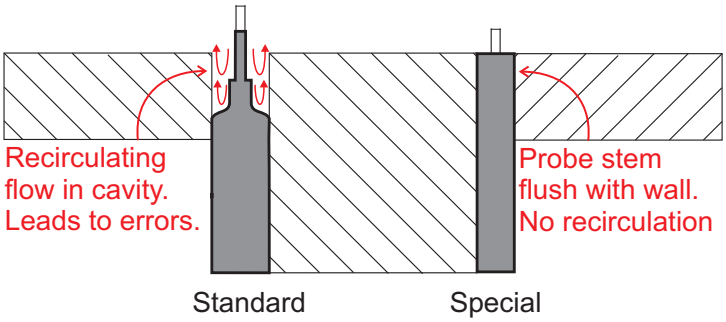

Diagram 3.5: *Schematic diagram of hotwire designs.*

3.3.5 Rotor Speed

Initially, the motor driving the compressor was controlled by a variable frequency drive. This gave accurate speed control and meant that the machine always operated at 3000 rpm. It was found, however, that electrical noise from the drive system was affecting the signal from the fast-response pressure transducers. This noise is high frequency, and is only an issue if, as in this work, frequencies greater than the blade passing frequency are of interest.

The only way to eliminate the electrical noise was to remove the speed controller and to operate the motor with a direct connection to the three-phase laboratory power supply[3]. This meant that the speed of the compressor could not be controlled, and it was subject to variations as the supply voltage changed. The speed during stable operation has been found to vary from approximately 2975 to 2995 rpm (0.7%) over the course of the experiments. The variation in speed during each experiment, however, was generally below 0.25%.

To minimise errors due to the slight changes in speed, the speed was measured and recorded between runs when steady data was being acquired. When unsteady measurements were being taken, the once-per-revolution shaft signal was recorded alongside the rest of the data. A larger change in speed occurs when the compressor stalls, but recording the once-per-revolution shaft signal alongside the unsteady data minimises any errors due to this change.

[3]A 'soft-start' unit was fitted to limit the acceleration on start-up so as to avoid damaging the compressor.

3.3.6 Atmospheric Conditions

The atmospheric pressure was measured using a mercury manometer in the laboratory at the start of each experiment and hourly during longer runs. Temperature was measured at the start of every experiment with a thermometer next to the compressor. The aim was to keep temperature fluctuations during each measuring session under 0.5°C (a temperature change of 0.5°C will lead to an error in the measured flow coefficient of 0.1%).

3.4 Measurements

3.4.1 Characteristics

The compressor is instrumented with total and static pressure tappings at the inlet, and static pressure tappings at rotor and stator exit, as shown in Diagram 3.1. This enables rotor-only and whole-stage total-to-static characteristics to be recorded. The pressure transducers chosen could be sampled at high frequencies, and an average measurement was taken every 0.1 seconds. This meant that it was possible to measure the characteristics 'live' (i.e. the throttle was being closed continuously during logging to give a detailed characteristic), and to record the compressor behaviour right up to the point of stall.

Once the compressor had stalled, the hysteresis loop was measured by opening the throttle slowly until the machine came out of stall and started operating normally again.

The errors in the measurements of the characteristics will be mainly due to the errors in pressure transducer measurements already discussed. In the datum configuration (see Table 3.1), the stall point of the machine was found to vary by 1% of average stall flow coefficient both during back-to-back tests and over a period of several months.

The inlet total pressure is measured at midspan, and the static pressures (at inlet, and downstream of the rotor and stator rows) are measured at the wall. It would be usual to use correction factors to convert the point-wise measured pressures into spanwise-averaged values. However, in this case, the static pressure correction factor

was found to vary over the operating range of the machine (due to separation of the flow over the stator blades) and the total pressure correction factor was found to be very small (0.3% of inlet dynamic head). For this reason, correction factors were not used. This means that the values presented are not absolutely correct, but can be compared with each other with consistency.

3.4.2 Blade Passing Irregularity

To measure the blade passing signal, fast-response pressure transducers (Kulites) were fitted to the rotor casing. The standard configuration was 14 evenly-spaced pressure transducers mounted at the rotor leading edge - giving one every four stator pitches. This is shown schematically in Diagram 3.6. The optimum location for the pressure transducers (in terms of detecting a pre-stall ramp-up in irregularity) was found by testing several locations from 10% chord upstream of the blades to the trailing edge. This is discussed in more detail in Chapter 6.

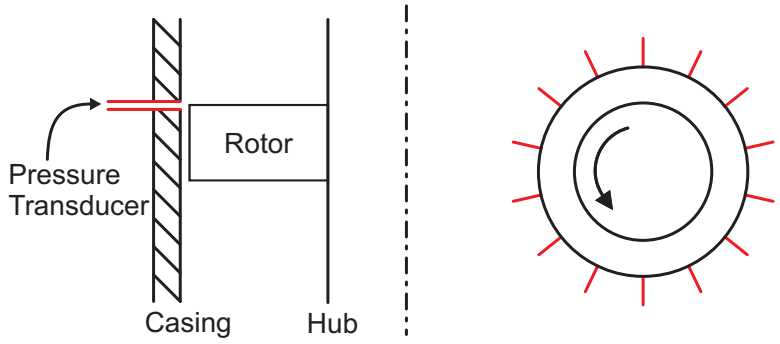

Diagram 3.6: *Schematic diagram of standard pressure transducer arrangement.*

To study the irregularity in the blade passing signal as the compressor was driven towards stall, the signals from the 14 pressure transducers were recorded for 45 revolutions at successive stationary throttle positions (about 20 or 30 positions between full flow and the stall point). As explained above, a sampling rate of 100 kHz was used, with a low-pass filter set to 50 kHz.

3.4.3 Stall Inception

Measurements of stall inception were taken from the 14 pressure transducers already described, and from a further set of six probes located 10% chord upstream of the

rotors. Data from the set upstream of the rotors were also recorded at 100 kHz, with 50 Hz, 100 Hz and 50 kHz filter settings - 50 and 100 Hz being low enough to filter out the blade-passing signal and allow only modal/spike disturbances through, making the stall inception mechanism easier to identify.

The recording of the stall inception process was achieved by using a buffered logging system, triggered by the sudden drop in stage exit static pressure that accompanies the compressor entering stall. Once the trigger signal dropped below the threshold level, the previous 800 ms, and the following 200 ms of data were recorded, giving one second's worth of data with the stalling event located approximately 75% of the way through. In this way, stall inception and the build-up to it could be captured reliably without having to acquire and discard vast amounts of data.

3.4.4 Traverses

In the course of this project, radial traverses were performed both upstream and downstream of the rotor blade row. Measurements were taken using a three-hole cobra probe and a hotwire.

The compressor is fitted with an automated traverse gear, which could originally be used for traverses both upstream and downstream of the rotor and stator rows. However, when the new rotor casing ring was fitted, a traverse slot downstream of the rotor blades was not included. This was to avoid the risk of introducing out-of-roundness to the ring during machining, but it also meant that the traverse gear could no longer be used downstream of the rotors. To overcome this issue, a manual traverse gear was used to obtain simple radial traverses downstream of the rotors.

The numbers of measuring positions used in both manual and automated traverses are given in Table 3.3. In both cases, the traverse points were clustered toward the endwalls, to give greater resolution in the boundary layer regions.

During traverses, the flow coefficient was monitored at each measuring position, and data was only recorded if the value obtained was within 0.2% of the required value.

Three-Hole Probe A three-hole cobra probe was used to measure the time-averaged flow speed and direction upstream and downstream of the rotor blades. At each tra-

Position	Type	Distance from blade row (% b_x)	No. of points	Resolution of traverse gear
Upstream of rotors	Automated	43	55	6.5μm/step
Downstream of rotors	Manual	14	39	25μm markings

Table 3.3: *Traverse locations and resolutions.*

verse position, the probe was allowed to settle for 0.5 seconds and then the average reading was taken over a 1 second period.

In the upstream traverses, the probe was automatically nulled at each measuring position, i.e. the difference in pressure between the left and right holes was minimised, so that the probe was within 0.3°(1 step) of the average flow direction. This meant that the most linear part of the probe calibration could be used.

The use of the manual traverse gear downstream of the rotors meant that the probe could not be nulled at each point in the downstream traverses. The probe was therefore rotated to the approximate midspan flow direction at the start of the traverses to minimise the angular extent over which the calibration was used.

Hotwire For turbulence measurements, the hotwire signal was logged at 100 kHZ and filtered at 30 kHz, while for all other traverses, the logging frequency was reduced to 50 kHz and the filter reduced to 10 kHz. In all cases, the raw data was recorded, and averaging took place during the post-processing.

For hotwire measurements downstream of the rotor bladerow, the ensemble-average of 50 revolutions was computed. The yaw angle of the hotwire was not altered, it was aligned to the axial direction, so only the quasi-axial velocity was measured.

In some specific circumstances, the hotwire was rotated in the traverse gear to get more accurate flow direction measurements. This process is explained in later chapters when the relevant data is discussed.

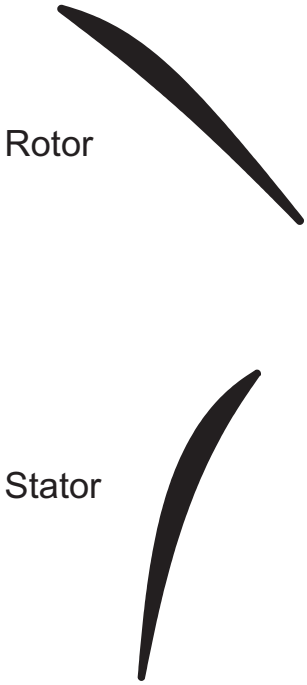

Figure 3.1: *Mid-span blade profiles for the test compressor.*

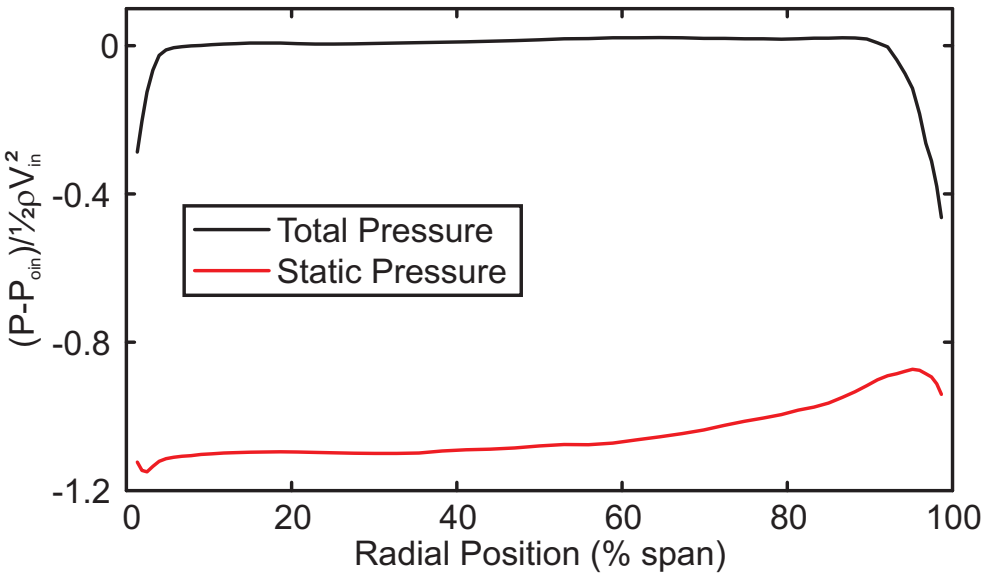

Figure 3.2: *Inlet total and static pressures for the test compressor with datum tip-clearance (1.7% chord, concentric) at design flow coefficient ($\phi = 0.5$).*

Chapter 4

Effect of Tip-Clearance on Compressor Performance - Part 1: Tip-Clearance Size

In this chapter, the results of a parametric study into the effect of tip-clearance size on compressor performance and stall margin are presented. This subject is important because the size of the tip-clearance gap will vary throughout each flight cycle as thermal and centrifugal effects change both the length of the blades and the size of the casing at different engine operating points. Over the lifetime of an engine, the blade tips will also rub on the casing from time to time, leading to a gradual increase in the tip-clearance gap size. It is therefore important to understand the likely impact of these changes on compressor behaviour, and in particular on stall margin.

It is believed that the results shown here form the most comprehensive data set available in terms of the number of tip-clearances tested and the range of gap sizes. For this work, the tip-clearance was varied in ten steps from 1.1% to 10.0% chord (the datum, or design, clearance being 1.7% chord). In a typical engine, the tip-clearances will vary from about 1 to 5% chord, so the larger values shown here are probably not representative of real engine conditions. These larger clearances are, however, found in the rear stages of large industrial gas turbines, due to the large thermal mass of the rotor and casings.

The structure of this chapter is as follows: First, the effect of tip-clearance size on the

stall point and stalling behaviour will be discussed. After this, the performance of the machine will be reviewed, both in terms of pressure rise and blockage.

4.1 Stall Point

Figure 4.1 shows the total-to-static characteristics of the compressor when operating with ten different levels of tip-clearance. From these characteristics, it can be seen that the peak pressure rise drops and the stall point moves to the right as the tip-clearance is increased. The latter trend is quantified in Fig. 4.2, which is a plot of stalling flow coefficient against tip-clearance size.

It can be seen that the effect of tip-clearance size on stability changes noticeably as the tip-clearance increases. For clearances smaller than 3% chord, the relationship between tip-clearance size and stall point is approximately linear. However, with tip-clearances between 3% to 6% chord, the stalling flow coefficient is constant. From 7% to 9% chord, increasing the tip-clearance leads to a further increase in stall point, but the stalling flow coefficient is lower again for a clearance of 10% chord.

The increase in stalling flow coefficient at 6 to 7% chord is accompanied by a transition from full-span to part-span stall (see below). Once the transition is complete, the stalling flow coefficient returns to the previous value of 0.46.

The results shown above do not reveal an optimum clearance level at which the stalling flow coefficient is minimised. This appears to be contrary to the theory of Peacock and others [18], and the experimental findings of Wennerstrom [19]. It may be, however, that an optimum clearance does exist but it is smaller than the minimum safe clearance in this machine (1.1% chord, or 0.4 mm).

4.2 Stall Inception Mechanisms

As stated above, the compressor began to show signs of part-span stall once the tip-clearance reached 6% chord. A comparison of the throttle hysteresis for full-span and part-span stall is shown in Fig. 4.3. With smaller tip-clearances (1.1 - 5.8% chord), the

compressor drops straight into full-span stall and the throttle hysteresis is extensive. In the cases with 6.7% clearance or more, it can be seen that the compressor goes into part-span stall. In the largest tip-clearance case (10% chord), if the throttle is fixed at the stall point, the compressor will switch repeatedly from clean flow to part-span stall. Further throttling from this point produces a flat part-span stall characteristic, not shown here, until full-span stall develops, and only then is a small amount of hysteresis observed.

Returning to Fig. 4.1, it can also be seen that the characteristic becomes less smooth once the compressor starts exhibiting part-span stall. This is due to the operating point of the compressor showing signs of increased unsteadiness (see characteristics for 6.7, 8.5 and 10.0% clearance). The stall point also becomes less clear, and so is harder to pinpoint. At tip-clearances below 6% chord, the spread in stall point is only around 1% of the average when five characteristics are compared. At the larger clearances, however, the spread is closer to 3%.

In Fig. 4.2, it is also interesting to note that the stall inception mechanism changes from spike to modal at a clearance of approximately 3% chord. This change from spike to modal stall occurs at the same clearance level as the change from a linear increase in stalling flow coefficient to a constant value.

The change in stall inception mechanism can be seen by comparing data from six pressure transducers mounted 20% chord upstream of the rotor leading edges. Figure 4.4 (a) shows a typical stall inception event in the compressor operating with the smallest tip-clearance (1.1% chord, 0.4 mm). The traces show a classic spike-type stall event, with a small spike appearing suddenly and travelling at approximately 70% of rotor speed. Within about 3 revolutions of first appearing, the spike has grown into a fully-developed stall cell.

A typical modal stall trace is shown in Fig. 4.4 (b), which is from a stall inception event with 3.3% clearance. In contrast to the spike case shown in Fig. 4.4 (a), modal waves can be observed for many revolutions before stall. These modal waves travel at about 40% of rotor speed and gradually grow into a stall cell.

In the cases where the compressor went into part-span stall, the stall inception traces were very similar to those shown in Fig. 4.4 (b), i.e. the inception mechanism remained modal. There was no clear way of telling whether the stall was full- or

Regime	Tip-Clearance Range (% chord)	Inception Mechanism	Change in ϕ_{stall} with clearance	Full- or Part-span?
1	1.1 - 1.7	Spike	Linear	Full-span
2	3.3 - 5.8	Modal	Constant	Full-span
3	6.7 - 10	Modal		Part-span

Table 4.1: Stalling behaviour by tip-clearance size.

part-span from the unsteady pressure transducer data, so the characteristics were used to determine the extent of the stall (see Fig. 4.3).

The stalling behaviour of the compressor with different tip-clearance sizes can be split into three regimes - spike, modal and part-span. The change in stalling flow coefficient with increasing tip-clearance is also different in each regime. The three regimes are summarised in Table 4.1, they are also labelled in Fig. 4.2.

The changes in stalling behaviour, from spike to mode and from full-span to part-span, will occur at different clearance levels in different compressors. The changes are, however, thought to be of a general nature. The change from spike to modal behaviour accompanying an increase in tip-clearance has been observed in another Whittle Laboratory machine [76]. The reason for the change is unclear, and will be discussed briefly in Section 4.4.2 below.

The change from full-span to part-span stall can be explained by considering the change in the shape of the characteristic as the tip-clearance is increased; Day et al. [9] showed that a compressor will tend to favour part-span stall when the pressure rise is low and the stalling flow coefficient is reasonably high. As the clearance is increased, the pressure rise at stall decreases and the stalling flow coefficient increases (see Fig. 4.1), thus making the compressor tend towards part-span stall. As the change in shape of the characteristic with tip-clearance is likely to be similar in all machines, the change from part-span to full-span stall is also likely to be a general phenomenon.

4.3 Pressure Rise

As well as reducing the stall margin, it is clear from the characteristics in Fig. 4.1 that enlarging the tip-clearance leads to a drop in pressure rise. It is also the case that the pressure rise continues to drop when the clearance is increased above 4% chord, despite the fact that the stalling flow coefficient remains relatively constant. This is demonstrated in Fig. 4.5 (a), which is a plot of maximum pressure rise against tip-clearance. Additionally, Fig. 4.5 (b) shows the pressure rise at the design flow coefficient (ϕ = 0.5) against tip-clearance. In both cases, the three regimes of stalling behaviour identified above are shown for reference.

Figure 4.5 (a) shows that there is a linear loss of maximum pressure rise with increasing tip-clearance once the stall mechanism has changed to modal (i.e. in regimes 2 and 3, where the clearance is greater than 3% chord). In regime 1, when the clearance is under 3% chord and the compressor shows spike-type stall, the loss of pressure rise with clearance is more rapid. A similar relationship was seen by Khalid et al. [53] in their experimental data, but they did not comment on any changes of stall inception mechanism.

Figure 4.5 (b) shows that the pressure rise at design flow coefficient drops at an increasing rate over the range of tip-clearances tested. Extrapolating the line of best fit to the x-intercept (not shown in Fig. 4.5 (b)) suggests that a tip-clearance of 20 - 30% chord would produce no pressure rise at all. While it is unlikely that any compressor would ever be built with such large clearances, this result may be of interest in terms of engine rundown behaviour in cases of severe mechanical damage.

As with stalling flow coefficient, for the range of clearances tested, this compressor does not show an optimum tip-clearance in terms of stage pressure rise - all increases in clearance beyond the minimum cause a reduction in pressure rise.

4.4 Blockage Level

As shown above, there is a drop in stage pressure rise when the tip-clearance is increased. Close inspection of Fig. 4.1 also reveals that the maximum flow through the compressor is reduced as the tip-clearance is increased - i.e. the right-hand ends

of the characteristics move to the left. These two findings suggest that there is an increase in the level of blockage (lost flow area due to slow moving fluid in wakes, separations, boundary layers etc.) in the rotor passage as the tip-clearance is increased. For this reason, the rotor exit flowfield was measured and two methods were used to quantify the level of blockage: spanwise non-uniformity, and displacement thickness.

4.4.1 Spanwise Non-Uniformity

Spanwise non-uniformity, (S_{u}), is a measure of the radial distortion in the flowfield and is defined by Simpson and Longley [16] as:

$$S_{\mathrm{u}} = \frac{\int_{\mathrm{hub}}^{\mathrm{tip}} V_{\mathrm{x}}^2 \mathrm{d}A}{\left(\int_{\mathrm{hub}}^{\mathrm{tip}} V_{\mathrm{x}} dA\right)^2} \mathrm{x} \int_{\mathrm{hub}}^{\mathrm{tip}} \mathrm{d}A \tag{4.1}$$

where a spanwise non-uniformity of 1 would describe uniform flow. From hotwire traverses at the rotor exit, and using Equation 4.1, the spanwise non-uniformity was calculated for each tip-clearance tested in this project. In each case, the traverse was performed at a near-stall operating point. The results of this analysis are shown in Fig. 4.6, which shows that the relationship between spanwise non-uniformity and tip-clearance is linear.

Simpson and Longley [16] measured a higher level of spanwise non-uniformity in compressors showing modal stall than those which showed spike stall. The data in Fig. 4.6 supports this, as the spanwise non-uniformity is higher with larger clearances and these are the cases in which modal stall is observed.

One might expect there to be a change in the relationship between spanwise non-uniformity and tip-clearance at the point where the stall inception mechanism changed - a step increase, perhaps - if the two were linked. There is, however, no abrupt change in the relationship between tip-clearance and spanwise non-uniformity across the range of clearances shown in Fig. 4.6. This suggests that the increased value of spanwise non-uniformity is not directly linked to the stall inception mechanism in this case.

4.4.2 Displacement Thickness

The major advantage of using spanwise non-uniformity as a measure of blockage is that it does not require any assumptions to be made about the 'ideal' flow through the compressor. It does not, however, allow the blockage to be split into hub and tip blockage, and the lack of assumptions about the 'ideal' flow mean that spanwise velocity gradients that are part of the design flowfield are indistinguishable from non-uniformity due to blockage. To overcome these problems, a more conventional measure of blockage was used, i.e. the displacement thickness, δ^*, as follows:

$$\delta^* = sB \tag{4.2}$$

$$\text{Where} \qquad B = 1 - \frac{\int_{\text{hub}}^{\text{tip}} V_{\text{real}} \mathrm{d}A}{\int_{\text{hub}}^{\text{tip}} V_{\text{ideal}} \mathrm{d}A} \tag{4.3}$$

and s is the blade span. To see the development of blockage as the compressor is moved towards stall, the hotwire traverses were repeated at several operating points from full-flow to near-stall. The total blockage will be discussed first (i.e. that from the hub and casing combined) and then the individual contributions from the hub and casing will be shown[1].

The displacement thickness against stall margin is shown in Fig. 4.7. The nine lines on the graph represent the data from each of the nine tip-clearances tested. It can be seen from Fig. 4.7 that the blockage always increases as the compressor is throttled towards its stall point, as expected. Another noteworthy point is that the lines for the smallest four tip-clearances (1.7% to 4.2% span) are fairly similar to each other at all operating points and have the same value of blockage at near-stall operating conditions. This is in line with the ideas of Khalid et al. [53] who suggested that a compressor will stall when the blockage reaches a critical level.

The blockage measurements from the compressor with tip-clearances greater than 4.2%, however, do not fit the hypothesis of Khalid et al. [53]. From 4.9% clearance onwards, all blockage levels increase, and by the 10.0% clearance case, the compressor is supporting twice the blockage level recorded in the smaller clearance cases.

[1]The hub and tip displacement thicknesses were found by calculating the blockage over the inner and outer halves of the span respectively and multiplying by $\frac{s}{2}$.

Although the blockage at near-stall conditions is roughly constant for tip-clearances under 4% chord, the spanwise non-uniformity is increasing. The reason for this change can be seen in Fig. 4.8, which shows contour plots of axial velocity taken from rotor exit traverses at design and near stall for the compressor with 1.7% and 3.3% tip-clearance. For reference, the location of the blade tips is denoted by a dotted white line in each plot. In Fig. 4.8 (a), there is a small region of loss in the hub region and a further area of loss near the blade tips. When the compressor with small clearance is operating near its stall point (Fig. 4.8 (b)), there is a large loss in the hub region, due to separation on the rotor blade suction surface, with only modest blockage near the blade tips.

The flowfield at the design point with 3.3% clearance is shown in Fig. 4.8 (c). Comparison with Fig. 4.8 (a) shows more loss near the rotor tips, but apart from that the velocity distribution is similar to that observed with smaller clearance.

At near-stall conditions, however, the flow field is markedly different, as can be seen by comparing Fig. 4.8 (b) and (d). In the large clearance case (Fig. 4.8 (d), the tip blockage has increased dramatically and extends over a disproportionately large part of the blade span, while the hub loss is much smaller. The reasons for the reduction in hub blockage are two-fold; firstly, the large blockage in the tip region diverts the flow towards the hub, and secondly, the stall point moves to a higher flow coefficient. These two effects combine so that the hub ends up being more lightly loaded in the large tip-clearance case.

The increase in tip blockage due to enlargement of the tip-clearance from 1.7 to 3.3% chord is offset by the reduction in hub blockage so that the total blockage remains the same. However, the flow field has become less uniform, so the spanwise non-uniformity is increased.

The contributions to the total blockage from the hub and tip regions can be seen more clearly in Fig. 4.9, which is a plot of hub, tip and total displacement thickness against tip-clearance size, calculated from near-stall traverses. The black circles show the total blockage, which is constant for tip-clearances up to 4% chord, as discussed above.

It can be seen that, at small clearances, the increase in tip blockage (blue crosses) is offset by a corresponding reduction in hub blockage (red squares). At the smallest

clearance, the hub blockage is larger than the tip blockage, but, by 4% chord, the tip blockage makes up most of the total blockage.

The increase in near-stall blockage at larger clearances suggests that there is no critical blockage level at which the compressor will stall, as the level of blockage supported by the compressor just before it stalls is not constant. A similar result was reported by Smith and Cumpsty [22], who found that the pitchwise location of the blockage was also important. More work is required to understand the connection between blockage and stall.

As with the work of Dickens [15], the hub blockage is large when the compressor shows spike-type stall, and the tip blockage is large when the compressor stalls via modes. The reasons for this remain unclear, though it is possible that the presence of a large region of blockage at the tip prevents the formation of a spike.

4.4.3 Comparison with Smith's Relationship for Tip Blockage

In an experimental study of a multi-stage compressor, Smith [51] found that the near-stall tip blockage increased linearly with tip-clearance. From these results, Smith developed the following empirical relationship between tip blockage and non-dimensional gap size:

$$\frac{\delta_t{}^*}{g_t} = 0.20 + \frac{\epsilon}{g_t} \tag{4.4}$$

where g_t is the 'staggered spacing', i.e. the blade pitch in the direction perpendicular to the stagger angle. Smith chose this as the quantity with which to non-dimensionalise his data because he argued that it has the biggest effect on the penetration of casing wall effects into the flow.

Figure 4.10 shows tip blockage non-dimensionalised by g_t against tip-clearance size. The black crosses show the experimental data.

The blue line shows Smith's relationship (Equation 4.4). It can be seen that the level of the blockage predicted by Smith is similar to that measured here, but the gradient

of the blue line is much too low to fit the data from the current work (although the agreement is not bad for the smaller clearances). The red line shows a linear fit to the experimental data, which is given by:

$$\frac{\delta_t{}^*}{g_t} = 0.06 + 2.6\frac{\epsilon}{g_t} \tag{4.5}$$

The red line line follows the data reasonably closely, especially at smaller clearance levels. From these two lines, it can seen that the relationship between blockage and tip-clearance size is linear, as stated by Smith. However, the increase in tip blockage with clearance is smaller in the results from this work than in Smith's work, with the discrepancy becoming more apparent at larger clearances.

4.5 Conclusions

The results presented in this chapter show that, in a concentric machine, increasing tip-clearance is detrimental to compressor performance, both in terms of stall margin and pressure rise. The following specific conclusions can be drawn:

1. The stalling behaviour of the compressor over a range of tip-clearances can be divided into three regimes:

   Regime 1: With clearances lower than 3% chord, the compressor shows spike-type stall and the relationship between stalling flow coefficient and tip-clearance is linear.

   Regime 2: With clearances between 3% and 6% chord, the compressor shows modal stall and the stalling flow coefficient remains constant. In both regimes 1 and 2, the compressor goes straight into full-span stall.

   Regime 3: When the clearance is greater than 6% chord, the inception mechanism remains modal, but part-span stall is observed, and the compressor operating point becomes much more unsteady. The stall point is harder to define and there is more variation between test runs.

   It is thought that this behaviour will be common to all compressors, but the gap sizes at which the regime changes occur will vary from one compressor to another.

2. The maximum pressure rise of the compressor drops linearly with increasing clearance in regimes 2 and 3 (tip-clearance greater than 3% chord). With smaller clearances, a more rapid loss of maximum pressure rise is observed. The pressure rise at the design flow coefficient ($\phi = 0.5$) drops at an increasing rate over the range of tip-clearances tested

3. No optimum clearance level was found for the compressor tested here. The minimum stalling flow coefficient and maximum stage pressure rise were both recorded at the smallest safe clearance.

4. A study of the relationship between tip-clearance size, rotor exit blockage, and stalling flow coefficient yields the following conclusions:

   (a) Spanwise non-uniformity was found to increase linearly with an increase in tip-clearance gap. Part-way through the range of gap sizes tested, the stall inception mechanism of the compressor changed from spike to modal. The increase in spanwise non-uniformity thus favours the assertion of Simpson and Longley that spikes occur when spanwise non-uniformity is low and modes occur when the non-uniformity is higher. This relationship may, however, be coincidental, and the current work shows a continuous trend rather than a sharp distinction between compressors which show spike stall and those which exhibit modes.

   (b) With small clearances, the hub blockage is large and the tip blockage is small. This trend reverses as the clearance is increased. This adds weight to Dickens' finding that compressors which stall via modes show high blockage in the tip region while those which show spike stall have large hub blockage.

   (c) The level of blockage measured in the rotor exit flow at near-stall conditions is constant for tip-clearances up to 4% chord, because the increase in tip blockage is countered by the reduction in hub blockage. At clearances greater than 4% chord the tip blockage continues to increase but the hub blockage no longer decreases, leading to higher total blockage levels. This result shows that the idea that the compressor will stall when the blockage reaches a critical level is too simplistic.

   (d) Smith's empirical relationship between tip blockage and tip-clearance size shows a trend in the right direction but does not fit the data shown here - the gradient of the line is much steeper than predicted by Smith.

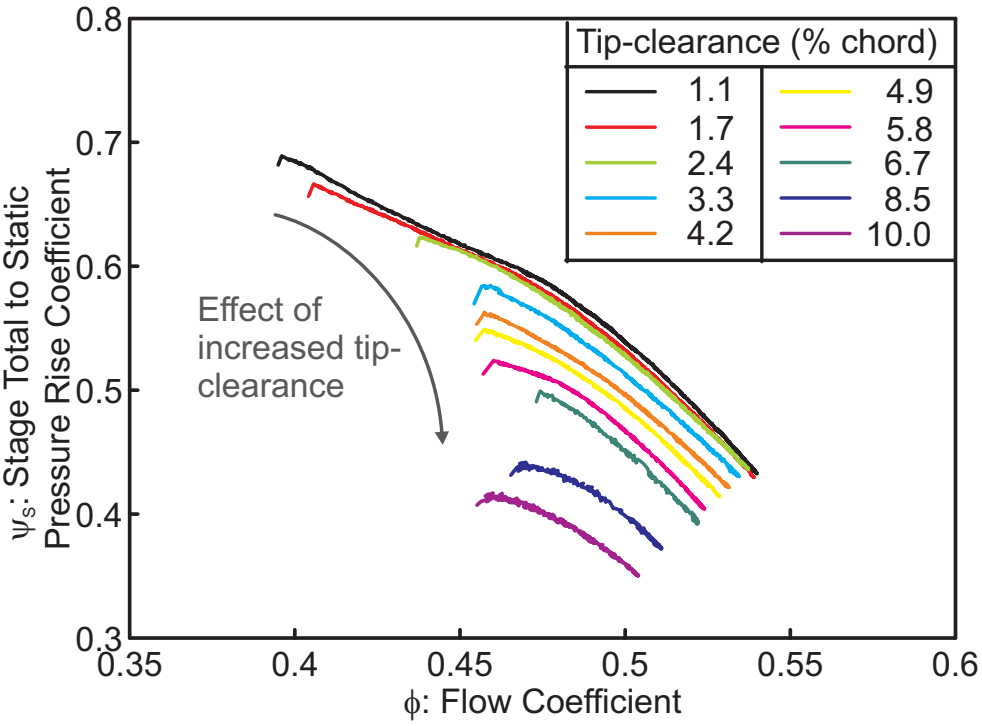

Figure 4.1: *Characteristics with different levels of tip-clearance.*

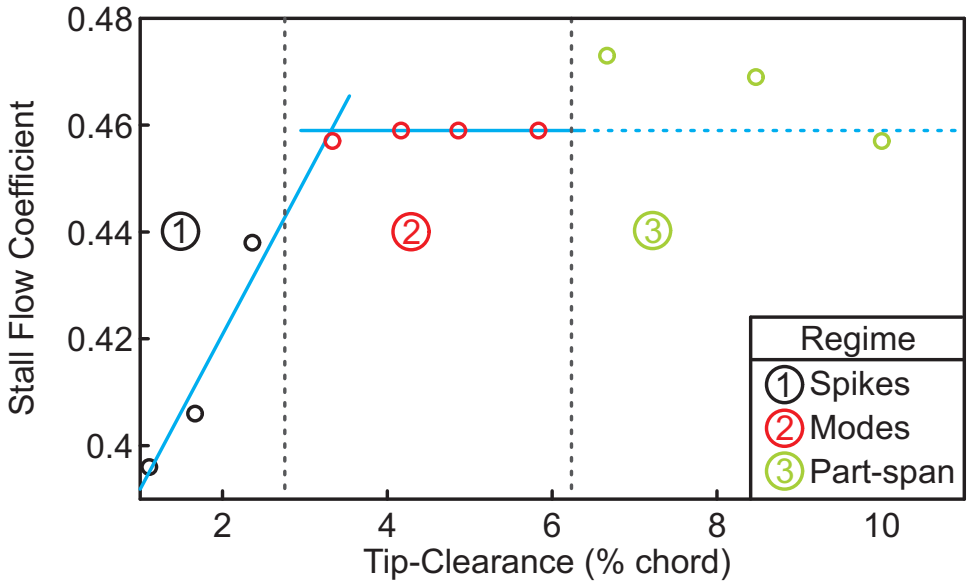

Figure 4.2: *Stalling flow coefficient with different tip-clearance sizes.*

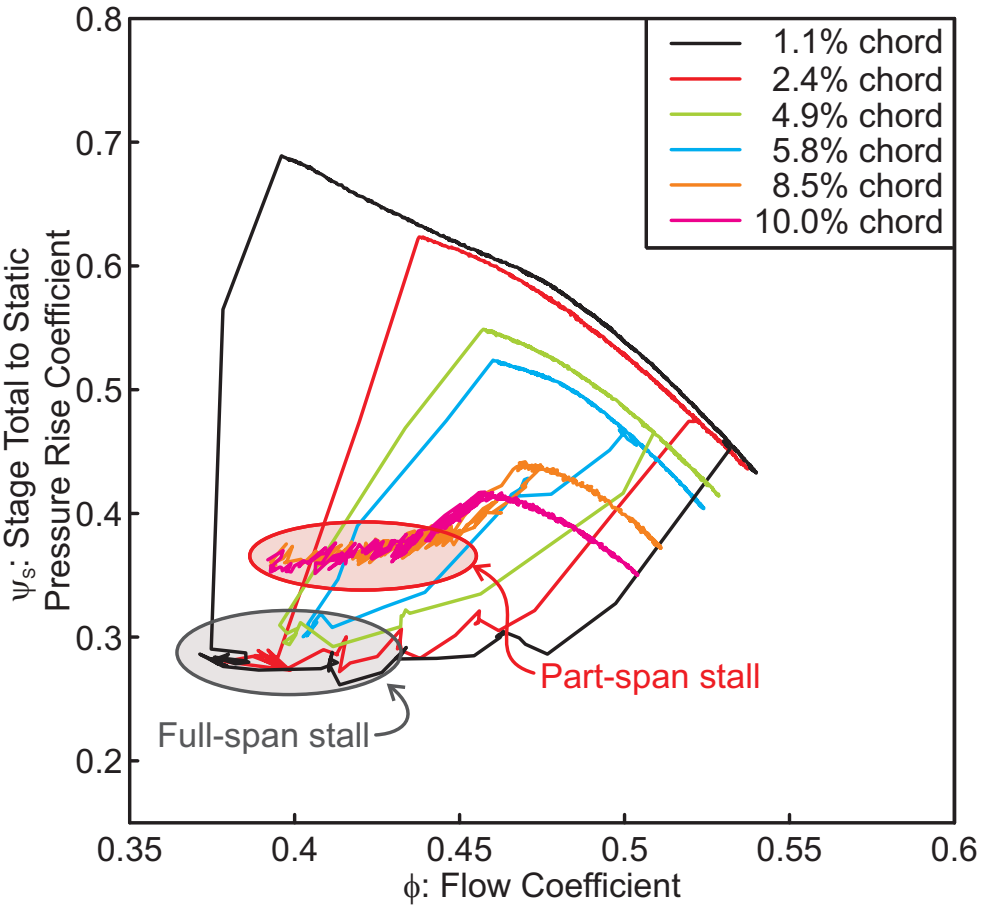

Figure 4.3: *Characteristics showing full-span and part-span stall with different levels of tip-clearance.*

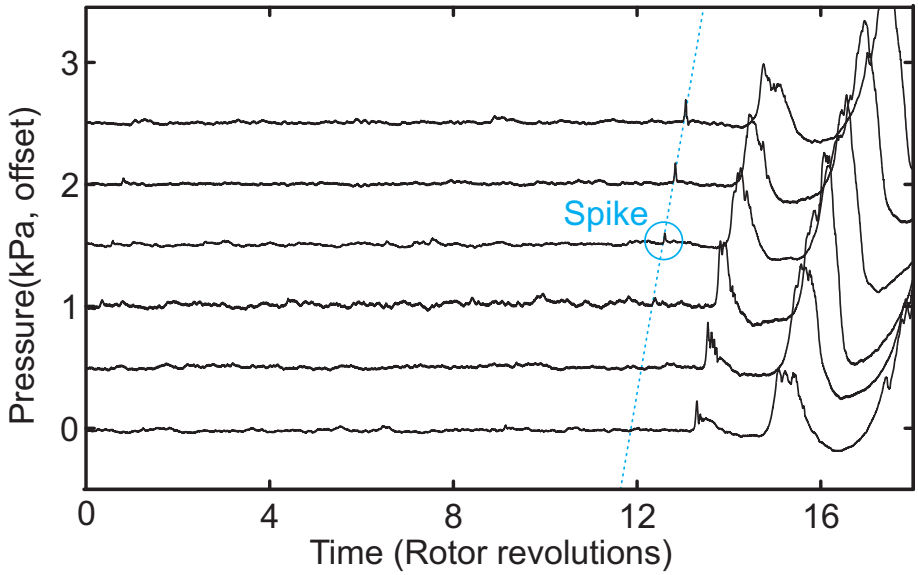

(a) Spike stall in the compressor with 1.1% clearance.

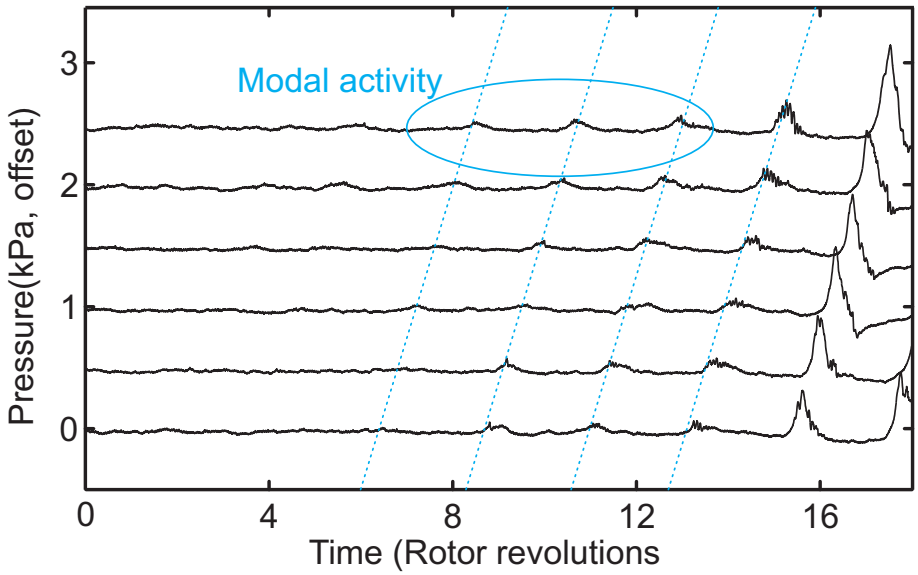

(b) Modal stall in the compressor with 3.3% clearance.

Figure 4.4: *Measurements of stall inception with different levels of tip-clearance from a set of pressure transducers 20% chord upstream of the rotor blades (100kHz logging frequency, 50Hz low-pass filter).*

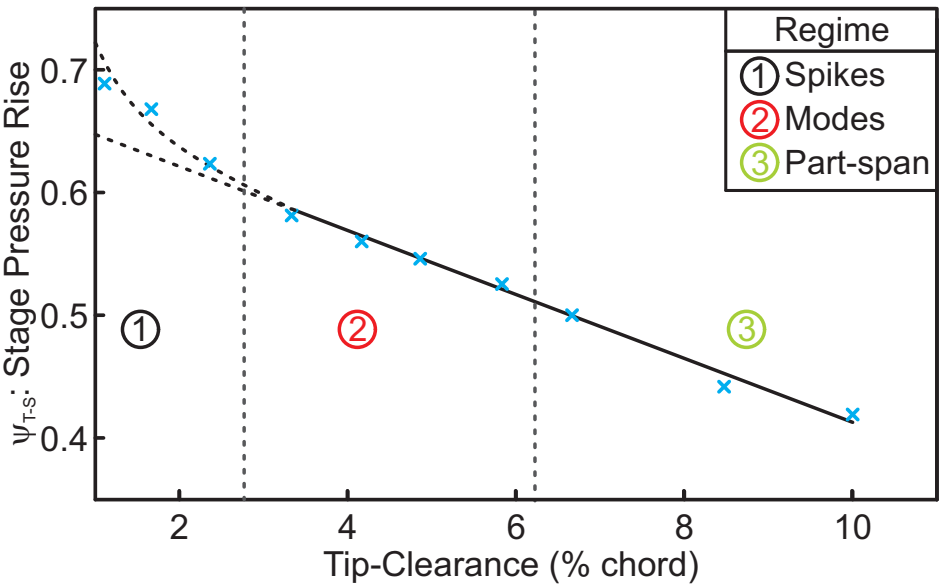

(a) Maximum pressure rise

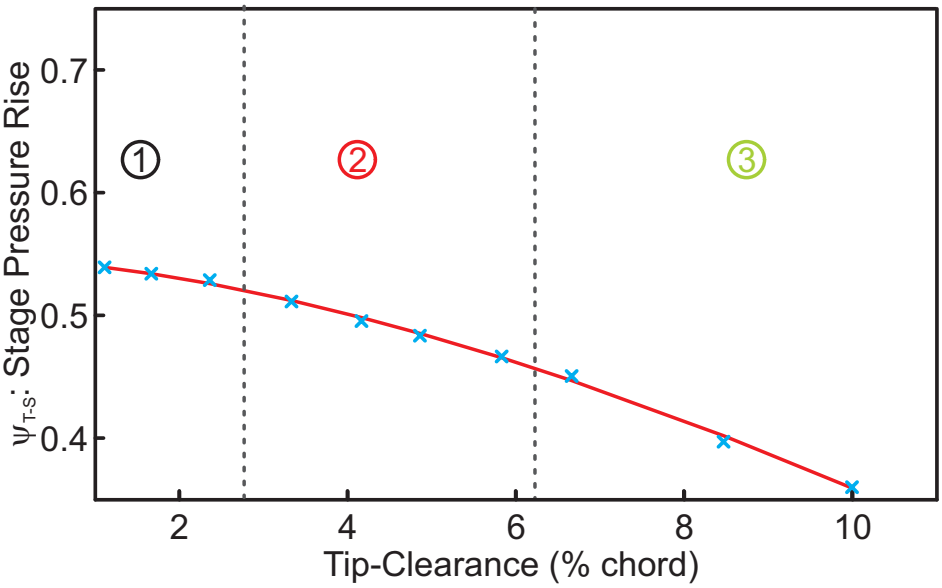

(b) Pressure rise at design flow coefficient ($\phi = 0.5$)

Figure 4.5: *Total-to-static pressure rise against tip-clearance.*

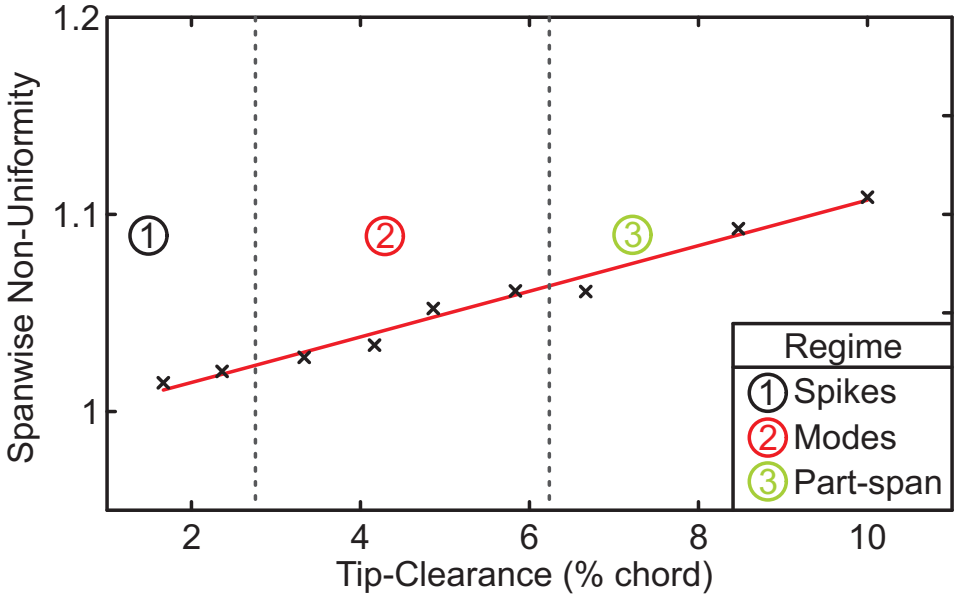

Figure 4.6: *Rotor exit spanwise non-uniformity against tip-clearance at near-stall conditions.*

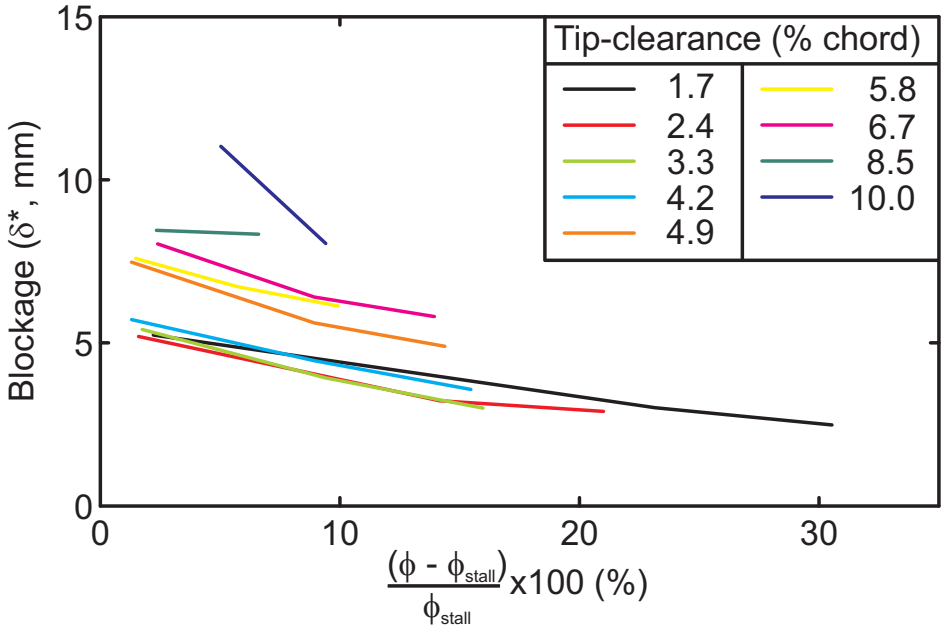

Figure 4.7: *Rotor exit blockage against stall margin for different clearance levels.*

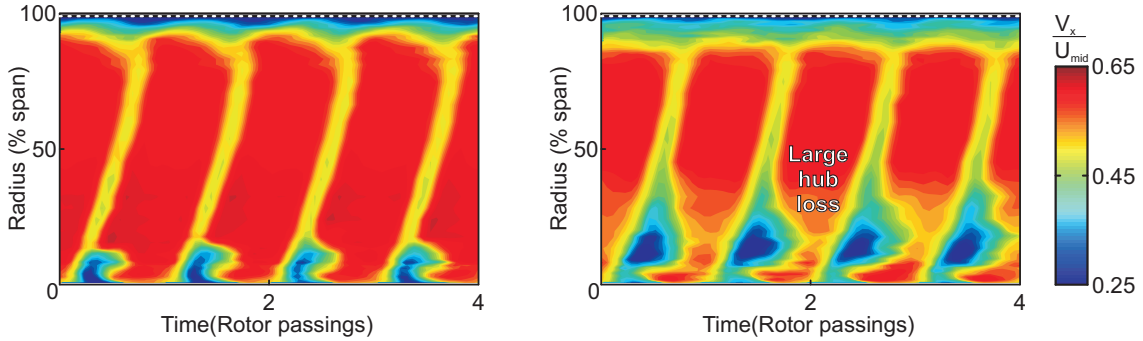

(a) 1.7% tip-clearance, design ($\phi = 0.5$).

(b) 1.7% tip-clearance, near stall ($\phi = 0.415$).

(c) 3.3% tip-clearance, design ($\phi = 0.5$).

(d) 3.3% tip-clearance, near stall ($\phi = 0.465$).

Figure 4.8: *Contours of axial velocity from radial hotwire traverses at design and near stall for two clearance levels.*

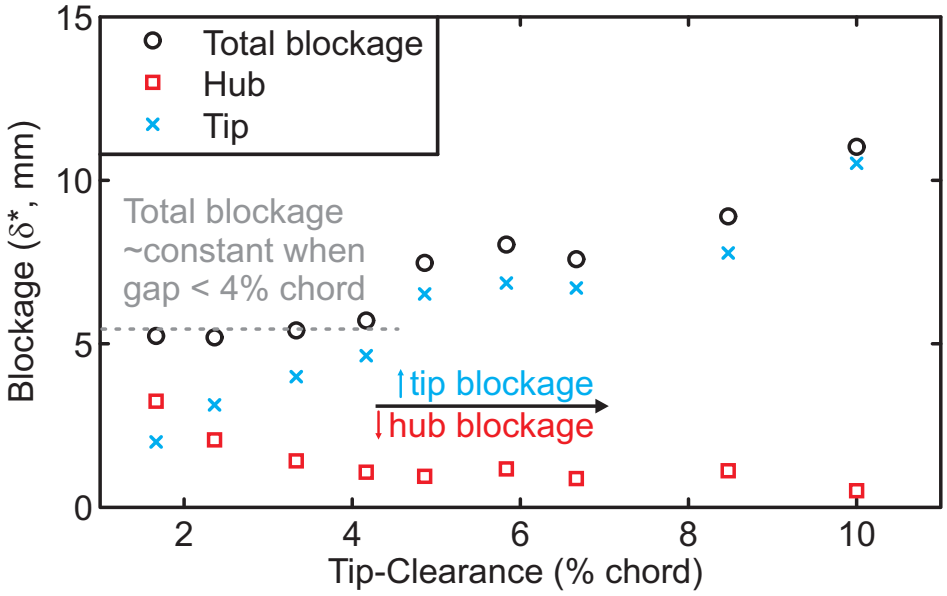

Figure 4.9: *Rotor exit blockage against tip-clearance.*

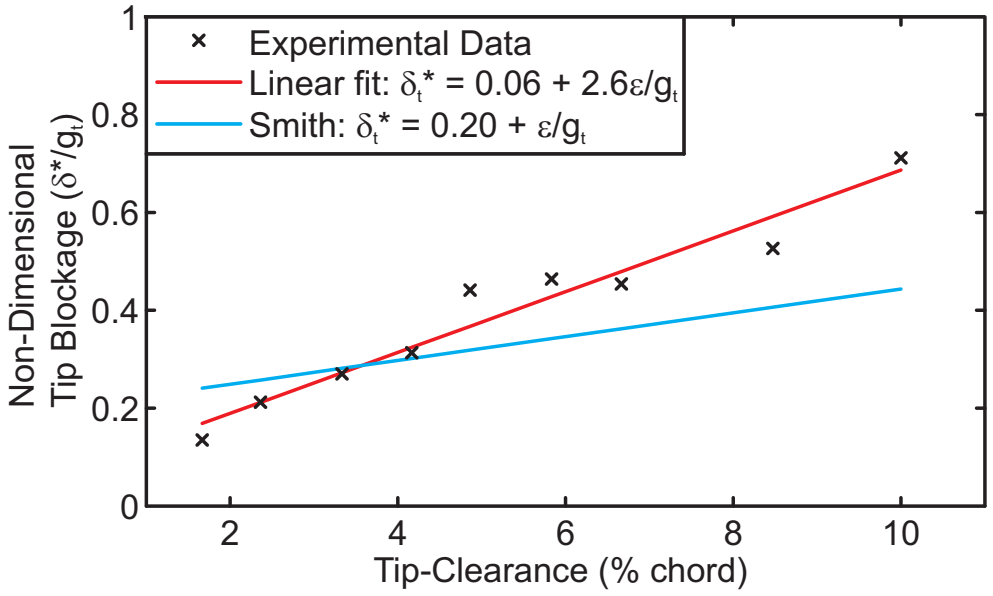

Figure 4.10: *Comparison of tip blockage to Smith's empirical correlation [51].*

Chapter 5

Effect of Tip-Clearance on Compressor Performance - Part 2: Tip-Clearance Eccentricity

In this chapter, the effect of tip-clearance asymmetry on the performance of a compressor will be discussed. This topic is not only of academic interest, as the tip-clearance in a real engine will become eccentric at various points during each flight cycle and over the life of the engine. Furthermore, previous work has shown that tip-clearance asymmetry has a detrimental effect on compressor stability.

The background to this work will be discussed first, in the form of a description of the factors affecting tip-clearance eccentricity in a real engine. This will be followed by an explanation of the configurations tested for this work. Experimental results showing the effect of eccentricity on compressor performance will then be given. From these results, an empirical relationship will be developed for relating the stall point of a machine relative to the tip-clearance size and eccentricity for small to moderate clearances. Freeman's rule of thumb (that the stall point in an eccentric compressor is determined by the worst tip-clearance) will then be discussed and shown to be inaccurate.

The model of Graf et al. [47] for flow redistribution in an asymmetric compressor will then be applied to the test compressor and the results compared with the experimental data. The effect of this flow redistribution on the stability the machine will

then be examined. Finally, local performance characteristics from different positions around the annulus will be considered.

5.1 Factors Affecting Tip-clearance Asymmetry

There are several sources of tip-clearance asymmetry in an aero-engine. These can be divided into two categories: transient and permanent.

Transient changes in tip-clearance asymmetry are caused by changes in the load from the engine to the pylon. Thrust from the engine is transmitted to the rest of the aeroplane through the pylon which connects the engine to the wing. The pylon is mounted on the compressor casing, whereas the thrust acts along the centre-line of the shaft. This radial offset creates a bending moment. At certain points during the flight cycle, this moment becomes large enough to bend the engine casing (for example at take-off). This means that the compressor tip-clearance will become eccentric.

Permanent changes in tip-clearance asymmetry are caused by holes and slots cut into the casing for tertiary systems such as bleed, which cause the casing to deform. Hard landings and stall events can also cause the blades to rub the casing and thus remove material from one side of the casing and not the other, again leading to permanent asymmetry.

Further to these, shaft bending due to gyroscopic effects during rotation and other manouevres can salso cause transient asymmetry and, where the bending is large enough, blade rubbing and permanent eccentricity.

When the blades rub the casing, the eccentricity reaches at least 200% by the definition used in this work (see Chapter 3). More commonly, levels of eccentricity of 50 – 75% are expected to occur [77], so the tests described in this chapter were generally undertaken with eccentricity levels from 0 to 75%.

5.2 Configurations Tested

The configurations tested in the course of this work are listed in Table 5.1. As the clearance size in a real engine will change due to thermal expansion and centrifugal forces, the effect of tip-clearance eccentricity on pressure rise and stalling flow coefficient was investigated at seven tip-clearance levels ranging from 1.7% to 6.7% chord.

The minimum safe tip gap in the compressor is 0.4 mm (1.1% chord), so it was not possible to test the compressor with eccentricity at this clearance level. At the largest two clearances tested in Chapter 4 (8.5% and 10.0% chord), the stall point of the compressor was found to be too variable for any useful conclusions to be drawn from testing the effect of eccentricity.

5.3 Effect of Eccentricity on Performance

Figure 5.1 shows the characteristics of the compressor with different levels of eccentricity at two sizes of average clearance. It can be seen that, at a given average clearance size, tip-clearance eccentricity leads to an increase in stalling flow coefficient.

It is interesting to note that there is no loss of stage pressure rise when eccentricity is introduced, i.e. the characteristics all lie on top of each other, and the only change is in the stalling flow coefficient. This result is different from the effect of a concentric increase in clearance (see Fig. 4.1). This is a surprising result, as it would be expected that the high levels of loss in the large tip-clearance part of the annulus would reduce the overall pressure rise. It appears, however, that the reduction in pressure rise in the large clearance sector is entirely offset by a higher pressure rise in the small clearance region. This will be discussed further in Section 5.6 below.

The stalling flow coefficients of all the test cases (concentric as well as eccentric) are plotted against maximum tip-clearance in Fig. 5.2. It can be seen that the trend is similar to that observed for concentric tip-clearances in Chapter 4 (see Fig. 4.2), i.e. there is a rapid increase in stalling flow coefficient with maximum tip-clearance for gap sizes under 3.5% chord, but after this the stall point becomes roughly constant. As

Tip-Clearance Size		Eccentricity Level	
% chord	**mm**	**%**	**mm**
1.7	0.60	5	0.030
		10	0.060
		25	0.225
		50	0.300
		75	0.450
2.4	0.85	5	0.025
		25	0.220
		53	0.450
		75	0.650
3.3	1.20	2	0.025
		37.5	0.450
		75	0.900
4.2	1.50	2	0.025
		30	0.450
		75	1.130
4.9	1.75	2	0.030
		26	0.450
		51	0.900
		75	1.310
		100	1.750
5.8	2.10	2	0.040
		9	0.190
		21	0.450
		29	0.610
		43	0.900
		75	1.575
6.7	2.40	2	0.050
		19	0.450
		75	1.800

Table 5.1: *Configurations tested for tip-clearance study*

with concentric clearances, this constant relationship between tip-clearance and stall point breaks down once part span stall is observed (with maximum tip-clearances of 5.8% chord and larger).

Another way of looking at the data from the smaller tip-clearance cases is to plot stalling flow coefficient against eccentricity level. This is shown for small to moderate clearances in Fig. 5.3. In each case, it can be seen that the data points fit well on a straight line, leading to a linear relationship between eccentricity level and stalling flow coefficient, for a given average clearance size. It can also be seen that the effect of eccentricity on the stall point of the machine diminishes as the average clearance is increased, i.e. the gradients of the lines in Fig. 5.3 get smaller as the tip-clearance increases.

5.3.1 Empirical Relationship between Tip-clearance and Stall Point

In this section, an empirical relationship between tip-clearance size and eccentricity and stall point will be developed for small to moderate clearances.

It was shown in Chapter 4 that, for average clearances under 4% chord, the relationship between average clearance size and stall point in a concentric machine is linear (see Fig. 4.2), i.e.:

$$\phi_{\text{stall,conc}} = \text{m}\bar{\epsilon} + \text{n} \tag{5.1}$$

where $\bar{\epsilon}$ is the average tip-clearance and m and n are constants. Furthermore, as the effect of eccentricity on stall point is linear at each tip-clearance, for a given average clearance:

$$\phi_{\text{stall}} = \phi_{\text{stall,conc}} + k\left(\frac{\Delta\epsilon}{\bar{\epsilon}}\right) \tag{5.2}$$

where k is the gradient of the relevant line in Fig. 5.3 $\left(\text{i.e. } k = \frac{\partial(\phi_{\text{stall}})}{\partial(\Delta\epsilon)}\Big|_{\bar{\epsilon}}\right)$. These gradients, k, are plotted against average tip-clearance in Fig. 5.4. It can be seen that

the relationship between k and the average clearance size, $\bar{\epsilon}$, is linear for the first three points (i.e. for average clearances of up to 3.3% chord), so:

$$k = p\bar{\epsilon} + q \tag{5.3}$$

again, p and q are constants. If this trend were to continue, then eccentricity would have no effect on the stall point of the machine once the average tip-clearance reached 3.9% chord, as the gradient would be zero.

For average clearances under 4% chord, substituting in for $\phi_{\text{stall,conc}}$ from Equation 5.1 and for k:

$$\phi_{\text{stall}} = m\bar{\epsilon} + n + (p\bar{\epsilon} + q)\frac{\Delta\epsilon}{\bar{\epsilon}} \tag{5.4}$$

Where m, n, p and q are constants. From the data shown in Figs 4.2 and 5.4, the values of the four constants can be found and are given in Table 5.2[1]. Substituting them into Equation 5.4 gives:

$$\phi_{\text{stall}} = 2.90\bar{\epsilon} + 0.36 + (0.47 - 1.22\bar{\epsilon})\frac{\Delta\epsilon}{\bar{\epsilon}} \tag{5.5}$$

The value for n obtained from the test data shown here suggests that a compressor with no tip-clearance would stall at a flow coefficient of 0.36. It is likely, however, that the relationship between tip-clearance and stall margin breaks down at very small tip-clearances, especially if an optimum clearance for this compressor exists (see Chapter 4).

The diminishing effect of eccentricity on stall point with increasing clearance can also be seen in the last term, where the effect will eventually become zero when $(0.47 - 1.22\bar{\epsilon}) = 0$, which will happen when the tip-clearance is increased above about 3.9% chord. This suggests that, if the average clearance is larger than 3.9%, eccentricity will have no effect on the stall point of the compressor.

[1]For these constants, eccentricity is measured as a fraction of average clearance and tip-clearance is defined as a fraction of chord (not in percent).

Constant	Value
m	2.90
n	0.36
p	-1.22
q	0.47

Table 5.2: *Constants for the empirical relationship between stall point and tip-clearance size and eccentricity given in Equation 5.4.*

At clearances greater than 4% chord, the above formula for stalling flow coefficient no longer applies. In the tests with 4.2% clearance, the stall point was almost unchanged between the concentric test and the test with 30% eccentricity (ϕ_{stall} = 0.459 and 0.460, respectively). This result is in line with the prediction that eccentricity will have no effect on stall point when the average clearance is greater than 3.9% chord. However, the test with 4.2% clearance and 75% eccentricity had a stalling flow coefficient of 0.465, a considerable increase.

This breakdown in the linear relationship between eccentricity and stalling flow coefficient can also be seen in Fig. 5.4, where the first three points (shown in red) lie on a straight line, but from 4.2% clearance onwards (blue crosses), there is no link between gap size and gradient. The change coincides with the start of the transition to part-span stall, which is discussed in more detail in the next section.

5.3.2 Stall Inception Mechanisms

As with the concentric cases, spike-type stall was observed in the eccentric tests with 1.7% average clearance. However, with larger average clearances and eccentricity, the stall inception mechanism was less clear-cut.

An example of this with 2.4% tip-clearance and 75% eccentricity is shown in Fig. 5.5. It can be seen that long-lengthscale modal activity is visible in the pressure traces after the maximum tip-clearance (top three lines). These modal waves appear to decay as they move through the small tip-clearance sector of the compressor.

As well as the modal disturbances in the large clearance sector of the annulus, it can also be seen in Fig. 5.5 that spikes appear in the bottom traces (i.e. just after

the minimum clearance) and then decay as they propagate. The final route into stall appears to be a combination of spike and modal stall inception.

At larger tip-clearances, the stall inception mechanism became harder to identify, due to the formation of large disturbances in the large tip-clearance part of the annulus. These decayed as they moved into the small tip-clearance region. These large disturbances obscured the developing stall cell. Pre-stall disturbances will be discussed in more detail in Chapters 6 to 8.

The transition from full-span to part-span stall at around 6% clearance is less clear-cut with eccentric clearance than in the concentric cases. It appears that the stall mechanism depends on both average and maximum tip-clearance size. This is why the transition is denoted by a grey band in Fig. 5.2 instead of a single line.

5.3.3 Freeman's Rule of Thumb

It is generally assumed that the stall point of an eccentric compressor will be the same as that of a concentric compressor with clearance equal to the maximum eccentric clearance. This idea was suggested by Freeman and is based on an engine test [2]. The experimental data discussed above will now be used to test this 'rule of thumb'.

Figure 5.6 is a plot of stalling flow coefficient against maximum tip-clearance for tests with 1.7% and 2.4% average clearance. The red circles show the stall points of two machines both with 1.7% average clearance, the left-hand point is for a concentric compressor and the right hand point is for one with 75% eccentricity, but the same average clearance, i.e. with a maximum clearance of 2.4% chord. The blue square shows the stall point of a concentric compressor with 2.4% clearance.

If the rule of thumb were correct, the right-hand red circle would lie on top of the blue square, as the compressors in these two tests have the same maximum tip-clearance and so should, according to the rule of thumb, have the same stalling flow coefficient. In Fig. 5.6, it can be seen that this is not the case. In this case, the increase in stalling flow coefficient due to eccentricity is only 60% of that given by a concentric case with tip-clearance equal to the maximum in the eccentric machine.

A similar, but less pronounced, pattern is observed in the cases with 2.4% and 3.3%

clearance. This is shown in Fig. 5.7, where it can be seen that the increase in stalling flow coefficient due to eccentricity at 2.4% clearance is 75% of the change due to opening the clearance to 3.3% axisymmetrically.

Returning to Fig. 5.2, the relationship between maximum tip-clearance and stall point can be seen for the entire range of tip-clearances tested. For maximum clearances of between 4% and 5.5%, the stalling flow coefficient is more-or-less constant. This trend is disrupted by the transition to part-span stall (see above), which brings about an upward hump in the stalling flow coefficient in Fig. 5.2 and a greater level of scatter in the results.

These results suggest that there may be some form of dynamic effect in play, where the large tip-clearance region of the compressor is able to operate beyond its normal stall point because of the stabilising effect of the small tip-clearance sector. This will be discussed in more detail in Section 5.5.

The results discussed in this section show that the rule of thumb that the stall point of a compressor is determined by the maximum tip-clearance is not accurate. The effect of defining an average 'worst clearance' over the large clearance sector (say, 60 or 90°) was also investigated and it was found that there was no consistent relationship between this 'worst clearance' and the compressor stall point.

In general, it may be concluded that an eccentric compressor retains more stall margin than a concentric compressor with tip-clearance equal to the maximum tip-clearance in the eccentric case. Freeman's rule of thumb is thus overly cautious.

5.4 Flow Redistribution due to Eccentricity

When a compressor is operating with tip-clearance asymmetry, there is an inevitable flow redistribution around the annulus, such that the flow coefficient is not the same at all circumferential positions. In this section, the theoretical model of Graf et al. [47] which is used to predict the flow redistribution around the annulus will be adapted for the test compressor used in this project. The flow redistribution derived from the model will then be compared with the experimental measurements.

5.4.1 Theoretical Model

The effect of tip-clearance eccentricity on the flowfield in a compressor has previously been studied both experimentally and analytically. Hynes and Greitzer [48] developed a model for flow redistribution in a compressor operating under inlet distortion. This model was later adapted for a compressor with eccentric tip-clearance by Graf et al. [47].

The model starts by assuming that there is a variation in flow coefficient around the annulus. This means that the fluid in the rotor passages must be accelerating and decelerating as it moves through the changing flowfield, and this acceleration must be balanced by a corresponding pressure fluctuation. This leads to the following equation:

$$\frac{p_2 - p_{01}}{\frac{1}{2}\rho U^2} = \psi_{\text{T-S}}(\phi, \epsilon) - \lambda \frac{d\phi}{d\theta} \tag{5.6}$$

This equation assumes that the compressor is insensitive to inlet swirl. As the test compressor used for this study was initially tested without Inlet Guide Vanes (IGVs), this assumption is invalid, and $\psi_{\text{T-S}} = \psi_{\text{T-S}}(\phi, \epsilon, \alpha)$, where α is the absolute inlet flow angle. This subject has been considered by Longley [78], and a full derivation of the resulting expression for the flowfield in an eccentric machine can be found in Appendix A. For the sinusoidal tip-clearance variation considered in the current work, the final equation for the perturbation in flow coefficient around the annulus is:

$$\delta\phi = -\Delta\varepsilon \frac{\partial\psi}{\partial\varepsilon} \left[\frac{\frac{\partial\psi}{\partial\phi}\cos\theta - (\lambda - \frac{\partial\psi}{\partial\alpha}\frac{1}{\phi})\sin\theta}{\left(\lambda - \frac{\partial\psi}{\partial\alpha}\frac{1}{\phi}\right)^2 + \left(\frac{\partial\psi}{\partial\phi}\right)^2} \right] \tag{5.7}$$

It can be seen that the sinusoidal tip-clearance distribution leads to a variation in flow coefficient (axial velocity) which is also sinusoidal, but that there is a phase lag,

which is given by:

$$\Delta\theta = -\tan^{-1}\left(\frac{\lambda - \frac{1}{\bar{\phi}}\frac{\partial\psi}{\partial\alpha}}{\frac{\partial\psi}{\partial\phi}}\right) \tag{5.8}$$

The experimental results for the magnitude and phase lag of the flow redistribution can now be compared with the theoretical model developed above.

5.4.2 Comparison of the Model with Experimental Results

From the characteristics for the compressor with different levels of (concentric) tip-clearance given in Chapter 4, values for $\frac{\partial\psi}{\partial\epsilon}$ and $\frac{\partial\psi}{\partial\phi}$ can be calculated. An expression for $\frac{\partial\psi}{\partial\alpha}$ can also be found from a separate set of experiments - as reported in Appendix A. Once these terms are known, Equation 5.7 can be evaluated for the test compressor.

The flow coefficient variation around the compressor was found by measuring the local static pressure just upstream of the rotor bladerow at eighteen positions around the annulus. The linearised Bernoulli equation was then used to translate this into a velocity perturbation, as described in Appendix A.

Equation 5.7 only predicts the first harmonic of the flow redistribution, and so the experimental results shown here also only show the first harmonic (i.e. in each case the Fourier transform of the raw data has been taken and the lines shown are a sine wave with the magnitude and phase lag of the first harmonic).

A comparison of the model with the experimental data for a compressor with 1.7% average clearance and 75% eccentricity is shown in Fig. 5.8. The tip-clearance variation is shown in Fig. 5.8 (a)[2], while the flow coefficient variation is shown for three different average flow coefficients ($\bar{\phi}$ = 0.50, 0.45 and 0.43) in Fig. 5.8 (b). In both cases the model input/output is shown in black, while the experimental data is shown as a red line with red circles denoting the measuring positions.

It can be seen that the sinusoidal tip-clearance variation gives rise to a sinusoidal

[2]As with the flow coefficient, a sinusoid based on the first harmonic of the actual tip-clearance in the machine is shown.

ϕ	Magnitude, A		Phase Lag $\Delta\theta$ (°)	
	Experiments	Model	Experiments	Model
0.50	0.0076	0.0016	9.7	41.6
0.45	0.0099	0.0033	8.2	27.8
0.43	0.0099	0.0049	16.0	25.9

Table 5.3: *Comparison between model outputs and actual flow redistribution in terms of magnitude and phase of the first harmonic (1.7% tip-clearance, 75% eccentricity).*

flow coefficient variation around the annulus, as is evident from Equation 5.7. The agreement between the experiments and the model is reasonable at lower flow conditions in terms of the magnitude of the redistribution. However, at the design point (top lines in Fig. 5.8, $\bar{\phi}$ = 0.5), the model predicts virtually no flow redistribution, while the experimental data shows a significant redistribution. More importantly, the phase lag is over-predicted by the model at all three operating points.

The magnitude and phase of the flow redistribution (expressed as $\phi = -A\cos(\theta - \Delta\theta)$) given by the model and the experiments is summarised in Table 5.3. Here, it can be seen that the model over-predicts the phase lag by 10 to 30°. It can also be seen that the model under-predicts the magnitude of the flow redistribution by almost a factor of 5 at $\bar{\phi}$ = 0.5, but that this error drops to a factor of two at the near-stall operating point, $\bar{\phi}$ = 0.43.

The same comparison between the experimental data and the model is shown in Fig. 5.9 for 25% eccentricity (also with 1.7% average clearance) at a near-stall operating point. The data from the 75% eccentricity case discussed above is plotted in black for reference, while the result from the test with 25% eccentricity is shown in red.

As expected, the flow redistribution becomes less pronounced as the eccentricity is reduced - a trend which is captured by both the model and the experimental data. As with the 75% eccentricity data, the model drastically under-predicts the magnitude of the flowfield redistribution in the case with 25% eccentricity.

A final comparison is given in Fig. 5.10, where the model outputs are compared with experimental data for the compressor with 3.3% clearance and 75% eccentricity. As with the smaller clearance cases discussed above, the magnitude of the flow

redistribution is under-predicted by the model, while the phase lag is over-predicted. Again, the discrepancy is less pronounced at near-stall conditions (lower lines) than at the design point (upper lines).

It is worth noting at this point that the results shown by Graf et al. (see Fig. 12 of [47]) also reveal a disagreement in phase lag between the experimental data and the model.

In the results shown in this chapter, the disagreement in phase between the model and the experimental data is mainly due to the inlet swirl sensitivity term, which is given in Appendix A as $\frac{\partial \psi}{\partial \alpha} = -7.1\phi + 2.7$. At low flow coefficients, this term is of a similar size to the other terms in Equation 5.7, and so creates a small additional phase lag, and a small reduction in the magnitude of the redistribution.

At flow coefficients away from the stall point, however, this term rapidly becomes larger and dominates the equation, leading to a disproportionate reduction in phase lag. This term is also the cause of the excessive attenuation of the magnitude of the redistribution at high flow coefficients, because it appears squared in the denominator of the expression for $\delta\phi$.

In response to these discrepancies between theory and experiment, it should be pointed out that a two-dimensional model will not be able to predict the flow redistribution accurately because the input which causes the redistribution, the tip-clearance eccentricity, is not applied evenly across the span, but is entirely applied in the outer 1%. The original model was developed to describe the response of a compressor to inlet distortion, which is often applied evenly across the span.

The validity of using a two-dimensional model to predict the flowfield redistribution is discussed in more detail in Appendix B. In particular, it seems that the change in absolute inlet swirl angle around the annulus (due to the flowfield redistribution caused by eccentricity) varies across the span. This goes some way to explaining why the inlet swirl sensitivity parameter seems to create an excessive phase lag. Removing the inlet swirl sensitivity and unsteady loss terms from the model would give better agreement with the experimental data (again, see Appendix B), but to do this would be to obtain the right answer with the wrong physics.

In conclusion, there is a significant circumferential flow redistribution in a compressor with eccentric tip-clearance. The model of Graf et al. is, however, not a reliable

means of predicting the magnitude or phase of this redistribution. In the next section, the effect of the flowfield redistribution on the stability of the compressor, and its likely impact on the stall point of the machine, will be discussed.

5.5 Effect of Flow Redistribution on Stability

Simply considering the variation in local flow coefficient shown above suggests that the flow would first become unstable in the region just after the maximum tip-clearance as the flow coefficient is lowest in this region. However, there is another factor which affects the stability of a given part of the annulus: the 'equivalent concentric stall point'. The equivalent concentric stall point is the point at which that part of the annulus would stall were it to be operating as a concentric compressor.

The relationship between tip-clearance and stall point in a concentric compressor was shown in Fig. 4.2 to be approximately linear for clearances up to 3.3% chord. Using this approximation, the equivalent concentric stall point was calculated for every circumferential position around the annulus of a compressor with 1.7% clearance and 75% eccentricity. This is shown by the red line in Fig. 5.11 (a). In this case, the equivalent concentric stall point is 11% higher in the maximum tip-clearance sector than in the small tip-clearance sector.

The local flow coefficient (taken from experimental data) at the stall point of this configuration ($\bar{\phi}$ = 0.425) is plotted in black on Fig. 5.11 (a). This can be compared with the local equivalent concentric stall point. It can be seen that there is a part of the annulus in which the compressor is being forced to operate at flow coefficients below the stability limit of the equivalent concentric compressor with the same local tip-clearance. The grey shaded area shows the region in which the compressor would be expected to be unstable. In this case, the unstable sector extends from 55° before the maximum tip-clearance to 65° after it.

If the eccentricity is lowered, the flow redistribution becomes less extreme, as shown in Fig. 5.9. The variation in equivalent concentric stall point around the annulus also becomes smaller. These effects are shown in Fig. 5.11 (b), which shows results for a compressor with 25% eccentricity operating at its stall point (also with 1.7% average clearance). Compared with the plot for 75% eccentricity (Fig. 5.11 (a)), the

unstable sector is wider than it was before, extending from 80° before the maximum tip-clearance to 190° after it. The extent to which any part of the compressor is being forced to operate beyond its natural stalling point is, however, reduced - i.e. the grey shaded region in Fig. 5.11 (b) is wider but flatter than the one in Fig. 5.11 (a).

It turns out that the areas of the two grey regions in Fig. 5.11 are approximately the same. This suggests that it may be possible to establish a criterion for stall in an eccentric compressor based on the width and depth of this unstable area, for example, by integrating it to find the area.

If there is a link between the unstable sector and stall, this link could prove to be a useful tool for designers as it would be an improvement on Freeman's rule of thumb. To test this hypothesis, a more accurate model for the flow redistribution would be required.

5.6 Local Characteristics in an Eccentric Machine

In a further investigation of the performance of an eccentric compressor, the local static pressure upstream of the compressor stage was measured simultaneously at six locations around the annulus while the compressor was throttled from full flow to near stall. Six 'local characteristics' were thus obtained.

The local total-to-static characteristics obtained in this way are shown in Fig. 5.12. The six coloured lines represent the local characteristics (see key), while the average characteristic is shown in grey. From Fig. 5.12, it can be seen that the large tip-clearance part of the compressor (black, dark blue and red characteristics) is operating to the left of the average characteristic, while the small clearance sector (light blue, green and orange) is operating to the right of the mean.

In order to compare the behaviour of different circumferential sectors of the annulus, it is more instructive to study the compressor performance at discrete operating points, as has been done in Fig. 5.13. The average characteristic is again shown in grey, and the local operating points are represented by coloured crosses joined by grey horizontal lines. The inlet total and exit static pressures are fixed, so the total-to-static pressure rise must be constant around the annulus, hence the local operating points all lie on a horizontal line.

Two additional characteristics are shown in Fig. 5.13 (a): one for a concentric compressor with tip-clearance equal to the maximum clearance and one for a concentric compressor with the minimum tip-clearance. From these, it can be seen that the locus of operating points in the eccentric machine extends beyond the area bounded by the two concentric characteristics (i.e. the grey horizontal lines are wider than the gap between the light and dark blue characteristics).

The equivalent concentric stall point of the maximum clearance (top left-hand end of the dark blue characteristic) is labelled 'A' in Fig. 5.13 (a). The local operating point for the maximum clearance sector in the eccentric compressor just before the compressor stalls is labelled 'B'. It can be seen that point B is above and to the left of point A.

This relative positions of points A and B show that the part of the annulus with the largest tip-clearance (dark blue crosses) is being forced to operate at a much lower flow coefficient, and to produce a higher pressure rise, than it would in an equivalent concentric compressor. This is interesting: the same blading with the same tip-clearance, but in an eccentric compressor, produces more pressure rise than it normally would in an equivalent concentric machine.

While the total-to-static characteristic is generally used to show the performance of a low-speed compressor, it is the total-to-total pressure rise which must be used to determine how much work (stagnation enthalpy input) is being put into the fluid by the compressor. The total-to-total characteristics derived from the data in Fig. 5.13 (a) are shown in Fig. 5.13 (b). These characteristics have been generated by assuming that the flow is axial at inlet and exit and is incompressible, such that:

$$\psi_{\text{T-T}} = \psi_{\text{T-S}} + \phi^2 \tag{5.9}$$

As in Fig. 5.13 (a), the equivalent concentric characteristics for the minimum and maximum tip-clearance are shown in light and dark blue, and the local operating points are represented by coloured crosses joined by grey lines. Because the exit total pressure is not constant in an eccentric machine (due to the variation in flow coefficient), the operating points now lie on diagonal lines.

In Fig. 5.13 (b), the maximum pressure rise of a concentric compressor with tip-clearance equal to the largest eccentric clearance (i.e. the peak of the dark blue characteristic) is marked 'A'. As in Fig. 5.13 (a), the operating point of the maximum tip-clearance part of the eccentric annulus just before the compressor stalls (the final blue cross) is labelled 'B'.

By presenting the characteristics in total-to-total format, it can be seen that point B is level with point A. This shows that the large tip-clearance part of the annulus does not do any more work on the flow than it would if it were operating in isolation from the rest of the compressor. However, the large clearance part of the compressor is able to operate at a lower flow coefficient than its equivalent concentric stall point. This is due to the stabilising effect of the small tip-clearance region of the annulus.

An alternative way of comparing the local pressure rise at the stall point of the eccentric machine with the local equivalent concentric maximum pressure rise can be made for the other five measuring positions around the annulus. This is shown in Fig. 5.14, which is a graph of total-to-total pressure rise against circumferential position. The black line shows the equivalent maximum total-to-total pressure rise of a concentric compressor with tip-clearance equal to the local clearance, while the coloured crosses represent the pressure rise measured at that location in the eccentric compressor while operating at the eccentric stall point.

As discussed above, the dark blue cross, which represents the data from the maximum clearance, is level with the black line in Fig. 5.14, so this part of the annulus is producing a total-to-total pressure rise equal to the maximum that it would produce if it were operating in an equivalent concentric machine.

The stall point total pressure rise measured at the two points either side of the maximum clearance are shown by the black and red crosses. It can be seen that the black cross also lies on the black line, and the red cross is just below it. This shows that, throughout the large clearance sector of the compressor, the compressor is operating at or near its maximum total-to-total pressure rise capability.

By contrast, in the small tip-clearance part of the annulus (light blue, orange and green crosses) the local total pressure rise is significantly lower than the maximum pressure rise of an equivalent concentric machine.

Putting this together, at the stall point of the eccentric compressor, the large clearance

part of the machine is producing a total-to-total pressure rise roughly equal to the maximum that it could produce were it to be operating in a concentric machine, while the small tip-clearance part of the machine is operating well below its peak pressure rise.

It appears that the compressor stalls when the part of the annulus around the large clearance reaches its maximum concentric total pressure rise. More work would, however, be required to confirm this, and this is discussed further in Section 9.4. If this is the case, then it may be possible to establish a critical sector size of the compressor which must reach the maximum pressure rise before stall occurs.

5.7 Conclusions

From this work, the following conclusions can be drawn:

1. It has been shown that tip-clearance eccentricity does not reduce the pressure rise at the design flow coefficient. It does, however, have the following effects on the stalling flow coefficient of the compressor:
   (a) For a given average clearance, there is a linear increase in stalling flow coefficient due to eccentricity.
   (b) The increase in stalling flow coefficient caused by eccentricity decreases as the average tip-clearance increases. The relationship between stall margin penalty due to eccentricity and average tip-clearance size is also linear.
   (c) The increase in stalling flow coefficient due to an eccentric tip-clearance is considerably less than that of a concentric compressor with the same maximum tip-clearance. This is contrary to Freeman's rule of thumb and suggests that the small tip-clearance part of the annulus has a stabilising effect on the large tip-clearance region.

   As with the results for a concentric machine, the linear relationships above break down once part-span stall is observed (at a tip-clearance of around 4% in this case).

   An empirical formula has been developed for the stalling flow coefficient of an eccentric machine with small to moderate tip-clearance (less than 4% chord).

This model is based on findings (a) and (b) and the linear relationship between tip-clearance and stalling flow coefficient in a concentric machine.

2. The stall inception mechanism in an eccentric compressor with average tip-clearance greater than 2% chord is unclear: both modes and spikes can be seen. Part-span stall was observed with clearances greater than 5% chord. The transition from full-span to part-span stall is less clear-cut than in a concentric machine and appears to depend on both the average and maximum clearance size.

3. Tip-clearance eccentricity leads to a circumferential redistribution of the flow in the compressor such that the flow coefficient is lower in the large tip-clearance sector than in the small clearance sector. The model of Graf et al. [47] for this flow redistribution was applied to the compressor used in this work. The model did not capture the behaviour of the compressor at full-flow conditions. At near-stall conditions, the errors were smaller, but there were still discrepancies in both the magnitude and phase lag of the redistribution. This is thought to be due to 3-D effects, which are not included in the two-dimensional model.

4. It has been found that, in an eccentric compressor operating at its stall point, a sector of the annulus is operating at a lower flow coefficient than its natural stall point. This sector would therefore be expected to be unstable. The size (both circumferential extent and 'depth') of this unstable sector may be useful for predicting the stall point of an eccentric machine if the flow field redistribution can be modelled accurately enough.

5. From the local characteristics generated at six locations around the annulus of an eccentric compressor it has been learned that:
   (a) The total-to-static characteristics showed that the large tip-clearance part of the annulus can operate at a lower flow coefficient and generate a larger pressure rise than it would if it were operating in a concentric machine.
   (b) The local total-to-total characteristics showed that the operating point of the maximum tip-clearance part of the annulus is never above the peak of its equivalent concentric characteristic. It is therefore the case that the large tip-clearance part of the annulus does not do any more work on the flow than it would if it were operating in a concentric machine.

(c) At the stall point of the eccentric compressor, the large tip-clearance sector of the annulus has been shown to produce a total pressure rise equal to the maximum that it could produce if it were operating in isolation. This suggests that the compressor stalls when a certain proportion of the annulus reaches its maximum pressure rise capability. More work would be required to confirm this idea.

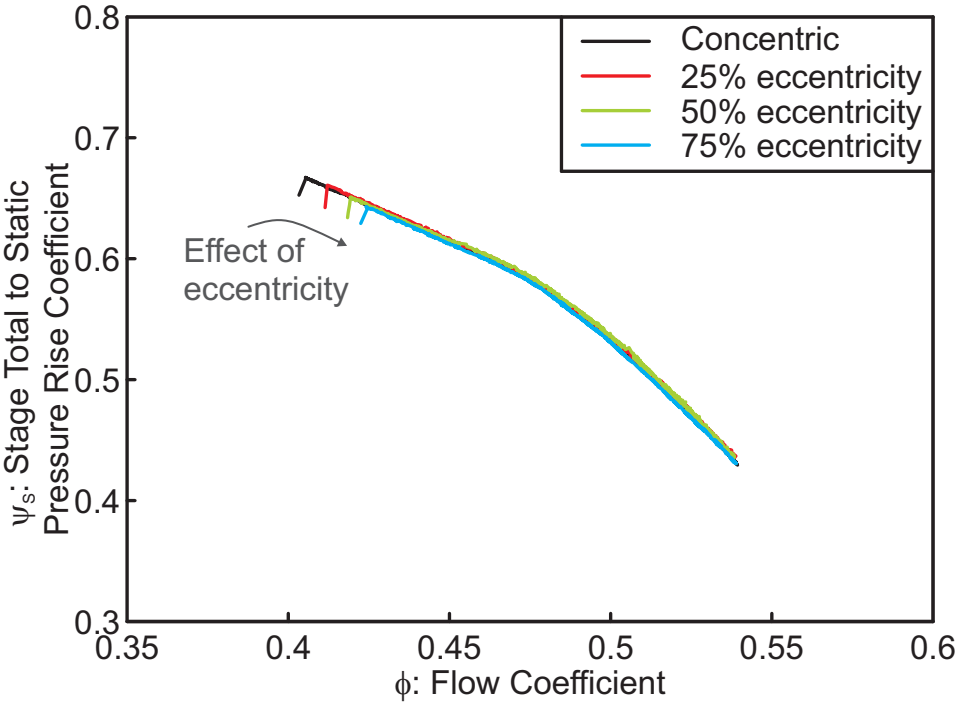

(a) 1.7% average clearance.

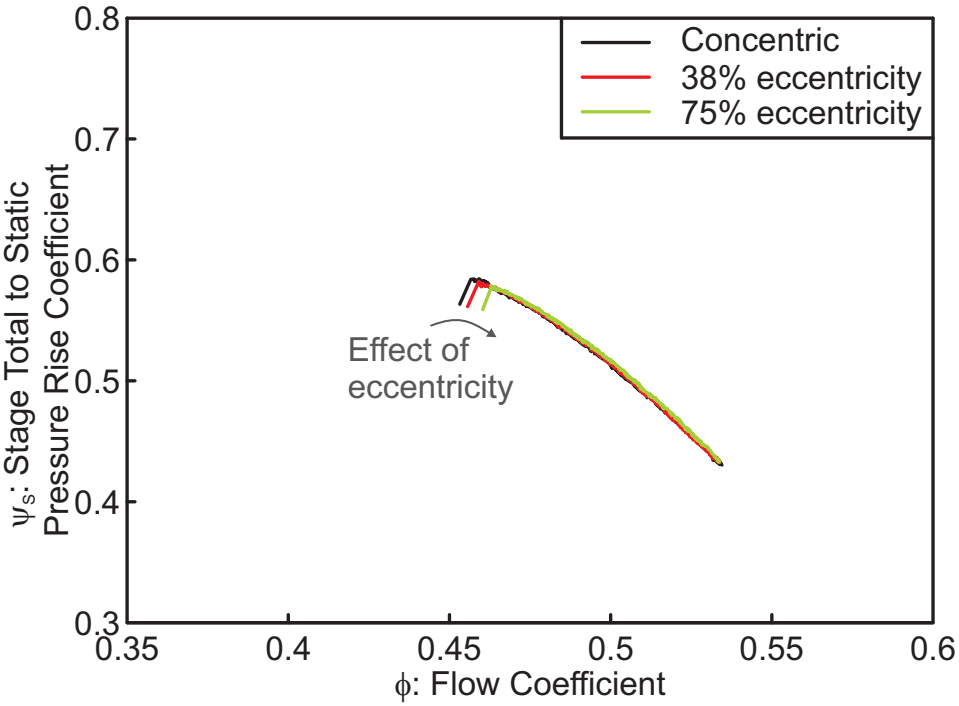

(b) 3.3% average clearance.

Figure 5.1: *Compressor characteristics with different levels of eccentricity for two average clearance levels.*

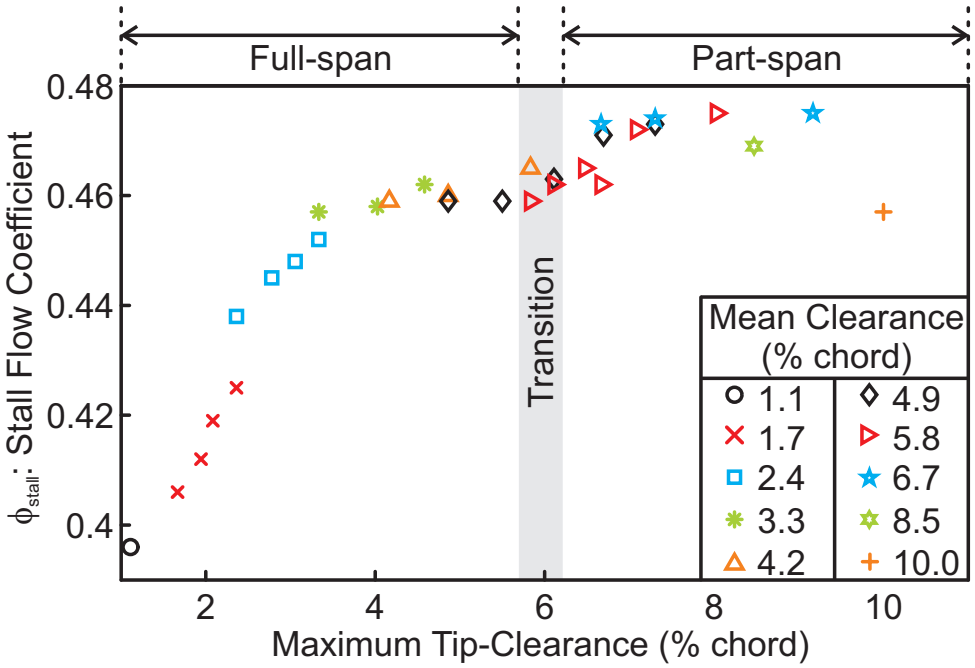

Figure 5.2: *Plot of stalling flow coefficient against maximum tip-clearance for all the test cases (concentric and eccentric).*

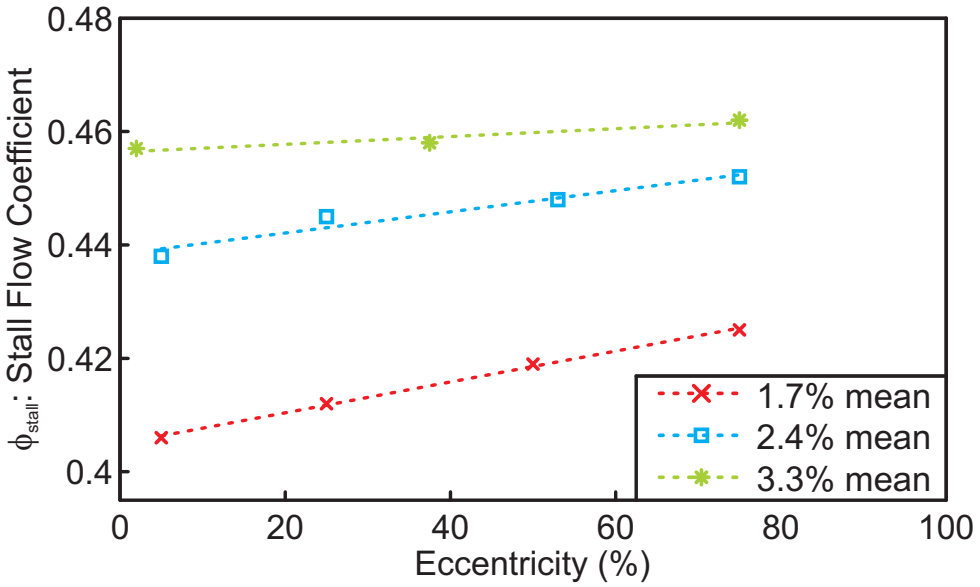

Figure 5.3: *Relationship between eccentricity level and stall point for three average clearance levels.*

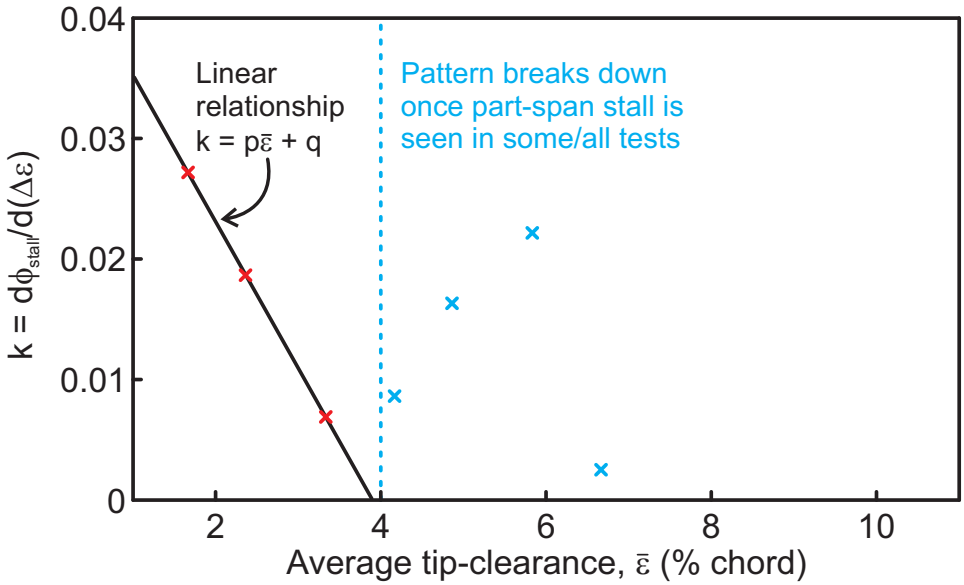

Figure 5.4: *Gradient of relationship between eccentricity and stalling flow coefficient* $\left(\frac{\partial(\phi_{stall})}{\partial(\Delta\epsilon)}\Big|_{\bar{\epsilon}}\right)$ *at different clearance levels.*

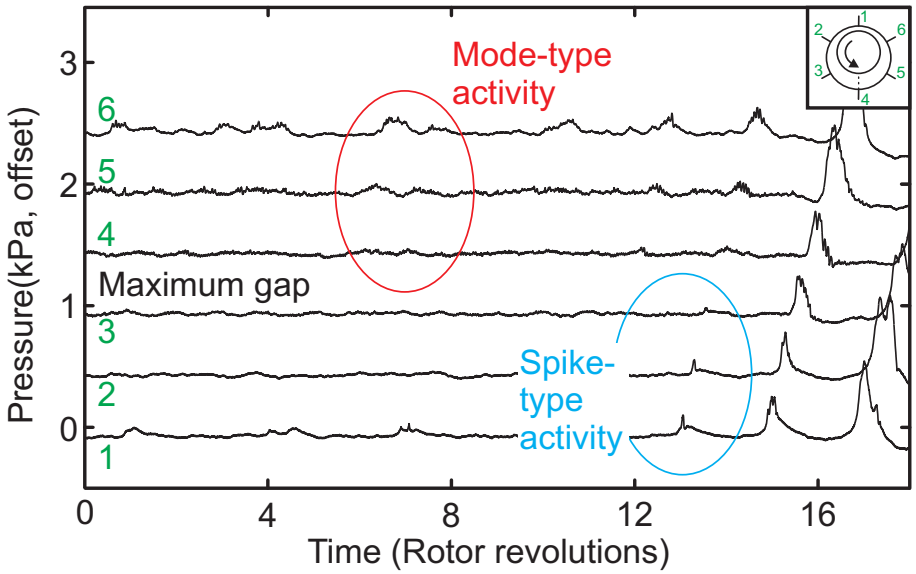

Figure 5.5: *Pressure transducer measurements of stall inception with 2.4% tip-clearance and 75% eccentricity. Data taken from transducers 20% chord upstream of the rotor blades (100kHz logging frequency, 50Hz low-pass filter).*

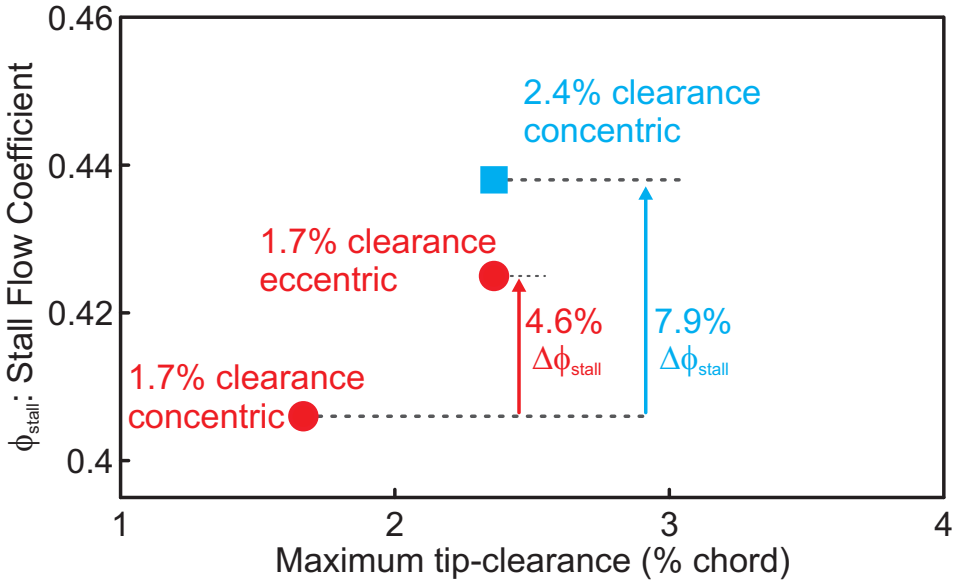

Figure 5.6: *Relationship between maximum tip-clearance and stall point in an eccentric machine (1.7% and 2.4% average clearance).*

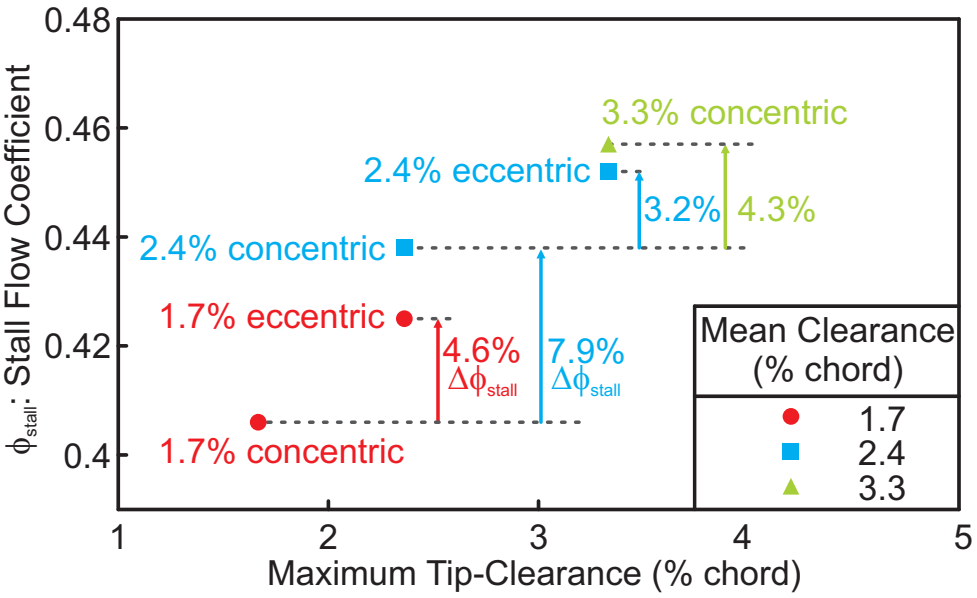

Figure 5.7: *Relationship between maximum tip-clearance and stall point in an eccentric machine (1.7% - 3.3% average clearance).*

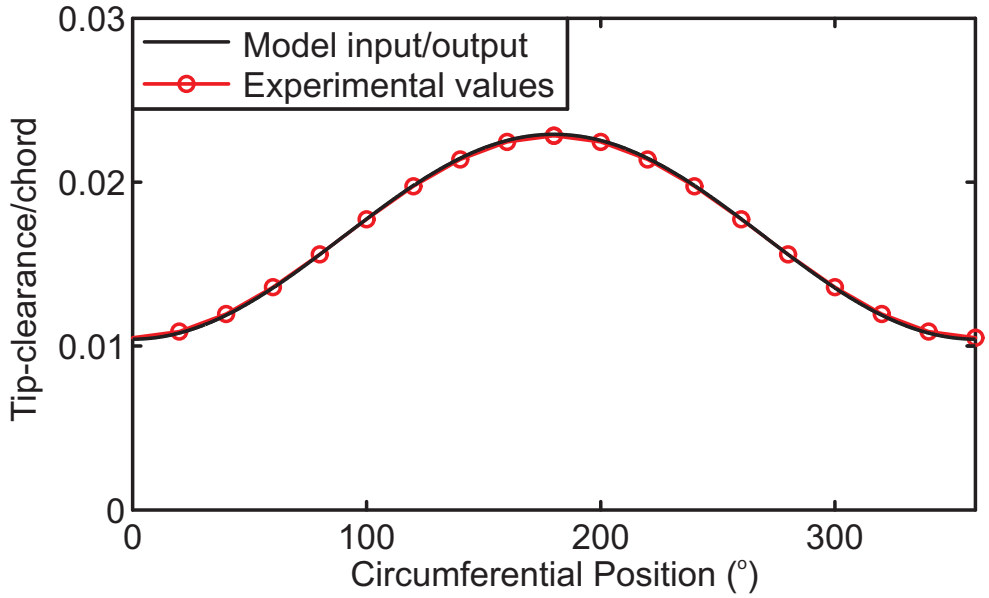

(a) Tip-clearance distribution.

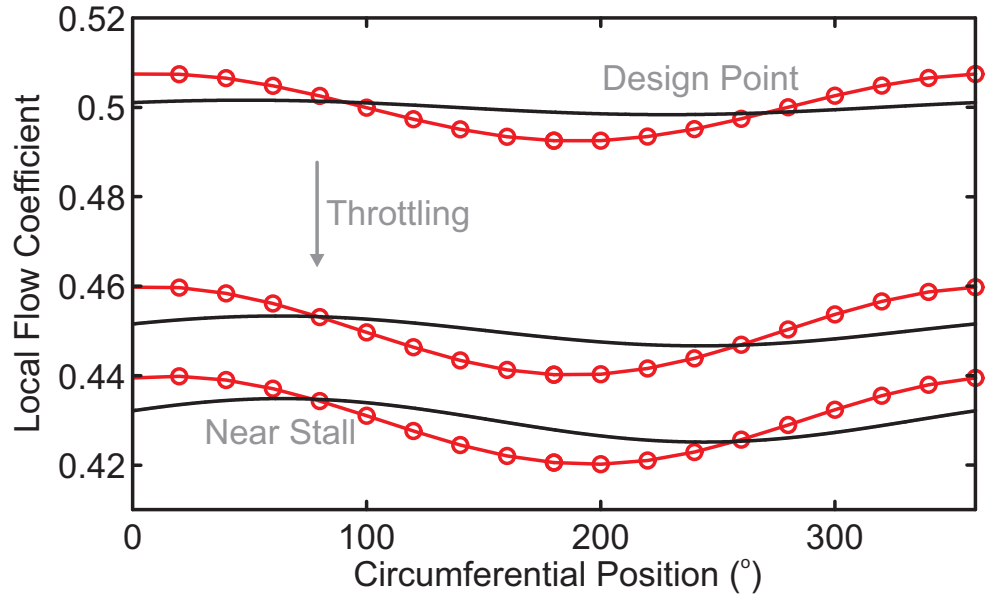

(b) Local flow coefficient.

Figure 5.8: *Flow redistribution in a compressor with eccentric tip-clearance (1.7% chord, 75% eccentricity). Comparison between the model of Graf et al. [47] and experimental data.*

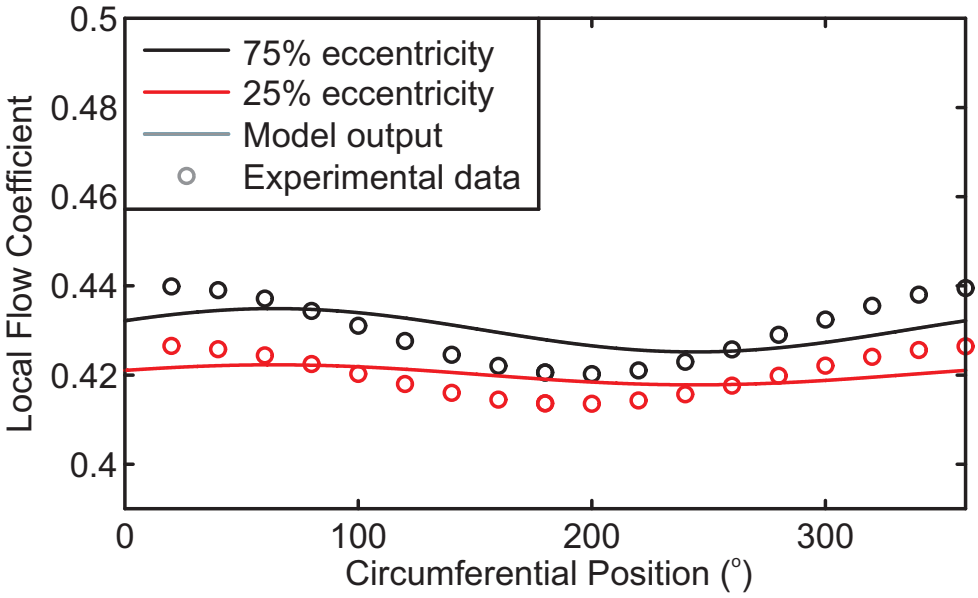

Figure 5.9: *Comparison between the model of Graf et al. [47] and experimental data for three levels of eccentricity (average clearance 1.7%, near-stall operating points).*

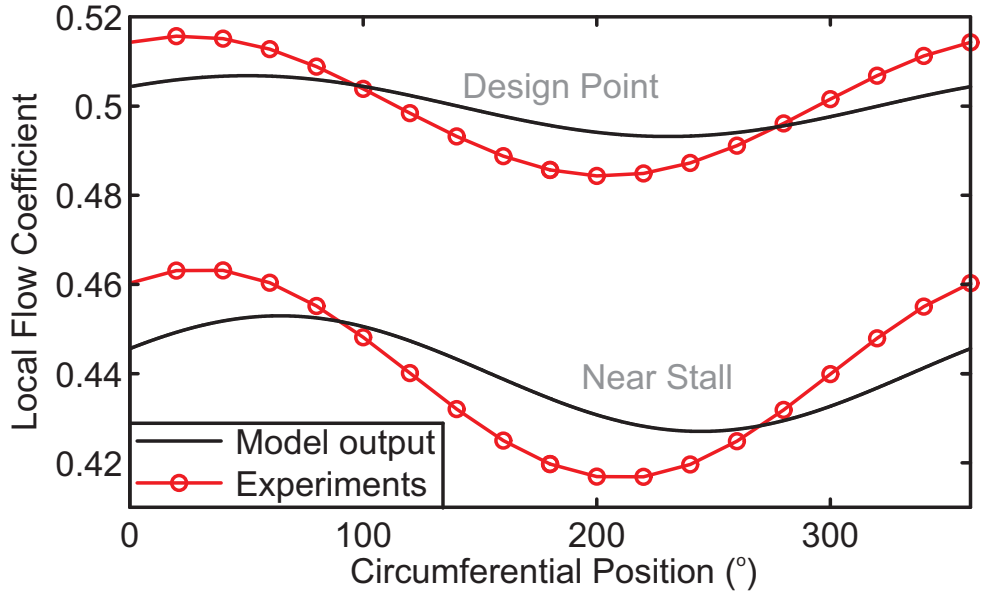

Figure 5.10: *Comparison between the model of Graf et al. [47] and experimental data for flowfield redistribution with larger tip-clearance at design and near-stall flow coefficients (3.3% clearance).*

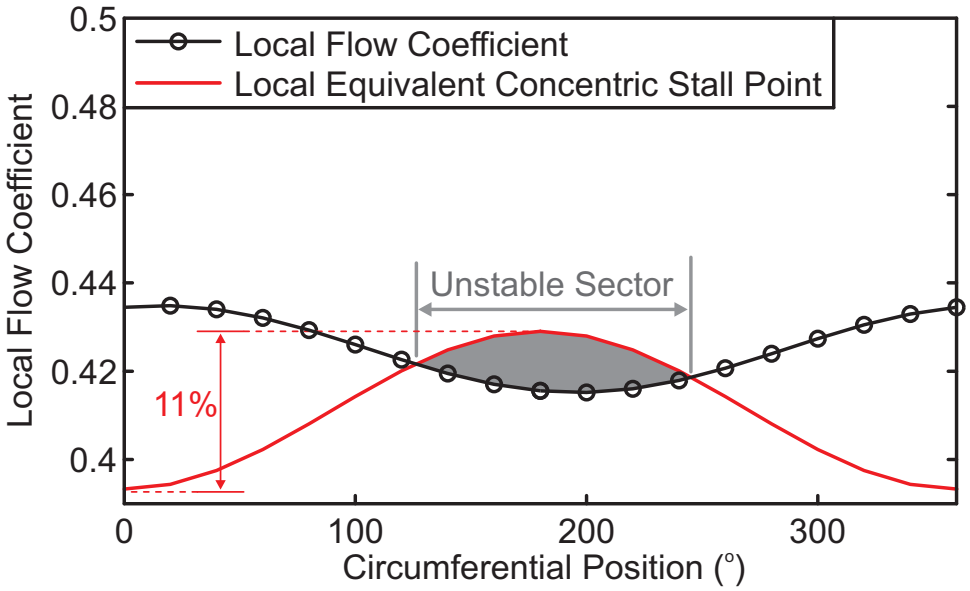

(a) 75% eccentricity.

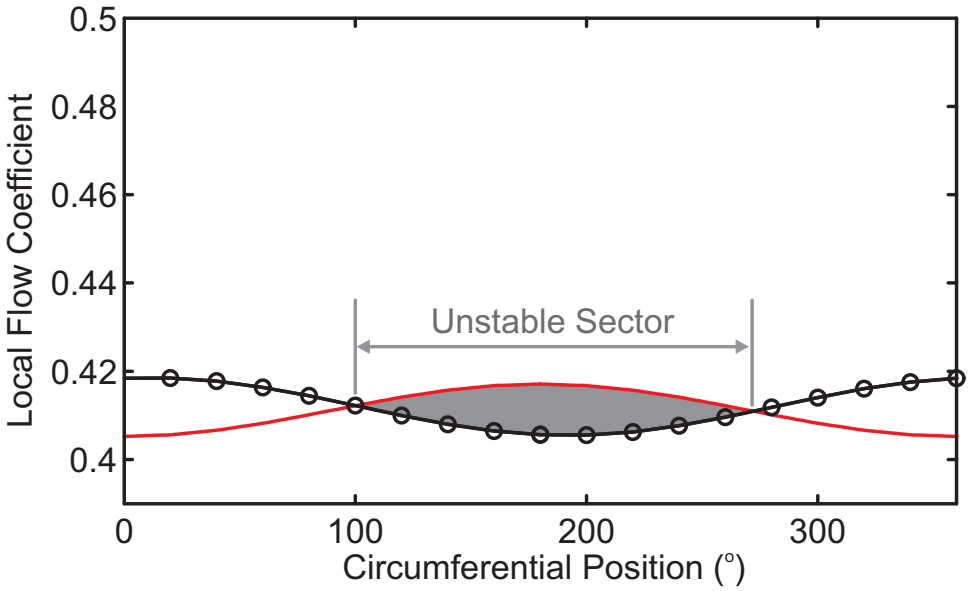

(b) 25% eccentricity.

Figure 5.11: *Effect of tip-clearance asymmetry on local stability with two levels of eccentricity - comparison between local flow coefficient and equivalent axisymmetric stall point (1.7% clearance).*

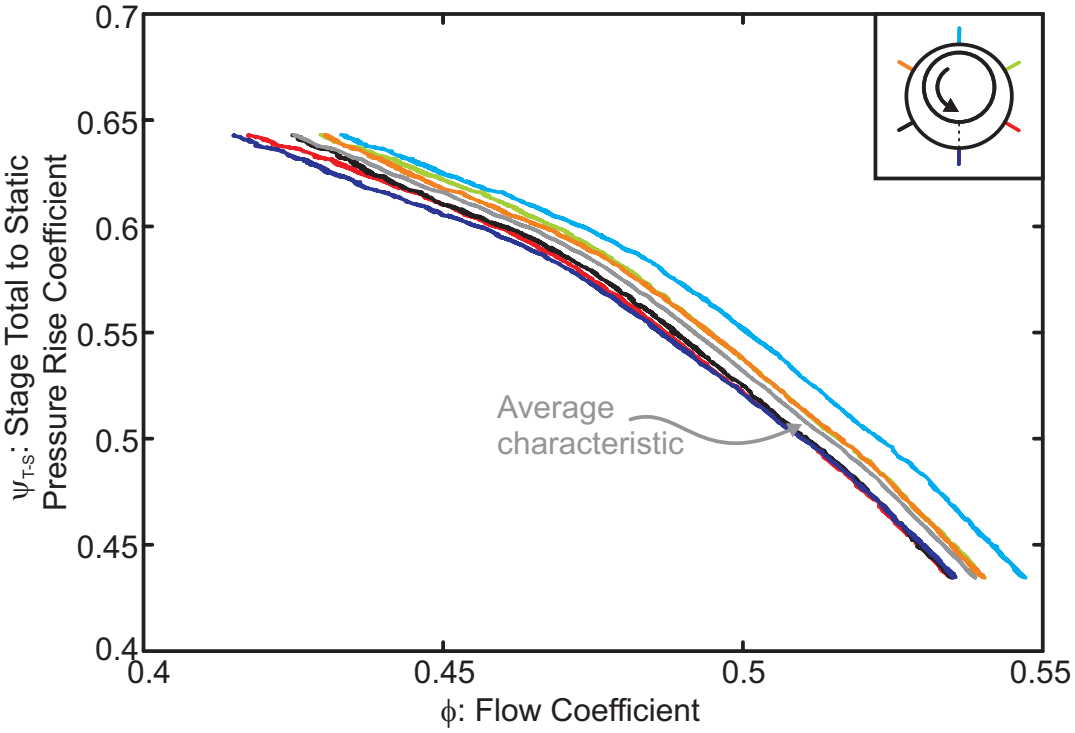

Figure 5.12: *Local total-to-static characteristics in a compressor with eccentric tip-clearance (1.7% clearance, 75% eccentricity).*

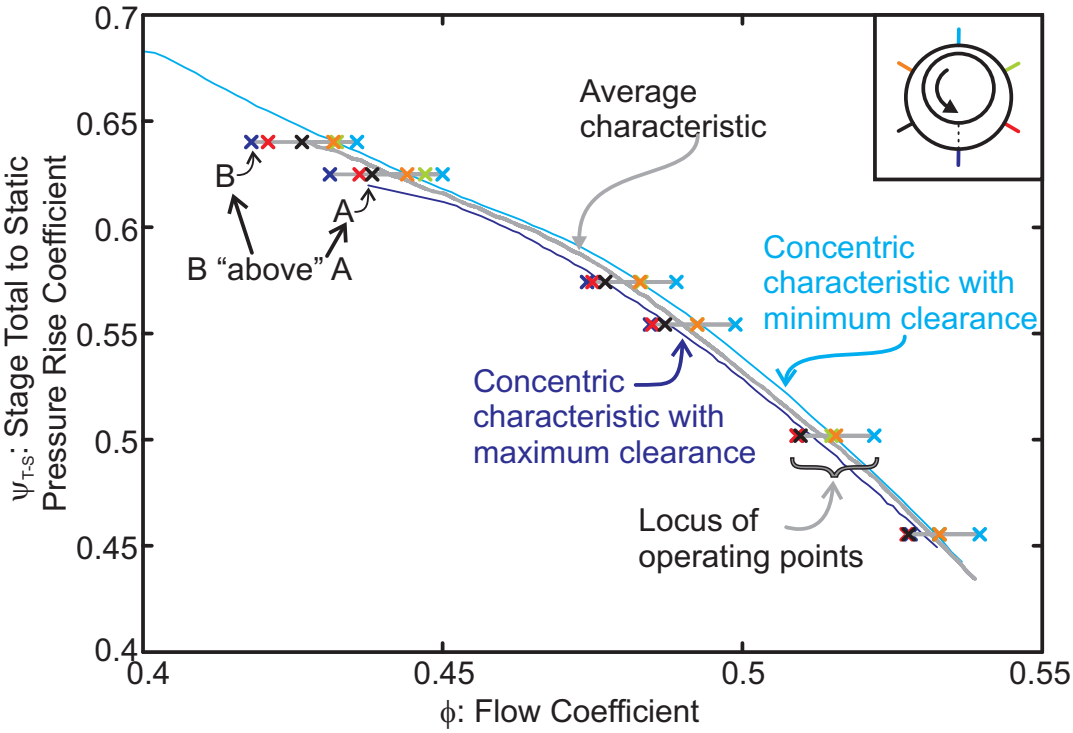

(a) Total-to-static characteristics.

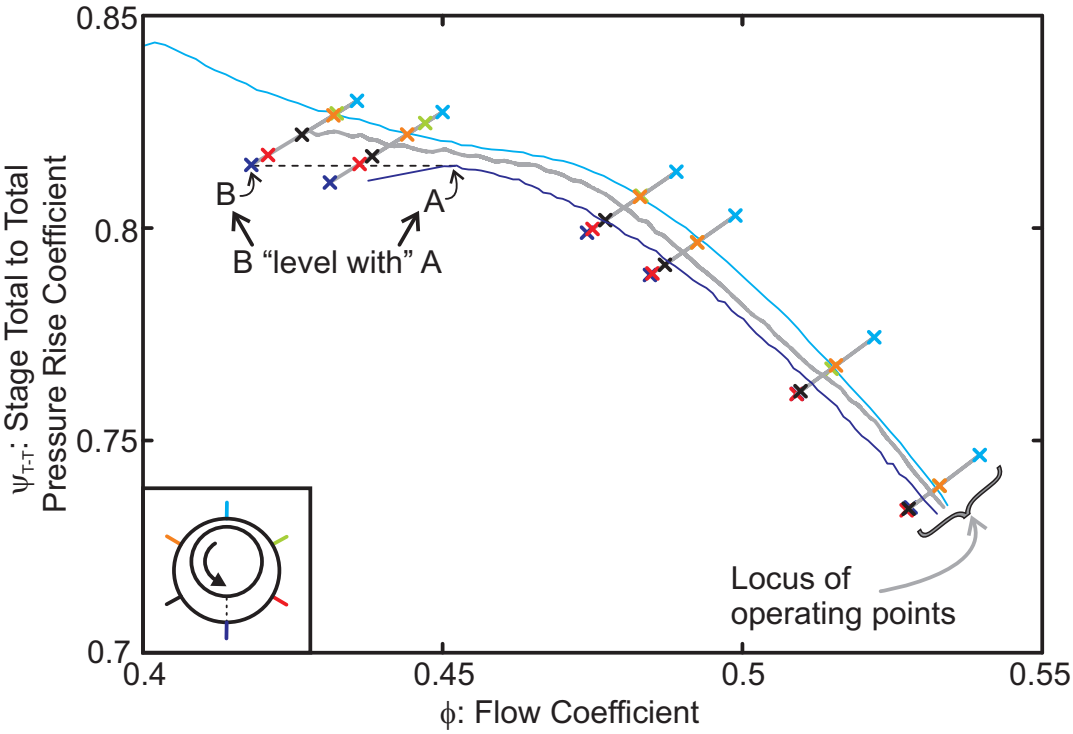

(b) Total-to-total characteristics.

Figure 5.13: *Local operating points in a compressor with eccentric tip-clearance (1.7% clearance, 75% eccentricity).*

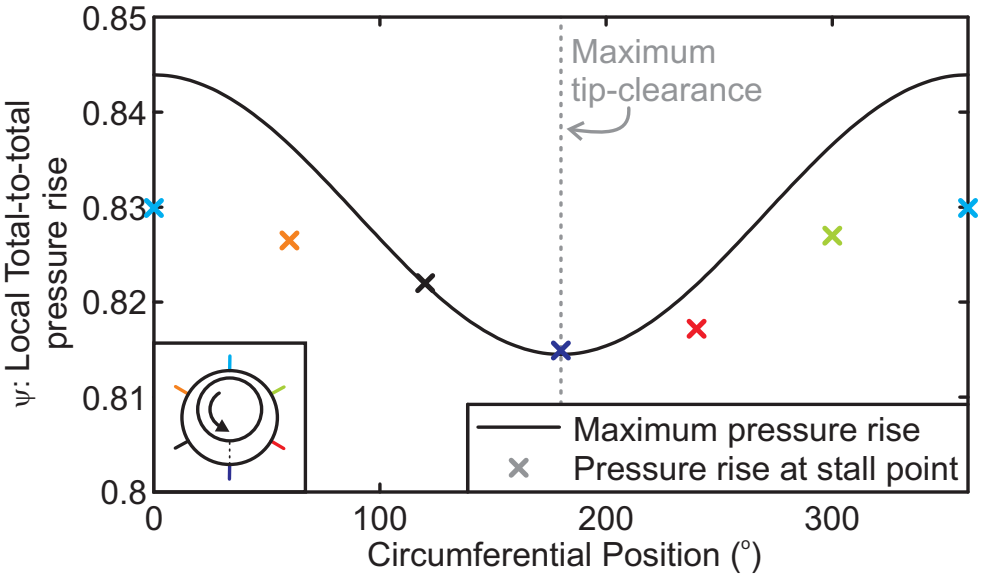

Figure 5.14: *Comparison of local maximum pressure rise with stall point pressure rise in an eccentric compressor (1.7% clearance, 75% eccentricity).*

Chapter 6

Blade Passing Signature and Stall Warning

The passing of each rotor blade causes the static pressure on the compressor casing to fluctuate. This fluctuation can be studied using unsteady pressure measurements from fast response pressure transducers mounted on the compressor casing over (or just upstream of) the blade tips. Each blade generates a unique pressure signal as it passes a particular probe, referred to here as its 'blade passing signature'.

The aim of this chapter is to establish whether or not the irregularity level in the blade passing signature can be used to give stall warning. This idea has been put forward by Dhingra et al. [66] and Christensen et al. [69], and is based on the assumption that the irregularity level in the blade passing signature will always rise dramatically when the compressor is operating close to stall, as indeed it does in their data.

The exact implementation of the system varies, but the principle is that a predetermined level of irregularity could be used as a trigger for an alarm which would indicate that the compressor is dangerously close to its stall point. The idea of connecting this alarm signal to an engine control system has been patented by General Electric [3]. The previous work on this topic was discussed in Section 2.5.3.

After some initial observations of the blade passing signature and a description of the data analysis technique, a detailed parametric study of the effects of both tip-clearance size and eccentricity on the blade passing irregularity level will be described. The results obtained by applying the same stall warning analysis to data

from a high-speed, multi-stage machine will then be presented. Finally, the potential usefulness of this stall warning technique in a real engine will be assessed.

6.1 Preliminary Measurements of the Blade Passing Signature

Looked at in detail, the blade passing signature is caused by the following process: As the pressure surface of the blade approaches the measuring position, the static pressure on the casing rises. When the blade passes, the pressure drops suddenly due to the pressure difference across the tip of the blade. After the blade has passed, the pressure returns to the original value as the effect of the suction surface of the blade dies away. This process is repeated by the next blade, leading to a continuous cycle of increasing and decreasing pressure. When the pressure measurements from the casing are plotted against time, they resemble a sawtooth pattern.

An example of data from the datum build (1.7% clearance, with concentric casing) is shown in Fig. 6.1. The data shown was acquired from six pressure transducers mounted 25% chord upstream of the rotor. Each signal has been ensemble-averaged over 45 revolutions at a fixed throttle setting (far from stall). In Fig. 6.1, the data from each probe has been laterally shifted so that the signal from a particular blade as it passes each probe is plotted at the same position on the x-axis (time), i.e. following a vertical line through the data gives the signal of the same blade as it passes each probe position in turn. The signals are also separated on the y-axis (pressure) by an arbitrary offset for ease of comparison.

All the transducers measure clear pressure fluctuations as each blade passes, but the precise shape of the signature varies from one blade to the next, i.e. one blade has a slightly different signature from the next. It can also be seen in Fig. 6.1 that one or two blades have signatures which are significantly different to those of the other blades. The most obvious example of this is highlighted by the red shaded area, where there is a smaller than normal drop in pressure over one particular blade. This smaller pressure drop is repeated at each measuring point, showing that the same blade has a similar effect on each transducer. It was also found to be repeatable throughout all the revolutions in the data set. These differences in blade passing

signal between blades are due to small variations in stagger angle (less than 0.5°), and minor variations in blade tip shape (such physical irregularities are present in all compressors, to a greater or lesser extent). As well as highlighting the difference in signature from one blade to the next, Fig. 6.1 reveals differences in the blade passing signatures recorded by each pressure transducer - i.e. a particular blade does not seem to have precisely the same effect as it passes from one transducer to the next. In fact, careful examination of the traces in Fig. 6.1 shows that probes which are diametrically opposite each other (e.g. 3 and 6) produce traces which are very similar in form and amplitude. The traces from probes 1 and 4, and 2 and 5, show the same behaviour.

The reason for this difference in shape and amplitude can be traced to the relative location of the downstream stator blades. There are 56 stator blades in the compressor and six evenly-spaced pressure transducers. This means that the pressure transducers are 60^0 apart and are therefore at three different positions relative to the stators, due to verniering, as shown in Diagram 6.1. The relative positions are summarised in Table 6.1.

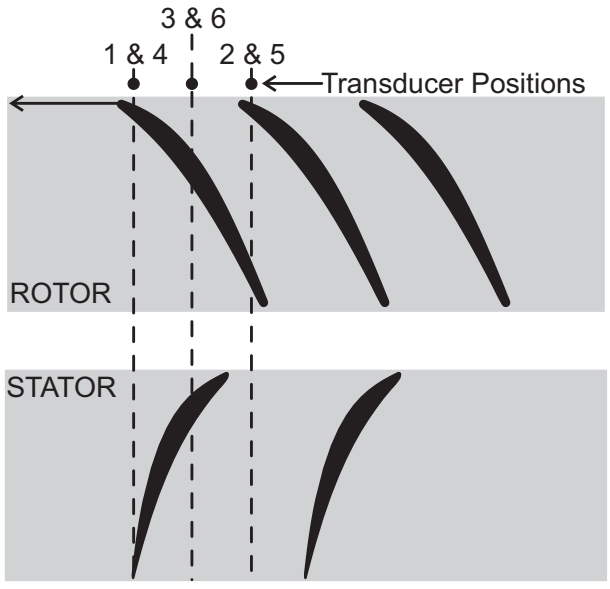

Diagram 6.1: *Positions of pressure transducers relative to stator blades.*

The results presented above show that the position of each pressure transducer relative to the downstream stator blades has a significant impact on the shape of the blade passing signal, even when the measurements are taken upstream of the rotor row. To remove any differences caused by this effect, care should be taken to ensure

Probe Numbers	Position Relative to Stator
1 & 4	Over trailing edge
2 & 5	Over blade near suction peak
3 & 6	Between blades

Table 6.1: *Positions of pressure transducers relative to stator blades.*

that all probes are at the same position relative to the stator blades, i.e. the number of measuring probes should be a proper fraction of the number of stator blades.

For this reason, the probe mounting positions in the test compressor were modified so that all the pressure transducers were at the same position relative to the stator blades. This was achieved by using eight or fourteen probes, to match the 56 stator blades, and by placing probes an integer number of pitches apart when more closely-spaced measurements were taken (see Chapter 7).

The importance of obtaining uniform signals from all the transducers will become clear when comparing signals from different circumferential locations.

6.2 Data Analysis

In order to measure the level of irregularity in the blade passing signature, unsteady data was recorded from a set of fourteen pressure transducers fitted to the casing at the same axial position as the rotor leading edge at the tip. The pressure transducers were evenly spaced around the circumference of the compressor and data was acquired at a fixed throttle setting for 45 revolutions.

The signal analysis process is designed to quantify the variation in the blade passing signal from the same blade on each successive revolution and is illustrated in Diagram 6.2. The Diagram shows a short section of data from one pressure transducer (in practice, an entire revolution's worth of data is used). First, the signal from the first revolution is plotted. The data from exactly one revolution later is then plotted on top, so that the blade passing signal of each individual blade can be compared with its own signal from the previous revolution, Diagram 6.2 (b). This plotting process is repeated for all 45 revolutions, and then the average blade passing signal is

computed, as shown by the red line in Diagram 6.2(c).

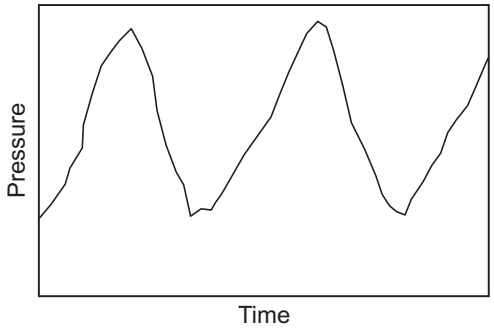

(a) Data from first revolution.

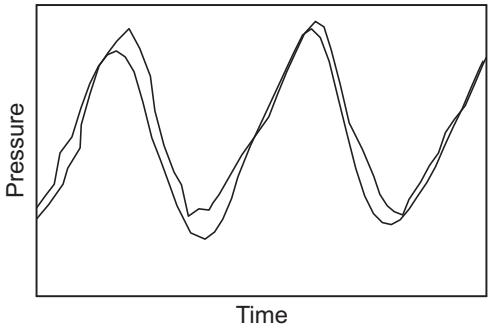

(b) Second revolution plotted on top.

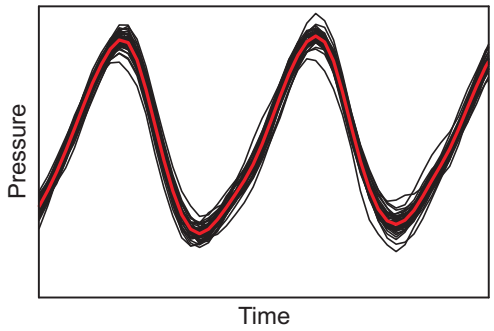

(c) All 45 revolutions and computed average.

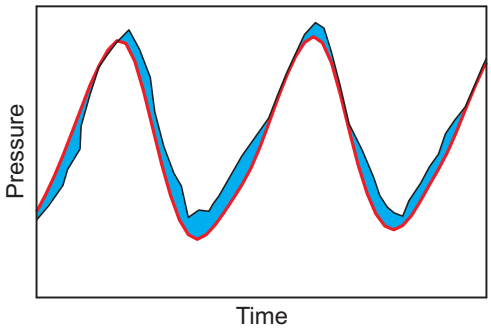

(d) Difference between average trace and individual revolution.

Diagram 6.2: *Data Analysis.*

If the pressure signal is given by p, where p(n,j) is the j$^{\text{th}}$ sample from the n$^{\text{th}}$ revolution (out of a total J samples and N revolutions), then the average trace is given by:

$$\bar{p}(\mathrm{j}) = \frac{1}{N}\sum_{n=1}^{N} p(\mathrm{n,j}) \tag{6.1}$$

Each of the 45 individual revolutions is then compared, in turn, with the average trace, and the difference between the two traces, δ(n,j), is found. This is shown in blue in Diagram 6.2(d). The RMS of this difference, δ_{RMS}, across the entire revolution is calculated, and then the mean of all 45 RMS differences is computed. The mean, $\bar{\delta}_{\text{RMS}}$, is non-dimensionalised by $\frac{1}{2}\rho U^2_{\text{mid}}$, in order to make it directly comparable to the total-to-static pressure rise across the stage. This final value is taken as a

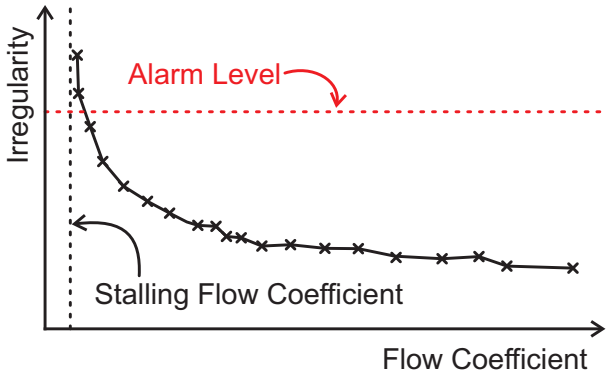

Diagram 6.3: *Sketch of irregularity against flow coefficient (data from one pressure transducer only).*

measure of the irregularity of the blade passing signal measured by this particular transducer. Each pressure transducer is analysed separately, so a value of irregularity is obtained for each probe (or for each circumferential location). The higher the value of irregularity, the greater the variation in the blade passing signal from one revolution to the next at this particular flow coefficient and transducer location.

$$\delta(\mathrm{n,j}) = \bar{p}(\mathrm{j}) - p(\mathrm{n,j}) \tag{6.2}$$

$$\delta_{\mathrm{RMS}}(\mathrm{n}) = \sqrt{\left[\frac{1}{J}\sum_{j=1}^{J}\left(\delta(\mathrm{n,j})\right)^2\right]} \tag{6.3}$$

$$\bar{\delta}_{\mathrm{RMS}} = \frac{1}{N}\sum_{n=1}^{N}\delta_{\mathrm{RMS}}(\mathrm{n}) \tag{6.4}$$

$$\text{Irregularity} = \frac{\bar{\delta}_{\mathrm{RMS}}}{\frac{1}{2}\rho U_{\mathrm{mid}}^2} \tag{6.5}$$

In order to build up an overall picture of how the repeatability of the blade passing signal changes as stall is approached, the irregularity measurement was repeated at about 20 flow coefficients from full-flow to near-stall. From this data, the variation of irregularity with flow coefficient was obtained. A hypothetical sketch of irregularity against flow coefficient for one pressure transducer is shown in Diagram 6.3. The crosses on the line represent the twenty constant flow coefficient points from open throttle to stall.

If the relationship between irregularity level and flow coefficient is as shown in Diagram 6.3, an alarm level could be set (as denoted by the dotted red line), to give stall warning when the compressor was within a certain margin of its stalling flow coefficient. This is the idea proposed by Dhingra et al. [66] and others [67] [69].

6.3 Stall Warning Measurements

In this section, the results of the study into the change in irregularity of the blade passing signature as stall is approached will be discussed. The results obtained from the compressor in its datum configuration will be presented first, followed by a study of the effects of tip-clearance size and eccentricity.

6.3.1 Datum Configuration

With the compressor in its datum, axisymmetric, configuration (i.e. a uniform tip-clearance of 1.7% chord), a small ramp-up in irregularity was observed as the compressor was throttled towards stall. This can be seen in Fig. 6.2, which is a plot of irregularity against flow coefficient. This ramp-up is similar to that observed by Christensen et al. [69] and Dhingra et al. [66], though here the rise in irregularity is small, especially compared to the stage pressure rise. It can be seen that there is some variation in ramp-up between the different pressure transducers. This variation is not thought to be of great significance and is probably caused, at least in part, by slight variations in the axial location of the pressure transducers (a drilling problem).

Figure 6.3 is a plot of near-stall irregularity against circumferential position for the datum configuration, i.e. the value of irregularity from each of the 14 pressure transducers at the measuring condition closest to stall, all the left-hand points in Fig. 6.2. It can be seen that there is no particular trend in irregularity level round the annulus. The broad grey line (horizontal) in Fig. 6.3 shows the envelope of the irregularity when the compressor is operating at full flow rate.

6.3.2 Effect of Tip-Clearance Size

The same irregularity tests were repeated with two larger levels of tip-clearance - 2.4% and 3.3% chord. The results for near-stall irregularity in a concentric compressor with increasing tip-clearance are shown in Fig. 6.4. The black lines show the data discussed above for the compressor with 1.7% clearance. With 2.4% clearance (blue lines), the pre-stall ramp-up starts further from the stall point of the machine, and the near-stall irregularity level is higher than before. The red lines show data from tests with 3.3% clearance. In this case, the ramp-up starts as soon as the flow-rate is reduced from full-flow and the near-stall level is higher still (note that the stalling flow coefficient increases as the tip-clearance is opened up).

Figure 6.5 shows the near-stall values of irregularity plotted against circumferential position. It can be seen that in all cases the level of irregularity near stall is approximately constant round the annulus, and that the irregularity level increases as the tip-clearance of the compressor increases. The lines in Fig. 6.5 are not perfectly constant because of small discrepancies in compressor geometry and probe position.

6.3.3 Effect of Eccentricity

As explained in Chapter 3, the casing of the test compressor can be offset to give a circumferential variation in tip-clearance. To illustrate the effect of tip-clearance asymmetry, with the tip-clearance set to 1.7% chord (datum level), the casing was moved to give a variation in tip-clearance around the annulus of 75% of the mean value.

The results from this test are shown in Fig. 6.6. It can be seen that the level in irregularity around the annulus is much more varied than in the concentric case, i.e. the left hand end points of the graph are spread out. The pressure transducers in the small tip-clearance region of the compressor show no real rise in irregularity, while the probes in and just after the maximum tip-clearance show a significant ramp-up as stall is approached. The maximum level of irregularity (green trace) is seen to occur just after the maximum tip-clearance.

To see the connection between local tip-clearance and irregularity more clearly, it is useful to plot the level of irregularity near stall against circumferential position. This

is shown in Fig. 6.7 for the concentric and eccentric configurations. In this graph, it is clear that the ramp-up in irregularity is confined to a sector starting just before the maximum tip-clearance and ending just before the minimum tip-clearance.

The compressor was also tested with more moderate levels of eccentricity. It was found that a peak in irregularity just after the maximum tip-clearance was the norm for all cases tested, even with as little as 10% eccentricity. The results clearly show that there will always be a ramp-up in irregularity as stall is approached in an eccentric compressor. This ramp-up is always confined to the large tip-clearance region of the annulus. Interestingly, no ramp-up at all is detectable in the small tip-clearance part of the annulus, even very close to stall.

Figure 6.7 shows that there is a phase lag of 30 - 70°between the maximum tip-clearance (which is at 180°) and the maximum level of irregularity (which is between 210 and 250°). This phase lag can be explained by considering the local stability of the compressor, as discussed in Section 5.5. In that section, a portion of the annulus was shown to be locally unstable when the eccentric compressor was operating close to stall.

The local stability is compared to the irregularity level in Fig. 6.8. Figure 6.8 (a) (a repeat of Fig. 5.11 (a)) shows a comparison between the local equivalent concentric stall point and the local flow coefficient around the annulus of the eccentric compressor operating near its stall point. The unstable sector, shaded in grey, represents the portion of the annulus over which the compressor is being forced to operate at a flow coefficient lower than its equivalent concentric stall point.

Figure 6.8 (b) shows the irregularity level around the annulus of the same compressor. The vertical grey lines which denote the start and end of the unstable sector in Fig. 6.8 (a) have been extended onto this figure for comparison. It can be seen that the irregularity level begins to rise at the start of the unstable region. Furthermore, the end of the unstable region coincides roughly with the location of the maximum irregularity. It appears that the irregularities grow in this unstable region and then begin to decay once the compressor becomes locally stable again.

6.3.4 Effect of Tip-Clearance Size with Eccentricity

In the sections above, the effects of tip-clearance size and eccentricity on the irregularity level of the blade passing signature have been presented. In this section, the effect of having a tip-clearance that is both large and eccentric will be discussed. The compressor was tested with eccentricity at three levels of average tip-clearance gap - 1.7, 2.4 and 3.3% chord. In each case a range of eccentricity levels up to 75% of the average clearance were tested. For the sake of clarity and brevity, only the results with 1.7% and 3.3% clearance and 75% eccentricity will be shown here.

Figure 6.9(a) shows results from the compressor with eccentricity equal to 75% of the average clearance with two different levels of average clearance: 1.7% and 3.3% chord. It can be seen that the maximum level of irregularity is approximately doubled between the case with average tip-clearance of 1.7% of chord (shown in red), and the case where the average tip-clearance is 3.3% chord (black line). The region over which there is little or no ramp-up in irregularity, near point B in Fig. 6.9(a), has become smaller in the case with larger average clearance, but still covers a sector of approximately 75°from the minimum clearance.

In terms of the absolute size of the tip-clearance gap, the minimum tip-clearance in the 3.3% average clearance case is approximately equal to the maximum clearance in the 1.7% clearance case, as shown by the dashed line in Fig. 6.9 (b). It is therefore interesting to compare the irregularity levels at three locations with the same local clearance - marked A, B and C. It can be seen that, out of the three positions, the irregularity is highest at position A (where the tip-clearance is at a maximum). The irregularity level measured at position C is slightly lower, and there is no ramp-up in irregularity at all at position B. This shows that the irregularity is not only a function of the local clearance, but of casing eccentricity as well.

It should be noted that the stall inception mechanism changed from spike to modal when the tip-clearance size was increased. This does not seem to have affected the observed pre-stall trends in irregularity.

From these results, it can be seen that the level of irregularity is not dependent on local tip-clearance alone, but on tip-clearance and the level of eccentricity. There appears to be a dynamic effect associated with the passage of the blades around the eccentric annulus which influences the irregularity level. Put another way, the

irregularity level appears to be affected by whether the blades are moving into a region of larger clearance or moving into a region of smaller clearance.

The dependence of irregularity level on tip-clearance size and eccentricity will have a profound impact on the design of any stall warning system based on measurements of blade passing irregularity. Considering the idea of defining a level of irregularity at which to trigger a stall warning alarm, it is clear that care must be taken when setting this level to take into account not only the local tip-clearance at the probe location, but also the size and relative position of any casing eccentricity.

The results shown above also go some way to explaining why some researchers see a clear rise in irregularity levels before stall but others do not. Compare the work of Dhingra et al. [66] and Gannon et al. [70], who differ over the question of a rise in irregularity before stall. Most research of this kind has been undertaken with one pressure transducer, and tip-clearance size and eccentricity have not been taken into account. It has been shown here, Fig. 6.9, that identical tests in compressors with different tip-clearance levels (or even the same clearance level but with the probe in different circumferential positions) will yield totally different results. Stall warning based on blade passing irregularity measurements is thus more complicated than originally envisaged by Dhingra et al. [66].

6.4 Effect of Axial Position on Stall Warning Results

The results shown so far have all been from pressure transducers at the leading edges of the rotor tips. However, the work of Dhingra et al. [66] found that the best transducer position for stall warning measurements was at mid-chord. The effect of axial position is important in a real engine, as the probe locations may be dictated by other design requirements (bleed slots, for example).

To test the effect of axial position on the blade passing irregularity, measurements were taken from a set of six pressure transducers 20% chord upstream of the rotor blades and from a set of eight pressure transducers (evenly spaced around the annulus) which were moved through six axial positions from the leading edge to the trailing edge of the rotor blades. Irregularity measurements were taken at approximately twenty stable operating points from full-flow to near-stall. For these tests, the

compressor had a small tip-clearance (1.7% chord), with 75% eccentricity. This set-up was chosen because it was a configuration in which measurements at the leading edge showed a marked ramp-up near stall at some circumferential locations but not others, so there was a greater chance of capturing any changes with axial position.

The data from the set of pressure transducers 20% upstream of the rotor blades showed the same patterns as the probes at the leading edge, but the signal was substantially smaller. This is because the blade passing signature decays rapidly away from the blades, so the signal size and the corresponding irregularities are smaller. From the data at 20% upstream of the rotor blades, it seems reasonable to conclude that probes positioned within 20% chord of the leading edge would be adequate for measuring the irregularity level. Any further upstream and the signal would probably be too small to be of any use.

The results of the tests at different positions over the rotor blade tips can be seen in Fig. 6.10, which shows plots of irregularity against flow coefficient for the six axial positions. Figure 6.10 (a) shows results with the probes at the leading edge, i.e. the same position that was used in the above work. Here, as discussed in Section 6.3.3, there is no ramp-up in the small tip-clearance sector, but a marked rise in irregularity in and just after the maximum tip-clearance.

The data from the probes at 20% chord downstream of the leading edge (Fig. 6.10 (b)) shows a higher near-stall irregularity level in the maximum tip-clearance than the leading edge results. However, the shape of the curve has also changed; the two lines showing data from the maximum tip-clearance and just after it (orange and green) show an initial ramp-up from $\phi = 0.5$ onwards, but the irregularity then levels off towards the stall point. The next probe round towards the small tip-clearance (blue) shows a continuously-rising level of irregularity. This result shows that it would be more difficult to use data from 20% chord than the leading edge data discussed above for stall warning, because the ramp-up begins further from stall, and the rate of change of irregularity with flow coefficient is erratic.

The results obtained with the transducers at 40% chord are shown in Fig 6.10 (c), where it can be seen that the near-stall irregularity levels are still higher than those recorded at the leading edge, but the shapes of the curves have changed again. The probe at the maximum tip-clearance point gives a near-linear increase in irregularity as the compressor is moved towards stall. Again, this data would be difficult to use

as part of a stall warning system because of the lack of a sudden rise in irregularity just before stall.

As the transducers are moved towards the rear of the compressor (Fig. 6.10 (d) - (f)), the near-stall irregularity levels fall, while the irregularity levels recorded at full-flow in the large tip-clearance region increase. This makes the ramp-up in irregularity almost non-existent. It is difficult to see how stall warning would be achieved using probes fitted aft of mid-chord.

The relationship between irregularity and circumferential position at the different axial locations is summmarised in Fig. 6.11. Again, it is clear that the highest irregularity levels are seen at 20% chord (represented by the red line). It can also be seen that the 'hump' in the curve becomes broader as the probes are moved back through the machine, i.e. there is less of a variation in irregularity levels between the large and small tip-clearance.

From this data, it is clear that a stall warning system will only work if the pressure transducers can be placed forward of mid-chord, and that the leading edge is the preferred location as the rise in irregularity here is steepest just before stall. Probes just upstream of the rotor leading edge (within 20% chord) could also be used.

6.5 Application to a Real Engine

In this section, data from a high-speed, multi-stage compressor will be examined. This will be followed by a discussion of engine life-cycle changes and the possibility of designing a reliable stall warning system.

6.5.1 High-speed Data

In order to examine the possibility of stall warning based on blade passing irregularity in a real engine, the data analysis technique described in Section 6.2 was applied to measurements from the NEWAC Compressor - a modern high-speed, six-stage compressor[1]. Data was acquired from 14 pressure transducers spaced over the six

[1]Measurements taken by Rolls-Royce Plc. as part of the NEWAC European Project.

stages (note that there were only two or three probes per stage, which is not enough to capture all the trends seen in the low-speed tests above). Again, unsteady data was taken at stable operating points between the working line and the surge line, and the irregularity of the blade passing signature was measured. These tests were carried out between 79 and 90.5% compressor speed with varying amounts of bleed taken from between stages 3 and 4. Some tests were also done with a new stability system involving air injection ('rotor blowing') in stages 1 and 2.

The overall performance of the compressor over the speed range is shown in Fig. 6.12. It can be seen that the surge point varies greatly with speed and bleed rate. For this reason, the graphs of irregularity to be shown in this section have an x-axis which represents the percentage mass flow away from stall for that particular configuration. This means that the level of irregularity at a given stall margin can be compared between test cases.

In nearly all the tests, the stalling process began in the first or second stage. An example of stall inception is shown in Fig. 6.13, which shows the stall cell starting in stage 1 and quickly propagating through the entire machine. This data is from a test at 79% speed with 3.5% bleed.

With high levels of bleed (16.5% and above), the stall was initiated in stage 4 of the compressor. This is to be expected as the front stages are operating at a higher mass flow rate than the stages downstream of the bleed, and so they are further from their individual stall points. The impact of the location of stall onset on the blade passing irregularity will be discussed below.

Blade Passing Signature

The ensemble-averaged blade passing signature taken from data near the working line for 84% speed, 3.5% bleed is shown in Fig. 6.14 for all 14 pressure transducers. The signals from each stage are shown in a different colour, with stage 1 at the bottom in blue and stage 6 at the top in pink. It can be seen that the signatures of individual blades are much more clearly-defined at the front of the machine, and that there is less variation from one blade to the next than in the rear stages. There is a sinusoidal variation in the magnitude of the signal in stages 5 and 6. The reasons for this are unclear.

As well as an increase in variation from one blade to the next, the repeatability of the blade passing signature drops towards the rear of the compressor. This means that the signal from each blade is less regular from one revolution to the next. This is demonstrated in Fig. 6.15 (a), which is a graph of irregularity level against stage number for two operating points at 84% speed with 3.5% bleed, one near the working line and one near the surge point. At both operating points, it can be seen that the irregularity level increases towards the rear of the compressor.

When the irregularity level is non-dimensionalised by the stage inlet total pressure, as shown in Fig. 6.15 (b) the level through the machine is more constant. This shows that, while the actual size of the fluctuations increases towards the rear of the machine, the increase is roughly in line with the rearward increase in density and pressure. Nevertheless, the higher absolute level of irregularity and greater difference between the working line and near stall in the rear stages of the compressor (Fig. 6.15 (a)) mean that measurements from the rear stages may be more useful for stall warning.

Now that the levels of irregularity at the working line and near surge in a typical case have been examined, the effect of changing the speed of the compressor and the bleed rate will be investigated. The implications of the results for a stall warning system based on irregularity level will also be discussed.

Effect of Compressor Speed

The data analysed here was taken at 79% and 84% speed (note: 90.5% is the design speed of the compressor). Graphs of irregularity against stall margin (based on flow rate) for each stage are shown in Fig. 6.16.

The relationship between speed and blade passing irregularity is not the same in all stages of the compressor. In the front stages, the irregularity level drops with increasing speed (red to black lines). This is logical because the front stages are more unstable at lower compressor speeds. There is no clear link between speed and irregularity in the rear stages, where the variation between probes in each stage is larger than the variation between speeds.

From the data at different speeds, it is clear that any stall warning system based on

the level of irregularity in the blade passing signature would have to be adjusted for each compressor speed because the ramp-up in irregularity changes with speed. It should also be noted that the ramp-up in irregularity is not very pronounced in any of the graphs in Fig. 6.16. A stall warning system which make tries to make use of signals which hardly change from the working line to stall will not be very effective.

Effect of Bleed Rate

Figure 6.17 shows the effect of bleed rate on irregularity at 79% speed, while Fig. 6.18 shows the same data at 84% speed.

At both speeds, it can be seen that the bleed level has a profound effect on the irregularity level in stage 4, which is immediately downstream of the bleed slots. In stage 4, the irregularity level does not necessarily rise as the operating point moves towards the surge line. This is because the blade passing signal is being dominated by disturbances and radial redistribution due to the bleed flow. The wide range of irregularity levels recorded in stage 4 is particularly apparent in Fig. 6.18 (d), which shows data from tests with 5 different bleed rates at 85% speed. This result reinforces the conclusion that stage 4 would not be a suitable location for obtaining stall warning measurements.

In the stages before the bleed offtake (stages 1 to 3), the effect of bleed tends to lower the irregularity level in the blade passing signature. This is to be expected, because the bleed has a stabilising effect on the front stages of the machine, by increasing the mass flow rate in these stages. In the rear two stages (5 and 6), the irregularity level is less affected by the bleed level, and the ramp-up as stall is approached is fairly consistent between test cases. This result suggests that stages 5 and 6 may be the most promising stages from which to obtain stall warning measurements.

Discussion

As has been shown above, there are changes in the pre-stall level of blade passing irregularity when the compressor changes speed and/or bleed rate. This leads to additional complications when designing a stall warning system for a high-speed, multi-stage machine, which will be considered here.

Because of the large effect of bleed on the irregularity levels in the first four stages, the best stages for installing a stall warning system would be stages 5 and 6. This is likely to be a general rule for any compressor - a stall warning system will be most successful in stages well downstream of any bleed offtakes.

If the rear stages are chosen, it may not be necessary to adjust the alarm level for bleed rate. As an example, consider the data from 84% speed (see Fig. 6.18). Examination of Fig. 6.18 (d) shows that the ramp-up in stage 5 changes very little with bleed rate. At this speed, if probe 2 in stage 5 were to be used for stall warning, an alarm level of 0.6% of stage inlet total pressure would give warning when the compressor was operating with corrected mass flow 0.5 - 2% from stall. If this were to be an acceptable range of stall margin at which the warning would occur, then the same alarm level could be used regardless of bleed rate. This result means that it might only be necessary to adjust the alarm level for the compressor speed, but care would need to be taken with this approach.

As stated above, stall tends to originate in stage 1 of the machine over the speed range tested here, except at very high bleed rates. It is interesting that stage 1 does not provide the most useful irregularity data for stall warning. This suggests that there is no solid link between irregularity and stall proximity, and any pre-stall ramp-up observed is a coincidence. This lack of a link between the stage which initiates stall and the irregularity levels in that stage casts doubt on the whole concept of this kind of warning system.

From the measurements, it can be seen that the multi-stage environment provides additional complications for stall warning as the irregularity level and size of any pre-stall ramp-up will vary from stage to stage, from speed to speed and from bleed rate to bleed rate.

Furthermore, the increase in irregularity from the working line to near stall tends to be small and gradual – there is generally no pronounced ramp-up in activity just before stall. This suggests that, based on the limited data available, it would be difficult to implement a reliable stall warning system in a high-speed machine.

6.5.2 The Prospects for Stall Warning in a Real Engine

In addition to the negative conclusions reached above, it will be useful to consider how the levels of tip-clearance and eccentricity change over the life of an engine. By returning to the data from the laboratory tests with different levels of tip-clearance and eccentricity, an assessment can be made of the likely impact of these changes on a stall warning system based on blade passing irregularity measurements.

A new engine operating on a test-bed will typically have small tip-clearances, and it will be relatively concentric. The relationship between irregularity and flow coefficient for this case is illustrated in Fig. 6.19(a) (the results from just three pressure transducers have been selected for clarity). The red dotted line shows an alarm level which would give warning when the flow coefficient was 1% above the stall point.

Thrust from the engine is transmitted to the aeroplane through the pylon which connects the engine to the wing. At certain points during the flight cycle, these forces become large enough to bend the engine casing (for example at take-off). This means that the compressor tip-clearance will become eccentric.

Figure 6.19(b) shows the same pressure transducers for a compressor with 75% tip-clearance asymmetry (still with small average clearance). This time, two of the pressure transducers will not trigger the alarm before the compressor stalls, while the third, which is just after the maximum tip-clearance, will set the alarm off at a flow coefficient 5% before stall – an excessive margin. Permanent tip-clearance asymmetry can also be caused by engine damage from hard landings and surge events. Again, this asymmetry will change the pre-stall ramp-up in irregularity.

Finally, towards the end of the engine's life, the blade tips will have rubbed and the tip-clearance will be larger. Fig. 6.19(c) shows irregularity against flow coefficient in a compressor with twice the normal tip-clearance and 75% eccentricity. In this case, one of the pressure transducers (in the tight tip-clearance) will fail to trigger the alarm, while the other two will trigger the alarm well before stall.

From the measurements presented above, it is clear that a stall warning system based on one pressure transducer at a fixed location (i.e. the system that has been patented by General Electric [3]) would fail to give reliable results under different flight conditions. On the other hand, the use of more than one transducer could lead to any

number of false alarms. In order to use blade passing signature analysis for stall warning, it is likely that at least one other parameter would have to be measured – tip-clearance size or eccentricity, for example – and care would have to be taken to ensure that bleed and any other sources of irregularity were accounted for.

Alternatively, if the problem is considered from another angle, an engine health warning system might be conceived. As blade passing signature irregularity is known to be a function of tip-clearance size and eccentricity (as well as bleed, speed and flow-rate, all of which can be measured), irregularity measurements could be used to measure the deterioration in tip-clearance through the life of the engine.

6.6 Conclusions

A detailed study has been carried out of the seemingly erratic way in which the blade passing signature of each rotor blade in an axial compressor is different from its neighbour – and from itself in the previous revolution. In this Chapter, the relationship between the level of blade passing irregularity and the proximity to stall of the compressor has been investigated for concentric and eccentric compressors. The following conclusions can be drawn:

1. The position of downstream stator blades relative to the measuring probes can change the magnitude and shape of the blade passing signature, even when measurements are taken upstream of the rotor bladerow. This is an important finding which has not previously been reported in the literature.

2. For the first time, a systematic study of blade passing signature irregularity has been carried out in a compressor with different levels of tip-clearance and casing eccentricity. The key findings are:

    a. The level of blade passing signature irregularity in a concentric compressor, with small tip-clearance, is generally low and rises very little as the compressor approaches stall.

    b. In a concentric compressor with large tip-clearance, however, the level of irregularity is low at full flow, but ramps up noticeably as the flow rate is reduced.

c. In an eccentric compressor, the level of blade passing irregularity in the large tip-clearance sector of the annulus will ramp up strongly as the compressor is throttled towards stall. By contrast, the irregularity will remain small and steady in the tight tip-clearance part of the annulus – this is true regardless of the actual size of the gap in this region.

d. In an eccentric compressor the blade passing irregularity will always be largest just after the blades pass the position of maximum clearance.

3. The above behavioural patterns appear to be unaffected by the fact that, at large tip-clearances, the stall inception mechanism will change from spikes to modes (see Section 4.2).

4. It has been found that the maximum level of irregularity in an eccentric compressor coincides roughly with the end of the unstable sector, where, at near-stall conditions, part of the annulus is operating at a lower flow coefficient than its natural stall point (see Section 5.5). Furthermore, the point at which the level of irregularity begins to rise coincides with the start of the unstable sector. This finding suggests that the irregularities form and grown throughout the unstable sector of the annulus and then begin to decay once the compressor becomes locally stable again.

5. It has been shown for the first time that the level of blade passing irregularity in an eccentric compressor is influenced by the average tip-clearance size *and* by the amount of casing eccentricity. There is a dynamic aspect to the level of blade passing irregularity which is not solely dependent on the size of the local tip-clearance. The irregularity level thus depends on whether the blades are passing into a region of large clearance or leaving it.

6. The optimum axial location for the probes in a stall warning system was found to be level with the rotor leading edge. While this is not the location with the highest near-stall irregularity, it is the position that gives the clearest pre-stall ramp-up in irregularity. Tests at different axial locations showed that probes mounted aft of mid-chord would not give useful data for stall warning, but probes at locations up to 20% chord upstream of the leading edge could be used.

7. Similar patterns in blade passing irregularity have been found by applying the same analysis to measurements from a high-speed compressor. In this case,

the irregularity level was found to be influenced by additional factors such as compressor speed and bleed rate, as well as stall proximity. Furthermore, the measurements also show that the general level of irregularity increases from the front to the back of the compressor and that this increase is in proportion to the rise in total pressure through the machine.

8. The experimental results from this work show that the level of irregularity in the blade passing signature cannot be used on its own to provide reliable stall warning in a real engine - at least one other parameter would have to be measured. This leads to the conclusion that any stall warning system based on the irregularity of the blade passing signature is unlikely to work. However, it is possible that blade passing irregularity could be used as part of an engine health monitoring system, to check tip-clearances in the compressor after a period of time in service.

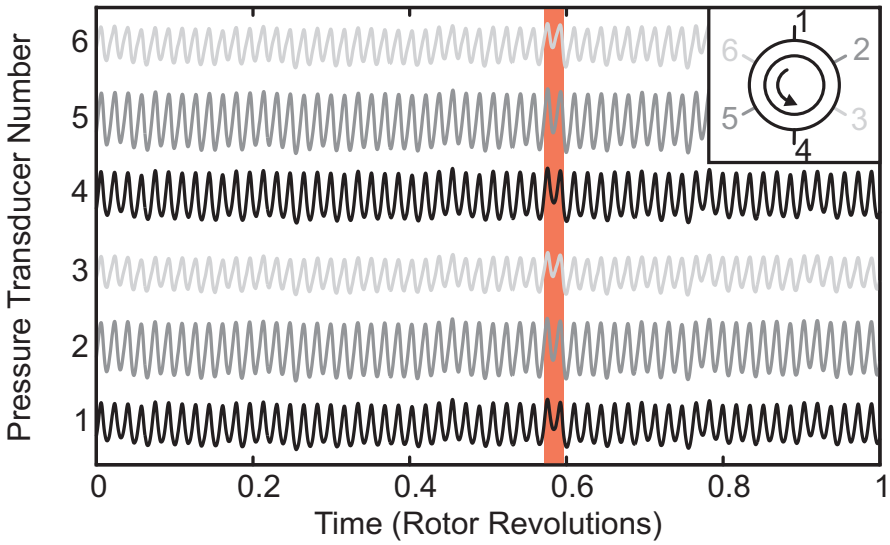

(a) Whole revolution.

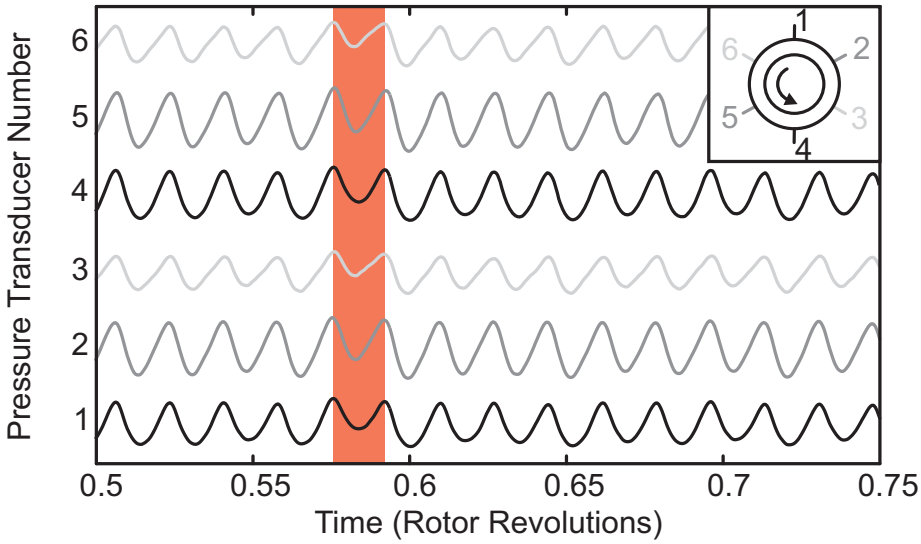

(b) Part-revolution.

Figure 6.1: *Example of ensemble-averaged blade passing signature around the annulus of the compressor.*

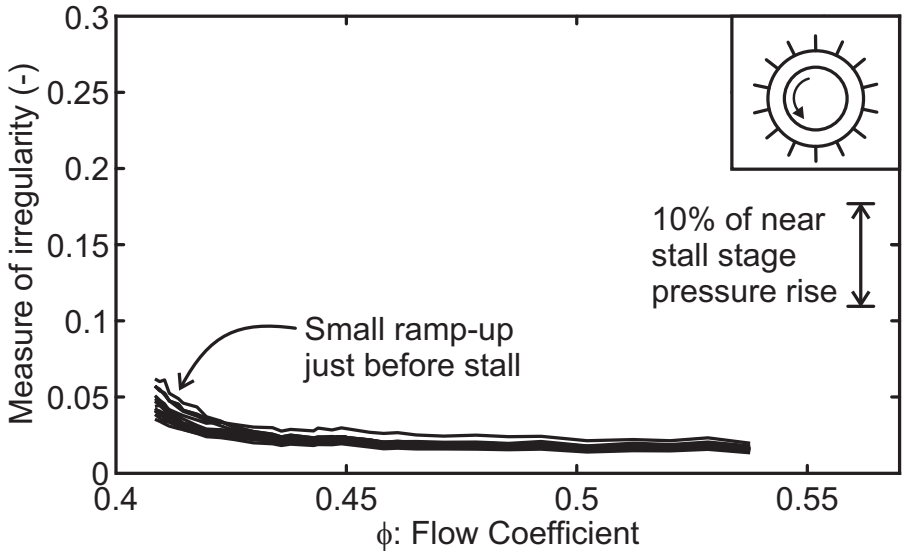

Figure 6.2: *Irregularity against flow coefficient for the datum concentric compressor (tip-clearance 1.7% chord; 0.6 mm).*

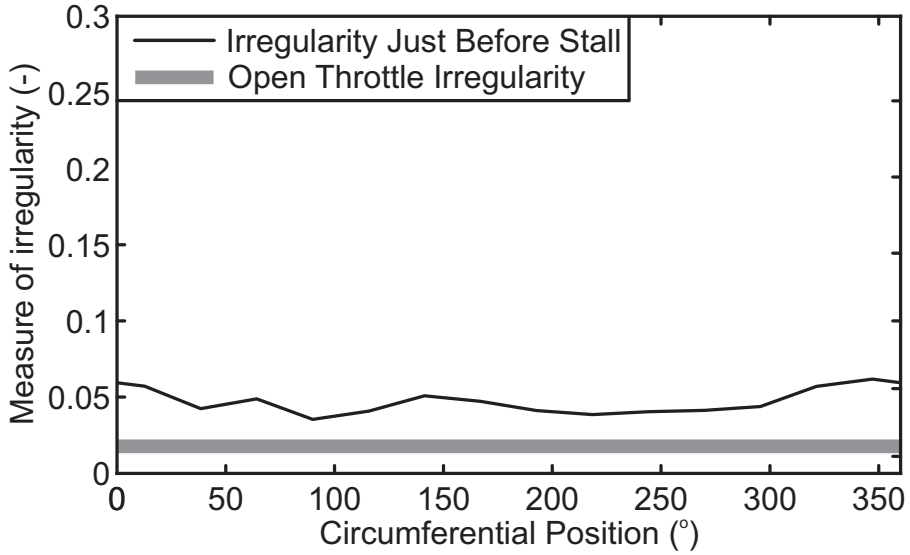

Figure 6.3: *Near-stall irregularity against circumferential position for the datum concentric compressor (1.7% clearance).*

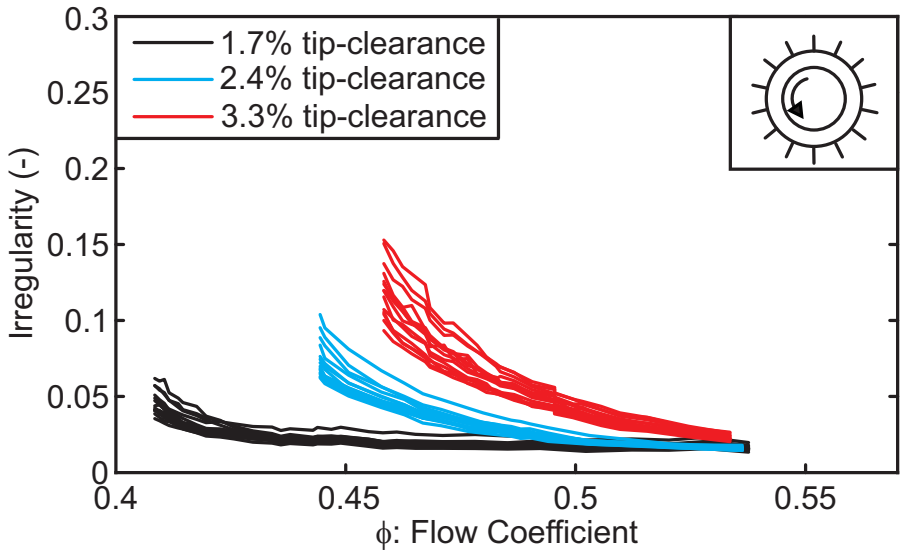

Figure 6.4: *Irregularity against flow coefficient with different levels of average tip-clearance (concentric).*

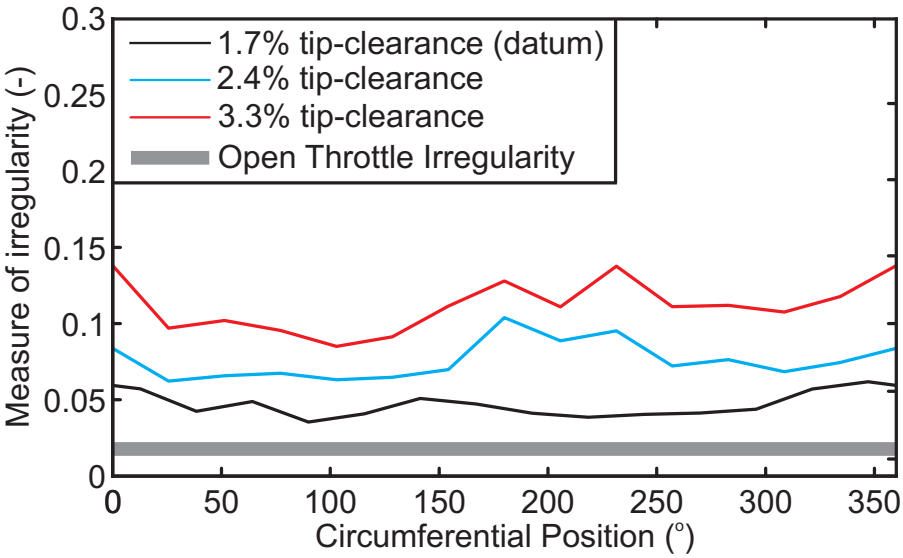

Figure 6.5: *Near-stall irregularity against circumferential position with different levels of average tip-clearance (concentric).*

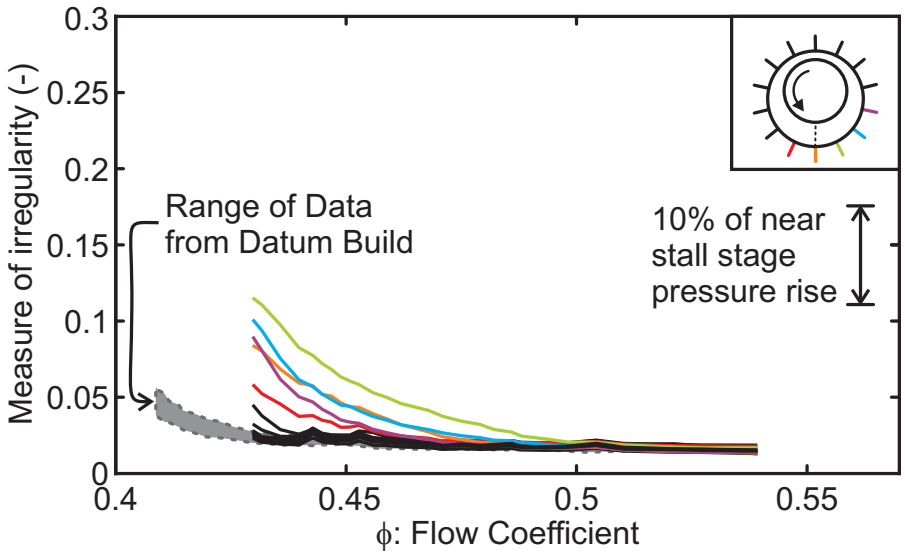

Figure 6.6: *Irregularity against flow coefficient for the compressor with eccentric tip-clearance (1.7% clearance, 75% eccentricity).*

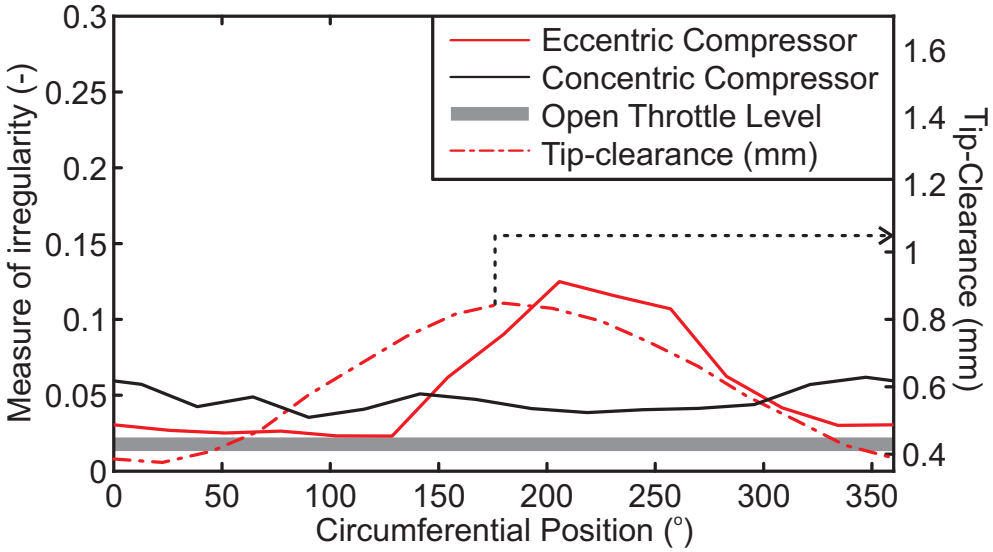

Figure 6.7: *Near-stall irregularity against circumferential position for concentric and eccentric compressors (1.7% clearance).*

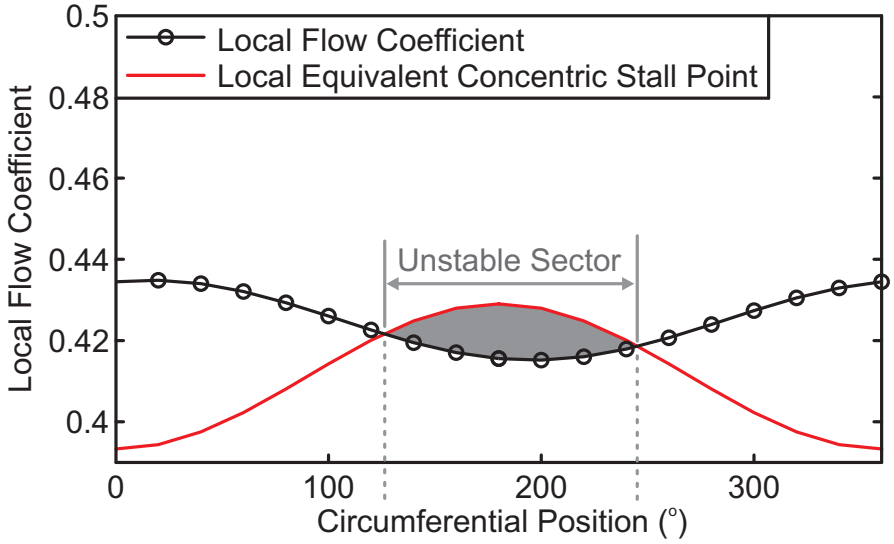

(a) Local stability.

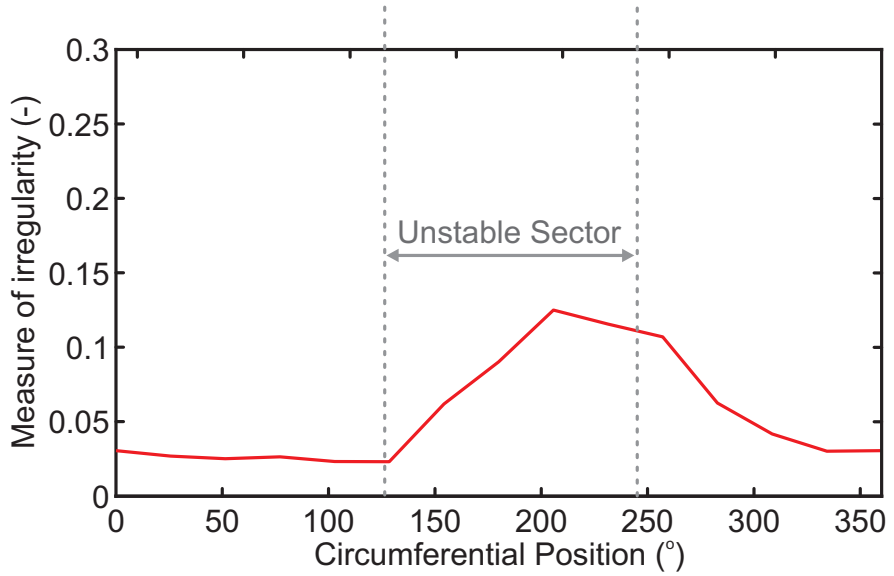

(b) Local irregularity level.

Figure 6.8: *Comparison of local stability to irregularity level at near-stall conditions in an eccentric compressor (1.7% clearance, 75% eccentricity).*

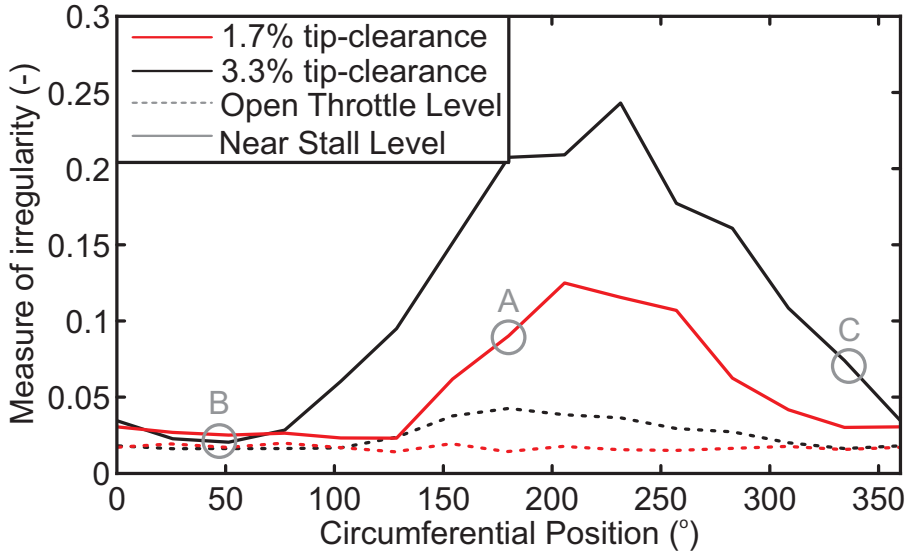

(a) Irregularity levels at open throttle and near stall operating points.

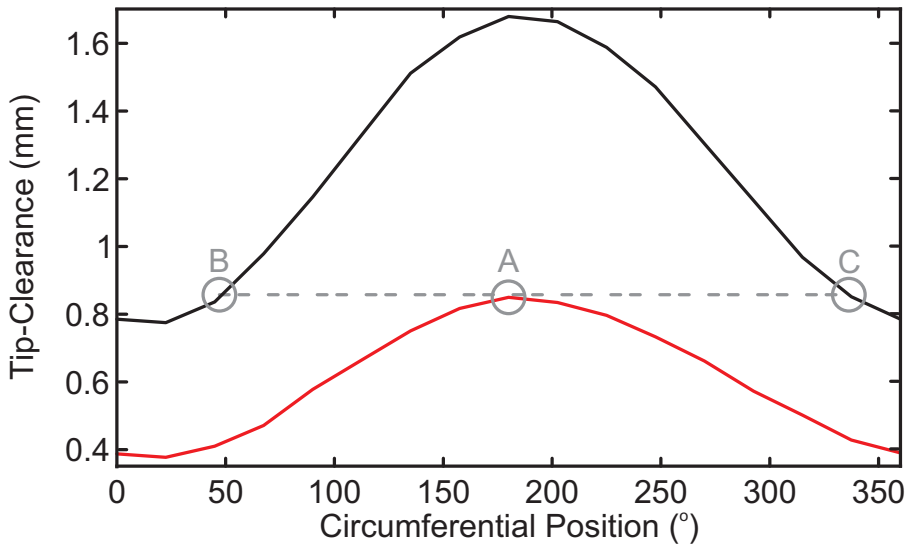

(b) Tip-clearance distributions.

Figure 6.9: *Comparison of near-stall irregularity levels with two levels of average tip-clearance (75% eccentricity).*

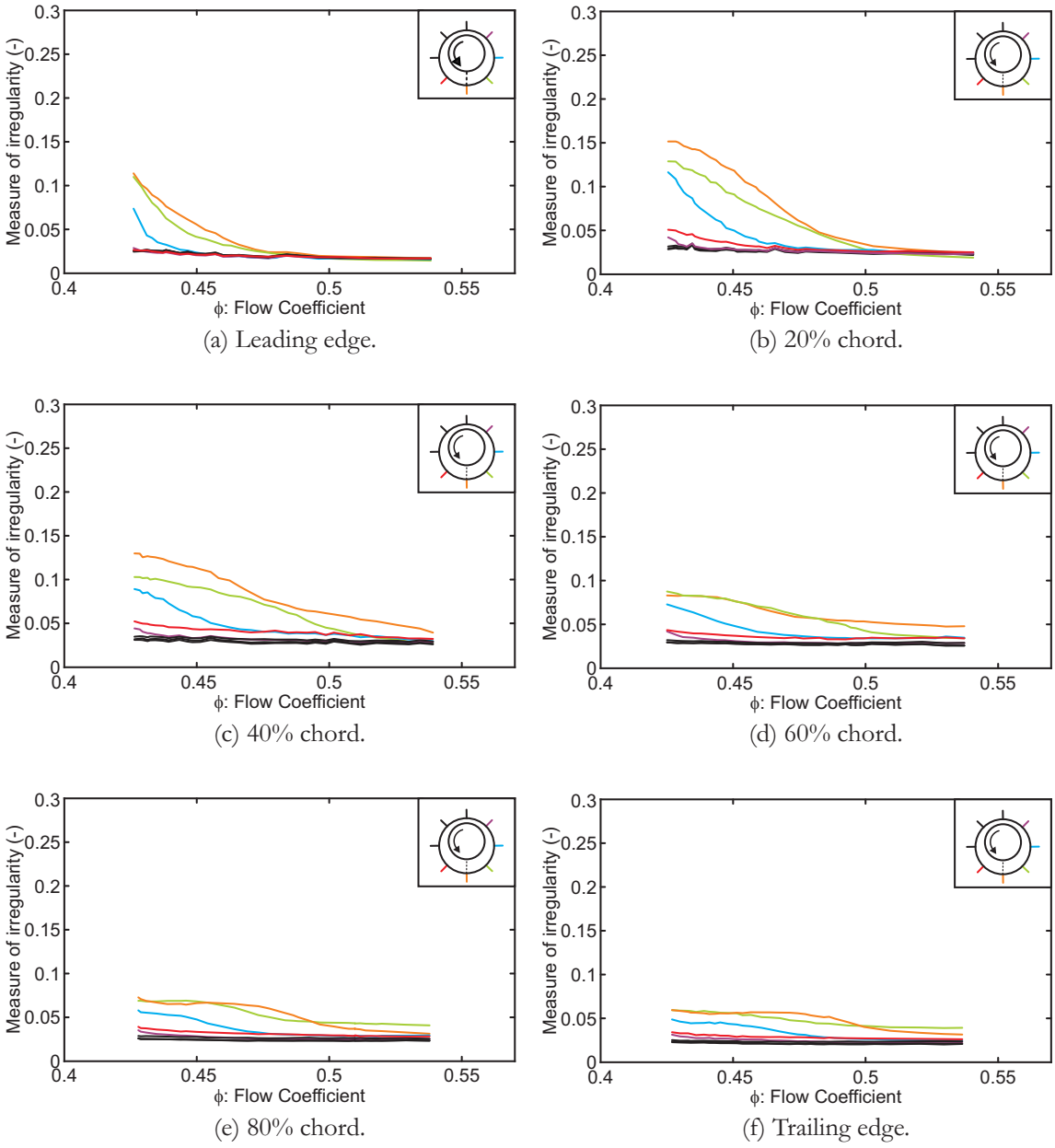

(a) Leading edge.

(b) 20% chord.

(c) 40% chord.

(d) 60% chord.

(e) 80% chord.

(f) Trailing edge.

Figure 6.10: *Irregularity against flow coefficient for different axial positions (1.7% clearance, 75% eccentricity).*

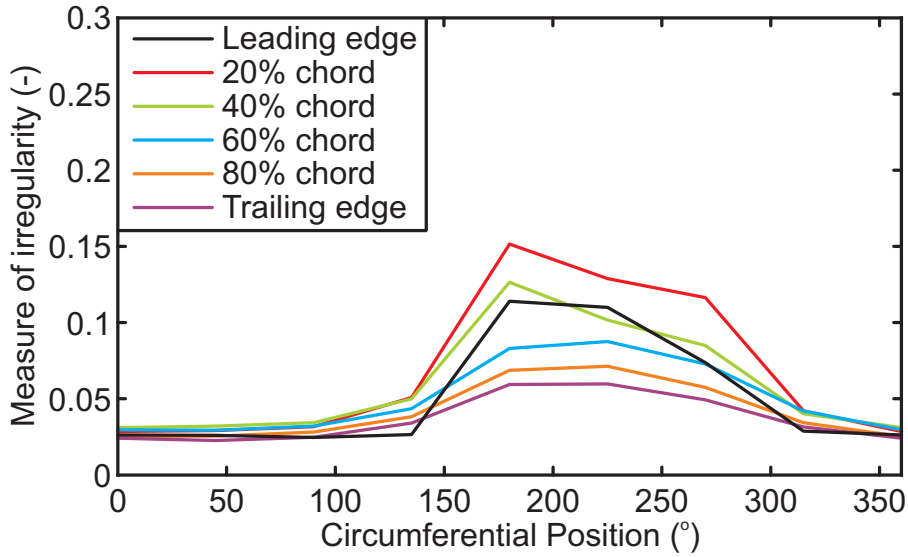

Figure 6.11: *Near-stall irregularity against circumferential position for different axial positions (1.7% clearance, 75% eccentricity).*

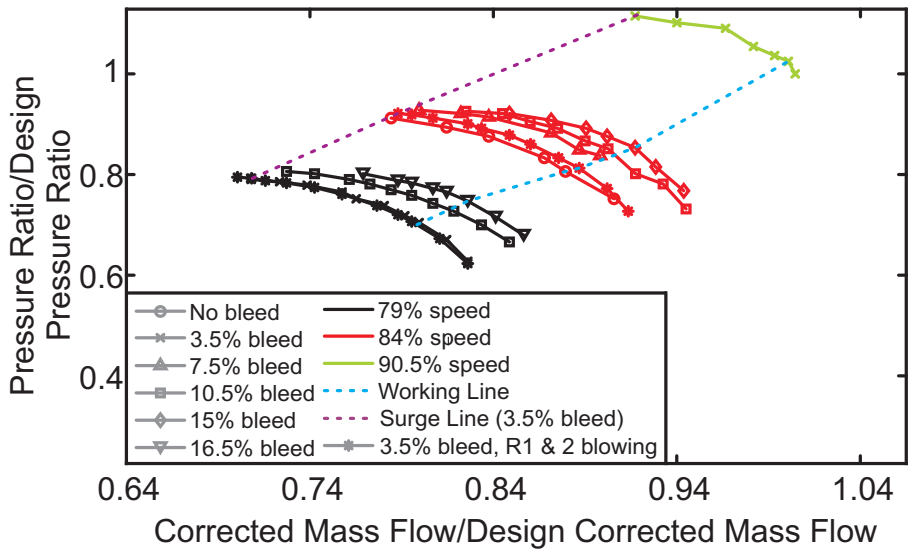

Figure 6.12: *Pressure rise characteristics from the NEWAC compressor.*

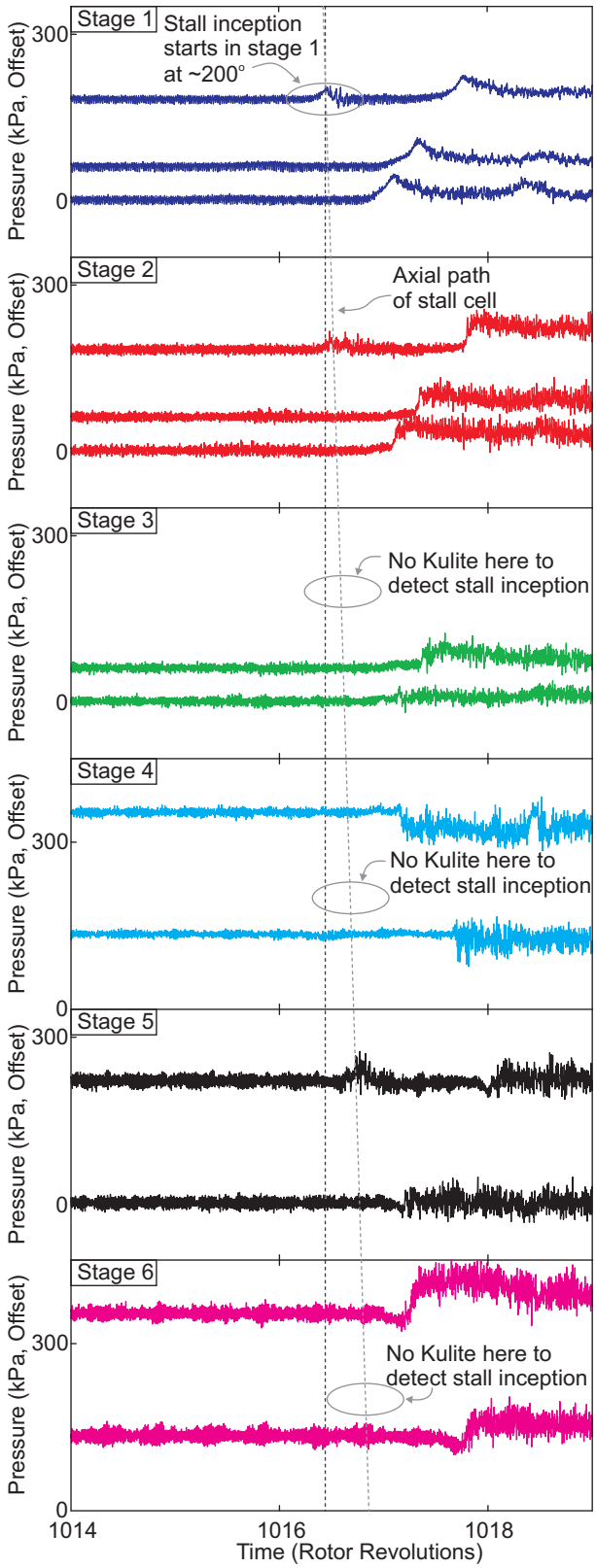

Figure 6.13: *Stall inception in the NEWAC compressor starting in stage 1 and propagating through the compressor (79% speed, 3.5% bleed).*

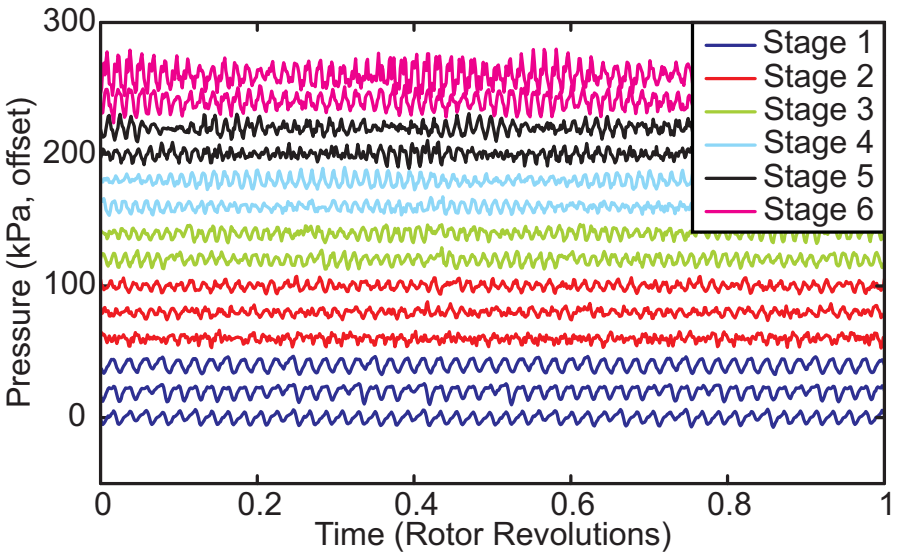

Figure 6.14: *Ensemble averaged blade passing signature from the NEWAC Compressor near the working line (84% Speed, 3.5% bleed).*

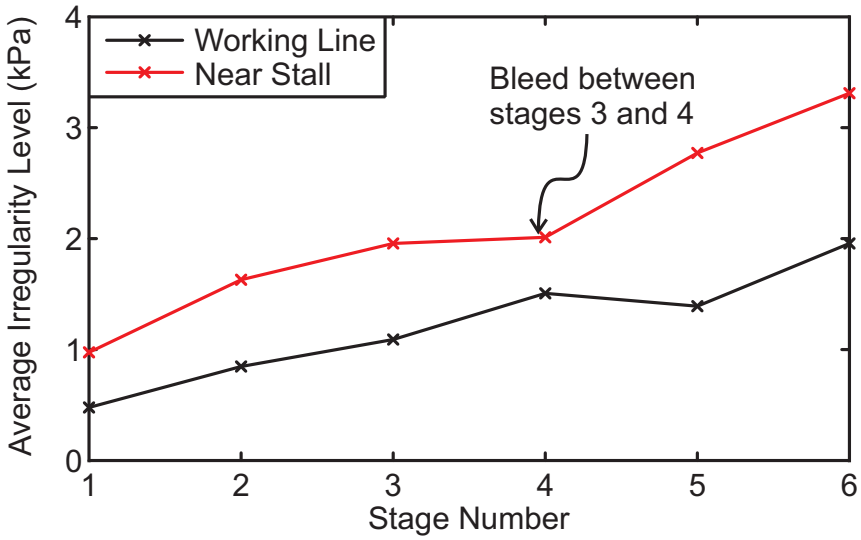

(a) Absolute level (kPa).

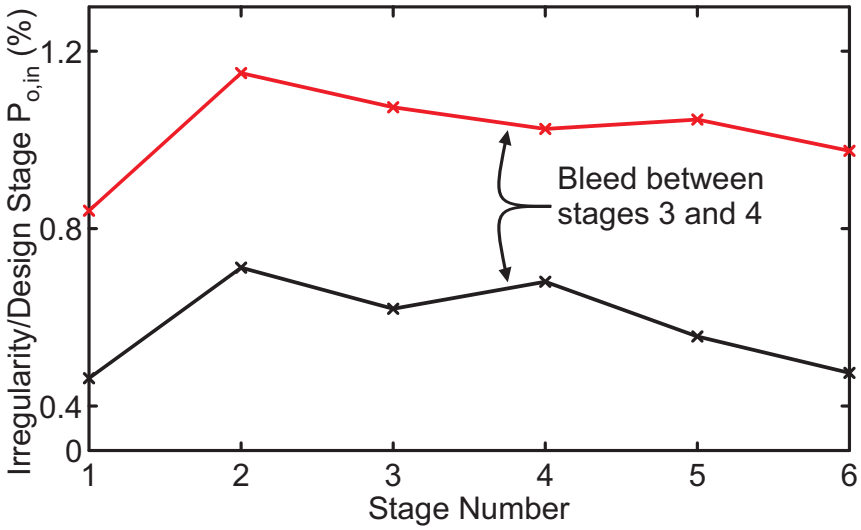

(b) Non-dimensionalised by stage inlet total pressure.

Figure 6.15: *Irregularity against stage number for the NEWAC compressor (84% speed, 3.5% bleed).*

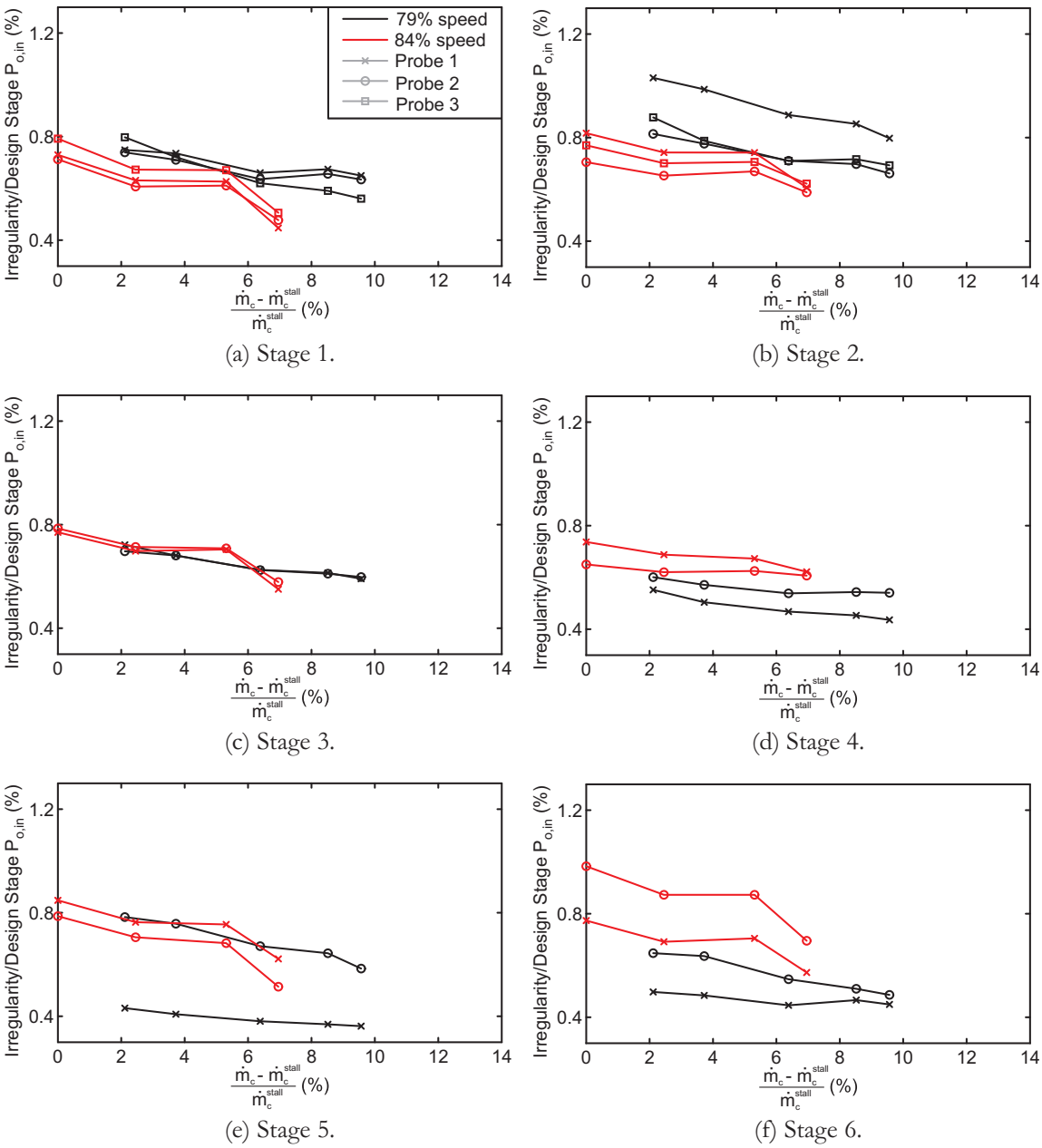

(a) Stage 1.

(b) Stage 2.

(c) Stage 3.

(d) Stage 4.

(e) Stage 5.

(f) Stage 6.

Figure 6.16: *Irregularity against flow rate for different speeds in the NEWAC compressor (3.5% bleed).*

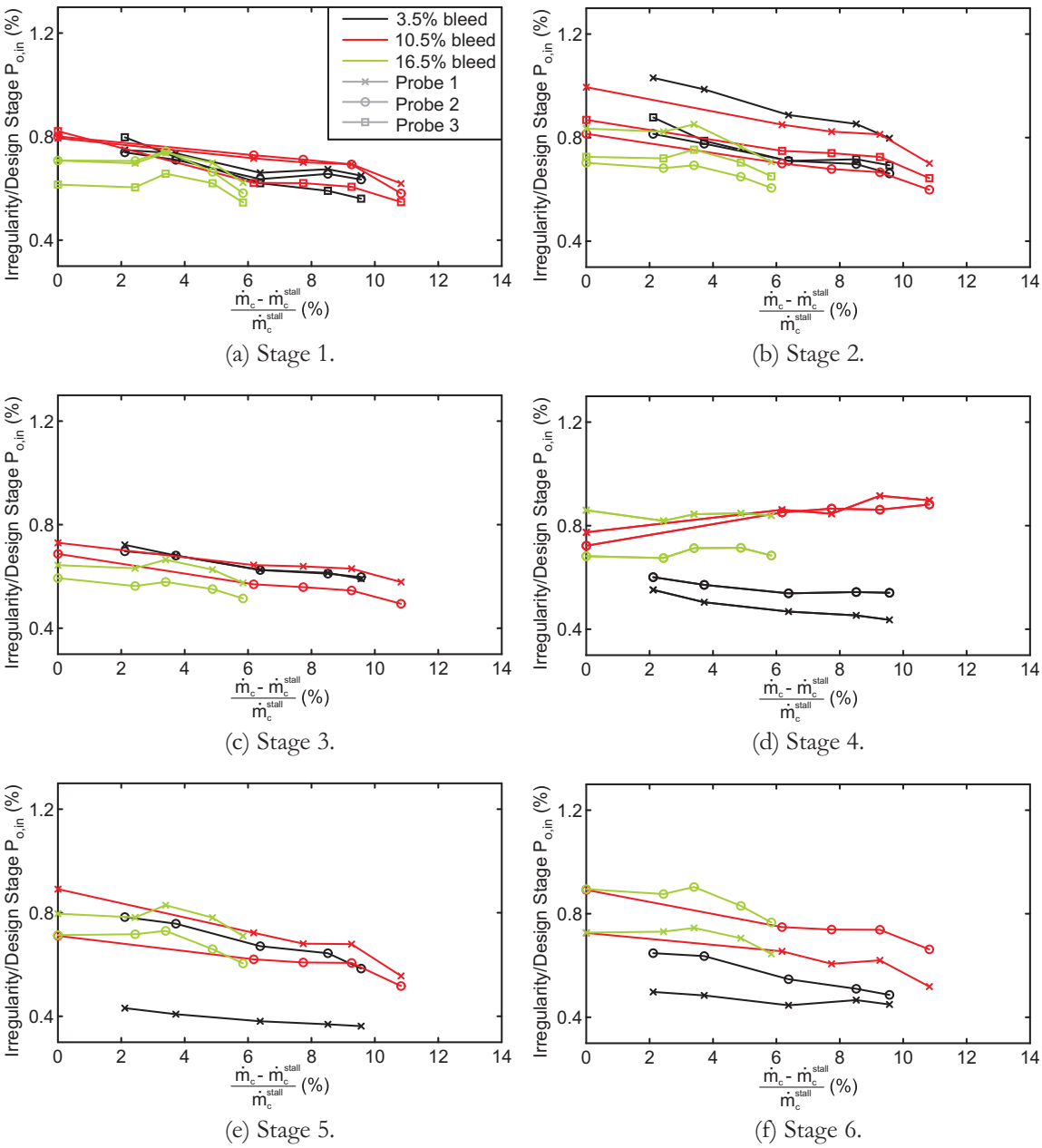

(a) Stage 1.

(b) Stage 2.

(c) Stage 3.

(d) Stage 4.

(e) Stage 5.

(f) Stage 6.

Figure 6.17: *Irregularity against flow rate for different bleed rates in the NEWAC compressor (79% speed).*

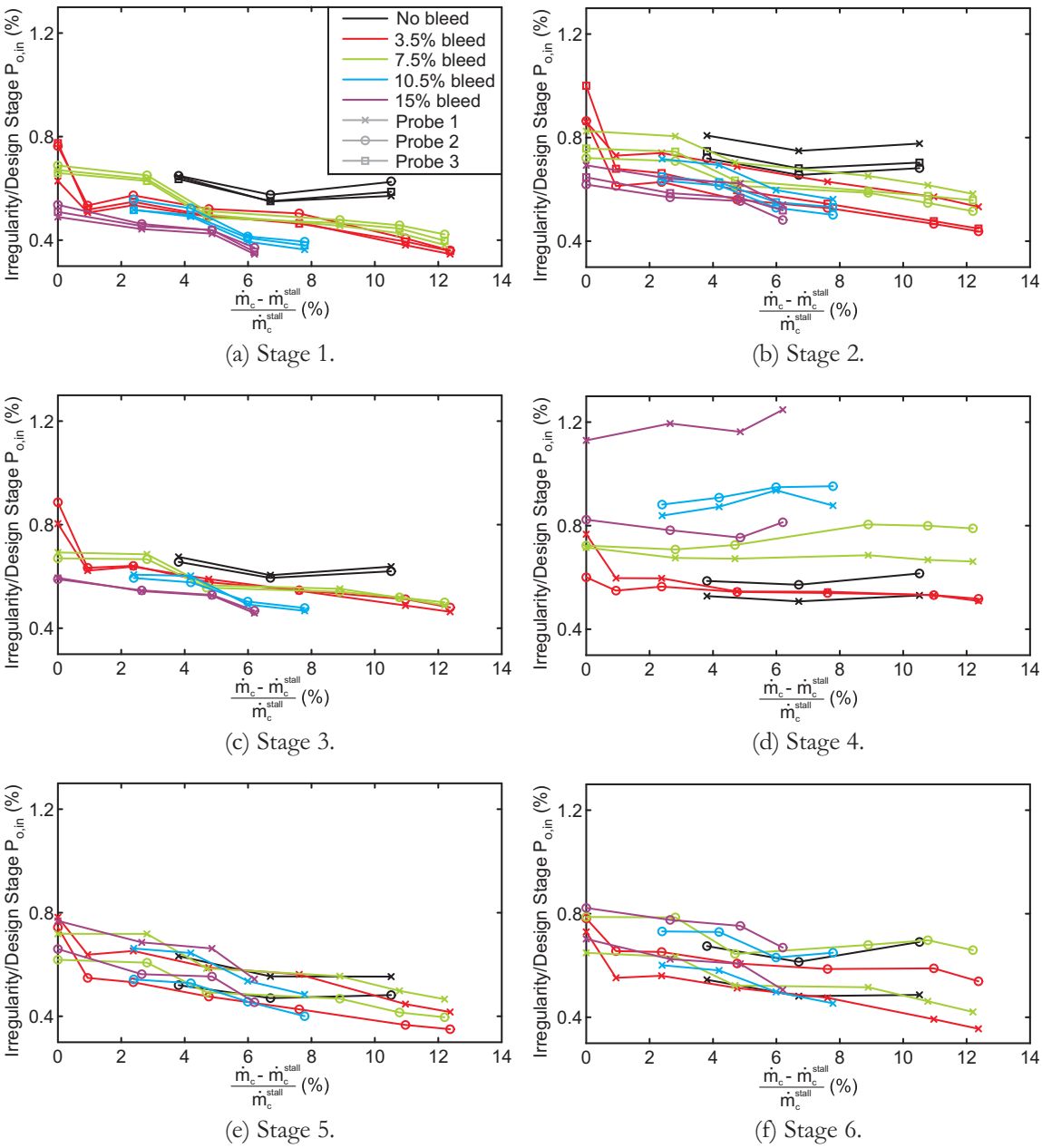

(a) Stage 1.

(b) Stage 2.

(c) Stage 3.

(d) Stage 4.

(e) Stage 5.

(f) Stage 6.

Figure 6.18: *Irregularity against flow rate for different bleed rates in the NEWAC compressor (84% speed).*

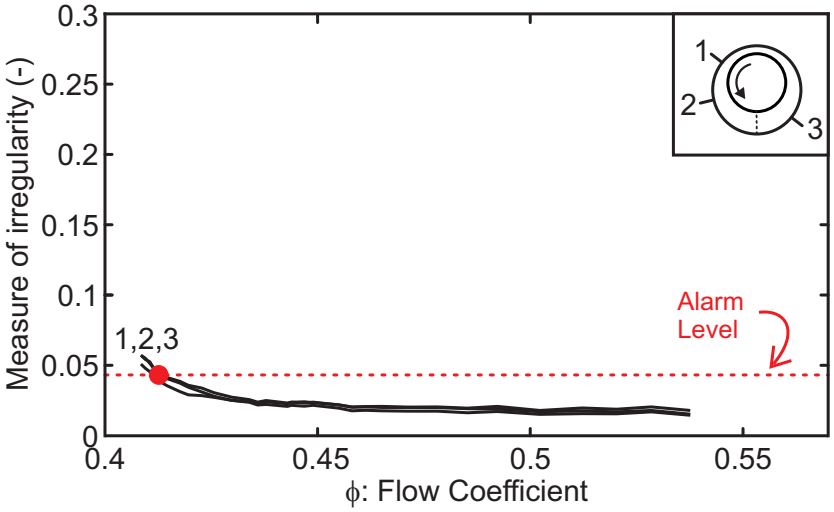

(a) Concentric compressor with 1.7% tip-clearance.

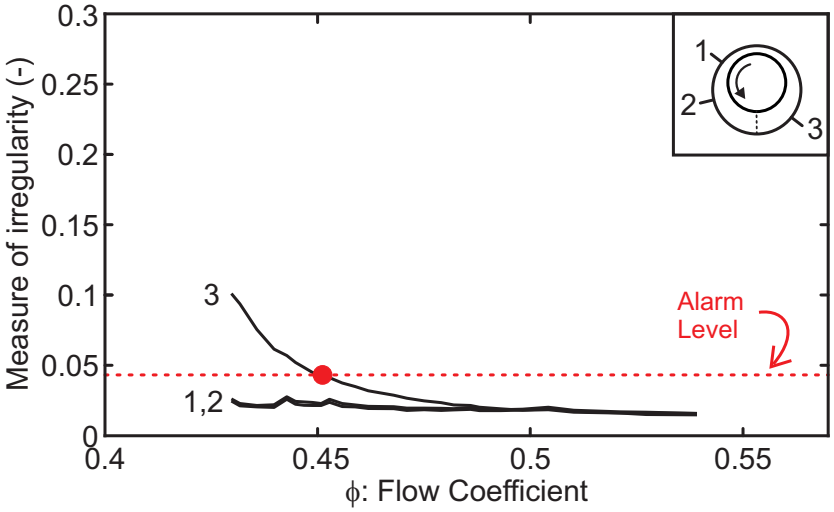

(b) Eccentric compressor with 1.7% tip-clearance.

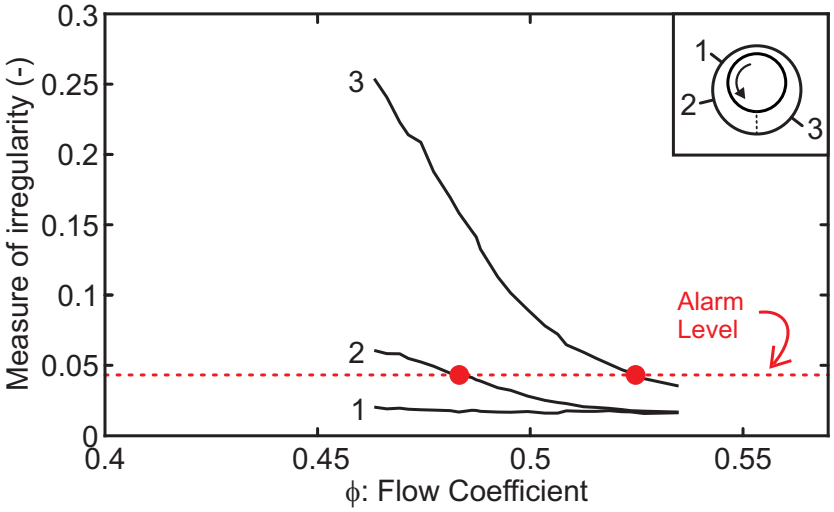

(c) Eccentric compressor with 3.3% tip-clearance.

Figure 6.19: *Effect of changing tip-clearance on a stall warning system with a fixed alarm level.*

Chapter 7

The Cause of Irregularity in the Blade Passing Signature

In the previous chapter, it was shown that there is an increase in irregularity in the blade passing signature as stall is approached. The extent of this increase, or ramp-up, has also been shown to be strongly dependent on both the tip-clearance size and eccentricity in the compressor.

Notwithstanding the problems in implementing a stall warning system based on irregularity that were discussed in Section 6.5.2, if such a system were to be designed then two questions must be answered first: what is the cause of the irregularity? and is there a link between the cause of the irregularity and stall inception? This chapter answers the first question, and the next chapter will address the second.

Previous work on stall warning has concentrated on measuring the rise in irregularity, but little attention has been paid to the *cause* of the irregularity itself, i.e. is it due to structured disturbances in the flow or simply due to a general increase in turbulent fluctuations? Furthermore, most work in this area has relied on Fourier analysis, as opposed to direct measurement of the flow features. This chapter presents the results of a detailed study into the underlying cause of the irregularity.

The results shown in this chapter are mostly from high-frequency casing static pressure measurements. First, the frequency content of these measurements will be examined to see whether there is a dominant frequency in the disturbances. The casing static pressure field over the rotor tips will then be examined to reveal, in unprece-

dented detail, the existence of discrete low-pressure disturbances which are the cause of the irregularity.

It will also be shown that the newly-identified disturbances propagate around the annulus, and that they initially form within the blade passage and move towards the rotor leading edge plane as the compressor operating point is pushed towards stall.

Once the existence of these disturbances has been proven, the changing flowfield around the annulus of a compressor with eccentric tip-clearance will be discussed. The effect of changing average clearance size will also be shown.

The factors affecting the propagation speed of the disturbances will also be examined, as well as the mechanism by which they propagate. This leads on to a discussion of the structure of the disturbances which is backed up by computational results from Dr Graham Pullan. Finally, a comparison of this work with previous research will be made.

7.1 Disturbances in a Concentric Machine

In this section, the cause of the rise in irregularity in a concentric machine with large clearance (3.3% chord) will be considered. This configuration has been chosen because there is a significant ramp-up in irregularity as stall is approached, so any disturbances should be easy to identify.

7.1.1 Frequency Content

Before embarking on a detailed measurement campaign, the frequency content of the casing static pressures was analysed to see whether there was a particular frequency that was present during times of high irregularity. The Fourier transform of a perfectly regular blade passing signal in a machine with identical blades would contain only the blade passing frequency and its harmonics. An additional frequency, measured in regions of high irregularity, would suggest a structured disturbance as opposed to a general increase in turbulent fluctuations (which would cause an increase in all frequencies).

Fourier transforms of data taken from a pressure transducer positioned at the rotor leading edge plane are shown in Fig. 7.1. The data in Fig. 7.1 (a) was taken at full flow, where the irregularity level in the blade passing signal is fairly low, while Fig. 7.1 (b) is from a near-stall operating point, where the irregularity level is much higher (see Chapter 6).

In Fig. 7.1(a), the blade passing signature can be seen as a sharp spike at just under 3kHz and there is a small hump at approximately one third of blade passing frequency. In Fig. 7.1(b), the blade passing signature is still clearly visible, but the hump at 1kHz is now much bigger. The humps at around 2 and 4kHz are harmonics of the large frequency content at 1kHz.

This data shows that the rise in irregularity as the compressor operating point is moved towards stall is accompanied by a large increase in activity at one third of the blade passing frequency. The hump, although broad in frequency content, suggests the possibility of a coherent structure to the disturbances, as opposed to a simple increase in turbulence.

7.1.2 Flow Structure of the Disturbances

In order to investigate the cause of the increased frequency content, measurements were taken from 40% chord upstream of the rotor leading edges to 60% downstream of the leading edge, as shown in Diagram 7.1. In preliminary tests, it was found that there was little irregularity downstream of the mid-chord position, so no measurements were taken in this region. This arrangement allowed for more instrumentation elsewhere.

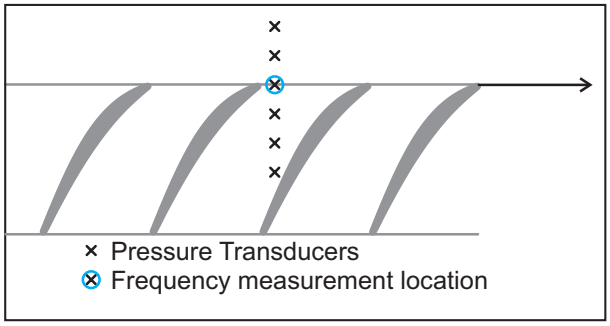

Diagram 7.1: *Measuring positions for detailed casing pressure measurements.*

At this point, a brief note about the behaviour of the fast-response pressure transducers is necessary. While the calibration gradient of the transducers was found to be stable to within 1% over long periods of time, the zero level was found to drift to such an extent that the average pressure levels were not reliable. For this reason, static pressure probes were installed at the same axial locations and the steady pressure levels from these probes (D.C.) were added to the fluctuations from the fast-response pressure transducers (A.C.) to give a signal that both captured the high-frequency fluctuations and had a reliable mean value.

Before examining the measurements with high levels of irregularity, it will be useful to consider an example of the instantaneous static pressure on the casing in a 'quiet' machine with low irregularity levels. Such a measurement is shown in Diagram 7.2 (a), which is a contour plot of the pressure fluctuations caused by the passing of the blades. It can be seen that there is a regular rise and fall of pressure as each blade passes, and that all the blades behave in a similar manner.

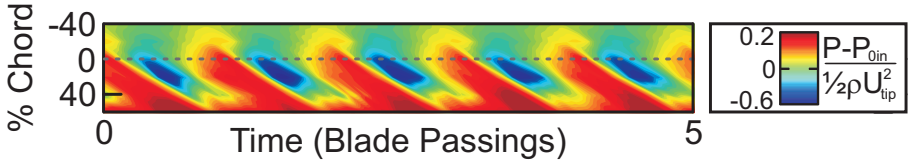

(a) Instantaneous Static Pressure.

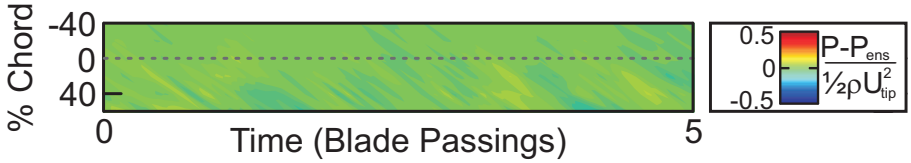

(b) Ensemble-average removed.

Diagram 7.2: *Casing static pressure measurements before and after removal of ensemble-average.*

An alternative way of looking at the data is to subtract the ensemble-averaged pressure signal from the plot itself so that only the irregularities remain. This process is demonstrated in Diagram 7.2 (b), which was created from the same raw data as Diagram 7.2 (a). As expected, there is very little to see in Diagram 7.2 (b), because this data was purposely chosen to have a low irregularity level.

We now consider data taken from a concentric compressor with large tip-clearance (3.3%) operating near stall - a configuration in which high irregularity levels are observed - Fig. 7.2. Figure 7.2(a) shows instantaneous static pressure measurements which are much less regular than those in Diagram 7.2 (a). It is still just possible to

discern the passing of individual blades, but there are also large deviations from the expected pressure pattern. In particular, some passages appear to have low-pressure disturbances in them, which are not present in Diagram 7.2 (a).

A clearer picture is obtained in Fig. 7.2(b), which is a plot of the same data with the ensemble-average removed. In this plot, the disturbances show up clearly as intense patches of low pressure (or 'blue holes'). These 'blue holes' appear every two to three rotor blade passings, occupy roughly half a blade pitch and extend from the leading edge to 40% chord. The depression in static pressure represented by the blue holes is of approximately the same magnitude as the inlet dynamic head of the compressor, i.e. these blue holes create an extremely large deviation from the expected pressure level.

The most likely cause of these sudden low pressure patches is a radial vortex. This will be discussed in more detail in Section 7.5.3, where measurements from downstream of the rotor bladerow will be considered, and in Section 7.6, where a comparison will be made between the experimental data shown in this chapter and some computational simulations by Graham Pullan.

7.1.3 Propagation of the Blue Holes

The question now arises; do the disturbances (the blue holes) form and die in quick succession, or are they coherent structures which propagate around the annulus?

To answer this question, data from three closely spaced sets of pressure transducers (see Diagram 7.3) were analysed for signs of propagation. Three contour plots are shown in Fig. 7.3, where the blue holes can be seen to move, along the dotted lines, from one measuring location to the next.

We now consider the propagation speed of the blue holes and the spacing between the blue holes in the absolute frame of reference (i.e. as seen by the stationary pressure transducers). The speed, spacing and characteristic frequency (see above) of the blue holes can be combined to find their spacing in the rotor relative frame.

The propagation speed of the blue holes is found by measuring the time taken for

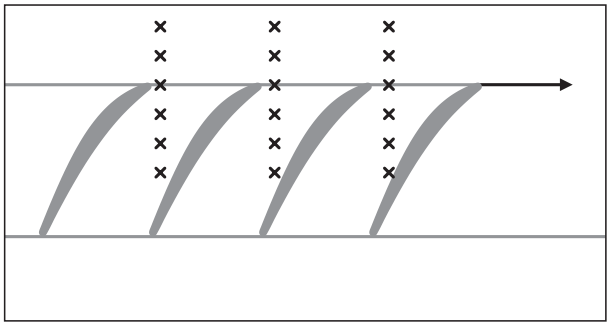

Diagram 7.3: *Measuring positions for propagation tests.*

each disturbance to pass from the first set of pressure transducers to the third set. From this measurement, the average propagation speed was found to be 46% of blade tip speed, though there was significant scatter in the data.

From the Fourier transforms, the dominant frequency of the disturbances can be seen to be approximately 1030Hz, which is just over a third of the blade passing frequency. The circumferential spacing of the disturbances can then be found by dividing the propagation speed by the frequency from the Fourier transform. This gives an average spacing of 1.3 rotor pitches.

As the disturbances are propagating at just under 50% of rotor speed with a spacing of about 1.3 rotor pitches, they will appear at each measuring location every 2-3 rotor pitches. This is consistent with the blue hole spacing seen in Fig. 7.3. Factors affecting the propagation speed of the blue holes and the mechanism by which they propagate will be discussed in more detail below.

7.1.4 Growth

So far, the blue holes have been shown to exist at near-stall conditions in a concentric compressor with large clearance. In this tip-clearance configuration, the ramp-up in blade passing irregularity begins at full flow conditions and ramps up gradually as stall is approached (see Fig. 6.4). This means that if the irregularity in the blade passing signal is caused by blue holes, then the blue holes should also be visible (in some lesser form) at full flow conditions.

The existence of blue holes in the compressor across the entire operating range is shown in Fig. 7.4. The figure shows contours of casing static pressure measurements

with the ensemble-average signal removed. Measurements are shown from four flow coefficients between full flow and near stall.

In Fig. 7.4 (a), which shows data from the full flow operating condition, pale blue patches can be seen approximately every three blade passings. These patches appear to be embryonic blue holes. At this flow coefficient, the blue holes are well behind the leading edge plane. At the design point, shown in Fig. 7.4 (b), the blue holes are more recognisable; being both 'deeper' (i.e. having lower pressure at the centre) and larger in axial and circumferential extent. They are still, however, well aft of the leading edge.

Data from halfway between the design point and stall point (ϕ = 0.480) is shown in in Fig. 7.4 (c), where again the blue holes are deeper and larger than before. At this point, the blue holes are still mainly downstream of the leading edge of the blades. By Fig. 7.4 (d), which shows data taken near stall, the blue holes are very clear and are level with, or slightly upstream of, the leading edge.

Comparing the four plots in Fig. 7.4, as the compressor operating point is moved towards stall, the blue holes grow in axial and circumferential extent and become deeper. They also move closer to the rotor leading edge plane.

Considering now the blade passing irregularity level and the size of the blue holes at each operating point, it can be seen that the there is agreement. The level of irregularity rises from full flow to near-stall, while the blue holes are small at full flow and large near stall. This suggests that the blue holes are, indeed, the cause of the irregularity.

7.2 Disturbances in an Eccentric Machine

Having observed the behaviour of the blue holes in a concentric machine with 3.3% clearance, the changing flowfield round the annulus of an eccentric compressor (again with 3.3% average clearance, but with 75% eccentricity) will be examined. In this configuration, the compressor showed a large pre-stall ramp-up in irregularity in the part of the annulus just after the maximum tip-clearance, but no ramp-up at all in the small tip-clearance sector of the annulus (see Fig. 6.7).

The change in irregularity levels around the annulus means that blue holes should only be seen in the large tip-clearance part of an eccentric compressor. To test this theory, the measurements undertaken in the concentric machine described in Section 7.1 were repeated at eight evenly-spaced locations around the annulus so that the circumferential changes could be observed. As with the concentric measurements, the frequency content of the signals from the rotor leading edge will be considered first, followed by an analysis of blue hole activity around the annulus.

Figure 7.5 shows the Fourier transforms of the signals from one of the pressure transducers at the leading edge plane in each of the eight locations around the annulus (denoted by the blue circle in Diagram 7.1). The data shown was taken with the compressor running near stall (ϕ = 0.465, 0.6% above stall).

It can be seen that the pressure transducers in the small tip-clearance sector (Fig. 7.5(a) and (b)) show very little frequency content apart from the blade passing frequency (around 2900 Hz). In the large tip-clearance sector, however, a broad peak centred on approximately 1000 Hz is clearly present (plots (c) to (g)). This broad band peak reaches a maximum just after the maximum tip-clearance. This coincides with the location at which the highest level of blade passing irregularity is observed in the raw data. As with Fourier transforms from the concentric machine, the average frequency of this peak is approximately 30% of the blade passing frequency.

An example of the casing pressure contours at each of eight locations around the circumference is shown in Fig. 7.6, which shows contours of raw static pressure (without the ensemble-averaged signal removed). The data was acquired with the compressor operating near stall (ϕ = 0.465, 0.6% above stall). In Fig. 7.6(a), which shows data from just after the minimum tip-clearance, there is a clear rise and fall in pressure as each blade goes past, and no significant departure from the regular blade passing pattern. In this region of the compressor, the measured level of blade passing irregularity near stall (Fig. 6.7) was very low.

At positions further round the annulus, where the tip-clearance gap is larger, the regular rise and fall of pressure as each blade passes becomes less clear. In Fig. 7.6(c), it seems that every third blade has lost a significant proportion of its lift (as denoted by the lack of blue in every third passage). In the data from the maximum tip-clearance (Fig. 7.6 (d) and (e)), the blade passing signal is no longer the major feature of the pressure traces. Instead, low-pressure patches appear approximately every

three blade passings. Figure 7.6 (e) shows the static pressure contours at the location where the highest irregularity level is recorded (see Fig. 6.7). After this point, the blade passing signal becomes clearer and more predictable as the rotor blades move back into the small tip-clearance region. In Fig. 7.6 (h), the blade passing signal is almost regular again.

Figure 7.7 shows the same data as Fig 7.6 but with the ensemble-average removed. This makes the blue holes easier to observe. In Fig. 7.7 (a) and (b), there are almost no discernible irregularities, as expected from the very regular blade passing signal in Fig. 7.6 (a) and (b). In Fig. 7.7 (c) and (d), where the blade passing signature is less repeatable and the irregularity level starts to rise, small blue holes begin to appear aft of the leading edge.

In the data from the maximum tip-clearance (Fig. 7.7 (d) and (e)), these disturbances have grown in both size and intensity, covering half a blade pitch and the forward part of the chord. Figure 7.7 (e) shows the disturbances at the location where the irregularity level recorded in Chapter 6, Fig. 6.7, is highest.

In Fig. 7.7 (h), some small disturbances are still visible. This data is from a part of the annulus with approximately the same tip-clearance level as Fig. 7.7 (a). The disturbance level here is, however, higher because the blades are moving towards the minimum tip-clearance not away from it. As discussed in Section 6.3, this shows that the disturbances are linked to some sort of dynamic effect, and are not just dependent on the local tip-clearance.

The results shown here for an eccentric compressor add substance to the argument presented in Section 7.1 that the blue holes are the cause of the blade passing irregularity observed in Chapter 6. At near-stall conditions, blue hole activity is observed in the same regions as those where high levels of irregularity were detected (i.e. the large tip-clearance sector). Furthermore, blue holes are not detected in those parts of the annulus where the irregularity level remains low (near the minimum clearance). Furthermore, the largest and deepest blue holes are seen just after the maximum tip-clearance, where the highest levels of blade passing irregularity were observed in Chapter 6.

7.3 Effect of Changing Average Tip-Clearance

7.3.1 Larger Clearances

Irregularity measurements similar to those discussed in Chapter 6 were taken in the compressor with larger tip-clearances, i.e. at 4.2, 4.9 and 5.8% chord. Both concentric and eccentric cases were investigated. It was found that the same patterns existed in these machines, i.e. the irregularity level increased with increased average clearance, but in an eccentric machine the near-stall level of irregularity is low in the small clearance sector of the annulus and high in the maximum tip-clearance sector.

When the blue hole measurements were repeated with the larger clearances, the results were similar in terms of the circumferential spacing and axial and circumferential extent of the 'blue holes', but the minimum pressure at the centre of each hole was lower with larger tip-clearances, i.e. the 'holes' got deeper and thus more blue as the clearance increased.

It appears that increasing the tip-clearance size enables the compressor to operate with very large blue holes in the flow field without stalling. (The connection between blue holes and stall inception will be discussed in Chapter 8.)

7.3.2 Smaller Clearances

The tests were also repeated in a compressor with smaller clearance - 1.7% chord. With this level of clearance, very little irregularity in the blade passing signature was observed near stall (see Section 6.3).

Casing static pressure contours for the concentric compressor with 1.7% clearance are shown in Fig. 7.8. The data was taken at an operating point near stall, and the ensemble-averaged signal had been removed so that only the irregularities remain. In this case, a few small blue holes are visible, but it is not possible to track them as they propagate, suggesting that they are forming and decaying rapidly, and not propagating over large portions of the annulus as in the larger tip-clearance cases. At operating points further from stall, the blue holes were not visible. This is consistent with the low level of irregularity measured at these operating points in Fig. 6.2, and

again supports the idea that blue holes are the cause of irregularity in the blade passing signal.

With a small concentric clearance, it appears that the compressor is unable to support mature blue holes, and stall occurs at an operating point close to that at which the blue holes first appear. The compressor with 1.7% clearance exhibited spike-type stall inception. It could be that the embryonic blue holes seen in Fig. 7.8 are somehow related to spike-type stall. This idea will be discussed in more detail in Chapter 8.

Data for the compressor with 1.7% average tip-clearance and 75% eccentricity presents a very different picture from that shown in Fig. 7.8. In Fig. 7.9, data is taken from the large tip-clearance region of the eccentric machine, where there is known to be a substantial pre-stall ramp-up in irregularity. The data was obtained near stall. In this case, the blue holes are clearly visible. Also, unlike in the concentric case (Fig. 7.8), the blue holes can be tracked from one set of pressure transducers to the next. As in the eccentric machine with 3.3% clearance, the blue holes grew and decayed as they moved from the small clearance to the large clearance and back again.

The results from these tests with help to demonstrate the overlap between blue hole activity and the pre-stall ramp-up in irregularity. The reason why the compressor can operate stably with large blue holes in some cases but not others will also be discussed in more detail in Chapter 8.

7.4 Propagation Speed

It was shown in Section 7.1.3 that the blue holes appear to move around the annulus by propagating relative to the rotor blades. This section deals with the factors affecting the speed at which the disturbances propagate and the next section describes the mechanism by which they do so.

In an eccentric machine, it has been shown that the blue holes grow in axial and circumferential extent as they move into the less stable part of the annulus. They also grow larger as the compressor operating point is moved towards stall. It has also been shown that the blue holes become deeper as the average clearance of the machine is increased. The relationship between blue hole size and depth and the propagation speed will now be discussed.

7.4.1 Effect of Flow Coefficient

The propagation speed of the blue holes in a concentric compressor was measured at five flow coefficients from full flow to near stall. These measurements were repeated at four clearance levels (3.3, 4.2, 4.9 and 5.8% chord). The results are shown in Fig. 7.10, which is a graph of propagation speed (normalised by rotor tip speed) against flow coefficient. The speeds were found by tracking each blue hole from one array of pressure transducers to another set located two stator pitches away. In each case, the average speed of all the blue holes in one revolution's worth of data was taken (roughly 20 blue holes).

From Fig. 7.10, it can be seen that the blue hole speed increases as the compressor moves towards stall, i.e. the blue holes speed up as they grow in size. This is the opposite of a spike stall cell, which will slow down as it grows larger. The relationship between flow coefficient and propagation speed is linear, and the four lines in Fig. 7.10 lie on top of each other, showing that the size of the tip-clearance gap, and thus the 'depth' of the blue hole has no impact on propagation speed.

The speeding up of the blue holes as they grow can also be seen in Fig. 7.11, which shows casing static pressure measurements taken at full flow (Fig. 7.11 (a)) and near stall (Fig. 7.11 (b)) in an eccentric compressor with 3.3% clearance. In each plot, the propagation is marked by a black dotted line, while the red dotted line shows 50% blade speed. In Fig. 7.11 (a), the blue holes are moving at significantly less than half blade speed, while in Fig. 7.11 (b), the red and black lines are almost parallel, as the blue holes have sped up to almost 50% blade speed.

7.4.2 Effect of Local Tip-clearance

In Fig. 7.10 it can be seen that the blue holes speed up as they grow in axial and circumferential extent, but that the average tip-clearance size (and therefore the blue hole 'depth') has no effect on the propagation speed. It is therefore interesting to consider what will happen to the speed of the blue holes as they grow and decay while propagating around the annulus of an eccentric machine, i.e. will the speed of propagation change in unison?

The propagation speed of the blue holes in an eccentric compressor with 3.3% aver-

age tip-clearance is shown in Fig. 7.12, which is a graph of blue hole speed (again normalised by blade tip speed) against circumferential position. In this graph, the maximum tip-clearance is at 180°and the size of the blue holes will be at a maximum at approximately 200°(see Fig. 7.7). In Fig. 7.12, the average propagation speed is shown by the squares joined by a solid line, while the crosses and circles denote the fastest and slowest speeds in a revolution's worth of data (i.e. they give an idea of the scatter in the data).

It can be seen that there is an increase in average speed in the regions where the blue holes are larger. The maximum speed occurs between 200°and 250°, i.e. at the location of the largest blue holes. Similar patterns were seen in the test data from larger clearances, though again there was a significant amount of scatter in the speeds.

As with the relationship to flow coefficient, in an eccentric machine the size (i.e. axial and circumferential extent) of a blue hole determines its propagation speed. This means that the blue holes speed up and slow down as they grow and decay around the annulus.

7.5 Mechanism of Propagation

The blue holes have been shown to propagate from blade to blade. There are two ways in which this can happen: either the presence of a disturbance in one passage triggers a similar disturbance in the next passage, or the actual fluid in the original blue hole somehow migrates around the annulus.

When the blue holes first form (at flow coefficients away from stall), they are well aft of the rotor leading edges. This means that it is unlikely that the fluid in the blue hole is spilling round the leading edge from one blade to the next. It is far more likely that each blue hole is swept across the blade passage and out of the rotor with the bulk of the flow, and, as it does so, it precipitates the formation of a new blue hole in the adjacent passage.

If the disturbance propagates, but the fluid involved in each blue hole does not, then

individual blue holes must be washed out of the rotor passages with the bulk flow. This means that the remnants of the blue holes should be detectable downstream of the rotor. To test this idea, measurements were taken downstream of the rotor trailing edge plane in a part of the annulus where blue holes are in abundance.

It should be noted that the measurements presented in this section, Figs. 7.13 to 7.17, are all from near-stall conditions in the large tip-clearance of an eccentric machine with 3.3% average clearance. The use of measurements from near-stall conditions assumes that the propagation mechanism of the blue holes does not change as they grow and move towards the rotor leading edge.

7.5.1 Downstream Frequency Content

Before any detailed measurements of the flowfield downstream of the rotor bladerow were carried out, preliminary measurements of the rotor exit flow were taken. The frequency content of this data was examined to see whether the familiar frequency hump was present.

Initially, experiments were carried out with four special hotwire probes as described in Chapter 3. The probes were all at 15% chord downstream of the rotor trailing edge plane and were evenly spaced over one stator pitch - just after the circumferential location of the maximum tip-clearance. The probes were at four different depths of immersion: 0.8, 4, 6 and 10 mm (the depths corresponded to the prong length on each probe), as shown in Diagram 7.4. The hotwires were all aligned to record the axial component of the flow, i.e. with the filaments tangential.

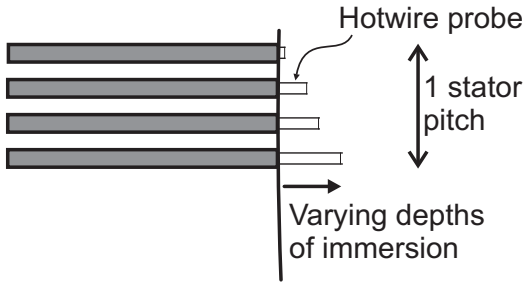

Diagram 7.4: *Schematic diagram of hotwires used to measure frequency content downstream of the rotor bladerow (axial view).*

Figure 7.13 shows the Fourier Transforms from the four hotwires with the compressor running at a near-stall operating condition. Comparison with Fig. 7.1 (b) reveals

a similar 'hump' in the frequency content at around one third of the blade passing frequency (though the harmonics seen in the casing static pressure measurements are not seen in Fig. 7.13). The hump is present in the Fourier Transforms from all the hotwires, though it is smallest in the data from the hotwire nearest the casing.

The frequency content of the hotwire data suggests that the presence of the blue holes is felt downstream of the rotor, and that they have considerable spanwise influence by the time they leave the rotor bladerow, as they can be detected by a hotwire that is 10 mm (almost 20% span) from the casing.

Regarding the spanwise extent of the blue holes, analysis of the hotwire data from the traverses in a concentric machine with 3.3% clearance described in Chapter 4 showed that the blue hole frequency content was minimal when the probe was more than 20% span from the casing, suggesting that the blue holes do not spread to more than 20% span as they convect downstream.

7.5.2 Traverse Method and Data Analysis

To understand more about the blue holes as they leave the blade row, a series of traverses were conducted using a hotwire probe. The hotwire traverse was conducted across the whole span of the blade, and measurements were taken at 39 radial points (clustered towards the endwalls).

In order to build up a picture of a blue hole at the rotor exit from traverse data, it was necessary to phase-lock the data with the blue holes themselves (in much the same way as a conventional hotwire traverse is phase-locked to the shaft rotation). This enabled a picture of an 'average blue hole' to be built up using data from each radial location. As the blue holes are seen very clearly in casing static pressure measurements, the averaging process was triggered by a signal from a casing pressure transducer in the rotor path at 20% chord. This meant that it was necessary to record data from a casing pressure transducer at the same time as the traverse data was logged.

In order to preserve the data for detailed analysis, each data set was recorded as a single sample of 1 second (50 revolutions) and then analysed at a later point, i.e. the averaging was done off-line. Another advantage of this method is that it allowed the

data to be ensemble-averaged on both the shaft signal and the blue hole trigger.

The procedure for creating an ensemble-averaged picture of a blue hole is shown in Diagram 7.5, and is described below:

Step 1: An individual blue hole is found by looking for instances where the irregularity level in the casing static pressure measurement drops below a threshold value (step 1(a)). The pressure signal is then examined to find the minimum pressure (step 1(b)), indicating the centre of the blue hole.

Step 2: A sample window straddling the centre point is used to pick out the blue hole (step 2(a)). The same sample window is then applied to the data from the hotwire probe (step 2(b)).

Step 3: This procedure is then repeated for the next blue hole and for all the selected blue holes in the data set - there are usually around 250 blue holes in 1 seconds' worth of data.

Step 4: The accumulated hotwire sample sets are then overlaid (step 4(a)) and ensemble-averaged to give an 'average blue hole' (step 4(b)).

In Figures 7.14 to 7.17, the plots on the left-hand side are ensemble-averaged in the conventional manner, using the once-per-revolution trigger signal, while those on the right-hand side are ensemble-averaged using the blue hole trigger technique described above.

7.5.3 Hotwire Traverse

The results of the hotwire traverse with the probe aligned to measure axial flow are shown in Fig. 7.14. Figure 7.14 (a) shows the data ensemble-averaged in the conventional manner, using the once-per-revolution shaft signal as a trigger. In this plot there are clear blade wakes, and a small corner separation loss at the hub, as expected. There is also a large region of low axial velocity covering the outer 20% span.

When the same data is ensemble-averaged using the blue hole minima as described above, the plot shown in Fig. 7.14 (b) is obtained. In this plot, there is much more

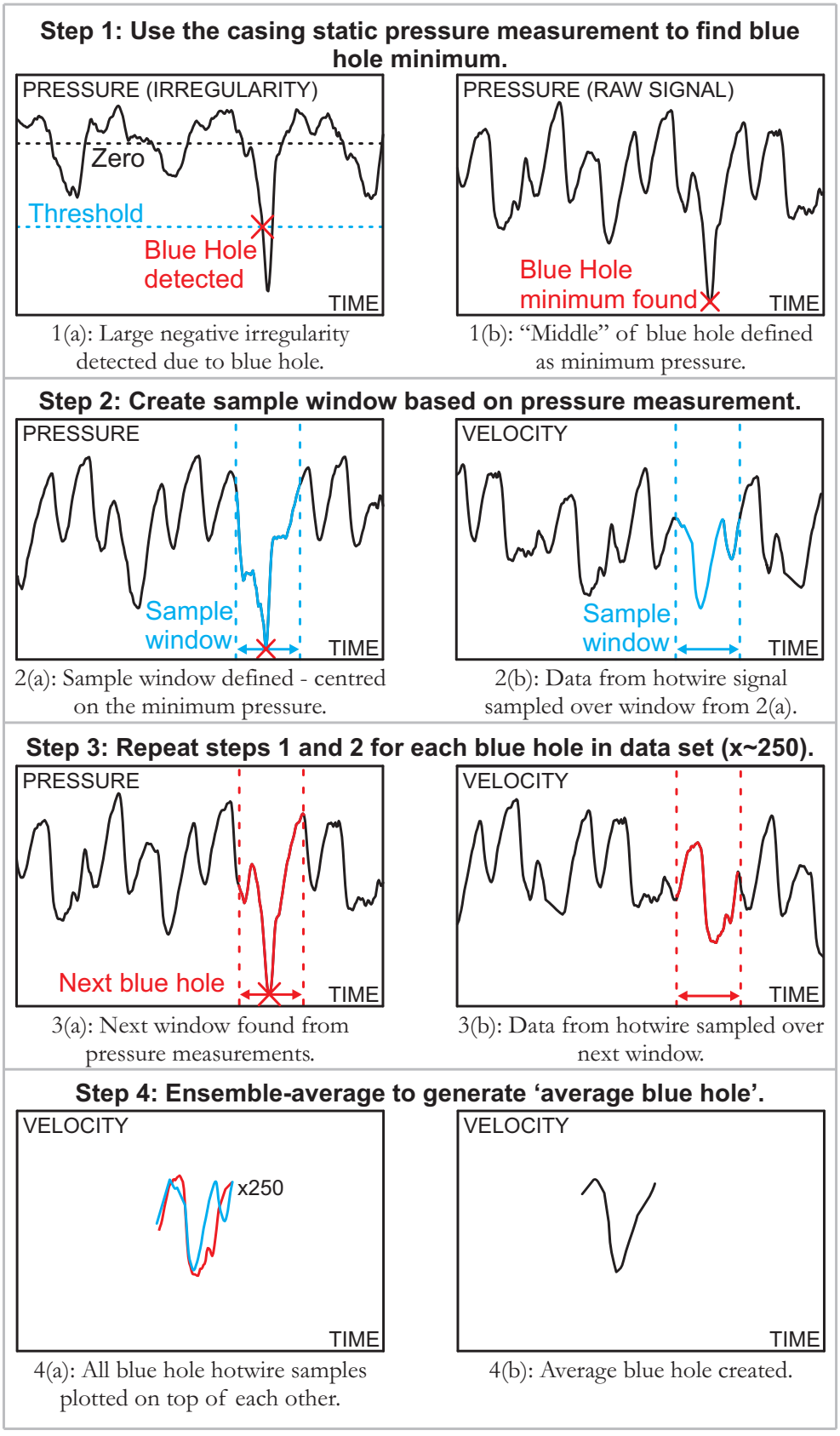

Diagram 7.5: *Procedure for ensemble-averaging 'blue holes'.*

structure to the flow in the outer 20% of span. At time 0.5 in Fig. 7.14 (b), the low axial velocity fluid only occupies the outer 5% of the span, whereas around the centre of the plot, it occupies 20% of span, (as in Fig. 7.14 (a)). This changing spanwise extent of the low velocity fluid at the rotor tips is highlighted by the black line in Fig. 7.14 (b) (the same velocity contour is also shown in black in Fig. 7.14 (a) for comparison).

This result shows that the large region of loss in Fig. 7.14 (a) (and discussed in Chapter 4) contains coherent structures which are only detected if the data is ensemble-averaged using the passing of each blue hole as a trigger. It is thus believed that the loss is caused by blue holes being swept out of the rotor passage.

It can also be seen that, compared to Fig. 7.14 (a), the blade wakes are not clearly defined. This shows that the blue holes are not locked to the blades, as they do not always leave the bladerow at the same pitchwise position.

Figure 7.15 shows data from a similar hotwire traverse, but this time aligned to measure tangential flow. Again, the rotor wakes are clearly discernible in Fig. 7.15 (a), but in Fig. 7.15 (b) the main feature is a high velocity patch which starts after two rotor passings. Again, this shows evidence of the blue holes being swept out of the rotor.

In order to get more information about the flow direction, the hotwire traverses were repeated at 25 angles from +90°to -90°; the probe was rotated in 5°steps from -15°to 65°and 15°steps elsewhere. The angle of the flow was found using a cosine fit.

The flow velocity and direction as calculated from the hotwire traverses at 25 yaw angles are shown in Fig. 7.16. As with the previous two figures, the plots on the left (Figs. 7.16 (a) and (c)) have been ensemble-averaged on the once-per-revolution signal, while those on the right (Figs. 7.16 (b) and (d)) are averaged on the blue hole minima. The top plots show velocity magnitude, while the bottom plots show absolute flow angle (positive in the direction of rotor rotation).

The main feature of interest is inside the dotted ellipse in Fig. 7.16 (b) (velocity magnitude ensemble-averaged on the centre of the blue holes). Here, a region of slow fluid is observed right next to a region of much faster fluid. This is accompanied by a change in flow direction, Fig. 7.16 (d). This sudden change in speed and direction is likely to indicate the presence of a vortex, and suggests that the blue holes are in

fact vortical structures, as proposed in Section 7.1.2.

7.5.4 Fast-response Total Pressure Probe Traverse

The problem with using a single-element hotwire is that it is unable to give accurate information in a highly three-dimensional flow, as forward and reverse flow cannot be distinguished from each other. In the case of the 'blue holes', there is likely to be significant flow reversal. This means that, while the hotwire data shows that there is a structured disturbance leaving the rotor passages, the flow direction cannot be reliably resolved.

In order to check whether the picture of the flow created from the hotwire data (Fig. 7.16) was correct, the traverses were repeated using a fast-response total pressure transducer. The advantage of this probe is that it distinguishes between forward and reverse flow as shown in Diagram 7.6.

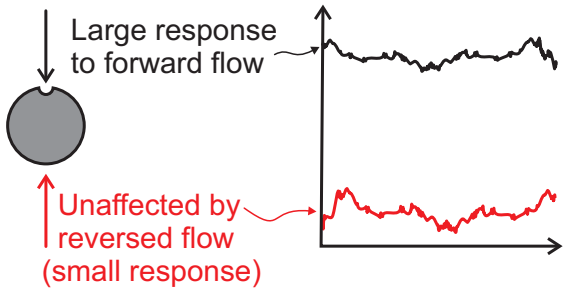

Diagram 7.6: *Fast-response total pressure probe.*

The total pressure probe was traversed at 14 yaw angles from -150°to +180°, and the data analysed in a similar manner to the hotwire traverse data[1]. The total pressure ensemble-averaged both on the once-per-revolution signal and on the blue hole minima can be seen in Figs. 7.17 (a) and (b). Again, in Fig. 7.17 (b), there is a structure near the casing which could be a vortex.

As a 'sense check', readings from the probe pointing axially upstream (i.e. to measure forward axial flow) are shown in Figs. 7.17 (c) and (d). Qualitatively, these are

[1]The construction of the total pressure probe is such that it is not possible to get within 20% span of the hub. As established above, the influence of the blue holes does not extend this far so this limitation is not of importance.

very similar to the hotwire axial velocity results shown in Fig. 7.14, suggesting that the hotwire results are showing a generally correct flowfield despite the lack of flow direction sensitivity.

Taken together, the results from the hotwire and total pressure probe give strong evidence that the blue holes are in fact vortical structures. The results also show that the blue holes leave the blade row thus adding weight to the argument that the disturbance propagates by setting off a new instability in the next blade passage, i.e. the disturbance propagates, but the fluid does not.

7.6 Comparison with CFD

Computational work by Pullan at the Whittle Laboratory [1] [79] has revealed similar structures to the blue holes described above. In his initial simulations on a different compressor with large tip-clearance, Pullan saw distinct structures propagating near the rotor tips, which had similar frequency content to the blue holes low-pressure patches on the rotor casing were similarly observed. The experimental data shown in this chapter provided validation of the computational results and the computational results have since been used to elucidate the experimental results.

To validate his findings, Pullan repeated his simulations on the concentric compressor discussed in this chapter with 3.3% clearance[2]. The computational results discussed here are taken from a quarter-annulus, unsteady simulation at an operating point near to the numerical stall point.

In his work, Pullan uses the λ_2 criterion as a means of showing showing vorticity that is associated with a swirling flow (i.e. a vortex) while neglecting that associated with a shear layers (see Jeong and Hussain [80] for further details). Figure 7.18 shows an iso-surface of the λ_2 criterion from the computational simulation at an operating point near to the numerical stall point.

In Fig. 7.18, two vortices are apparent near the rotor tips. The first is the tip-leakage vortex, which emerges near the leading-edge of the blade - circled red and white in the Fig. 7.18. In a machine with a stable tip-leakage flow, the tip-leakage vortex is

[2]For details of the computational approach, and the agreement between the computational and experimental results see Pullan et al. [1].

the only vortex that one would expect to see in this region. However, in this case, a second vortex appears to emerge from the tip-clearance flow. This is circled in black and white. Further examination of the simulation confirms that this structure is the blue hole, thus confirming the idea that the blue holes are radial vortices.

These simulations back up the hypothesis put forward in the previous section that the blue holes are vortical structures. Further to this, the computational results also show that the blue holes seen in a compressor with large tip-clearance are caused by instability of the tip-leakage flow [79]: the simulations appear to show the shear layer between the tip-leakage flow and the main flow becoming unstable and rolling up to form a vortex. The physical cause of blue holes in a compressor with smaller clearance will be discussed in the next chapter.

7.7 Links to Previous Work

Disturbances of a similar type to those reported here were seen in casing static pressure measurements by Inoue et al. [56], [57]. In their work, the same characteristic low pressure patches were observed, but the spacing between events was larger (every 5 rotor pitches, in a rotor with 24 blades). Inoue et al. [57] postulated that each low pressure patch was caused by a vortical structure with one end attached to the blade and the other on the casing. This structure is remarkably similar to that seen by Pullan (see Fig. 7.18 [79]).

Inoue et al. described the disturbances they saw as 'mild stall'. From the characteristic given it seems likely that they were observing some form of part-span stall, as there is a sharp drop in stage pressure rise between the main characteristic and the operating points at which the disturbances were seen. Furthermore, the disturbances appear upstream of the rotor leading edges in their casing static pressure measurements, they do not report seeing disturbances within the actual bladerow.

Apart from the work of Inoue et al. [56], [57], most of the remaining work in this area has relied on frequency analysis as opposed to direct measurements of the disturbances themselves.

Mailach et al. [54], [55] reported seeing 'rotating instabilities' of the same frequency and propagation speed to the blue holes seen in this work. Their measurements

were, however, taken in a multistage machine with the tip-clearance increased in one stage. Wisler et al. [20] repeated the measurements in an identical machine with large tip-clearance in all the stages, they saw no sign of the instabilities. This led Wisler et al. to suggest suggestion that the 'rotating instabilities' in Mailach et al.'s data were due to the fact that the stage with larger tip-clearance was partially stalled but was being supported by the other, more stable, stages.

März et al. [60] also detected 'rotating instabilities' in a fan, though the characteristic of their machine had a positive slope at the point where the disturbances were observed, suggesting that the machine was already operating in an unstable regime (again, see Wisler et al. [20]).

More work on 'rotating instabilities' was carried out by Kameier and Niese [59]. Their experiments in a fan with large tip-clearance showed disturbances in a similar frequency range to those observed here. They suggested that the rotating instabilities could be removed by making the flow in the tip-clearance region turbulent. In support of this, they repeated the tests with a piece of Velcro stuck to the casing at the rotor leading edge tips and reported that the rotating instabilities had disappeared. It is, however, probable that the Velcro was blocking the tip-clearance flow and so effectively making the tip gap smaller - they also found no rotating instabilities in tests with smaller tip-clearance.

It is believed the current efforts represent the first time these disturbances have been seen so clearly in a machine that is operating stably and is not being artificially supported by adjacent stages. Furthermore, many of the pieces of work discussed above have only considered the frequency content of unsteady pressure measurements, but have not studied not the structure or nature of the disturbances causing the characteristic 'hump' in the Fourier transform.

7.8 Conclusions

1. The irregularity in the blade passing signature observed in Chapter 6 has been shown to be caused by discrete disturbances ('blue holes') propagating from one blade to the next at approximately 50% of rotor speed.

   Detailed rotor casing pressure contour maps and Fourier analysis of the blade

passing signal in a compressor with large, concentric clearance have been used to show that these disturbances:

   a. Produce a frequency of approximately one third of the blade passing frequency.
   b. Are patches of intense low pressure similar in magnitude to the compressor inlet dynamic head. At near-stall operating conditions, these low pressure patches extend from the leading edge to mid-chord and occupy half a rotor pitch circumferentially.
   c. Are also visible at operating points far from stall, but initially appear well aft of the leading edge. As the compressor operating point is moved towards stall, the disturbances grow in axial and circumferential extent and become 'deeper'.

2. In an eccentric machine, blue holes are not observed in the small tip-clearance sector of the annulus. In regions of large tip-clearance, blue holes appear in abundance. They grow as they propagate towards the maximum tip-clearance part of the annulus and then decay as they move back towards the minimum clearance. The blue holes are largest just after the maximum tip-clearance. This location is in line with the highest irregularity reported in Chapter 6.

3. In tests with numerous combinations of tip-clearance size and eccentricity, the growth pattern of pre-stall blade passing irregularity matched perfectly with the growth in blue hole activity. Furthermore, larger, deeper blue holes were observed when the irregularity level was highest. This confirms that the blue holes are the cause of the ramp-up in irregularity measured in Chapter 6.

   This work is the first time that a link between blue holes and the rise in irregularity near stall has been established, as previous work has treated the two phenomena as separate subjects.

4. The blue holes have been shown to propagate from one blade to the next.

   a. As the blue holes grow in axial and circumferential extent, they propagate more quickly. This is the opposite of spike stall cells, which slow down as they grow. The propagation speed of a blue hole is not affected by its intensity.

b. The mechanism of propagation is that a blue hole in one blade passage sets off a similar disturbance in the next blade. This means that the disturbance propagates but the fluid in the disturbance does not. Each individual blue hole ends up convecting downstream with the bulk flow. This is confirmed by the disturbances detected in traverse data from downstream of the rotor bladerow.

5. The blue holes have all the the characteristics of vortical structures. They are characterised by regions of low static pressure on the casing, which are most easily described as radial vortices. The vortical structure is seen in hotwire traverse data from downstream of the rotor bladerow and is confirmed by computational results, which show that unsteadiness in the shear layer between the tip-clearance flow and the bulk flow gives rise to blue holes in compressors with large or eccentric clearances.

6. The disturbances shown here are more clearly defined than in any previous work, and it is believed that this is the first time that such disturbances have been seen in a compressor that is not operating in a partially-stalled state. This work also confirms for the first time the structure behind the 'rotating instabilities' which have previously been measured via the remote tool of Fourier analysis.

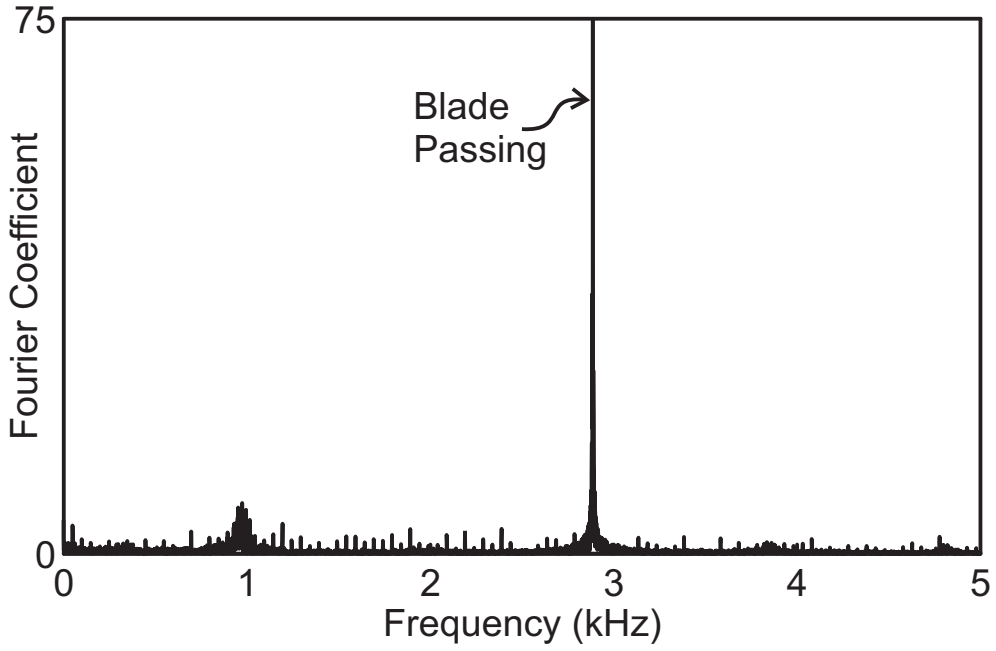

(a) Full Flow ($\phi = 0.530$).

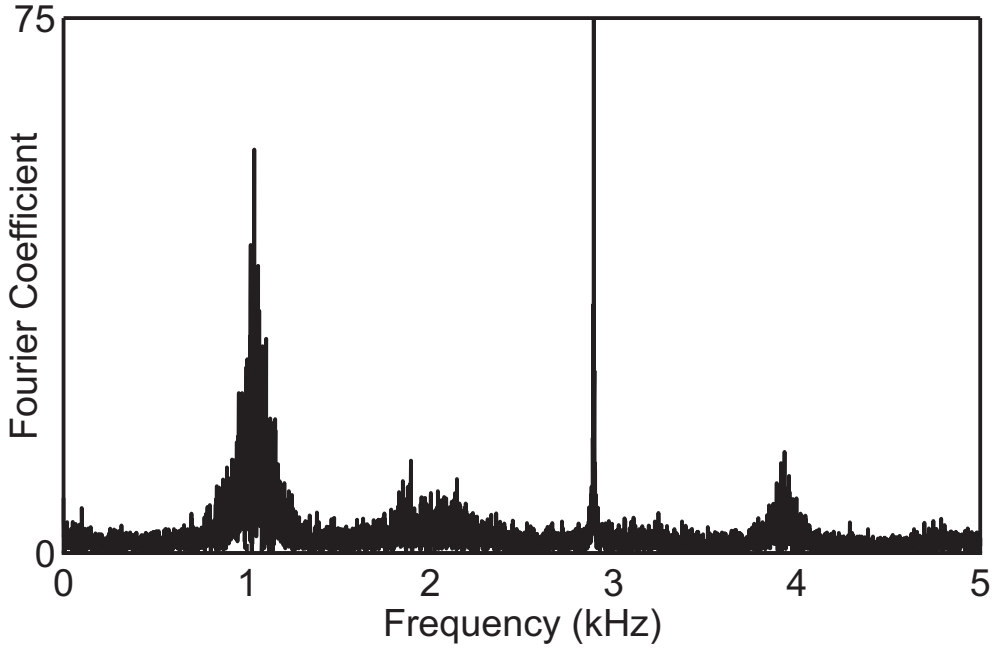

(b) Near Stall ($\phi = 0.460$).

Figure 7.1: *Fourier transform from a pressure transducer level with the rotor leading edge in a concentric compressor with large clearance operating at full flow and near stall (3.3% clearance).*

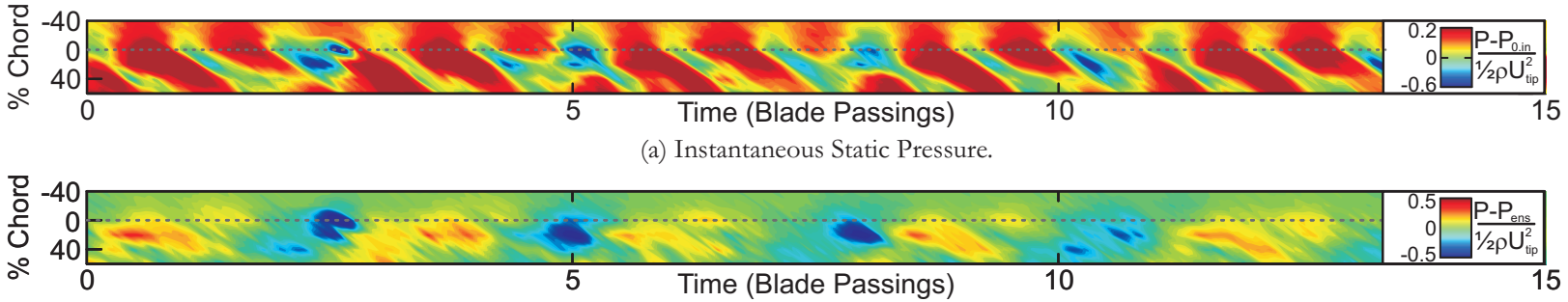

(a) Instantaneous Static Pressure.

(b) Ensemble-average removed.

Figure 7.2: *Instantaneous casing static pressure at a near-stall operating point in a concentric compressor with large clearance (3.3% clearance, $\phi = 0.460$).*

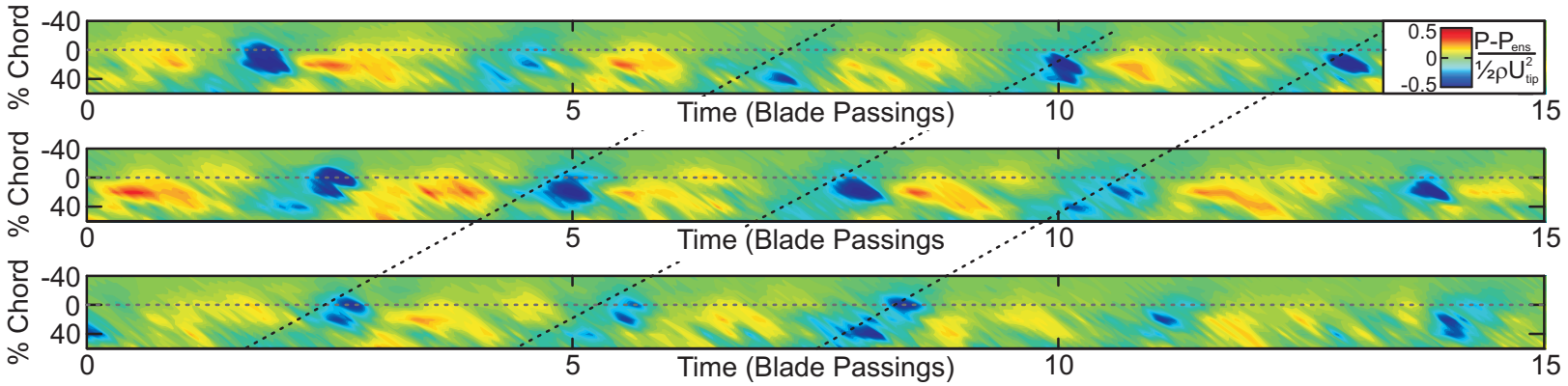

Figure 7.3: *Propagation of 'blue holes' in a concentric compressor with large clearance (3.3% clearance, $\phi = 0.460$). Casing static pressure with ensemble-average removed.*

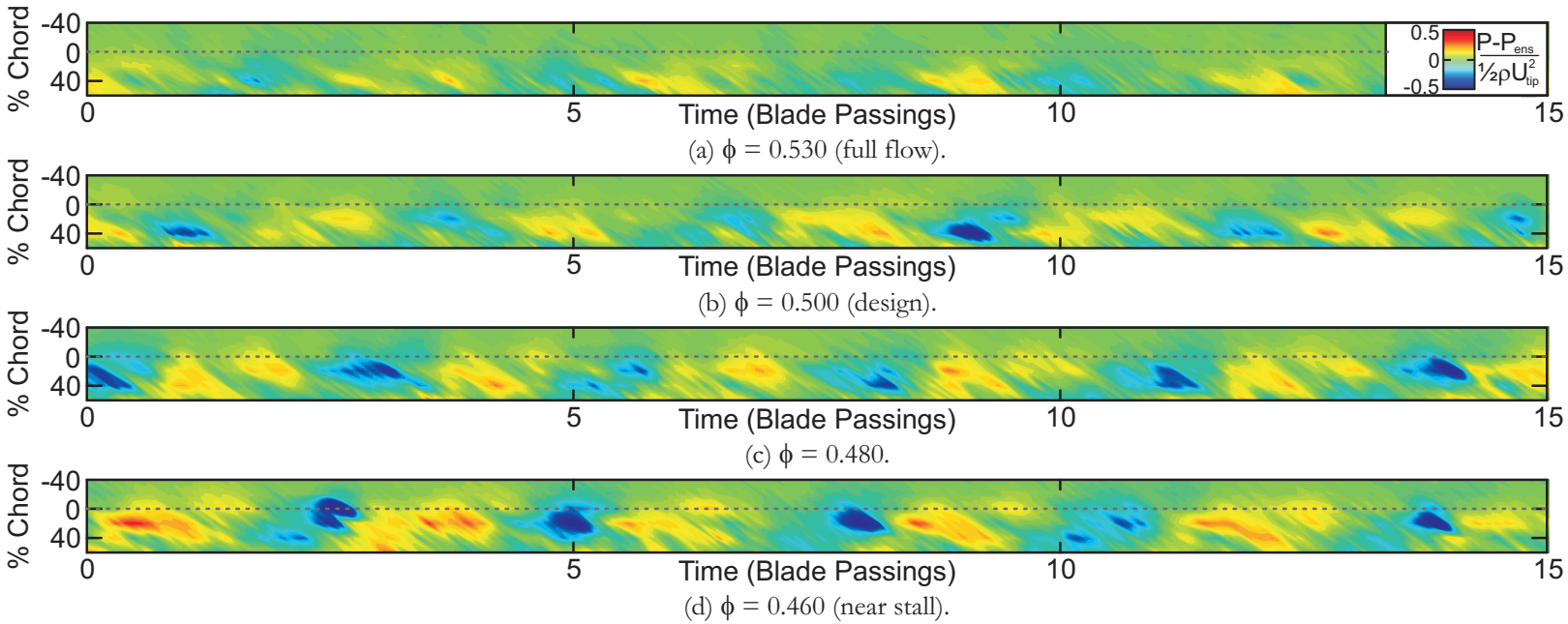

(a) $\phi = 0.530$ (full flow).

(b) $\phi = 0.500$ (design).

(c) $\phi = 0.480$.

(d) $\phi = 0.460$ (near stall).

Figure 7.4: *Casing static pressure with ensemble-average removed showing the development of 'blue holes' in a concentric compressor at different flow coefficients (3.3% tip-clearance).*

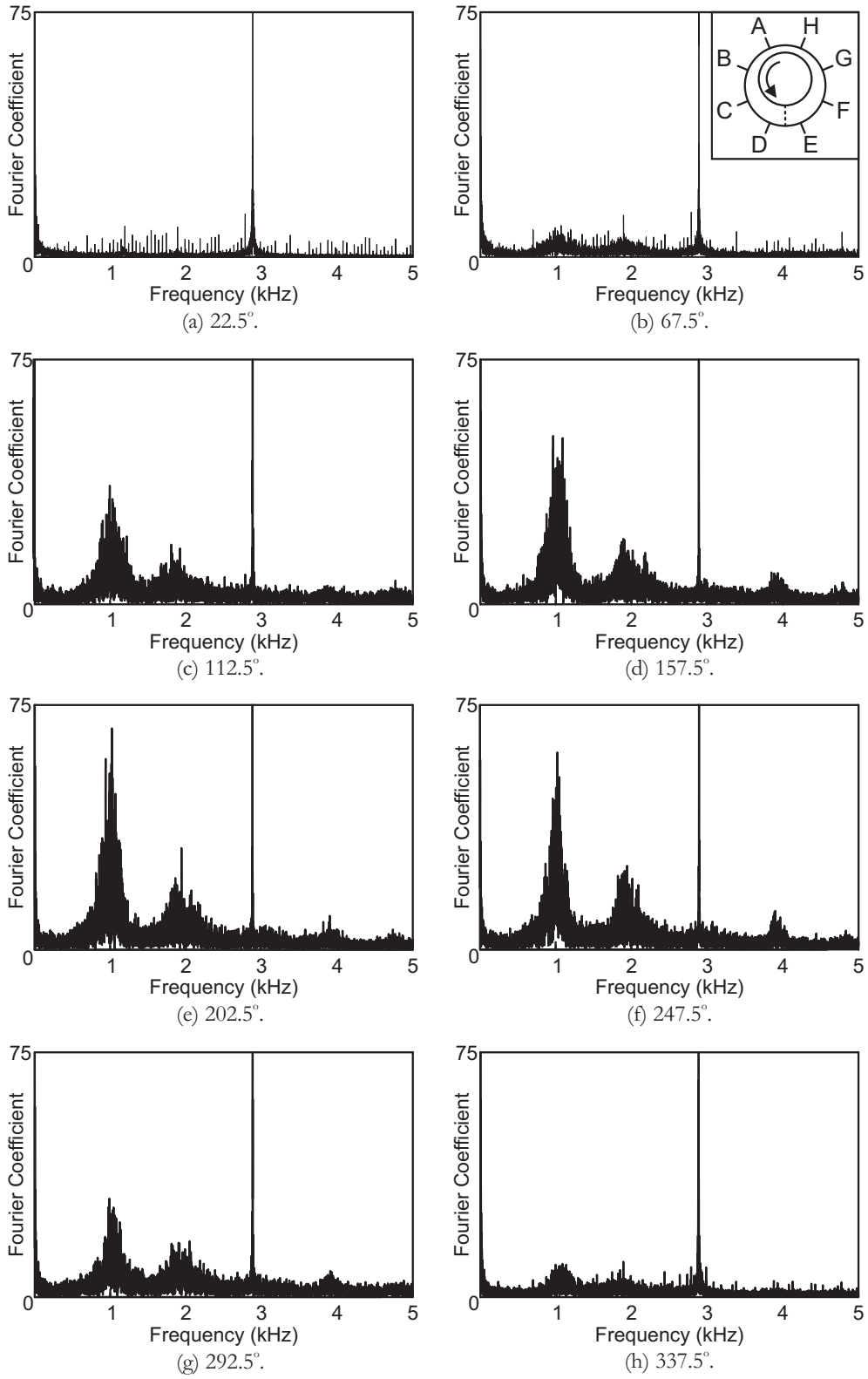

(a) 22.5°. (b) 67.5°.

(c) 112.5°. (d) 157.5°.

(e) 202.5°. (f) 247.5°.

(g) 292.5°. (h) 337.5°.

Figure 7.5: *Fourier transforms of near-stall data from pressure transducers in different circumferential locations (3.3% tip-clearance, 75% eccentricity, $\phi = 0.465$).*

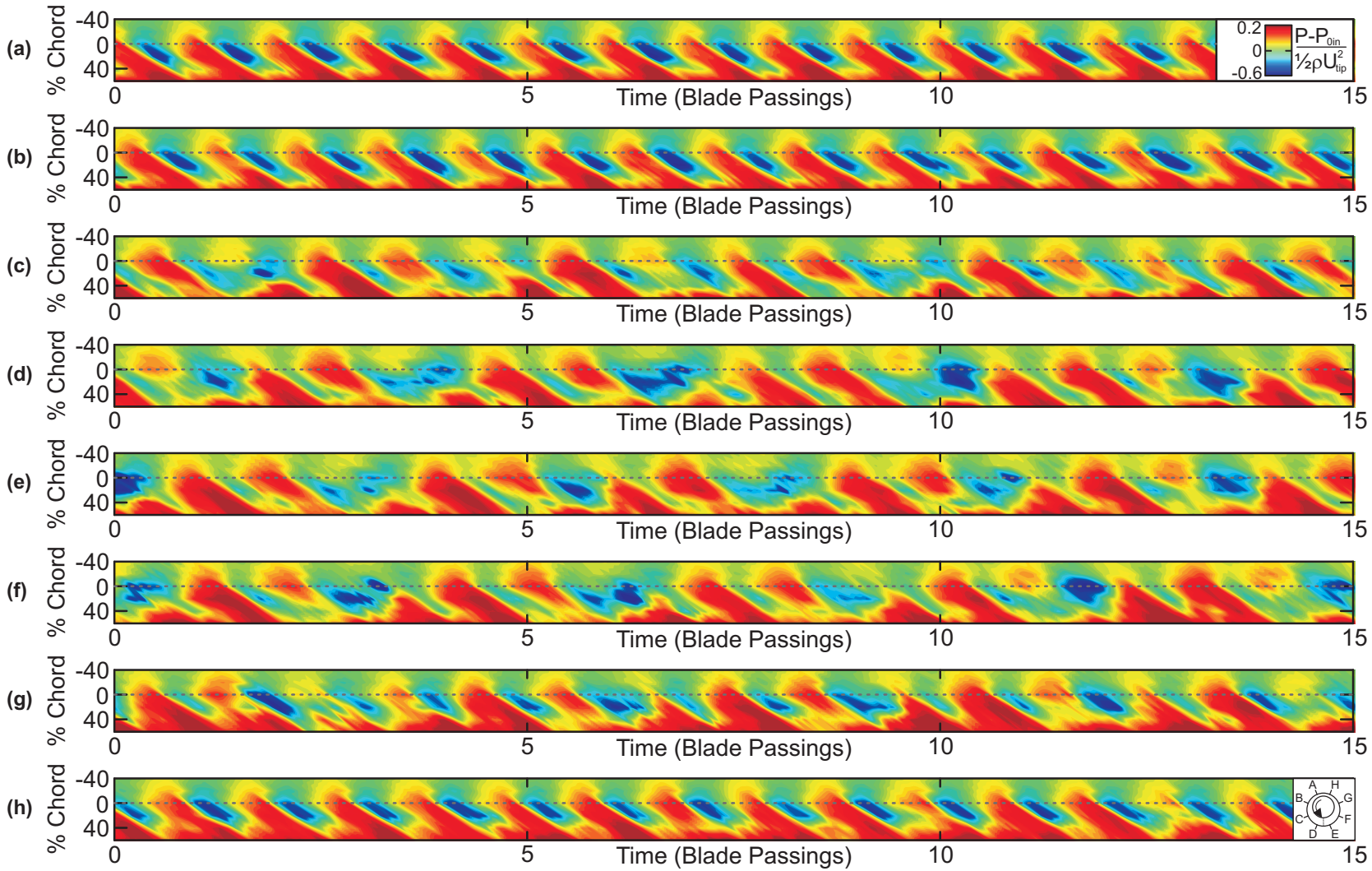

Figure 7.6: *Instantaneous casing static pressure near stall at different circumferential positions in an eccentric compressor (3.3% tip-clearance, 75% eccentricity, $\phi = 0.465$). NB: Data sets were not recorded simultaneously, so disturbance tracking is not possible.*

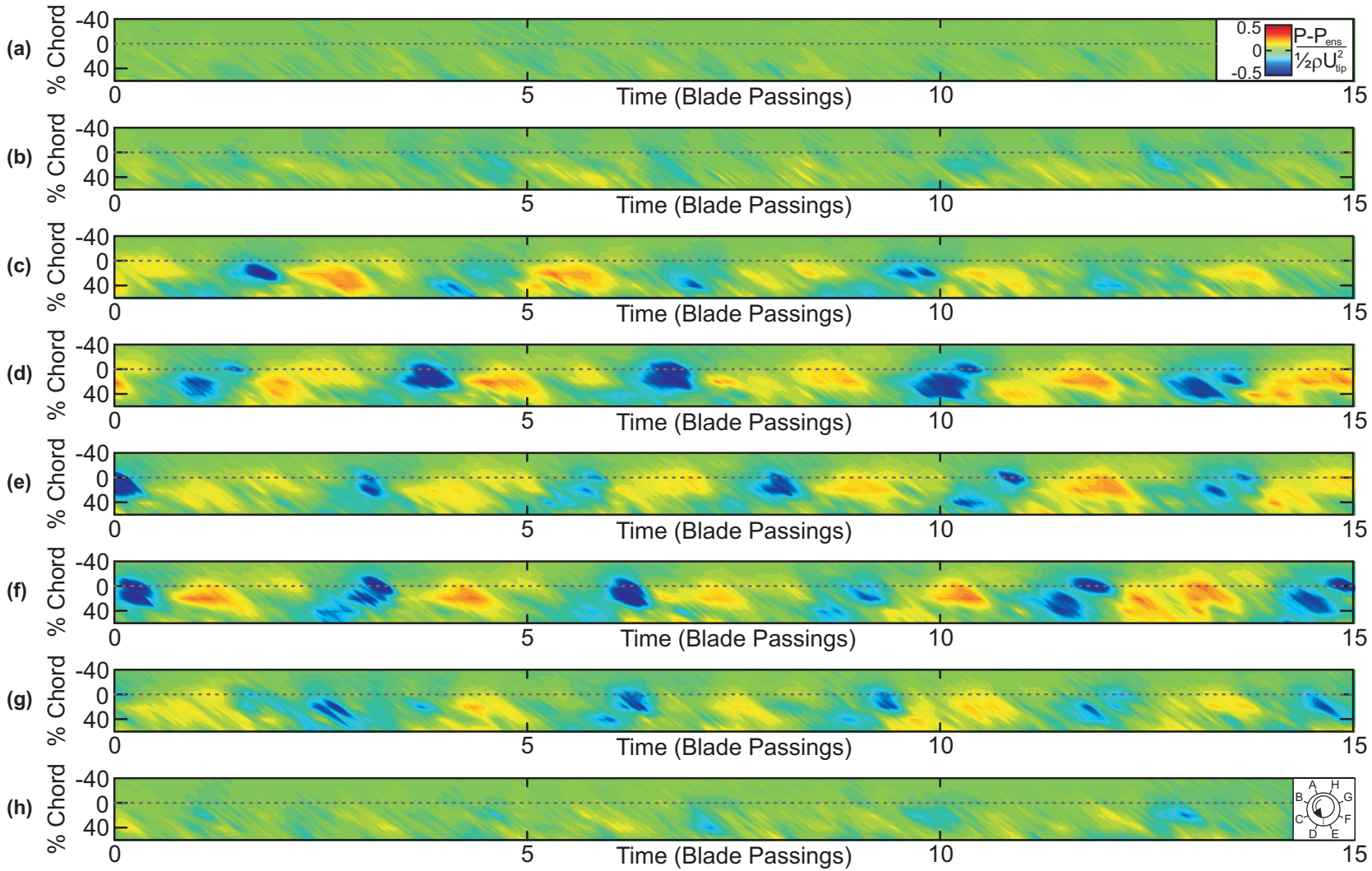

Figure 7.7: *Irregularities in casing static pressure at different circumferential positions in an eccentric compressor at a near-stall operating point (3.3% tip-clearance, 75% eccentricity, $\phi = 0.465$). NB: Data sets were not recorded simultaneously, so disturbance tracking is not possible.*

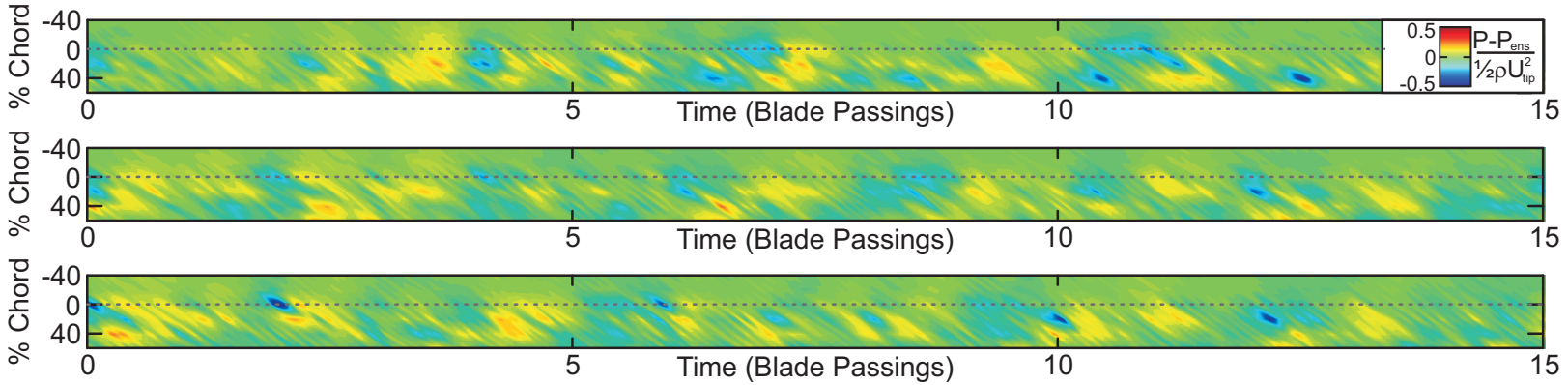

Figure 7.8: *Blue holes measured near stall in the compressor with small, concentric tip-clearance (1.7% tip-clearance, $\phi = 0.415$).*

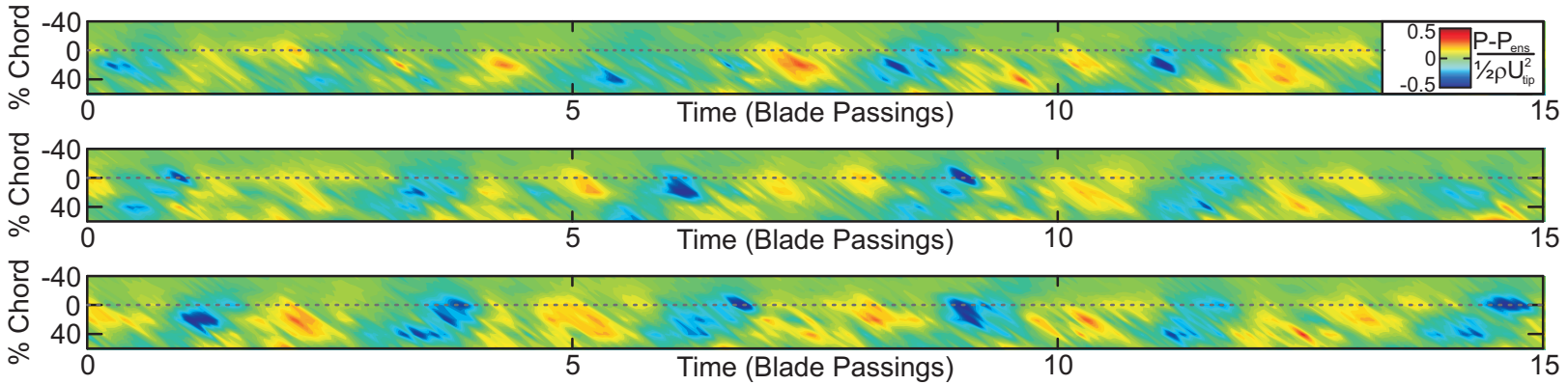

Figure 7.9: *Blue holes measured near stall in the large clearance region of the compressor with small, eccentric clearance (1.7% tip-clearance, 75% eccentricity, $\phi = 0.430$).*

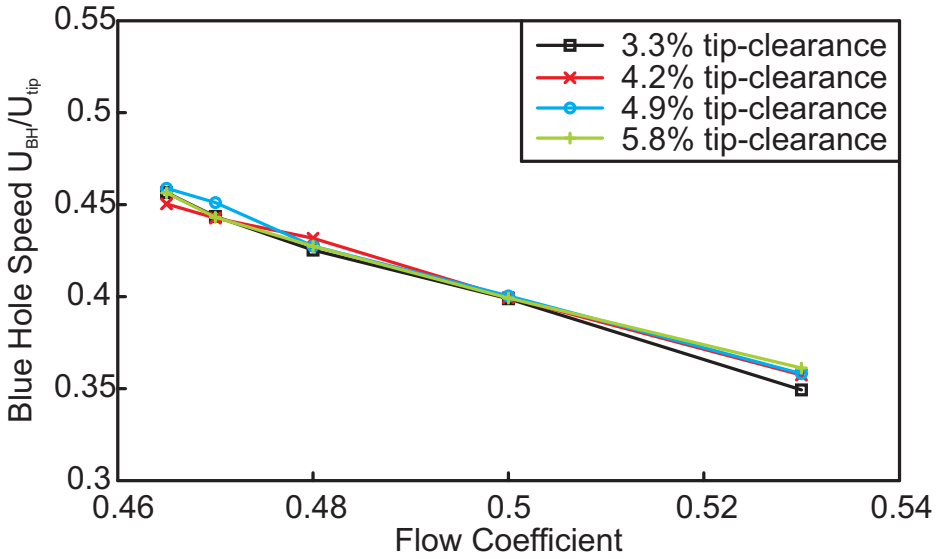

Figure 7.10: *Blue hole propagation speed against flow coefficient in concentric compressors with different average clearance levels.*

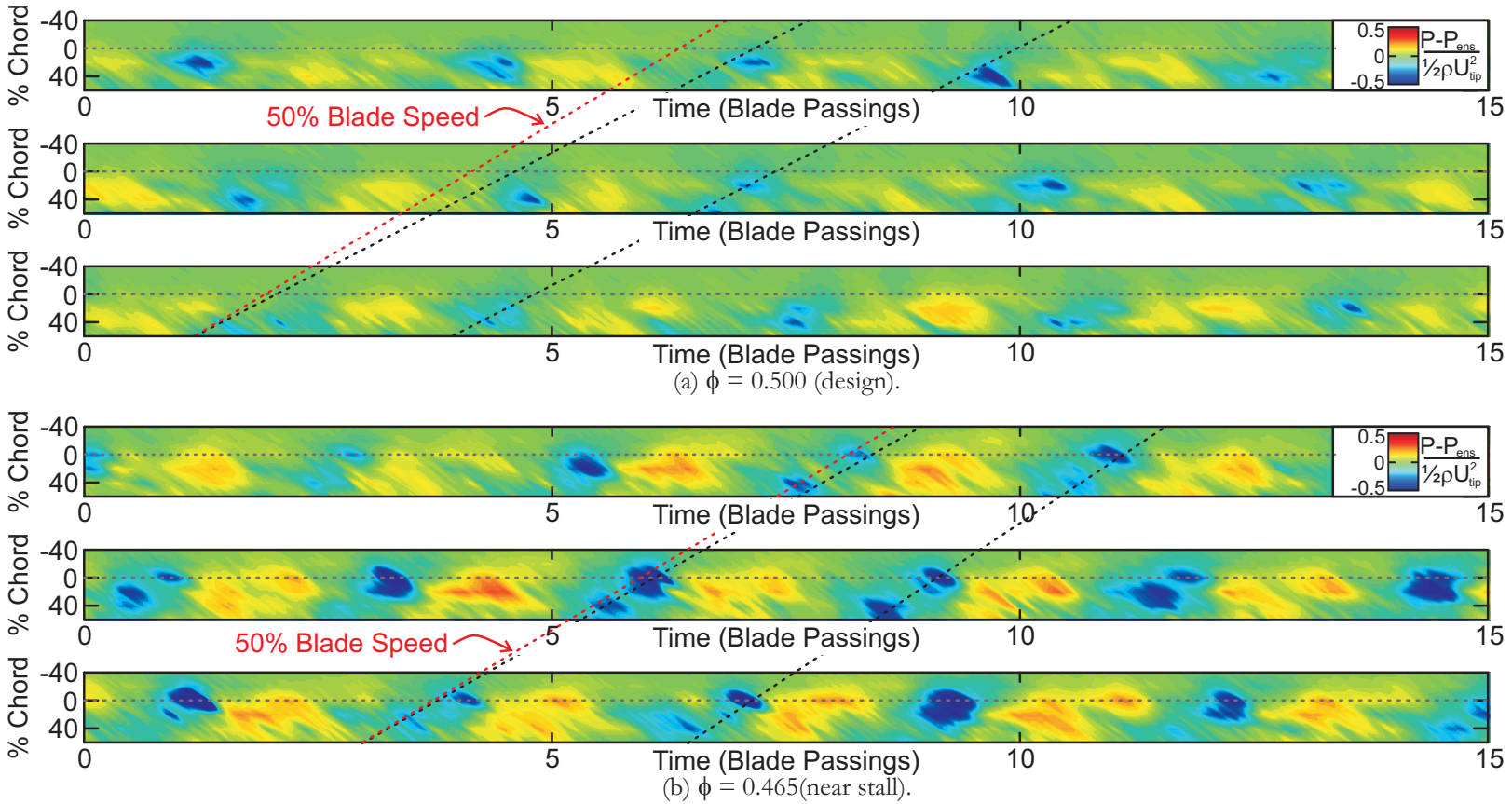

(a) $\phi = 0.500$ (design).

(b) $\phi = 0.465$(near stall).

Figure 7.11: *Propagation of blue holes at full flow and near stall in an eccentric compressor (3.3% tip-clearance, 75% eccentricity, 22.5°after maximum tip-clearance).*

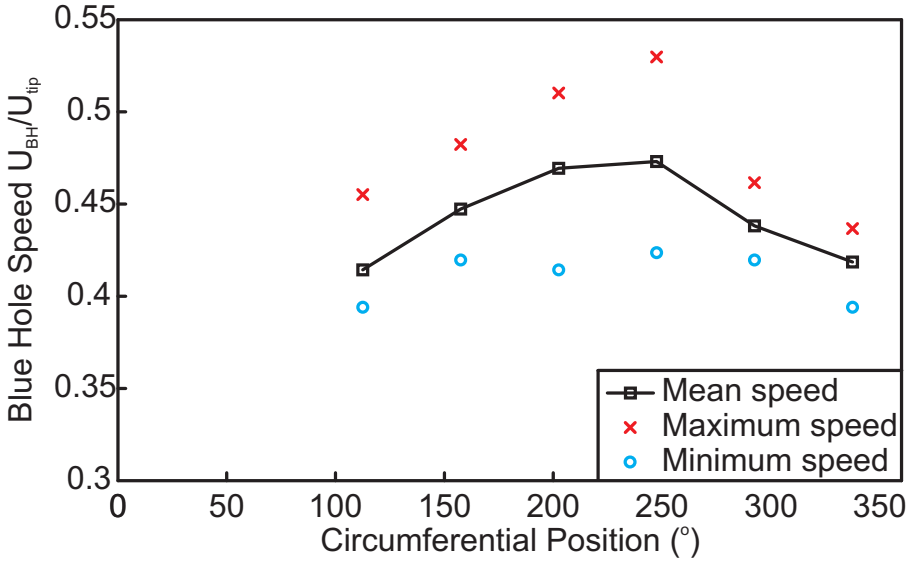

Figure 7.12: *Blue hole propagation speed against against circumferential position in an eccentric compressor at a near-stall operating point (3.3% clearance, 75% eccentricity, ϕ = 0.465).*

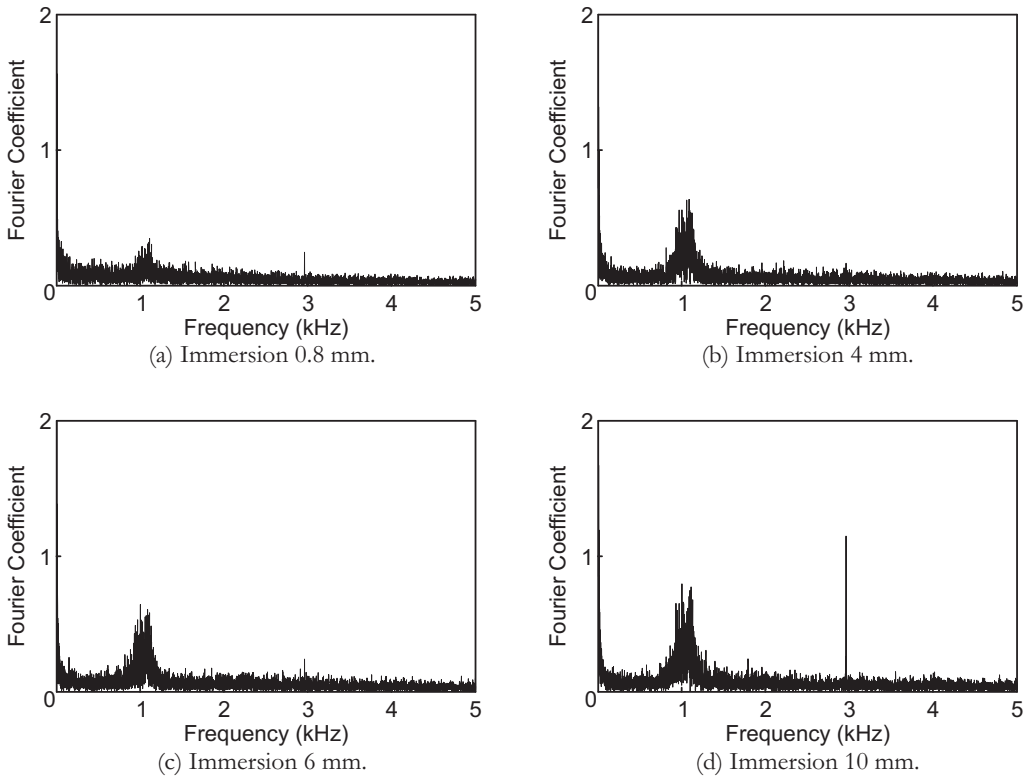

(a) Immersion 0.8 mm.

(b) Immersion 4 mm.

(c) Immersion 6 mm.

(d) Immersion 10 mm.

Figure 7.13: *Fourier transforms of data from hotwires downstream of the rotor at different depths of immersion (3.3% tip-clearance, 75% eccentricity, maximum tip-clearance, ϕ = 0.465).*

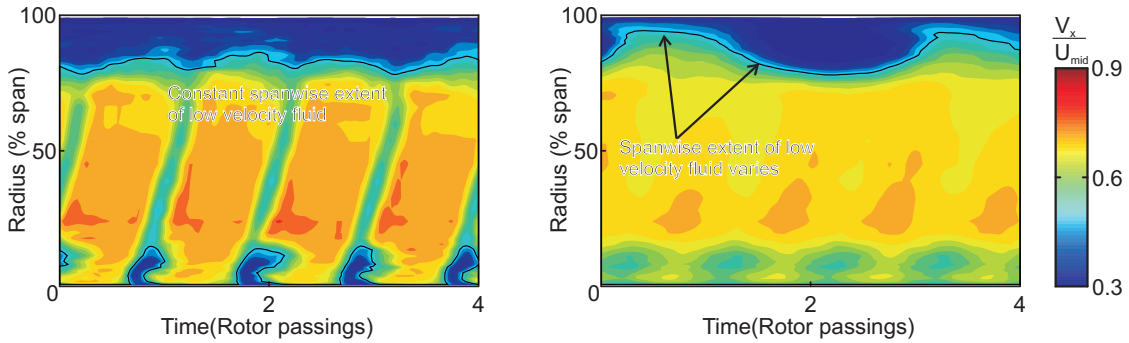

(a) Axial velocity, ensemble-averaged on once-per-revolution signal.

(b) Axial velocity, ensemble-averaged on 'blue hole' minima.

Figure 7.14: *Hotwire traverse downstream of rotor at near-stall condition. Axial velocity (3.3% tip-clearance, 75% eccentricity, maximum tip-clearance, ϕ = 0.470).*

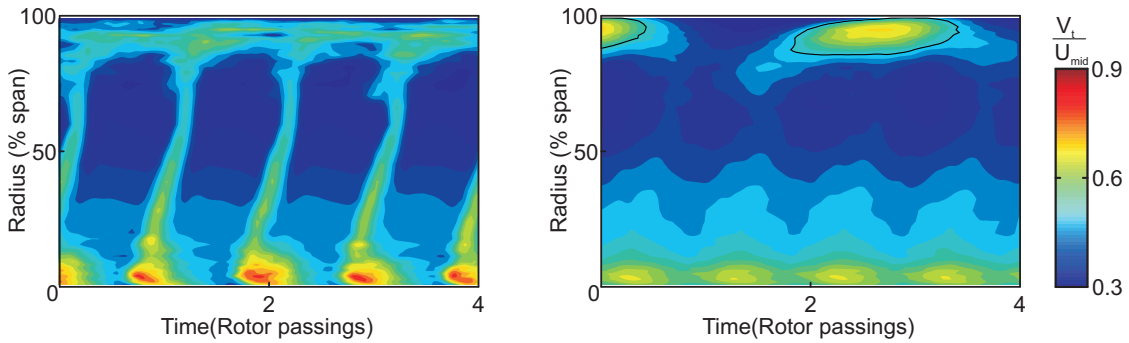

(a) Tangential velocity, ensemble-averaged on once-per-revolution signal.

(b) Tangential velocity, ensemble-averaged on 'blue hole' minima.

Figure 7.15: *Hotwire traverse downstream of rotor at near-stall condition. Tangential velocity (3.3% tip-clearance, 75% eccentricity, maximum tip-clearance, ϕ = 0.470).*

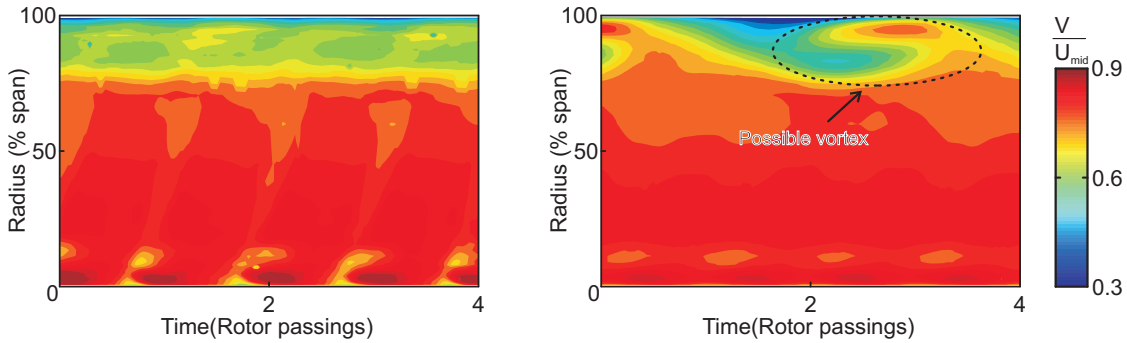

(a) Velocity, ensemble-averaged on once-per-revolution signal.

(b) Velocity, ensemble-averaged on 'blue hole' minima.

(c) Flow angle, ensemble-averaged on once-per-revolution signal

(d) Flow angle, ensemble-averaged on 'blue hole' minima.

Figure 7.16: *Hotwire traverse downstream of rotor at near-stall condition. Velocity and flow angles (3.3% tip-clearance, 75% eccentricity, maximum tip-clearance, $\phi = 0.470$).*

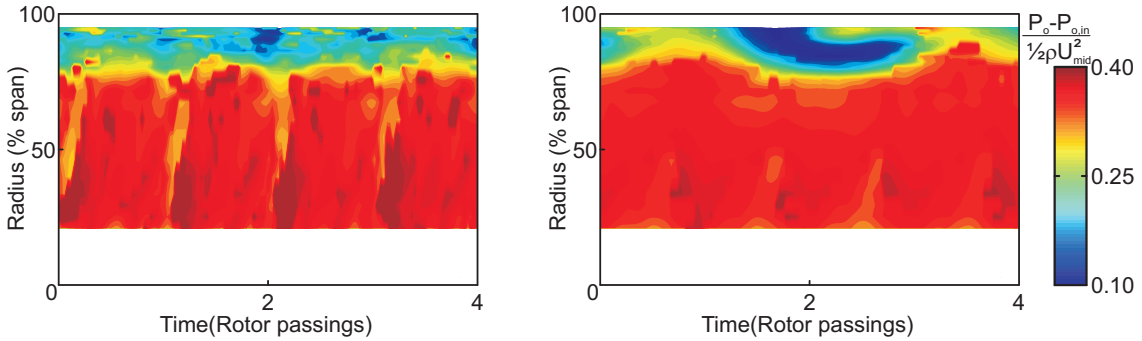

(a) Total Pressure, ensemble-averaged on once-per-revolution signal.

(b) Total pressure, ensemble-averaged on 'blue hole' minima.

(c) Readings from total pressure probe aligned axially, ensemble-averaged on once-per-revolution signal.

(d) Readings from total pressure probe aligned axially, ensemble-averaged on 'blue hole' minima.

Figure 7.17: *Fast-response total pressure probe traverse downstream of rotor at near-stall condition (3.3% tip-clearance, 75% eccentricity, maximum tip-clearance, $\phi = 0.470$).*

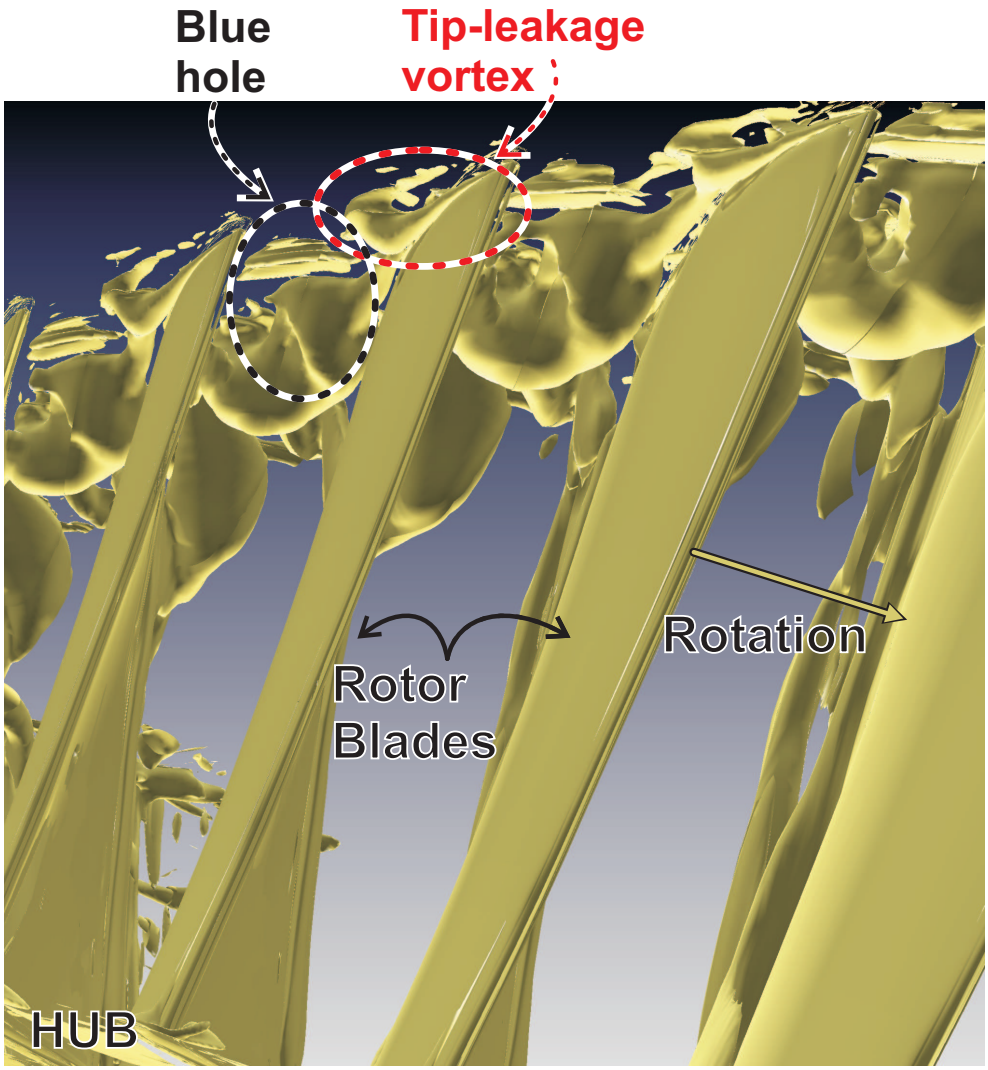

Figure 7.18: *Iso-surface of λ_2 vortex criterion in the concentric compressor with 3.3% clearance from an unsteady quarter-annulus simulation (Courtesy of Graham Pullan [79]).*

Chapter 8

Relationship Between Blue Holes and Stall Inception

The results discussed in Chapter 6 show that there is generally an increase in irregularity in the blade passing signature as stall is approached, though the magnitude of this increase, or ramp-up, is dependent on the tip-clearance size and eccentricity. In Chapter 7, the cause of the increase in irregularity was linked to the presence of blue holes - distinct disturbances which propagate in the tip-clearance region. The link between blade passing irregularity and blue holes is a significant step forward and its credibility is heightened by the recent computational work of Pullan [1], [79]. In the following pages, the link between blue holes and the stall inception process will be examined, particularly with reference to the formation of spikes.

In Chapter 7, it was shown that, under some circumstances, the compressor can operate stably with large blue holes propagating all the way around the annulus. For example, a compressor with large, concentric tip-clearance (3.3% chord) can sustain blue hole activity over most of the operating range. However, in a compressor with small, concentric tip-clearance (1.7% chord), once the blue holes begin to form the compressor immediately goes into rotating stall. It appears that the blue holes are instantly destabilising in the case of small tip-clearance, but not when the clearance is large.

This chapter addresses the link between blue holes and stall inception, and is divided into two sections. First, the stall inception process in a compressor with small tip-

clearance will be discussed. Second, a hypothesis will be put forward explaining why the compressor with larger clearance can operate stably when large blue holes are present.

8.1 Stall Inception with Small Clearance

In order to investigate the relationship between the blue holes and stall inception, measurements were taken with eight pressure transducers at the rotor leading edges and evenly spaced around the annulus. The arrangement is shown in Diagram 8.1. As well as the eight pressure transducers, five transducers were fitted at one particular circumferential location, marked 'A' in Diagram 8.1. These five probes were in an axial line from 40% chord upstream of the leading edge to 40% downstream of it.

Axial view. Radial view at point A.

Diagram 8.1: *Probe positions for stall inception measurements.*

Figure 8.1 shows stall inception in the test compressor with small, concentric tip-clearance. Figure 8.1 (a) shows the raw data from eight pressure transducers evenly spaced around the annulus as the compressor is driven into stall (the sample rate was 100kHz and the data was filtered at 50kHz prior to logging).

A mature stall cell can be seen in the traces from 29 revolutions onwards. The accepted characteristic trait of a spike stall cell is an upward pressure disturbance (see Fig. 4.4 (a)). In the traces shown in Fig. 8.1 (a), the upward spike is first visible in the data from transducer 5. The disturbance can, however be tracked back in the traces from transducer 4 to transducer 1.

More information about the disturbances from which the spike grows can be obtained by examining the data from the five transducers at position A, just before

transducer 1, where the stall cell can first be seen in Fig. 8.1. The pressure contour plot from these probes is shown in Fig. 8.1 (b)[1]. Just after 28.2 revolutions, a small blue hole can be seen just level with the leading edge of the blade row. A clearer picture of the disturbance can be seen in Fig. 8.1 (c), where the ensemble-averaged signal has been removed from the data. From this figure, it is clear that the spike stall cell follows immediately after the appearance of a blue hole.

Closer inspection of the pressure traces in Fig. 8.1 (a) reveals that the upward disturbance in the spike stall cell is also accompanied by a downward pressure spike. This downward pressure spike is actually the blue hole itself, so it can be said that the blue hole *is* the spike stall cell, and the upward pressure spike is a consequence of the presence of the blue hole.

A joint project was undertaken with Dr Pullan[2], with the aim of gaining a better understanding of the stall inception process in the light of the discovery of the blue holes. This has been reported by Pullan et al. [1]. In this paper, Pullan undertook a computational study of spike-type stall inception in a series of compressors, including the one discussed here.

Pullan et al. [1] show that the cause of the blue holes in compressors with small clearance is vorticity shed from a flow separation at the leading edge of the rotor tip. Their work also found that the blue holes propagate and grow into a spike stall cell.

The CFD work suggests that, in a compressor with small tip-clearance, the vortex is swept across the blade passage and triggers a new separation at the next blade leading to the formation of a new blue hole. However, instead of convecting downstream and out of the passage with the bulk of the flow, as is the case in a large clearance machine, the flow sweeps the original blue hole on a near-tangential trajectory around the leading edge of the next blade. This means that the two blue holes combine and move tangentially towards the next blade. This process is illustrated in Diagram 8.2. As fluid is being added to the blue hole, there is the potential for it to grow rapidly into a stall cell.

Figures 8.2 and 8.3 show a comparison of computational and experimental data at two different stages in the stall inception process.

[1]Note: a different colour scale to the one in Chapter 7 is used in this chapter to facilitate comparison with the computational results

[2]Those involved with the project were: G. Pullan, A. Young, I. Day, E. Greitzer and Z. Spakovszky.

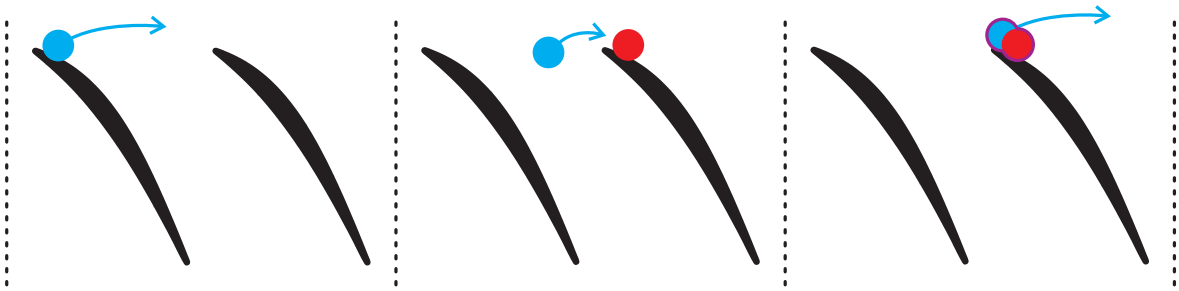

(a) Blue hole forms and convects across passage.

(b)New blue hole triggered in next passage.

(c) Two blue holes join together.

Diagram 8.2: *Mechanism of propagation and growth of blue holes in a compressor with small tip-clearance.*

Figure 8.2 shows an embryonic spike stall cell - i.e. data from the first point at which the characteristic up/down spike is seen. In Figure 8.2 (a), the top line traces show the data from the pressure transducer 40% chord upstream of the rotor leading edge (the solid line is raw data, while the dotted line shows the ensemble-averaged signal). The contour plot beneath shows pressure contours from the five probes at position 'A' in Diagram 8.1. Figure 8.2 (b) shows the same information as in Fig. 8.2 (a) but this time derived from the CFD calculation. Figure 8.2(b) also includes a plot of radial vorticity.

The blades marked 'G' in Fig. 8.2 show a loss of loading at their leading edges - i.e. the plot is less blue. This loss of loading is due to flow separation from the leading edge. Also visible in the pressure contour plots is a small blue hole at location 'F' (though this is a little more difficult to discern in the experimental data[3]).

The same set of plots is repeated in Figure 8.3, but at a later time. By this point, the low pressure zone (seen at t = 6 blades in Fig. 8.3 (a)) has grown significantly and now covers more than one blade passage. In the passages to the left of the low pressure region, small blue holes can be seen propagating forward of the leading edges. Further computational simulations can be seen in Pullan et al. [1], where the physical mechanism of spike stall cell propagation and growth is also shown in other compressors, suggesting some generality to the pattern.

The computational results shown here confirm the hypothesis that, in a compressor

[3]Note: Exact agreement between the experimental and computational data would not be expected in this situation, because the stall inception process in a real machine is not a perfectly repeatable event.

with small tip-clearance, blue holes lead directly to stall inception. Additionally, the blue holes have been shown to be due to shed vorticity from separation of the flow around the blade tips at the leading edge.

8.2 Stall Inception with Large Clearance

In the case of a compressor with large tip-clearance, blue holes form within the blade passage and can exist at operating points far from stall. They are therefore not thought to be caused by leading edge separation, unlike those in the small tip-clearance machine as discussed above.

Further computational studies have been carried out by Pullan in machines with larger tip-clearances [79]. These show blue holes forming from unsteadiness of the shear layer between the tip-leakage flow and the main flow. At operating points far from stall, at the design point for example, the blue holes are well aft of the leading edge and convect out of the rotor bladerow without causing stall inception, as shown in the experimental data in Section 7.1.3.

The connection between the blue holes which are formed further back in the blade row and stall inception has not been established. It is known that these blue holes move forwards as the compressor is throttled (Fig. 7.4), and eventually reach the leading edge. The hypothesis is that, upon reaching the leading edge, the blue holes cause a leading edge separation which leads to stall inception via a similar mechanism to that seen in a compressor with smaller tip-clearance. This has been seen in unpublished computational work by Pullan [79] on two different compressors, suggesting some generality to the trends.

Similar data to that shown in Fig. 8.1 for a compressor with small tip-clearance was obtained with a large clearance, but the vastly increased number of disturbances in the flow when the compressor was running at near-stall conditions meant that it was impossible to distinguish the eventual cause of stall inception. More CFD work is in progress and will be compared with the existing experimental results.

8.3 Conclusions

From the experimental data, guided and enhanced by the computational work of Pullan, the following conclusions can be drawn:

1. The effect of blue holes on compressor stability depends on the size of the tip-clearance gap:
    a. In a compressor with small tip-clearance (1.7% chord), the formation of blue holes leads directly to spike-type stall inception.
    b. A compressor with a larger tip-clearance (3.3% chord) can support large blue hole activity while continuing to operate stably. These blue holes remain within the blade passage and only move forwards when the flow coefficient is reduced. The blue holes do not appear to cause stall until they reach the rotor leading edge plane. Further work is required to clarify the connection between blue holes and stall inception in this case.
2. There is a distinction between the cause of the blue holes in a compressor with small tip-clearance and one with larger clearance:
    a. In the case of a compressor with small clearance, the blue holes are caused by shed vorticity from a separation at the rotor leading edge tip.
    b. In the case of a compressor with larger clearance, the blue holes form due to instability in the shear layer between the tip-leakage flow and the core flow.
3. In both the small and large clearance cases, each blue hole convects across the passage and triggers the formation of a new blue hole when it reaches the next blade. However, there is a distinction to be made between the path that the fluid in the original blue hole takes:
    a. In a compressor with a small clearance, the blue hole moves tangentially across the rotor passage and triggers, but also amalgamates with, a new blue hole. This creates the potential for a disturbance which will grow rapidly into a stall cell.
    b. In the case of a compressor with larger clearance, the blue holes convect downstream and out of the blade passage with the bulk flow, setting off a

new disturbance in the next passage as they do so. In this way the disturbances propagate but the fluid in them does not, the blue holes themselves do not necessarily grow in size.

4. The current hypothesis is that the blue holes cause a leading edge separation once they reach the rotor leading edge, which leads to stall in the same manner as that seen in a compressor with small tip-clearance.

The fact that the above trends have been observed in computational results for compressors of different designs suggests that the stall inception patterns observed here might be of a general nature.

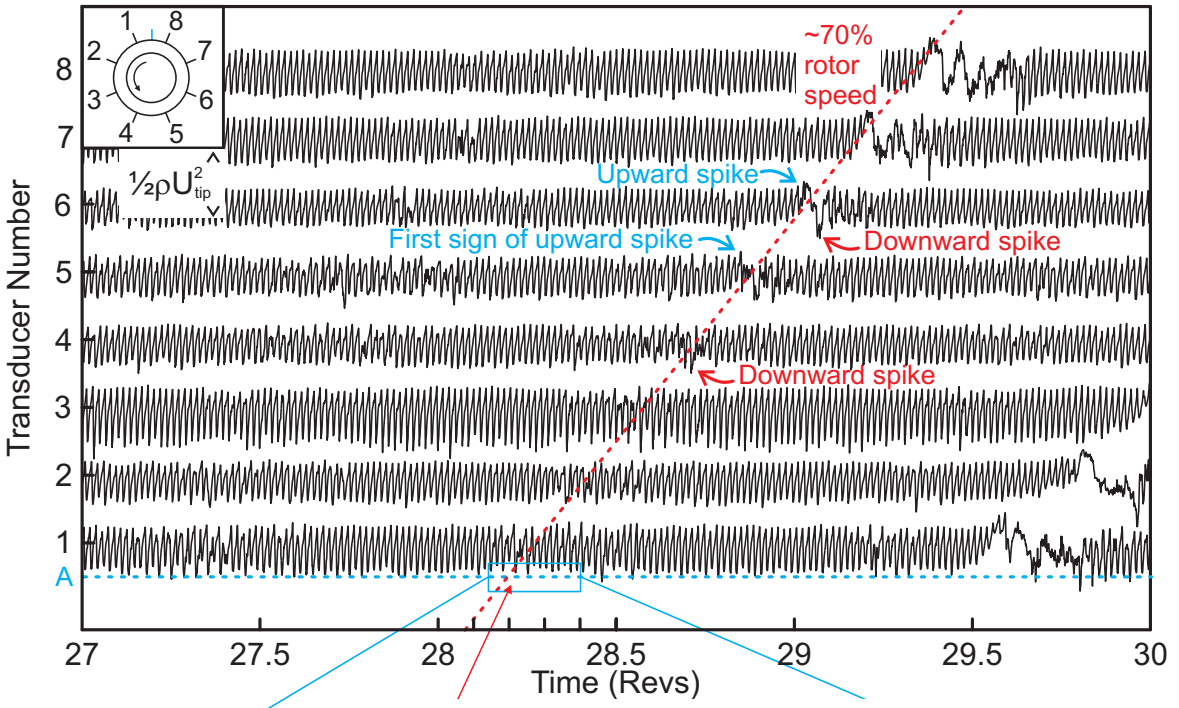

(a) Signal from 8 pressure transducers around the annulus.

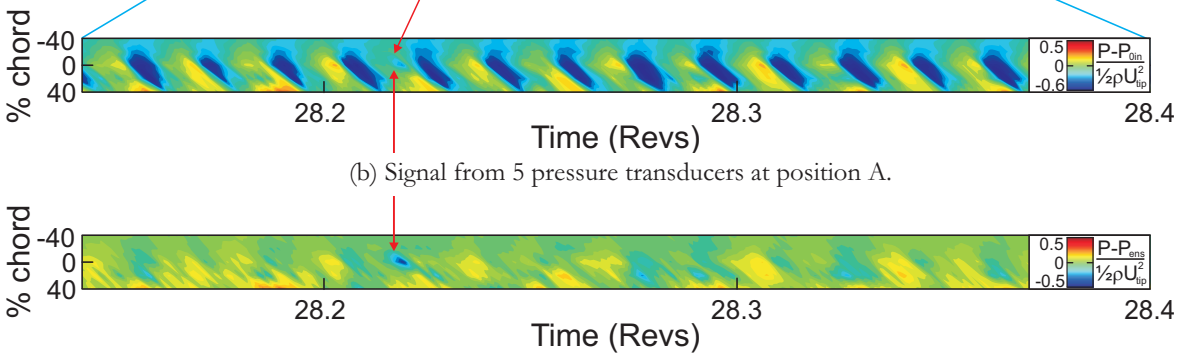

(b) Signal from 5 pressure transducers at position A.

(c) Signal from position A with ensemble-average removed.

Figure 8.1: *Stall inception observed with pressure transducers around the annulus and across the rotor tips (1.7% tip-clearance, concentric).*

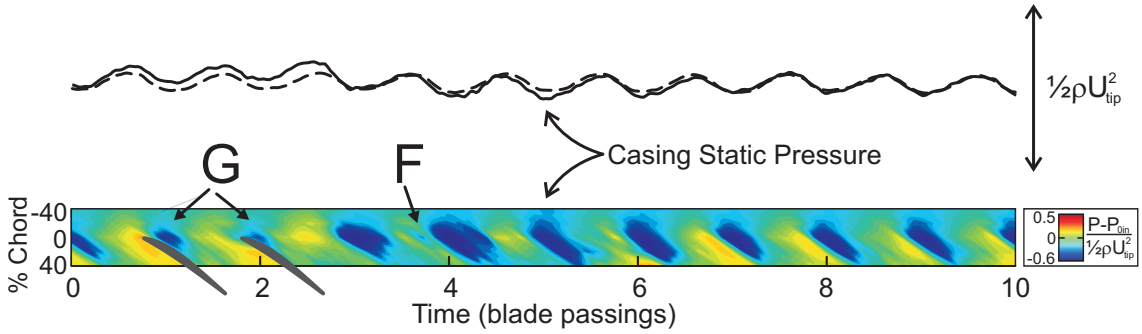

(a) Experimental Data (Anna Young).

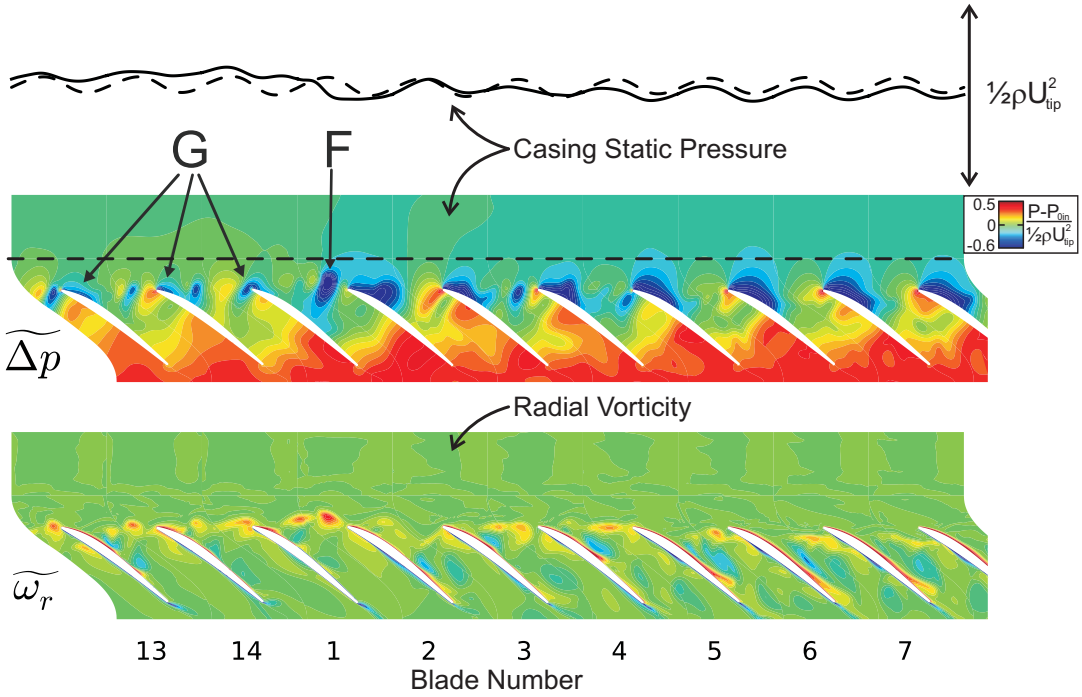

(b) Computational Simulation (Graham Pullan).

Figure 8.2: *Embryonic spike stall cell: comparison of casing measurements from experiments and CFD (1.7% tip-clearance, concentric).*

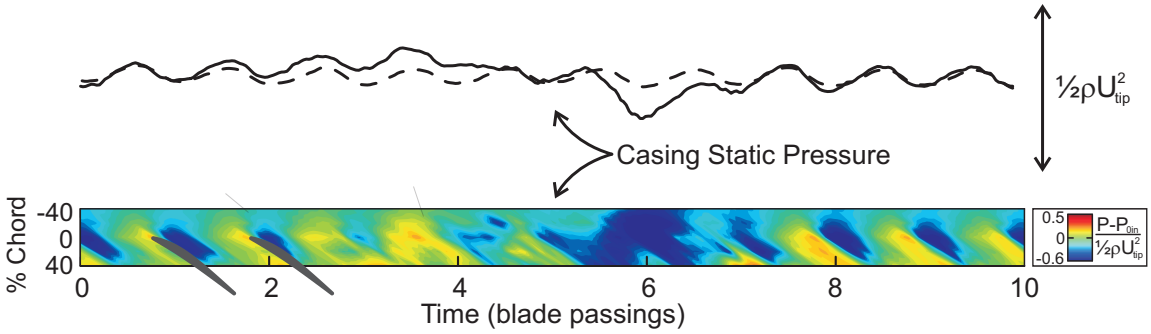

(a) Experimental Data (Anna Young).

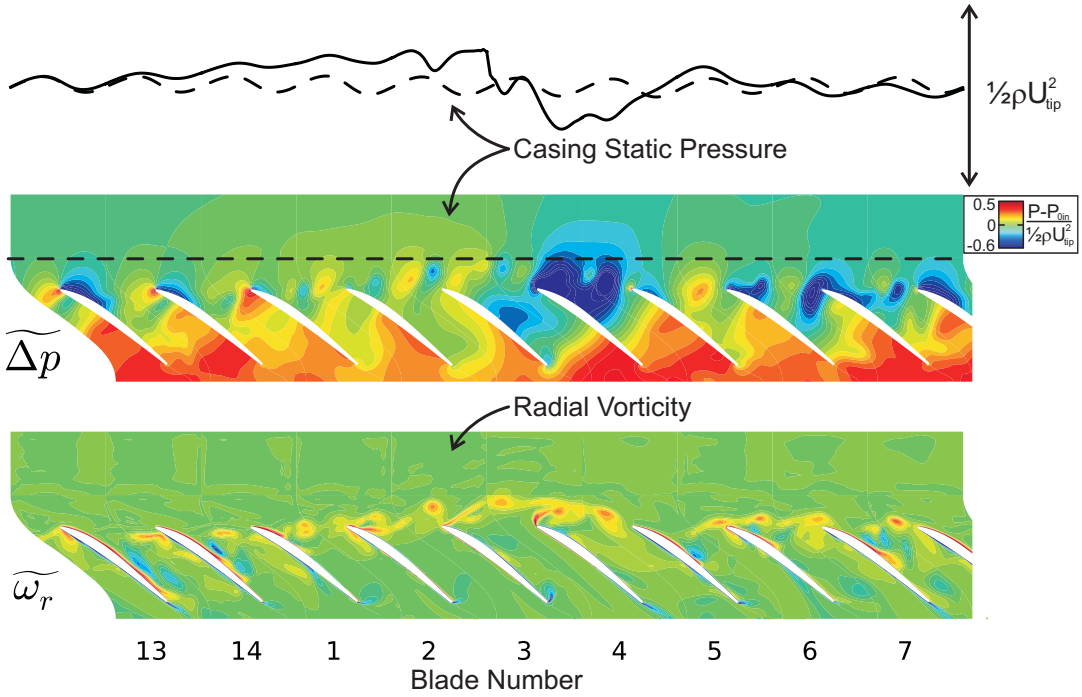

(b) Computational Simulation (Graham Pullan).

Figure 8.3: *Mature spike stall cell: comparison of casing measurements from experiments and CFD (1.7% tip-clearance, concentric).*

Chapter 9

Conclusions and Suggestions for Future Work

The subjects of tip-clearance flows and their effect on the performance and stalling behaviour of a compressor have been studied extensively over the past half-century but many questions remain. This chapter summarises the key contributions that this thesis has made in answering some of these questions.

The current work has studied the impact of tip-clearance size and eccentricity on the overall performance of a compressor. Attention was also focused on the highly unsteady flow in the tip region of the compressor and new revelations made about disturbances which appear in the flow before stall. The role of these disturbances in the stall inception process was also examined.

The chapter is divided into four parts. The first three parts list the key findings on the link between tip-clearance size and compressor performance, the irregularity level in the blade passing signature, and the pre-stall disturbances in the tip-clearance gap. In the final part, suggestions will be made for future work on the topics covered in this project.

9.1 Tip-Clearance Size and Compressor Performance

Measurements of stall inception in a concentric compressor with a range of tip-clearances have shown, for the first time, that the stalling behaviour of a compressor (i.e. its inception mechanism and stall cell type) changes as the tip-clearance is increased. Two trends been revealed: Firstly, the stall inception mechanism changes with tip-clearance from spike at small tip-clearances (1 to 3%) to modal with moderate clearances (3 to 6%), and secondly that the compressor begins to exhibit part-span stall with large clearances (greater than 6% chord).

It was also observed that there is a step change in the relationship between tip-clearance size and stalling flow coefficient which occurs as the gap size increases. With small clearances, the degradation in stalling flow coefficient with tip-clearance size is linear. Once the change to modal stall has occurred, the stalling flow coefficient remains roughly constant. It is thought that the trends observed here are general, but the gap sizes at which the changes occur will vary from one compressor to another.

It has also been shown that the idea put forward by Khalid et al. [53] and others, that the blockage level in the compressor is directly linked to how close the machine is to its stall point, is too simplistic. The level of blockage in the rotor exit flow at near-stall conditions was found to be constant for tip-clearances up to 4% chord, because the increase in tip blockage associated with each increase in gap size was countered by a corresponding reduction in hub blockage. At clearances greater than 4% chord, however, the tip blockage continued to increase but the hub blockage no longer decreased, leading to higher overall blockage levels.

The movement of blockage from the hub to the tip with increasing tip-clearance adds weight to Dickens' finding [15] that compressors which stall via modes show high blockage in the tip region while those which stall via spikes have more blockage at the hub.

In cases where tip-clearance eccentricity was introduced, it was found that there was no reduction in the pressure rise produced by the compressor. Eccentricity did, however, have a detrimental effect on the stall margin of the compressor.

The observed relationship between eccentricity level and stalling flow coefficient has

been used to develop an empirical model for the stall point of an eccentric machine with small to moderate tip-clearance (less than 4% chord). The new findings were that:

1. At a given average clearance, the increase in stalling flow coefficient due to eccentricity is linear, and,
2. Increasing the average tip-clearance leads to a linear reduction in the effect of eccentricity on the stalling flow coefficient.

Were this decreasing effect of eccentricity to continue indefinitely, the stalling flow coefficient would be unaffected by eccentricity if the average gap size was above 4%. The model was, however, shown to break down at larger clearances, when part-span stall was observed.

The industry rule of thumb, that the stalling flow coefficient of an eccentric compressor will be the same as that of a concentric compressor with clearance the same clearance as the maximum eccentric clearance, has been shown to be overly pessimistic. This suggests that the small tip-clearance part of the annulus has a stabilising effect on the large tip-clearance region.

The two-dimensional model of Graf et al. [47] for flowfield redistribution in an eccentric compressor was applied to the compressor used in this work. There was a considerable discrepancy between the model output and the experimental results, in terms of both the magnitude and phase lag of the redistribution. These errors arise because it is not appropriate to assume that the flow is two-dimensional.

The stability of the flow in an eccentric compressor was shown to vary around the circumference when it was operating near its stall point. This was found by comparing the local flow coefficient (at a near-stall average flow coefficient) to the local equivalent concentric stall point. This calculation showed an unstable sector in which the compressor was operating at a lower flow coefficient than its natural stall point. This result led to the suggestion that the size (both circumferential extent and 'depth') of this unstable sector may be useful for predicting the stall point of an eccentric machine if the flow field redistribution can be accurately modelled.

At the stall point of an eccentric compressor, the large tip-clearance sector has been shown to produce a total pressure rise equal to the maximum that it could produce if

it were operating in a concentric machine with the same clearance. This suggests that the compressor stalls when a certain proportion of the annulus reaches its maximum pressure rise capability. More work would be required to confirm this idea.

9.2 Blade Passing Irregularity and the Prediction of Stall

The unsteady pressure fluctuations on the rotor casing caused by the passing blades (the blade passing signature) have been observed by some researchers to become more irregular as the compressor operating point moves towards stall. Previous work by Dhingra et al. [66] and Christensen et al. [69] has suggested that this rise, or ramp-up, in irregularity just before stall could be used as an input to a stall warning device. Prototype systems based on these measurements have shown some promise, and the idea has been patented by General Electric [3].

Experiments undertaken as part of the current work have revealed that the level of irregularity is not just dependent on the proximity of the compressor to stall, but also on the tip-clearance size and eccentricity. This is a hitherto unappreciated complication.

The level of blade passing signature irregularity in a concentric compressor, with small tip-clearance, was found to be comparatively low and rose very little as the compressor approached stall. In a concentric compressor with large tip-clearance, the level of irregularity was low at full flow, but ramped up noticeably as the flow rate was reduced.

In an eccentric compressor, the level of blade passing irregularity varies around the annulus. In the large tip-clearance sector, the level of irregularity was found to ramp up strongly as the compressor was throttled towards stall. By contrast, the irregularity remained small and steady in the tight tip-clearance part of the annulus - surprisingly, this was found to be true regardless of the actual size of the gap in this region.

It has also been shown for the first time that the level of blade passing irregularity in an eccentric compressor is a function of the average tip-clearance size *and* the amount of casing eccentricity. There is a dynamic aspect to the level of blade passing irregularity which is not solely dependent on the size of the local tip-clearance gap.

The likely changes in tip-clearance size and eccentricity in a real engine - both over a flight cycle and over the life of the engine - were considered. This led to the conclusion that the level of irregularity in the blade passing signature cannot be used on its own to provide reliable stall warning in a real engine. At least one other parameter would have to be measured, and so the system patented by General Electric is useless in its current form.

9.3 Rotating Disturbances in the Tip-Clearance Region

For the first time, the cause of the increase in irregularity in the blade passing signature has been identified. This was achieved by using detailed rotor casing pressure contour maps and a novel data analysis technique. The irregularity is caused by discrete, pre-stall, disturbances ('blue holes') propagating from one blade to the next.

This work is the first to establish a link between blue holes and the rise in irregularity near stall, as previous work has treated the two phenomena as separate subjects. In tests with numerous combinations of tip-clearance size and eccentricity, the occurrence of a pre-stall ramp-up in irregularity and the presence of blue holes matched exactly, confirming this link.

Previous work by Mailach et al. [54] concentrated on Fourier transforms of casing pressure measurements which revealed a distinct hump at a frequency approximately one third of the blade passing frequency. The blue holes found in this work have a similar frequency content, but their existence and structure has now been revealed. Furthermore, it is believed that this is the first time that such disturbances have been seen in a compressor that is not operating in a partially-stalled state (see for example the work of Inoue et al. [57]).

The blue holes are characterised by regions of low static pressure on the casing which are similar in magnitude to the compressor inlet dynamic head. At near-stall operating conditions in a compressor with large tip-clearance (3.3% chord), these low pressure patches extend from the leading edge to mid-chord and occupy half a rotor pitch circumferentially. The low pressure patches are most easily explained as vortex structures of a radial nature. The vortical structure is seen in hotwire traverse data and confirmed by Pullan's computational results (see [1]).

In the tests with large clearance, the blue holes were present at operating points far from stall. At these operating conditions, their location was was aft of the leading edge. As the compressor operating point was moved towards stall, the blue holes grew in axial and circumferential extent and became 'deeper'.

It was also found that, as the compressor operating point is moved towards stall, the blue holes propagate more quickly as they grow in size. This is the opposite of spike stall cells, which slow down as they grow. The blue holes have been shown to propagate by convecting across the passage and triggering the formation of a new blue hole in the next blade passage. In this way, the disturbance propagates, but the fluid in the blue hole does not.

New light has also been shed on the link between the blue holes and the stall inception process. In a compressor with small tip-clearance, the blue holes are caused by shed vorticity from a separation at the rotor leading edge tip and the formation of blue holes leads directly to spike-type stall inception.

While blue holes lead directly to stall in a compressor with small tip-clearance, a compressor with large clearance can support vigorous blue hole activity while continuing to operate stably. This is because the blue holes do not augment each other as they propagate, but convect downstream and out of the blade passage with the bulk flow. The blue holes do not appear to cause stall until they reach the rotor leading edge plane. In the case of a compressor with large clearance, the blue holes are believed to form due to instability in the shear layer between the tip-leakage flow and the core flow.

The findings presented here have been enhanced and backed up by computational work by Pullan et al, which is to be published in June 2012 [1]. These calculations were initially carried out on a different compressor but were then repeated on the test compressor from this work, suggesting some generality to the findings.

9.4 Recommendations for Future Work

It has been shown that the size of the tip-clearance gap can influence the stall inception mechanism of a compressor. It would be interesting to understand more clearly

why this is, as this might help to shed more light on the general reasons why a compressor stalls via one mechanism and not the other. One potential avenue of research would be to calculate the rotor blade tip loading and see how this changes with tip-clearance size. This would be best achieved through a combination of computational and experimental work.

In the current work, it was shown that, when an eccentric compressor is operating near its stall point, there is a sector of the annulus which would be expected to be unstable if it were operating in isolation. This unstable sector exists because of the combined effects of the change in stall point associated with a change in tip-clearance, and the redistribution in the flowfield due to the tip-clearance asymmetry. If an improved flowfield model could be developed and used to predict this redistribution, then it may be possible to develop a better rule of thumb for the stall point of an eccentric machine based on the unstable sector.

It also appears that an eccentric compressor will stall when the large tip-clearance sector of the annulus is producing a total pressure rise equal to the maximum that it could produce if it were operating in a concentric machine with the same clearance. More work would be required to confirm this hypothesis, which also revolves around the local flow coefficient (because $\psi_{\text{T-T}} = \psi_{\text{T-S}} + \phi^2$ and $\psi_{\text{T-S}}$ is constant around the annulus). This means that an improved flow redistribution model would be of use here, too.

While it has been shown that the level of irregularity in the blade passing signature is unlikely to be useful as a stall warning signal, there are other possible uses for such measurements. In particular, it is possible that blade passing irregularity could be used as part of an engine health monitoring system, to check tip-clearances in the compressor after a period of time in service. This idea merits further research as the benefits will be significant.

In terms of the structure and behaviour of blue holes and their link to the stall inception process, it is hoped that the computational simulations currently being undertaken by Pullan will answer the remaining questions. In particular, further work is required to clarify the relationship between blue holes and stall in a compressor with large tip-clearance.

Appendix A

Derivation and Application of Flow Redistribution Model

In this appendix, the background to the model of Graf et al. will be explained. The application of the model to the test compressor used in this work will then be described, along with the method used to compare the model output with experimental data.

Initial Model

The Hynes-Greitzer model [48], as adapted by Graf et al. for asymmetric tip-clearance [47], starts by assuming that there is a variation in flow coefficient around the annulus. This means that the fluid in the rotor passages must be accelerating and decelerating as it moves through the changing flowfield, and this acceleration must be balanced by an unsteady pressure fluctuation. This leads to the following equation::

$$\frac{p_2 - p_{01}}{\frac{1}{2}\rho U^2} = \psi(\phi, \epsilon) - \lambda \frac{d\phi}{d\theta} \tag{A.1}$$

where λ is an inertia parameter and is defined by:

$$\lambda = \frac{b_x}{\frac{1}{2} r \cos^2 \gamma} \tag{A.2}$$

The test compressor used in this work was not initially fitted with Inlet Guide Vanes (IGVs). This means that the inlet absolute and relative flow angles are not fixed, and so the stage pressure rise is not only a function of flow coefficient and tip-clearance but also of inlet angle[1], α. Thus:

$$\frac{p_2 - p_{01}}{\frac{1}{2}\rho U^2} = \psi(\phi, \epsilon, \alpha) - \lambda\frac{d\phi}{d\theta} \tag{A.3}$$

For small perturbations, this becomes:

$$\frac{\delta p_2 - \delta p_{01}}{\frac{1}{2}\rho U^2} = \frac{\partial\psi}{\partial\phi}\delta\phi + \frac{\partial\psi}{\partial\epsilon}\delta\epsilon + \frac{\partial\psi}{\partial\alpha}\delta\alpha - \lambda\frac{d(\delta\phi)}{d\theta} \tag{A.4}$$

The inlet total pressure is fixed and thus cannot change around the annulus, and the same is true of the exit static pressure. This means that the left-hand side of the equation is zero, thus:

$$\lambda\frac{d(\delta\phi)}{d\theta} - \frac{\partial\psi}{\partial\phi}\delta\phi - \frac{\partial\psi}{\partial\alpha}\delta\alpha = \frac{\partial\psi}{\partial\epsilon}\delta\epsilon \tag{A.5}$$

Equation A.5 can be solved by expressing the flowfield and the tip-clearance distribution as Fourier series.

Fourier Series Expressions

The tip-clearance distribution can be expressed as a Fourier series:

$$\delta\epsilon = \sum_{\substack{n=-\infty \\ n\neq 0}}^{\infty} \mathrm{A_n} e^{in\theta} \tag{A.6}$$

Where $\mathrm{A_n}$ are Fourier coefficients, which will be known if the circumferential variation in tip-clearance is known.

The Hynes-Greitzer model is two-dimensional, so any radial variations in the flowfield are ignored. Furthermore, the flowfield must be periodic in the tangential direction and perturbations from the mean flow coefficient must decay upstream of

[1]The subject of incorporating inlet swirl sensitivity into the Hynes-Greitzer model is discussed in depth in Longley's PhD thesis [81].

the rotor bladerow. This means that the velocity potential, Φ, of the flowfield is of the form:

$$\Phi = \sum_{n=-\infty}^{\infty} \mathrm{B_n} e^{in\theta+|n|\frac{x}{r}} \tag{A.7}$$

where $\mathrm{B_n}$ are unknown Fourier coefficients. In cylindrical polar co-ordinates, the velocity field, $\underline{u}$, is related to the velocity potential as follows:

$$\underline{u} = \frac{1}{r}\frac{\partial \Phi}{\partial \theta}\underline{e}_\theta + \frac{\partial \Phi}{\partial x}\underline{e}_x \tag{A.8}$$

thus

$$\delta V_\mathrm{x} = \frac{\partial \Phi}{\partial x} \qquad \text{and} \qquad \delta V_\theta = \frac{1}{r}\frac{\partial \Phi}{\partial \theta} \tag{A.9}$$

Differentiating Equation A.7 and substituting into Equations A.9:

$$\delta V_\mathrm{x} = \sum_{\substack{n=-\infty \\ n\neq 0}}^{\infty} \mathrm{B_n}\frac{|n|}{r} e^{in\theta+|n|\frac{x}{r}} \qquad \text{and} \qquad \delta V_\theta = \sum_{\substack{n=-\infty \\ n\neq 0}}^{\infty} \mathrm{B_n}\frac{in}{r} e^{in\theta+|n|\frac{x}{r}} \tag{A.10}$$

To simplify Equations A.10, let $\mathrm{C_n} = \frac{\mathrm{B_n}|n|}{\bar{U}r}$:

$$\delta\phi = \frac{\delta V_\mathrm{x}}{\bar{U}} = \sum_{\substack{n=-\infty \\ n\neq 0}}^{\infty} \mathrm{C_n} e^{in\theta+|n|\frac{x}{r}} \tag{A.11}$$

$$\text{and} \qquad \frac{\delta V_\theta}{\bar{U}} = \sum_{\substack{n=-\infty \\ n\neq 0}}^{\infty} \mathrm{C_n}\frac{i|n|}{n} e^{in\theta+|n|\frac{x}{r}}$$

$$= \sum_{\substack{n=-\infty \\ n\neq 0}}^{\infty} [\delta\phi]_\mathrm{n}\,\frac{i|n|}{n} \tag{A.12}$$

An expression for $\frac{\partial(\delta\phi)}{\partial\theta}$ can be obtained by differentiating Equation A.11 with respect to theta:

$$\frac{\partial\,(\delta\phi)}{\partial\theta} = \sum_{\substack{n=-\infty \\ n\neq 0}}^{\infty} in\mathrm{C_n} e^{in\theta+|n|\frac{x}{r}}$$

$$= \sum_{\substack{n=-\infty \\ n\neq 0}}^{\infty} in\,[\delta\phi]_\mathrm{n} \tag{A.13}$$

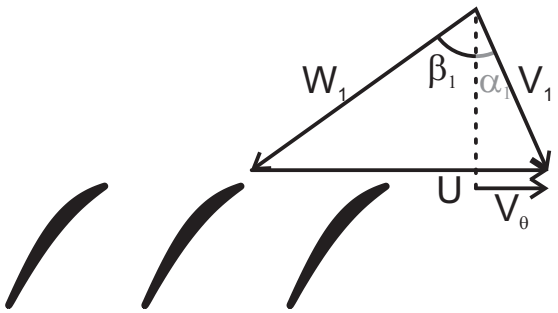

Figure A.1: *Rotor inlet velocity triangle.*

An expression for $\delta\alpha$ can be found by considering the velocity triangle shown in Fig. A.1:

$$V_x \tan\alpha_1 = V_\theta \tag{A.14}$$

$$\text{so} \qquad \delta V_x \tan\alpha_1 + V_x \sec^2(\alpha_1)\delta\alpha = \delta V_\theta \tag{A.15}$$

For axial inflow (as in the case of a compressor with no IGVs), $\alpha = 0$, therefore $\tan\alpha_1 = 0$ and $\sec\alpha_1 = 1$, so:

$$\begin{aligned} \delta\alpha &= \frac{\delta V_\theta}{V_x} \\ &= \frac{1}{\bar{\phi}}\frac{\delta V_\theta}{\bar{U}} \end{aligned}$$

Substituting in from Equation A.12 for $\frac{\delta V_\theta}{\bar{U}}$:

$$\delta\alpha = \frac{1}{\bar{\phi}} \sum_{\substack{n=-\infty \\ n\neq 0}}^{\infty} [\delta\phi]_n \frac{i|n|}{n} \tag{A.16}$$

The expressions derived above for $\frac{\partial(\delta\phi)}{\partial\theta}$, $\delta\epsilon$ and $\delta\alpha$ (Equations A.6, A.13 and A.16)can

now be substituted into Equation A.5, and rearranged to obtain an expression for $\delta\phi$:

$$\delta\phi = \sum_{\substack{n=-\infty \\ n\neq 0}}^{\infty} A_{\mathrm{n}} e^{in\theta} \frac{\frac{\partial\psi}{\partial\epsilon}}{\left(\lambda n - \frac{1}{\bar{\phi}}\frac{|n|}{n}\frac{\partial\psi}{\partial\alpha}\right) i - \frac{\partial\psi}{\partial\phi}} \tag{A.17}$$

Application of the model to the test compressor

Tip-clearance Distribution The tip-clearance distribution in the test compressor is sinusoidal, such that $\delta\epsilon = \frac{\Delta\epsilon}{2}\cos\theta$. The Fourier coefficients, A_{n}, are therefore:

$$A_{\mathrm{n}} = \begin{cases} \frac{\Delta\epsilon}{2}, & n = \pm 1 \\ 0, & \text{otherwise} \end{cases} \tag{A.18}$$

Substituting these coefficients into Equation A.17 gives:

$$\begin{aligned} \delta\phi &= -\frac{\Delta\varepsilon}{2}\frac{\partial\psi}{\partial\varepsilon}\left[\frac{e^{i\theta}}{\frac{\partial\psi}{\partial\phi} - \left(\lambda - \frac{1}{\bar{\phi}}\frac{\partial\psi}{\partial\alpha}\right)} + \frac{e^{-i\theta}}{\frac{\partial\psi}{\partial\phi} - \left(-\lambda + \frac{1}{\bar{\phi}}\frac{\partial\psi}{\partial\alpha}\right)}\right] \\ &= -\Delta\varepsilon\frac{\partial\psi}{\partial\varepsilon}\left[\frac{\frac{\partial\psi}{\partial\phi}\cos\theta - (\lambda - \frac{1}{\bar{\phi}}\frac{\partial\psi}{\partial\alpha})\sin\theta}{\left(\lambda - \frac{1}{\bar{\phi}}\frac{\partial\psi}{\partial\alpha}\right)^2 + \left(\frac{\partial\psi}{\partial\phi}\right)^2}\right] \end{aligned} \tag{A.19}$$

Equation A.19 shows that, given a sinusoidal variation in tip-clearance, the flowfield redistribution will also be sinusoidal, but with a phase lag. The phase lag, $\Delta\theta$ is given by:

$$\Delta\theta = -\tan^{-1}\left(\frac{\lambda - \frac{1}{\bar{\phi}}\frac{\partial\psi}{\partial\alpha}}{\frac{\partial\psi}{\partial\phi}}\right) \tag{A.20}$$

Compressor-Dependent Parameters The expressions derived for flowfield redistribution and phase lag depend on several aspects of the compressor's performance: $\frac{\partial\psi}{\partial\phi}$, $\frac{\partial\psi}{\partial\epsilon}$ and $\frac{\partial\psi}{\partial\alpha}$. In order to calculate the theoretical flow redistribution, values for these terms must be found. This was done empirically, as follows:

Values for $\frac{\partial\psi}{\partial\phi}$, and $\frac{\partial\psi}{\partial\epsilon}$ were found from measured compressor characteristics with different levels of tip-clearance (see Chapter 4). The increase in stalling flow coefficient which accompanies an increase in tip-clearance means that the value of $\frac{\partial\psi}{\partial\epsilon}$ has to be estimated at flow coefficients close to the stall point of the eccentric compressor (because no data is available for the large clearance compressor at these points).

The sensitivity of the compressor to inlet swirl, $\frac{\partial\psi}{\partial\alpha}$, was found by testing the compressor with IGVs fitted at three stagger angles (to give inlet flow angles of approximately -3, 0 and +3°). It was found that:

$$\frac{\partial\psi}{\partial\alpha} = -7.1\phi + 2.7$$

In the analysis above, the inertia parameter, λ, is dependent only on geometric features of the compressor (see Equation A.2). However, the inertia of the flow in the compressor is increased by the changing losses as the blades move through a changing flowfield. Chue et al. [82] undertook an analysis of this additional term and suggested that λ be replaced with λ_{eff}, where:

$$\begin{aligned} \lambda_{\text{eff}} &= \lambda - \tau\frac{d(\text{Loss}_{\text{rotor}})}{d\phi} \qquad \text{(A.21)} \\ \text{where} \qquad \tau &= \frac{b_x}{r\phi} \\ \text{and} \qquad \frac{d(\text{Loss}_{\text{rotor}})}{d\phi} &= \left.\frac{\partial\psi}{\partial\phi}\right|_{\text{ideal}} - \left.\frac{\partial\psi}{\partial\phi}\right|_{\text{real}} \end{aligned}$$

Experimental Method for Measuring the Flow Redistribution

The flow redistribution in the test compressor was found by measuring the local static pressure just upstream of the rotor blades at eighteen evenly-spaced locations around the annulus. The relationship between the static pressure and local flow

coefficient can be derived from the linearised form of Bernoulli's equation as follows:

$$\begin{aligned}
\delta p_0 &= \delta p + \rho \bar{v}_x \delta v_x + \rho \bar{v}_\theta \delta v_\theta \\
\text{but} \qquad \bar{v}_\theta &= 0 \text{ (no bulk inlet swirl)} \\
\text{so} \qquad \rho \bar{v}_x \delta v_x &= \delta \left(p_0 - p \right) \\
\delta \phi = \frac{\delta v_x}{\bar{U}} &= \frac{\delta \left(p_0 - p \right)}{\rho \bar{v}_x \bar{U}} \\
&= \frac{\bar{U}}{\bar{v}_x} \frac{\delta \left(p_0 - p \right)}{\rho \bar{U}^2} \\
\text{therefore} \qquad \delta \phi &= \frac{1}{\bar{\phi}} \frac{\delta \left(p_0 - p \right)}{\rho \bar{U}^2}
\end{aligned} \tag{A.22}$$

From the above equation, it is clear that the flowfield redistribution can be found by measuring the static pressure around the annulus, as long as the compressor speed and inlet total pressure are known.

Appendix B

Some Comments on the Validity of the Flow Redistribution Model

In Chapter 5, it was shown that the output from the model of Graf et al. [47] did not fit the experimental data.

The main cause of this discrepancy was shown to be the inlet swirl sensitivity parameter, which increases the phase lag between the maximum tip-clearance and minimum flow coefficient. The inlet swirl sensitivity parameter also becomes large at high flow coefficients, leading to excessive attenuation of the flow redistribution.

Two major assumptions implicit in this work are are that the exit static pressure is constant around the annulus, and that the flow is two-dimensional. These will be examined in this appendix, along with a qualitative check of the effect of inlet swirl sensitivity on the compressor.

Exit Static Pressure

The Hynes-Greitzer model assumes constant exit static pressure. To test the validity of this assumption, the exit static pressure was measured 5 chords downstream of the stators at twelve locations around the annulus. The results are shown in Fig. B.1 (a), which is a plot of the change in stage total-to-static pressure rise coefficient $\left(\frac{\delta p_2}{\frac{1}{2}\rho U^2}\right)$

against circumferential position[1].

The dotted lines in Fig. B.1 (a) show measurements in the concentric case, while the solid lines show the results from the compressor with 75% eccentricity. The two sets of measurements are very similar, so it can be concluded that the presence of eccentricity does not lead to increased variation in the exit static pressure.

In addition, by comparing the results for the eccentric compressor at its design point (solid black line) and at near stall conditions (solid red line), it can be seen that there is no noticeable increase in the variation in exit static pressure between the design point and near stall.

To emphasise the point that the exit static pressure is constant, it is interesting to compare the variation in exit static pressure with the variation in flow coefficient for the same set of configurations. This is shown in Fig. B.1 (b). In the concentric case (dotted lines), the variation in flow coefficient is negligible, and almost the same from design to near stall. In the case with 75% eccentricity (solid lines), however, there is a large redistribution of the flow, and the variation in flow coefficient is greater near stall than at the design point. This change in behaviour is due to the eccentric tip-clearance and is clearly much greater than the variation in total-to-static pressure rise coefficient seen in Fig. B.1 (a). From these results it can be concluded that the assumption of constant exit static pressure is valid.

Qualitative Check of the Effect of Inlet Swirl Sensitivity

In an eccentric compressor, the inertia parameter, λ, introduces a phase lag between the maximum tip-clearance and the minimum flow coefficient. The original analysis by Graf et al. assumes that the compressor is not sensitive to changes in inlet swirl, i.e. it is fitted with Inlet Guide Vanes (IGVs). In a compressor with no IGVs, there is an extra term in the phase lag due to the inlet swirl sensitivity, as discussed above, which changes the numerator in the phase lag expression from λ to $\left(\lambda - \frac{1}{\bar{\phi}}\frac{\partial \psi}{\partial \alpha}\right)$ (see Equation A.20).

Increasing the inlet swirl leads to a reduction in pressure rise, so $\frac{\partial \psi}{\partial \alpha}$ is negative,

[1] the inlet total pressure is constant, so any changes in pressure rise are due to variations in the exit static pressure.

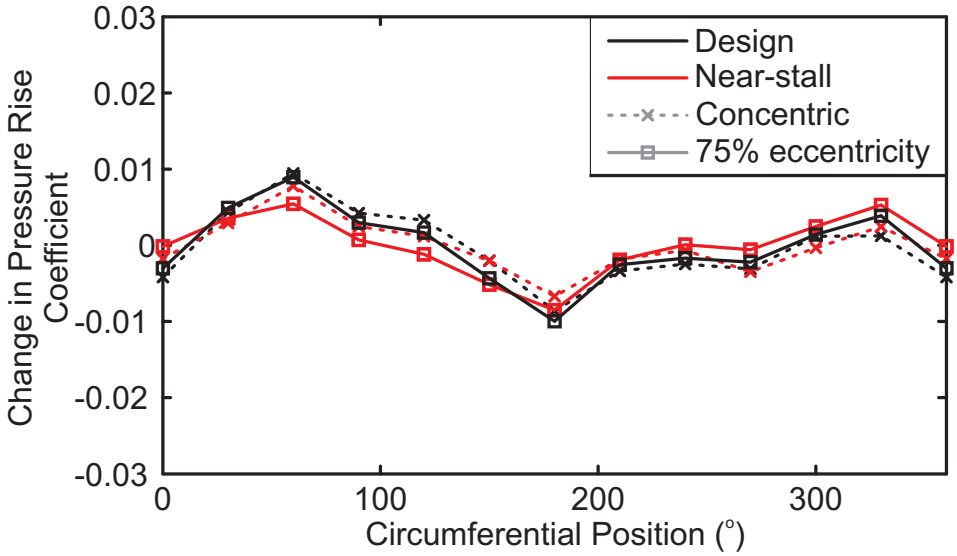

(a) Variation in total-to-static stage pressure rise coefficient.

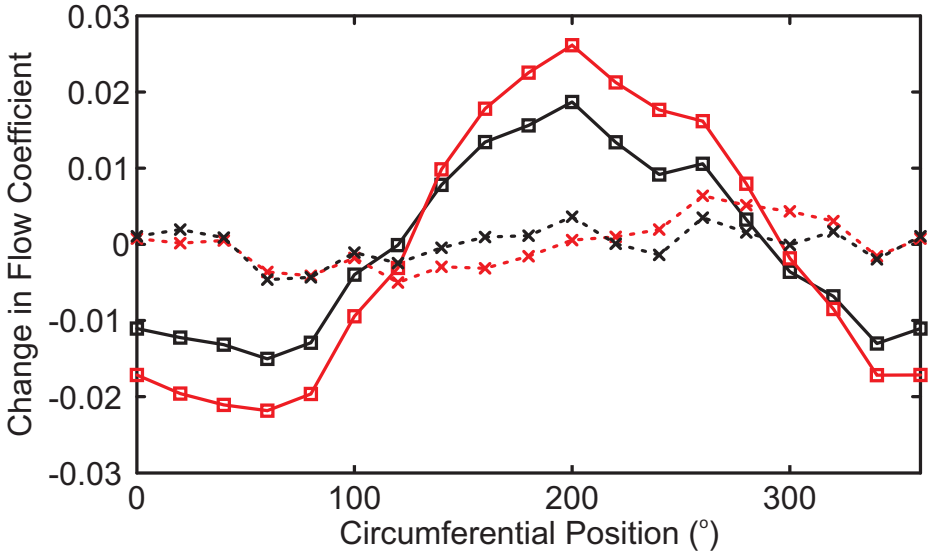

(b) Variation in flow coefficient.

Figure B.1: *Variation in stage loading and flow coefficient around the compressor (concentric and eccentric, 3.3% average clearance).*

as shown in Equation A.21. This means that the inclusion of the inlet swirl sensitivity term will increase the phase lag, as $\left(\lambda - \frac{1}{\bar{\phi}}\frac{\partial\psi}{\partial\alpha}\right)$ will be greater than λ (see Equation A.20).

Considering now the expression for the flowfield redistribution:

$$\delta\phi = -\Delta\varepsilon\frac{\partial\psi}{\partial\varepsilon}\left[\frac{\frac{\partial\psi}{\partial\phi}\cos\theta - (\lambda - \frac{1}{\bar{\phi}}\frac{\partial\psi}{\partial\alpha})\sin\theta}{\left(\lambda - \frac{1}{\bar{\phi}}\frac{\partial\psi}{\partial\alpha}\right)^2 + \left(\frac{\partial\psi}{\partial\phi}\right)^2}\right] \tag{B.1}$$

it can be seen that including the inlet swirl sensitivity term will lead to a reduction in the magnitude of the flow redistribution, as the term appears squared in the denominator of the equation.

It is thus clear that the inclusion of the inlet swirl sensitivity term in the model will ***increase*** the phase lag and ***decrease*** the magnitude of the predicted flowfield redistribution.

As a qualitative test of the effect of inlet swirl sensitivity on the flowfield redistribution, the compressor was fitted with non-turning IGVs which provided axial inflow. Once the IGVs are fitted, the compressor is no longer sensitive to inlet swirl, as the inlet flow angle is fixed. The model thus predicted a larger flow redistribution, with a smaller phase lag, compared with the case without IGVs.

The upstream static pressure measurements described in Chapter 5 were then repeated with the IGVs in place and the results are compared with those obtained without IGVs in Fig. B.2 for a near-stall operating point. As in Chapter 5, the lines shown are the first Fourier harmonics of the raw data.

It is clear that the magnitude of the flowfield redistribution is larger in the compressor with IGVs (red line) than the one without (black line). It is also clear, however, that the phase lag is much larger with the IGVs in place. It is the case, therefore, that the model correctly predicts an increase in magnitude, but is incorrect in predicting a reduction in phase lag. This result is summarised in Table B.1.

The disagreement between the model and the experimental results is likely to be

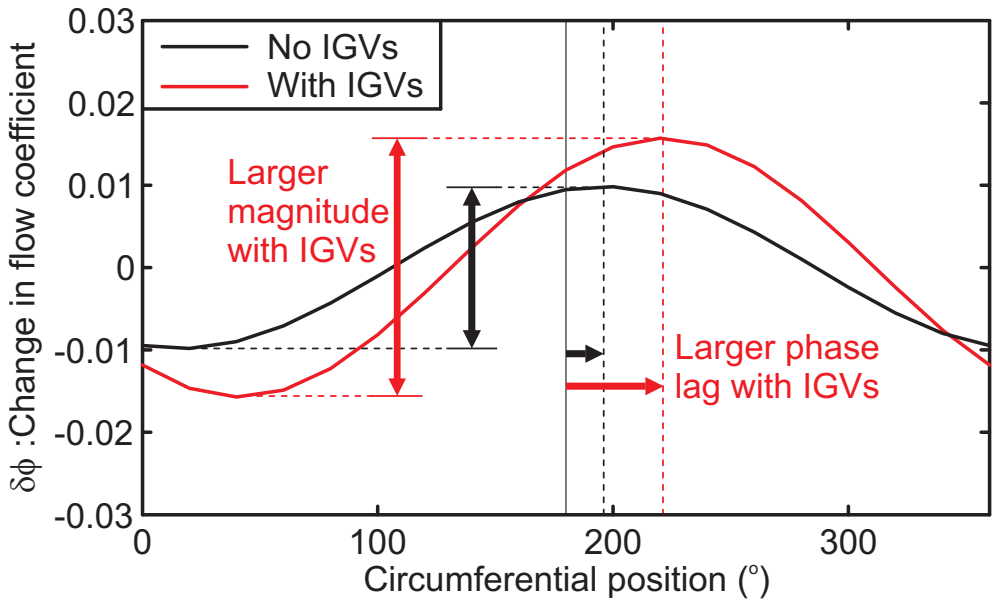

Figure B.2: *Comparison of flow redistribution near-stall with and without Inlet Guide Vanes (1.7% clearance, 75% eccentricity, $\phi = 0.430$).*

Effect of IGVs on:	Experiments	Model
Magnitude	Increase	Increase
Phase	Increase	Decrease

Table B.1: *Comparison of predicted and actual effect of fitting IGVs to the compressor (i.e. removing the inlet swirl sensitivity) on the flowfield redistribution.*

due to the assumption that the flowfield is two-dimensional and that any spanwise variations in the flowfield can thus be ignored. This will be discussed further in the next section.

Validity of the Assumption that the flowfield is Two-Dimensional

To test the validity of the assumption that the inlet flowfield is two-dimensional, a series of three-hole (cobra) probe traverses were conducted 40% axial chord upstream of the rotor bladerow.

The spanwise variations in total and static pressure in the concentric compressor (1.7% clearance) at its design point are shown in Fig. B.3. The total pressure (black line) is constant outside the endwall boundary layers (inner 5% and outer 10% span). The static pressure (red line), however, is not constant across the span. The change in static pressure from the hub to the casing is roughly 20% of the inlet dynamic head[2], and this non-uniformity is large enough to suggest that the assumption of two-dimensional flow in the Graf model is invalid.

In Appendix A, the midspan velocity triangle at inlet was used to derive an expression for the change in inlet flow angle $\delta\alpha$, which was then related to the flowfield redistribution, $\delta\phi$.

Again, this assumes two-dimensional flow, i.e. that the change in inlet flow angle at a given circumferential location will be constant across the span. To test this, inlet flow angle measurements from the maximum and minimum tip-clearance of an eccentric machine are compared in Fig. B.4. This data is also taken from cobra probe traverses at the design point.

Comparing the midspan flow angle measured in the minimum clearance (black line) with that in the maximum clearance (red line), it can be seen that there *is* a change in flow angle around the annulus of an eccentric compressor (i.e. $\delta\alpha$ is not zero).

It can also be seen, however, that the change in flow angle is not constant across the

[2]This variation in static pressure is assumed to be due to streamline curvature.

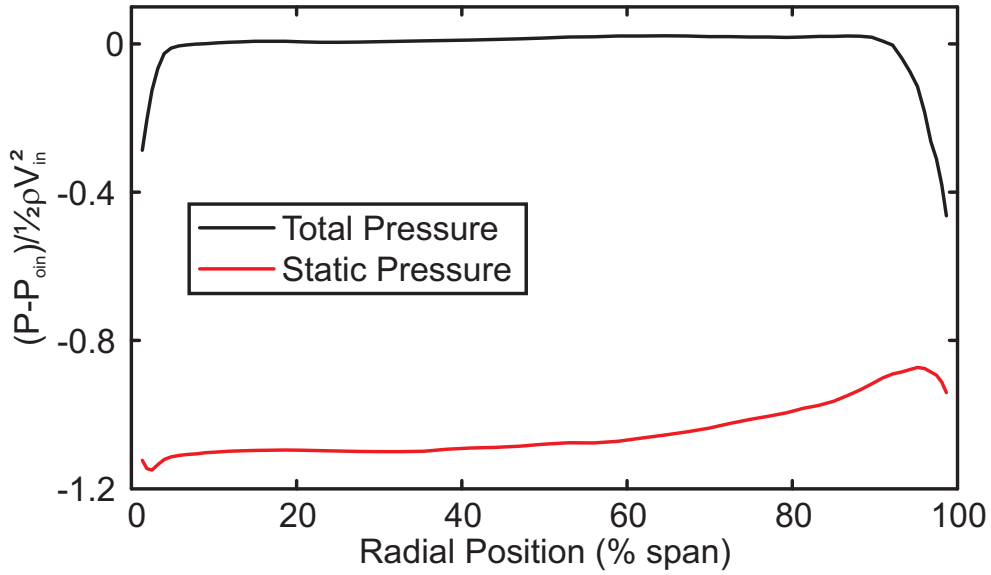

Figure B.3: *Radial variation in inlet total and static pressure in a concentric compressor with 1.7% clearance operating at design conditions (ϕ = 0.5).*

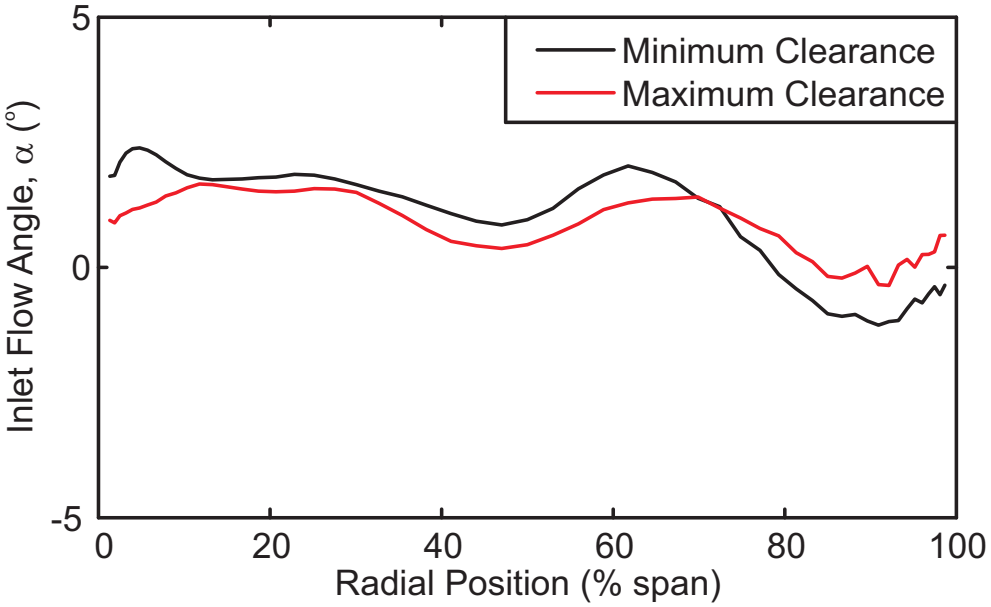

Figure B.4: *Radial variation in inlet flow angle in the maximum and minimum clearance of a compressor with 1.7% clearance and 75% eccentricity operating at design conditions (ϕ = 0.5).*

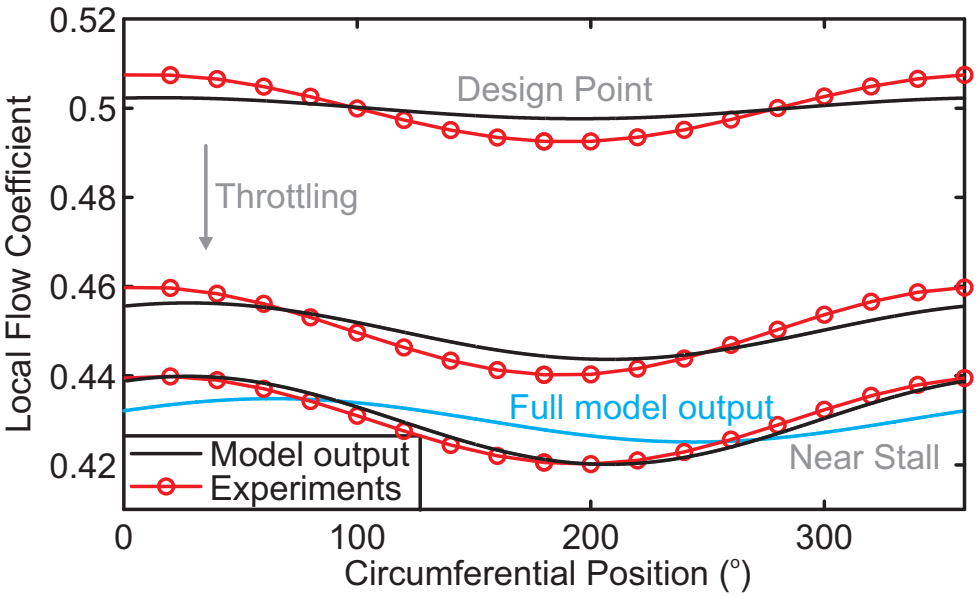

Figure B.5: *Comparison between experimental data and the output of the model of Graf et al. showing improved agreement due to the removal of the inlet swirl sensitivity and unsteady loss terms (1.7% clearance, 75% eccentricity).*

span. From the hub to 70% span, the red line is lower than the black line, so the flow angle is smaller in the large clearance sector than the small clearance sector. In the outer 30% span, the trend is reversed, and the flow angle is now lower in the small clearance sector. This shows that a two-dimensional expression for $\delta\alpha$ will be inaccurate.

Figure B.4 shows that averaging the change in flow angle (i.e. the difference between the red and black lines) across the whole span would give a number very close to zero. This means that it might be most accurate to neglect the inlet swirl sensitivity term in the Graf model altogether.

The Graf model without the inlet swirl sensitivity term is compared with the experimental data for a compressor with 1.7% clearance and 75% eccentricity in Fig. B.5. The flow coefficient variation is shown for three different average flow coefficients ($\bar{\phi}$ = 0.50, 0.45 and 0.43). As in Fig. 5.8, the model output is shown in black while the experimental data is in red. To further improve the agreement, the unsteady loss term which was added to λ in Equation A.21 has also been removed.

The upper pair of lines in Fig. B.5 show data from the design point. It can be seen that without the extra terms the model still under-predicts the magnitude of the redistribution. As the compressor is throttled, however, the agreement improves. In

particular, the near-stall prediction captures both the phase lag and magnitude with good accuracy.

To show the improvement in agreement more clearly, the output of the 'full model' (i.e. with the inlet swirl sensitivity and unsteady loss terms included) at the near-stall operating point is plotted in blue in Fig. B.5. It is clear that the black line (model without extra terms) follows the red line (experimental data) much more closely than the blue line (full model) does, both in terms of magnitude and phase lag.

It is clear from this result that the effect of inlet swirl sensitivity is much smaller than predicted by the model, and so the agreement can be improved by removing this term altogether. This is, however, not scientifically rigorous, as the 'right' answer has been obtained, but with the wrong physics. Essentially, this process is akin to adding terms to the model, or removing them from it, until agreement with the experimental data is achieved.

In the case of this compressor, the assumption that the flowfield is two-dimensional is not sufficiently close to reality for the model to predict the redistribution accurately. This is likely to be the case for all compressors, because the input to the model is not two-dimensional, i.e. the tip-clearance variation is applied near the casing only and not across the whole span. This is in contrast to inlet distortion (which is what the model was originally developed for), which is generally applied uniformly across the span.

Appendix C

Details of the Computational Method (taken from Pullan et al. [1])

The computations presented in Chapters 7 and 8 were performed using Turbostream. The code is a structured multi-block RANS solver that was developed using the method employed in the Denton code, TBLOCK. The approach is finite-volume timemarching, second order in space, with three levels of multigrid and a single step explicit time integration scheme. All simulations presented here used the Spalart-Allmaras turbulence model with adaptive wall functions and had fully turbulent boundary layers. All the runs were second order accurate in time using Jameson's dual timestepping technique, with 72 physical time steps per blade passing period.

The principal feature of Turbostream is its speed. As well as running on conventional CPUs, the code is also optimized to run on clusters of graphics processing units (GPUs). Turbostream runs 10 to 20 times faster on one GPU as compared to all cores of a contemporaneous CPU. This allowed an operating point of the quarter annulus ($\approx$ 20x10^5 node) calculations to be completed in one day on 32 GPUs.

The grids were generated using a Mitsubishi Heavy Industries in-house code that produced elliptically smoothed blade row meshes with H-O-H topology. Tip gaps were solved with two additional blocks (O-H topology) with 11 points in the gap. All blades were meshed with 293x37x74 points in the O-mesh, with approximately 30 points around the leading edge, and typical y+ values were below 5 on the blade surfaces. The computational domain extended 1.5 tip radii upstream and down-

stream of the blade rows. This gave an axial distance of approximately one quarter of a circumference between the compressor and the planes at which inlet or outlet boundary conditions were imposed. This was verified to be acceptable by comparing the solutions obtained for a two-dimensional linear cascade with those for the same cascade but with inlet and exit boundaries placed at 6 tip radii away from the blades. To reduce the mesh count required, the pitchwise node count per passage was reduced from 57 at the blade row, to 15 at the domain boundaries in 3 stages.

At the inlet of the domain, the total pressure and total temperature were specified as uniform. However, a portion at the start of the inlet duct was set to have zero skin friction in order to control the inlet endwall boundary layer thickness. The boundary layer thickness was matched to measurement data for the yellow compressor. At the exit of the domain, a convergent nozzle was employed to provide the compressor with a back-pressure that changes with mass flow rather than a fixed pressure boundary condition. The nozzle was not choked, so that altering the pressure downstream of the nozzle (specified to be uniform) caused the compressor operating point to change and the pressure upstream of the nozzle to vary according to the matching of the compressor characteristic and the characteristic of the nozzle.

Each operating point was run for five flow-through times (from domain inlet to exit); this was of the order of 4 rotor revolutions. Over the first rotor revolution, the back pressure at the exit of the nozzle was increased linearly with time and the flow coefficient typically reduced by 0.01. This procedure was done first with a single passage domain to obtain the approximate stall point, then with a quarter annulus domain, and finally with a full annulus.

Post-processing is a formidable task with unsteady datasets of order 10^8 nodes. The approach taken was similar to that of the experimentalist. Several measurement planes were output 12 times per rotor passing period, e.g. a selection of blade-to-blade planes, rotor blade surface, and rotor exit planes. From these, a particular range of times was identified for deeper analysis and the operating point was then re-run to obtain this data.

The characteristic obtained from the computational work is compared to the characteristic from experiments in Fig. C.1. (Note that the x-axis is now $\frac{V_X}{U_{\text{tip}}}$ as opposed to U_{mid}.) For this comparison, the inlet total and static pressures from the experimental data have been corrected using inlet three-hole probe traverses. It can be

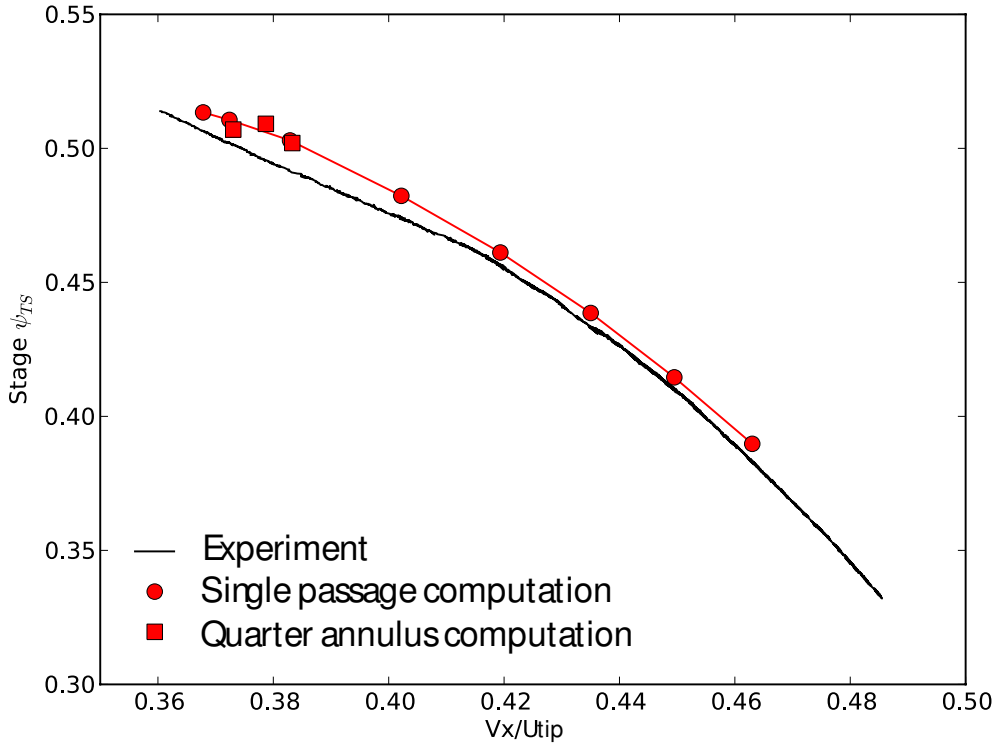

Figure C.1: *Comparison between characteristics obtained experimentally and computationally (from [1]).*

seen that the two characteristics agree well, with the computational stall point being at the same pressure rise as that in the experiments. The stalling flow coefficient is slightly higher in the CFD, and the 'kink' that is observed at about $\phi = 0.41$ in the experimental characteristic is not seen in the computations. This kink is thought to be due to separation on the stator, which the CFD does not capture correctly.

The results shown in Chapters 7 and 8 are from quarter-annulus (14 blades, 33x10^6 node) calculations.

Bibliography

[1] G. Pullan, A. M. Young, I. J. Day, E. M. Greitzer, and Z. S. Spakovsky. Origins and structure of spike-type rotating stall. In *Proc. ASME Turbo Expo, June 11-15 Copenhagen, Denmark*, number GT2012-68707, 2012.

[2] C. Freeman. Tip clearance effects in axial turbomachines. VKI Lecture Series, April 1985.

[3] Method and apparatus for an aerodynamic stability management system, us patent no. 7,827,803, 2010.

[4] H. W. Emmons, C. E. Pearson, and H. P. Grant. Compressor surge and stall propagation. *Transactions of the ASME*, 0:455–469, 1955.

[5] A. H. Stenning. Rotating stall and surge. *ASME Journal of Fluids Engineering*, 102:14–20, March 1980.

[6] T. R. Camp and I. J. Day. A study of spike and modal stall inception in a low-speed axial compressor. *ASME Journal of Turbomachinery*, 120:393–401, July 1998.

[7] I. J. Day and C. Freeman. The unstable behaviour of low and high-speed compressors. *ASME Journal of Turbomachinery*, 116:194–201, April 1994.

[8] E. M. Greitzer. Review - axial compressor stall phenomena. *ASME Journal of Fluids Engineering*, 102:134–151, June 1980.

[9] I. J. Day, E. M. Greitzer, and N. A. Cumpsty. Prediction of compressor performance in rotating stall. *ASME Journal of Engineering for Power*, 100(1):1–14, January 1978.

[10] F. K. Moore and E. M. Greitzer. A theory of post-stall transients in axial compression systems: Part i - development of equations. *ASME Journal of Engineering for Gas Turbines and Power*, 108:68–76, Jan 1986.

[11] E. M. Greitzer and F. K Moore. A theory of post-stall transients in axial compression systems: Part ii - application. *ASME Journal of Engineering for Gas Turbines and Power*, 108:231–239, April 1986.

[12] N. M. McDougall. *Stall Inception in Axial Compressors*. PhD thesis, University of Cambridge, March 1988.

[13] I. J. Day. Stall inception in axial flow compressors. *ASME Journal of Turbomachinery*, 115:1–9, Jan 1993.

[14] A. M. Young. Blade tip shape and compressor stall. 4th Year Undergraduate Project, Cambridge University Engineering Department, 2008.

[15] A. M. J. Dickens. *Highly Loaded Compressors*. PhD thesis, University of Cambridge, 2008.

[16] A. K Simpson and J. P. Longley. An experimental study of the inception of rotating stall in a single-stage low-speed axial compressor. In *Proc. ASME Turbo Expo, May 14-17, Montreal, Canada*, number GT2007-27181, 2007.

[17] A. T. Bowden and J. L. Jefferson. The design and operation of the parsons experimental gas turbine. *Proceedings of the IMechE*, 160:454–471, 1949.

[18] R. E. Peacock. A review of turbomachinery tip gap effects. part 1: Cascades. *International Journal of Heat and Fluid Flow*, 3(4):185–193, Dec 1982.

[19] A. J. Wennerstrom. Experimental study of a high-throughflow transonic axial compressor stage. *ASME Journal of Engineering for Gas Turbines and Power*, 106:552–559, Jul 1984.

[20] D. C Wisler, B. F. Beacher, and H.-W Shin. Effects of loading and clearance variation on tip vortex and endwall blockage. In *Proc. 9th International Symposium in Transport Phenomena and the Dynamics of Rotating Machinery, Honolulu, Hawaii, February 10-14*, 2002.

[21] C. C. Koch. Stalling pressure rise capability of axial flow compressor stages. *ASME Journal of Engineering for Power*, 103:645–656, Oct 1981.

[22] G. D. J. Smith and N. A. Cumpsty. Flow phenomena in compressor casing treatment. *ASME Journal of Turbomachinery*, 106:532–541, 1984.

[23] J. A. Storer and N. A. Cumpsty. Tip leakage flow in axial compressors. In *Proc. Gas Turbine and Aeroengine Congress and Exposition*, number 90-GT-127, 1990.

[24] D. A. Rains. *Tip Clearance Flows in Axial Compressors and Pumps*. PhD thesis, California Institute of Technology, 1954.

[25] J. A. Storer and N. A. Cumpsty. An approximate analysis and prediction method for tip clearance loss in axial compressors. *ASME Journal of Turbomachinery*, 116:648 – 656, Oct 1994.

[26] B. Lakshminarayana. Methods of predicting the tip clearance effects in axial flow turbomachinery. *ASME Journal of Basic Engineering*, 92:467–482, Sept 1970.

[27] B. Lakshminarayana and J. H. Horlock. Leakage and secondary flows in compressor cascades. Aeronautical Research Council Reports and Memoranda 3483, Ministry of Technology, March 1965.

[28] J. H. Horlock and J. D. Denton. A review of some early design practice using computational fluid dynamics and a current perspective. *ASME Journal of Turbomachinery*, 127:5–13, Jan 2005.

[29] J. H. Horlock. the determination of end-wall blockage in axial compressors: A comparison between various approaches. *ASME Journal of Turbomachinery*, 122:218–224, April 2000.

[30] R. Williams, D. Gregory-Smith, and L. He. A study of large tip clearance flows in an axial compressor blade row. In *Proc. ASME Turbo Expo, May 8-11, Barcelona, Spain*, number GT2006-90463, 2006.

[31] R. Williams, D. Gregory-Smith, L. He, and G. Ingram. Experiments and computations on large tip clearance effects in a linear cascade. In *ASME Journal of Turbomachinery*, volume 132, April 2010.

[32] M. Walker, D. Gregory-Smith, and L. He. A study of large tip clearance in a row of low speed compressor blades. In *Proc. 6th European Conference on Turbomachinery Fluid-Mechanics and Thermodynamics, Lille, March.*, 2005.

[33] Nasa website. http://www.aeronautics.nasa.gov/.

[34] H. D. Vo. *Role of Tip Clearance Flow on Axial Compressor Stability*. PhD thesis, Massachusetts Institute of Technology, 2001.

[35] H. D. Vo, C. S. Tan, and E. M. Greitzer. Criteria for spike initiated rotating stall. *ASME Journal of Turbomachinery*, 130:1–9, Jan 2008.

[36] M. Inoue and M. Kuroumoru. Structure of tip clearance flow in an isolated axial compressor rotor. *ASME Journal of Turbomachinery*, 111:250–256, July 1989.

[37] J. D. Cameron, S. C. Morris, S. T. Barrows, and J-P. Chen. On the interpretation of casing measurements in axial compressors. In *Proc. ASME Turbo Expo, Jun 9-13, Berlin, Germany*, number GT2008-51371, 2008.

[38] H. Saathoff and U. Stark. Tip clearance flow induced endwall boundary layer separation in a single-stage axial-flow low-speed compressor. In *Proc. ASME Turbo Expo*, number 2001-GT-0501, 2001.

[39] A. Deppe, H. Saathoff, and U. Stark. Stall inception phenomena in three single-stage low-speed axial compressors. In *Proc. 10th International Symposium on Transport Phenomena and Dynamics of Rotating Machinery, Hononlulu, Hawaii, March 07-11*, 2004.

[40] T. Houghton and I. Day. Enhancing the stability of subsonic compressors using casing grooves. In *Proc. ASME Turbo Expo, Jun 8-12, Orlando, FL, USA*, number GT2009-59210, 2009.

[41] T. Houghton. *Axial Compressor Stability Enhancement*. PhD thesis, University of Cambridge, Feb 2010.

[42] K. L. Suder and M. L. Celestina. Experimental and computational investigation of the tip clearance flow in a transonic axial compressor rotor. Technical report, NASA, 1994.

[43] N. A. Cumpsty. Part-circumference casing treatment and the effect on compressor stall. In *Proc. ASME Gas Turbine and Aeroengine Congress and Exhibition*, number 89-GT-312, 1989.

[44] J.F. Broukaert, N. Van de Wyer, B. Farkas, F. Ullmann, J. Desset, J. de Laborderie, M. Chomé, and S. Hiernaux. Unsteady pressure measurements in a single-stage low pressure axial compressor: Tip vortex flow and stall inception. In *Proc. ASME Turbo Expo, Jun 8-12, Orlando, FL, USA*, number GT2009-59771, 2009.

[45] S. A. Weichert and I. J. Day. Detailed measurements of spike formation in an axial compressor. In *Proc. ASME Turbo Expo, June 11-15, Copenhagen, Denmark*, number GT2012-68627, 2012.

[46] P. A. Seitz. *Casing Treatment for Axial Flow Compressors*. PhD thesis, University of Cambridge, 1999.

[47] M. B Graf, T. S. Wong, E. M. Greitzer, F. E. Marble, C. S. Tan, H.-W Shin, and D. C. Wisler. Effects of nonaxisymmetric tip clearance on axial compressor performance and stability. *ASME Journal of Turbomachinery*, 120:648–661, Oct 1998.

[48] T. P. Hynes and E. M. Greitzer. A method for assessing effects of circumferential flow distortion on compressor stability. *ASME Journal of Turbomachinery*, 109:371 – 379, July 1987.

[49] J. D. Cameron, M. A. Bennington, M. H. Ross, S. C. Morris, and T. C. Corke. Effects of steady tip-clearance asymmetry and rotor whirl on stall inception in an axial compressor. In *Proc. ASME Turbo Expo, May 14-17, Montreal, Canada*, number GT2007-28278, 2007.

[50] M. A. Bennington, M. H. Ross, J. D. Cameron, J. Morris, Du, F. Lin, and J. Chen. An experimental and computational investigation of tip clearance flow and its impact on stall inception. In *Proc. ASME Turbo Expo, Jun 14-18, Glasgow, UK*, number GT2010-23516, 2010.

[51] L. H. Smith. Casing boundary layers in multistage axial-flow compressors. In *Proc. Symposium on Flow Research on Blading. Baden, Switzerland. Ed. L. Z. Dzuyng.*, pages 275–304. Elsevier, 1969.

[52] K. L. Suder. Blockage development in a transonic, axial compressor rotor. *ASME Journal of Turbomachinery*, 120:465–476, July 1998.

[53] S. A. Khalid, A. S. Khalsa, I. A Waitz, C. S. Tan, E. M. Greitzer, N. A. Cumpsty, J. J. Adamczyk, and F. E. Marble. Endwall blockage in axial compressors. *ASME Journal of Turbomachinery*, 121:499–509, 1999.

[54] R. Mailach, I. Lehmann, and K. Vogeler. Rotating instabilities in and axial compressor originating from the fluctuating blade tip vortex. *ASME Journal of Turbomachinery*, 123:453–463, July 2001.

[55] R. Mailach, H. Sauer, and K. Vogeler. The periodical interaction of the tip clearance flow in the blade rows of axial compressors. In *Proc. ASME Turbo Expo, Jun 4-7, New Orleans, LA, USA*, number 2001-GT-0299, 2001.

[56] M. Inoue, M. Kuroumoru, T. Tanino, and M. Furukawa. Propagation of multiple short-length-scale stall cells in an axial compressor rotor. *ASME Journal of Turbomachinery*, 122:45–54, Jan 2000.

[57] M. Inoue, M. Kuroumoru, T. Tanino, S. Yoshida, and M. Furukawa. Comparative studies on short and long length-scale stall cell propagating in an axial compressor rotor. *ASME Journal of Turbomachinery*, 123:24–32, Jan 2001.

[58] N. C. Cumpsty. Discussion of inoue et al. "propagation of multiple short-length-scale stall cells in an axial compressor rotor". *ASME Journal of Turbomachinery*, 122:53, Jan 2000.

[59] F. Kameier and W. Neise. Experimental study of tip clearance losses and noise in axial turbomachines and their reduction. *ASME Journal of Turbomachinery*, 119:460–471, Jul 1997.

[60] J. März, C. Hah, and W. Neise. An experimental and numerical investigation into the mechanisms of rotating instability. In *Proc. ASME Turbo Expo, Jun 4-7, New Orleans, LA*, number 2001-GT-0536, 2001.

[61] A. H. Epstein, J. E. F Ffowcs Williams, and E. M. Greitzer. Active suppression of aerodynamic instabilities in turbomachines. *AIAA Journal of Propulsion and Power*, 5(2):204–211, 1989.

[62] J. D. Paduano, A. H. Epstein, L. Valavani, J. P. Longley, E. M. Greitzer, and G. R. Guenette. Acrive control of rotating stall in a low-speed axial compressor. *ASME Journal of Turbomachinery*, 115(1):48–56, Jan 1993.

[63] I. J. Day, T. Breuer, J. Escuret, M. Cherrett, and A. Wilson. Stall inception and the prospects for active control in four high-speed compressors. *ASME Journal of Turbomachinery*, 121:18–27, Jan 1999.

[64] I. J. Day. The fundamentals of stall and surge; part i: Stall. Cambridge Turbomachinery Course Lecture, 2008.

[65] S. Bindl, N. Niehuis, C. Zähringer, and F. Grauer. Retrofit of a digital engine control unit and integration of an active stability control system. In *ISABE-2007-1251*, 2007.

[66] M Dhingra, Y. Neumeier, J. V. R. Prasad, and H.-W Shin. Stall and surge precursors in axial compressors. In *Proc. 39th AIAA/ASME/SAE/ASEE Joint Propulsion Conference and Exhibit, July 20-23, Hunstville, AL*, number AIAA 2003-4425, 2003.

[67] Y. Liu, M Dhingra, and J. V. R. Prasad. Active compressor stability management via a stall margin control mode. In *Proc. ASME Turbo Expo, Jun 8-12, Orlando, FL, USA*, number GT2009-60140, 2009.

[68] M. Dhingra. *Compressor Stability Management*. PhD thesis, Georgia Institute of Technology, May 2006.

[69] D. Christensen, P. Cantin, D. Gutz, P. N. Szucs, A. R. Wadia, J. Armor, M. Dhingra, Y. Neumeier, and J. V. R. Prasad. Development and demonstration of a stability management system for gas turbine engines. *ASME Journal of Turbomachinery*, 130:1 – 8, July 2008.

[70] A. J Gannon, G. V. Hobson, and W. L. Davis. Axial transonic rotor and stage behaviour near the stability limit. In *Proc. ASME Turbo Expo, Jun 14-18, Glasgow, UK*, number GT2010-23713, 2010.

[71] D. C. Wisler. Loss reduction in axial-flow compressors through low-speed model testing. *Journal of Engineering for Gas Turbines and Power*, 107:354–363, 1985.

[72] T. R. Camp and H.-W. Shin. Turbulence intensity and length scale measurements in multistage compressors. *ASME Journal of Turbomachinery*, 117:38–46, Jan 1995.

[73] H. Schlichting and A. Das. On the influence of turbulence level on the aerodynamic losses of axial turbomachines. In *Flow Research on Blading. Ed. L. Z. Dzuyng.* Elsevier, 1970.

[74] A. K. Simpson. *An Investigation into Stall Inception in a Single-Stage, Low-Speed Axial-Flow Compressor*. PhD thesis, University of Cambridge, 2005.

[75] I. Day. Effect of blade irregularities on surge margin. NEWAC Project Report D3.5.1C, University of Cambridge, 2011.

[76] R. J. Miller. Private communication. 2011.

[77] C. Freeman. Private communication. 2009.

[78] J. P. Longley. Measured and predicted effects of inlet distortion on axial compressors. In *Proc. ASME Gas Turbine and Aeroengine Congress and Exposition*, number 90-GT-214, 1990.

[79] G. Pullan. Private communication. 2012.

[80] J. Jeong and F. Hussain. On the identification of a vortex. *Journal of Fluid Mechanics*, 285:69–94, 1995.

[81] J. P. Longley. *Inlet Distortion and Compressor Stability*. PhD thesis, University of Cambridge, 1988.

[82] R. Chue, T. P. Hynes, E. M. Greitzer, C. S. Tan, and J. P. Longley. Calculations of inlet distortion induced compressor flow field instability. *International Journal of Heat and Fluid Flow*, 10(3):211–223, Sept 1989.